JOURNAL OF

METALS

IN TWO SECTIONS—SECTION 1

January 1954

INDUCTION STIRRING

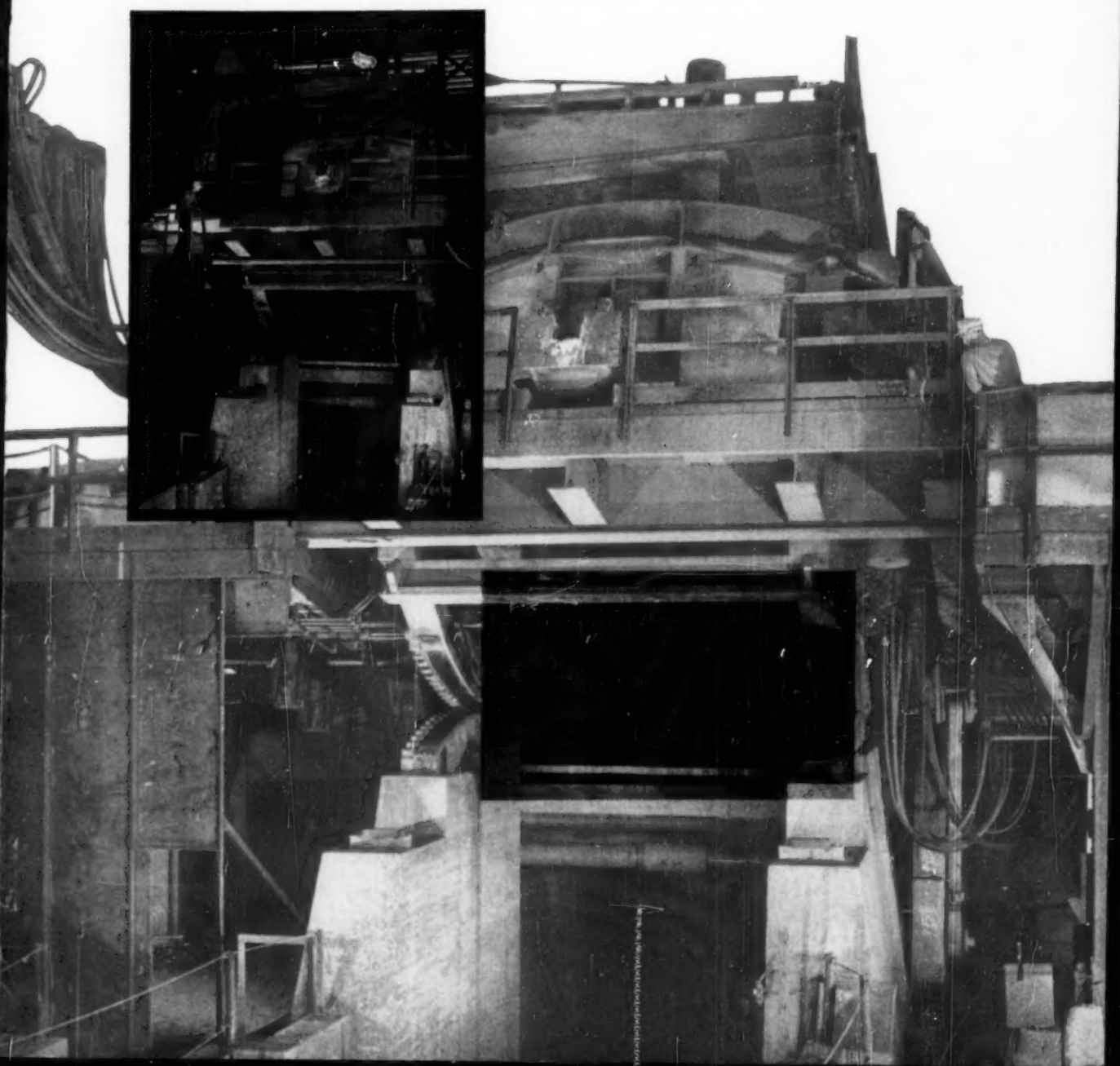

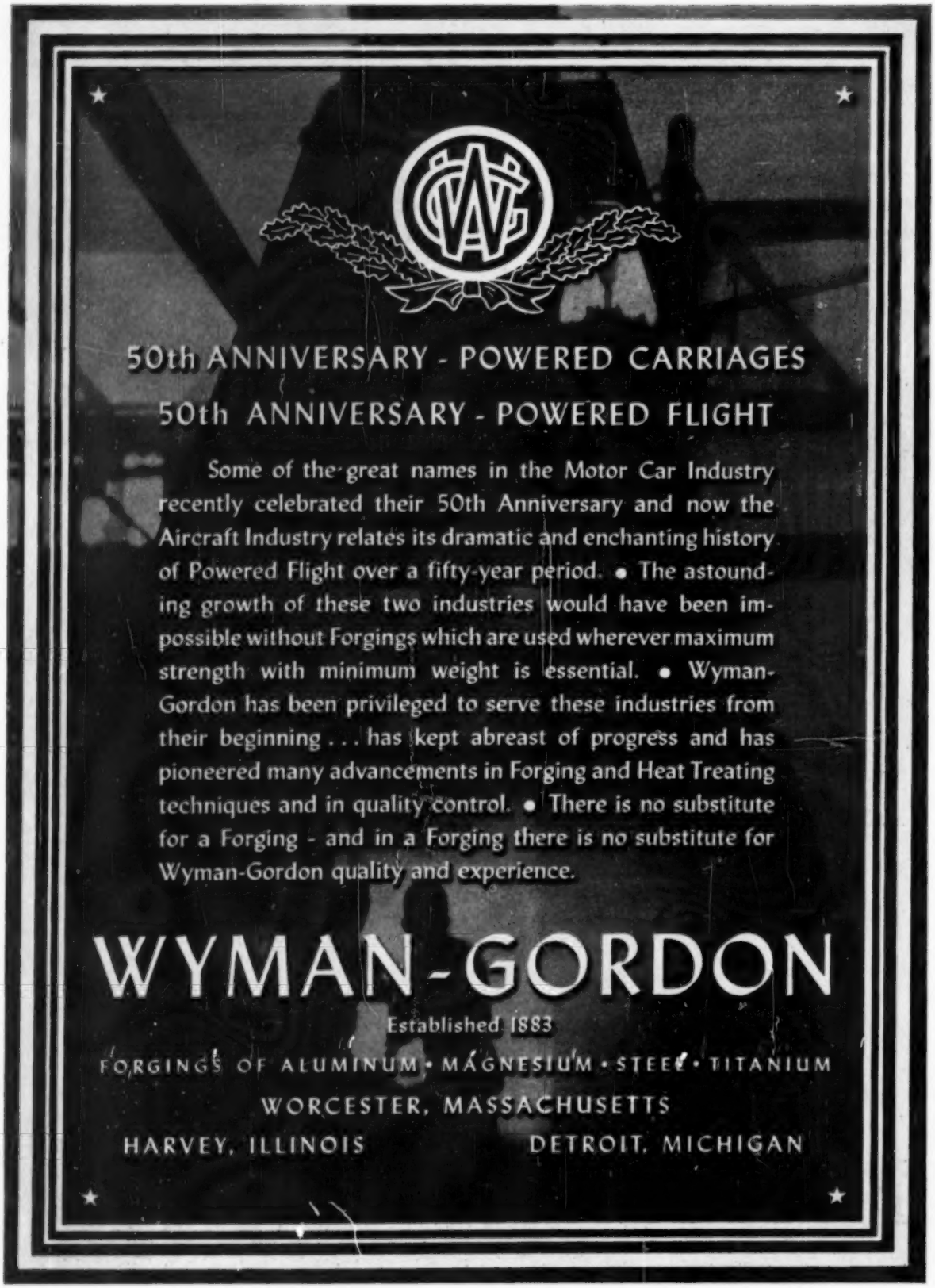

50th ANNIVERSARY - POWERED CARRIAGES

50th ANNIVERSARY - POWERED FLIGHT

Some of the great names in the Motor Car Industry recently celebrated their 50th Anniversary and now the Aircraft Industry relates its dramatic and enchanting history of Powered Flight over a fifty-year period. • The astounding growth of these two industries would have been impossible without Forgings which are used wherever maximum strength with minimum weight is essential. • Wyman-Gordon has been privileged to serve these industries from their beginning . . . has kept abreast of progress and has pioneered many advancements in Forging and Heat Treating techniques and in quality control. • There is no substitute for a Forging - and in a Forging there is no substitute for Wyman-Gordon quality and experience.

WYMAN-GORDON

Established 1883

FORGINGS OF ALUMINUM • MAGNESIUM • STEEL • TITANIUM

WORCESTER, MASSACHUSETTS

HARVEY, ILLINOIS DETROIT, MICHIGAN

Journal of

METALS

VOL. 6, NO. 1 JANUARY, 1954

In Two Sections — Section 1

COVER

Cover design shows the induction stirrer installation on one of the electric furnaces at Timken Roller Bearing Co., Canton, Ohio. The full report of the benefits obtained through use of the induction stirrer begins on page 21 of this issue.

NEWS

Meet the Authors	2	Journal of Metals Reporter	15
Employment Service	3	Drift of Things	16
Books for Engineers	5	Annual Meeting Program	81
New Products	7	AIME News	86
Industrial Notes	10	Electric Furnace Meeting	87
Trends	12	Personals	91

TECHNICAL FEATURES

Elliptical Electric Furnace Outperforms Conventional Circular Type — James K. Preston 18

Induction Stirring Provides Better Control of Operating Techniques — Harry F. Walther 21

17 Years of Stirring History Shows International Exchange of Ideas — Eric G. Malmlow 24

Tin Increases Strength of Ti-Al Alloys Without Loss in Fabricability — W. L. Finlay, R. I. Jaffee, R. W. Parcel, R. C. Durstein 25

Closed Electric Reduction Furnaces Permit Utilization of Furnace Gas — M. O. Sem 30

TRANSACTIONS

Optimum Composition of Blast Furnace Slag as Deduced from Liquidus Data for the Quaternary System CaO-MgO-Al_2O_3-SiO_2 — E. F. Osborn, R. C. DeVries, K. G. Gee, H. M. Kraner 33

Solidification of Aluminum-Rich Aluminum-Copper Alloys — A. B. Michael, M. B. Bever 47

Mechanism of Plastic Flow in Titanium: Manifestations and Dynamics of Glide — F. D. Rosi 58

Creep Correlations of Metals at Elevated Temperatures — O. D. Sherby, R. L. Orr, J. E. Dorn 71

TECHNICAL NOTES

Magnetic Transformation of Iron in Copper Matrix at Low Temperatures — R. E. Cech, D. Turnbull 45

Effect of Repeated Tensile Prestrain on the Ductility of Some Metals — E. C. Franz 56

Reaction of Oxygen and Nitrogen with Titanium from 700° to 1050°C — L. S. Richardson, N. J. Grant 69

Structure of Some Iridium-Osmium Alloys — H. C. Vacher, C. J. Bechtoldt, E. Maxwell 80

Published to provide a continuing, authoritative, and up-to-date record of technological, engineering, and economic progress in all branches of the metals industry by the Metals Branch American Institute of Mining and Metallurgical Engineers, Inc. 29 West 39th Street, New York 18

ALVIN S. COHAN
Manager of Publications
Editor, JOURNAL OF METALS

D. G. GARRETT M. A. MATZKIN
E. M. WEISS G. M. ZILL
Assistant Editors

GRACE PUGSLEY Production Manager
W. J. SEWING Asst. Prod. Mgr.

METALS BRANCH COUNCIL
K. C. McCutcheon Chairman
E. O. Kirkendall Secretary
M. Cohen IMD Chairman
T. J. McLaughlin ISD Chairman
R. R. McNaughton EMD Chairman
W. A. Dean R. D. Parks
T. D. Jones D. S. Eppelsheimer

EDITORIAL ADVISORY COMMITTEE
J. S. Smart, Jr. Chairman
W. A. Dean Evan Just
J. C. Kinnear, Jr. John Marsh
T. D. Jones M. Tenenbaum

TECHNICAL PUBLICATIONS COMMITTEES
Robert Aborn AIME Chairman
Otto Zmeskal ISD Chairman
S. J. Dickinson EMD Chairman
W. R. Hibbard, Jr. IMD Chairman
E. J. Kennedy, Jr. Secretary

JAMES A. STANGARONE
Advertising Manager
FRED STANLEY
Eastern Representative

The AIME Publishes:
Journal of Metals
Mining Engineering
Journal of Petroleum Technology

Published the first day of each month by the American Institute of Mining and Metallurgical Engineers, Inc., 29 West 39th Street, New York 18, N. Y. Telephone: PEnnsylvania 6-9220. Subscription $8 per year for non-AIME members in United States and North, South and Central America; $10, foreign; $6 for AIME members, or $4 additional in combination with a subscription to "Mining Engineering" or "Journal of Petroleum Technology." Single copies, 75 cents; single copies foreign, $1.00; special issues, $1.50 . . . The AIME is not responsible for any statement made or opinion expressed in its publications . . . Copyright 1954 by the American Institute of Mining and Metallurgical Engineers, Inc. . . . Registered cable address, AIME New York . . . Indexed in Engineering Index, Industrial Arts Index and Chemical Abstracts . . . Reentered as second-class matter Sept. 21, 1949, at the post office at New York, N. Y., under the Act of March 3, 1879. Additional entry established at Manchester, N. H.

Meet The Authors

E. G. Malmlow (p. 24) was born in Sweden and received his doctorate degree from the Royal Institute of Technology, Stockholm. From 1938 to 1946 he was in the research dept., ASEA, Vasteras, Sweden. He then transferred to the production dept. In 1948 Dr. Malmlow came to the United States as resident engineer. He is now president for Aros Electric, Inc., New York.

E. G. MALMLOW

W. L. FINLAY

Walter L. Finlay (p. 25) is presently associated with Rem-Cru Titanium, Inc., Midland, Pa., as research manager. He is a native Brooklynite and graduated from Lehigh and Yale Universities. From 1936 to 1946 he was engaged in small arms and ammunition ballistic research and metal processing development at Remington Arms Co., Bridgeport, Conn. Since 1946 he has been engaged in melting, alloying, casting, and fabrication of Ti and Ti base alloys. An AIME Member, his reason for not having a hobby is "too hobbled by that wench, Titania, so my occasional hobby is dreaming of hobbies."

K. G. Gee (p. 33) is a native of Elmira, N. Y. A graduate of the University of Arizona, he holds a B.S. in geology and mineralogy. Mr. Gee is presently a research associate at the School of Mineral Industries, Pennsylvania State University. Interests other than his work include tropical fish.

K. G. GEE

H. M. KRANER

Hobart McKinley Kraner (p. 33) has been research engineer for the Bethlehem Steel Co., Bethlehem, Pa., since 1935. Born in Columbus, Ohio, Mr. Kraner graduated from Ohio State University. In 1922 he joined the staff of the U. S. Bureau of Mines ceramic experiment station in Columbus as ceramic engineer. One year later he went to the AC Spark Plug Co, Flint, Mich., as ceramic engineer and in 1924 became superintendent of the Illinois Electric Porcelain Co., Macomb, Ill. He has also been associated with the Westinghouse Electric & Mfg. Co. and Corhart Refractories Co. Mr. Kraner has been active in the American Ceramic Society since 1919, serving as president at one time and also an officer of various committees. He also holds membership in the AISI, AIME, and Iron & Steel Institute (England). His varied hobbies include interest in photography and an interesting collection of unusual patents. Mr. Kraner also does quite a bit of golfing, consistently shooting in the 90's.

R. C. DeVries (p. 33) has been at Pennsylvania State University for approximately five years engaged in research and as a student. Dr. DeVries received his degrees from DePauw and Pennsylvania State Universities. As his hobbies, he enjoys woodcraft and photography.

R. C. DeVRIES

E. F. OSBORN

E. F. Osborn (p. 33) has degrees from DePauw and Northwestern Universities and California Institute of Technology. After receiving his doctorate in 1937, Dr. Osborn was an instructor at Northwestern. He then accepted a position in Quebec as mining geologist, returning to the United States to join the Carnegie Institution of Washington. He was engaged in research for the National Defense Research Committee from 1942 to 1945. Dr. Osborn joined the Eastman Kodak Co. as research chemist in 1945. He became a member of the staff at Pennsylvania State University in 1946. Prior to becoming dean of the School of Mineral Industries, Pennsylvania State University, he was head of the dept. of earth sciences. He is a Member of AIME and other technical societies. His spare time interests are golf and fishing.

Raymond L. Orr (p. 71), born in San Francisco, California, received his B.S. from the University of California. From 1949 to 1951 he was a chemist with the Best Fertilizers Co., Oakland. For approximately one year he was a member of the Bureau of Mines at Berkeley and is presently a graduate research engineer, University of California, Berkeley. His spare time hobbies include hiking, back-packing, and fishing.

James K. Preston (p. 18) is a supervisory trainee for the Timken Roller Bearing Co., Canton, Ohio. Mr. Preston is a graduate from Cornell University, (1951, B. Met.). Born at Benton Harbor, Mich., he joined the Auto Specialties Mfg. Co., St. Joseph, Mich., after graduation from Cornell. He was engaged in the development of adaptation of ductile iron and Croning process molds to castings made of steel. He joined Timken in July 1952.

John E. Dorn (p. 71) is associated with the dept. of metallurgy, engineering research projects, University of California, Berkeley. Born in Chicago, he attended Northwestern University and University of Minnesota (B.S., M.S., Ph.D.). In 1936 Dr. Dorn was a research associate with Battelle Memorial Institute. In 1938 he joined the staff at the University of California as an assistant professor. For one year he was a research metallurgist with Dow Chemical Co., and in 1942 was again with the University of California. Dr. Dorn was appointed associate professor in 1946; professor in 1948; and is presently professor of physical metallurgy. An AIME Member, he has presented about 10 papers since 1937. His spare time interests include gardening and stamp collecting.

METALLURGIST. Leading, progressive, Precision Investment Casting concern offers outstanding opportunity for capable metallurgist with High Temperature Alloys experience. Radiographic and Customer Contact experience helpful. TOP SALARY. APPLY TO: Personnel Manager, MICRO-CAST DIVISION, Austenal Laboratories, Inc., 7001 S. Chicago Ave., Chicago 37, Ill.

COLUMBIA UNIVERSITY
SCHOOL OF MINES

William Campbell Fellowships
Henry Krumb Scholarships

These grants are available for degree candidates in Mining, Mineral Engineering and Metallurgy. Applications are invited for the academic year 1953-54.

The William Campbell Fellowships, with the value of $1800-$2100 a year, are awarded for graduate study leading to the M.S. or doctoral degree, or for post-doctoral work.

The Henry Krumb Scholarships, in the amount of $1000 a year, are awarded to B.S., M.S., and professional engineering degree candidates.

Application blanks and further information may be obtained from the Office of University Admissions, Columbia University, New York, 27, N. Y. The closing date for applications is February 20th, 1954.

— Personnel Service —

THE following employment items are made available to AIME members on a nonprofit basis by the Engineering Societies Personnel Service, Inc., operating in cooperation with the Four Founder Societies. Local offices of the Personnel Service are at 8 W. 40th St., **New York 18;** 100 Farnsworth Ave., **Detroit;** 57 Post St., **San Francisco;** 84 E. Randolph St., **Chicago 1.** Applicants should address all mail to the proper key numbers in care of the New York office and include 6c in stamps for forwarding and returning application. The applicant agrees, if placed in a position by means of the Service, to pay the placement fee listed by the Service. AIME members may secure a weekly bulletin of positions available for $3.50 a quarter, $12 a year.

MEN AVAILABLE

Metallurgical Engineer—coordinator of research and development; B.S., M.S. plus graduate work in industrial engineering. Age 30; 9½ years experience, married. Qualified plan and direct basic and applied research and development programs, maintain liaison with production and sales, new product specialist. Numerous published articles, patents. M-117.

Graduate Metallurgist, M.S. Fourteen years experience metal fabrication, laboratory supervision materials selection and troubleshooting. Heavy experience forging, heat treatment, welding, press working stainless, carbon and low alloy steels. Excellent knowledge chemical laboratory practices. Location, immaterial. Publications. Acknowledgment of all inquiries. M-118.

Ferrous Metallurgist desires work in production metallurgy, development or research. Has over 15 years background in open hearth and electric furnace metallurgy, also heating and mill practice. Good on surface quality including resulphurized grades. Experience includes all AISI carbon and alloy grades. Good organizer. M-119.

POSITIONS OPEN

Metallurgist, 25 to 35, recent graduate or better. Must have knowledge of metallography. Will supervise laboratory technicians handling heat treating of ferrous and nonferrous alloys. Company manufactures oils. Salary, $4420 to $5720 a year. Employer will pay fee. Location, Illinois. C1373(b).

Nonferrous metallurgist, up to 60. Must have had at least 5 years experience in rolling and fabricating nonferrous metals and/or foundry operations of nonferrous copper alloys. Company manufactures novelties. Duties will involve controlling of all metal operations in fabricating copper alloys. Salary up to $9000 per year. Employer will negotiate fee. Location, western Chicago suburb. C1357(a).

Metallurgist—Application Metallurgist or Metallurgical Engineer, 25 to 35. Must have had at least two years experience in metallurgical work pertaining to development or manufacture of radio tubes or similar products. Will work in sales dept. in developing or using rare metals for use in radio or TV tubes and allied products. Must have sales personality. Salary, $5400 to $7200 a year. Employer might negotiate fee. Location, northern Chicago suburb. C1412A.

Development Engineer, 25 to 35; engineering college or more. Company's field is fine metallurgy and duties will be to work on processes and equipment for producing composite metals. Must have good imagination to fit in with group already engaged in work. Salary, $4500 to 8400 a year. Employer will pay fee. Only incidental traveling. Location, New England. C1436W.

Metallurgical Engineer, 30 to 40, B.S. or M.S. in metallurgical engineering; ten years experience. Problems of welding and corrosion on stainless steel—also problems concerning metals in contact with sea water, such as copper, nickel and monel. Developing welding processes—representing company at meetings and engineering conferences. Salary, $8000 to $12,000 a year. Location, Connecticut. Y9408(b).

Instructor or Assistant Professor to teach physical metallurgy in engineering school. Day and evening classes. Starting Feb. 1, 1954. Salary, $4000 to $5000 a year. Location, New York metropolitan area. Y9388.

METALLURGIST

Technically trained with approximately five years' steel mill experience. Pittsburgh district. Excellent opportunity for a young man to work directly under Chief Metallurgist on open hearth and related operations.

Box A-1 AIME, 29 W. 39th St., New York

PROFESSOR OF PHYSICAL METALLURGY experienced in research direction and graduate instruction. Ph.D. or equivalent, to head educational option in physical metallurgy and direct thesis and contract research. Excellent opportunity for expansion in an outstanding center in the Middle Atlantic region.

Box A-2 AIME, 29 W. 39th St., New York

METALLURGIST

. . . needed as Process Metallurgist in brass mill manufacturing beryllium-copper, phosphor-bronze and nickel-silver in the form of strip, wire and rod.

Excellent position offering advancement and many benefits.

Reply fully giving age, experience and salary desired to: The Riverside Metal Co., Riverside, N. J.

Metallurgical Consultant

Applications are invited from graduate Metallurgical Engineers, preferably in the age range 40 to 45, who have had not less than ten years broad and responsible experience in the field of nonferrous extraction metallurgy, for the position of Assistant Consulting Metallurgist to the undermentioned Corporation for duties in connection with the important group of Northern Rhodesian mining companies producing copper, cobalt, lead, zinc and other base metals, to which the Corporation acts as Consulting Engineers.

The salary to be offered will be commensurate with the successful candidate's qualifications and experience. Membership of the Corporation's Pension Fund will be a condition of employment.

Applicants must be prepared to take up residence in Kitwe, Northern Rhodesia. The cost of transportation of the successful candidate, his wife and children up to 18 years of age and reasonable personal effects will be borne by the Corporation. A modern three-bedroomed brick house, with essential furniture, will be made available at a rental which will not exceed $28.00 per month.

Excellent medical facilities are provided and recreational amenities are outstanding.

Initially the engagement will be for a period of three years, after which service may be extended indefinitely, but will be subject to six months notice of termination by either party. Repatriation privileges on the same scale as above will be granted at the end of three years service. Leave is generous and amounts at present to 60 days per annum which can be accumulated up to a maximum of 180 days.

Applications stating age, marital status, educational and professional qualifications and giving details of past experience and positions held should be addressed to:

Personnel Officer,

Anglo American Corporation of South Africa, Limited,

P.O. Box 4587,
JOHANNESBURG.

Advertisement

ELECTROMET Data Sheet

A Digest of the Production, Properties, and Uses of Steels and Other Metals

Published by Electro Metallurgical Company, a Division of Union Carbide and Carbon Corporation, 30 East 42nd Street, New York 17, N. Y. • In Canada: Electro Metallurgical Company of Canada, Limited, Welland, Ontario.

COLUMBIUM and TANTALUM

Strategic Combination for Imparting Strength and Stability to High-Temperature Metals

Gas turbines for jet-aircraft engines, and for other similar engines being developed for marine and railway transportation, have greatly increased the demand for high-temperature metals. The present most satisfactory metals are either iron-base, nickel-base, or cobalt-base. They are used in the form of castings and hot-worked products, such as forgings, bars, and sheets.

Many of these special metals contain columbium because of its beneficial effect on high-temperature strength in both cast and wrought products. Investigations have shown that columbium is one of the key alloys for imparting high-temperature strength and stability in metals suitable for operating temperatures up to 1500 deg. F. and above.

Need for New Alloy

Originally, a ferrocolumbium alloy containing approximately 55 per cent columbium and 5 per cent tantalum was employed in the production of many of these high-temperature metals. However, with the increased use of high-temperature metals and columbium-bearing 18-8 stainless steels, the demand for columbium exceeded its availability.

ELECTROMET's Research Laboratories began investigations to ascertain whether an alloy containing more tantalum and less columbium would be equally satisfactory for producing the high-temperature metals. Columbium and tantalum alone, as well as combination alloys of columbium plus tantalum, were tested.

Results of Tests

The alloy N-155 was selected for tests. It is an iron-base alloy with the following approximate analysis:

Chromium	20 per cent
Nickel	20 per cent
Cobalt	20 per cent
Tungsten	3 per cent
Molybdenum	2 per cent
Columbium	1 per cent
Nitrogen	0.15 per cent
Carbon	max. 0.35 per cent

The data in the table below describe the mechanical properties, at room temperature, of this low-carbon N-155 alloy modified with columbium and tantalum alone, and with combinations of columbium plus tantalum. The metal modified with columbium has good strength and high ductility at room temperature. These same good properties are obtained when tantalum, or tantalum plus columbium, is substituted for the columbium.

Stress-to-rupture tests were also conducted on these same modified low-carbon N-155 alloys at 1350 and 1500 deg. F. The data show (see table) that when the columbium is replaced with a mixture of columbium plus tantalum, the strength of the metal remains substantially unaffected at 1350 and 1500 deg. F. Also, when all of the columbium is replaced with tantalum, the strength of the metal at 1500 deg. F. is equivalent to that obtained with columbium. Hence, from the standpoint of high-temperature strength, columbium and tantalum can be used interchangeably, or in combination.

Help to Industry

ELECTROMET has developed an alloy containing approximately 20 per cent tantalum and 40 per cent columbium for use in high-temperature metals and stainless steels. It is known as ELECTROMET ferrotantalum-columbium.

Industrial experience with this comparatively new alloy has confirmed the favorable results of the experimental work. The alloy has already aided considerably in augmenting the supply of columbium alloys, since it is just as effective as ELECTROMET ferrocolumbium, with 50 to 60 per cent columbium, for giving strength at high temperatures.

Furthermore, the new alloy is now preferred because of its greater availability. It should be added to a thoroughly deoxidized metal bath to obtain the best results. A recovery of about 90 per cent for the columbium and 80 per cent for the tantalum may be expected.

For further information regarding alloys for high-temperature metals, write to the nearest ELECTROMET office: in Birmingham, Chicago, Cleveland, Detroit, Houston, Los Angeles, New York, Pittsburgh, or San Francisco. In Canada: Welland, Ontario.

Properties of Modified N-155 Alloys Compared*

Typical Analysis, %**	With Columbium	With Columbium and Tantalum		With Tantalum
Columbium	1.13	0.58	0.49	....
Tantalum	0.08	0.64	0.53	1.47
Carbon	0.12	0.13	0.13	0.12
Nitrogen	0.13	0.14	0.14	0.14
At Room Temperature				
Tensile Strength, psi	119,000	123,200	117,500	122,100
Yield Strength, psi	56,700	59,500	52,000	59,100
Elongation in 2 in., %	52	47	57	54
Reduction of Area, %	69	65	69	56
At 1350 deg. F.				
Stress to Cause Rupture, psi				
In 100 hr.	31,000	34,000	33,500	....
In 1000 hr.	23,000	25,000	23,000	....
At 1500 deg. F.				
Stress to Cause Rupture, psi				
In 100 hr.	20,000	20,000	20,500	20,000
In 1000 hr.	15,000	14,000	15,500	15,000

* Tests made on standard samples from one-inch round bars, water-quenched from 2250 deg. Fahrenheit.
** Composition of the base alloy is given in the text.

The term "Electromet" is a registered trademark of Union Carbide and Carbon Corporation.

Books for Engineers

ORDER YOUR BOOKS THROUGH AIME—Address Irene K. Sharp, Book Department. Ten per cent discount given whenever possible. Order Government publications direct from the agency concerned.

Modern Electroplating, edited by Allen G. Gray. *John Wiley & Sons, Inc.* $8.50, 563 pp., 1953—In addition to practical aspects, the book accents basic theory as it is known today. Its purpose is to present commercially available processes, not only to the electroplating industry, but to those industries which may be considering or using the processes. Virtually all current practices are completely described, even to analytical control of the solution and the theory underlying each operation.

Dislocations in Crystals, by W. T. Read, Jr. *McGraw-Hill Book Co.* $5.00, 228 pp., 1953—The book is designed for use in industry and graduate school by those dealing with physical metallurgy and branches of solid state physics. This is the first work on the subject published in the U. S. and the only one confining itself to well established results. Treatment is by systematic development of what is definitely known—not a review of speculations. Presentation is based on simple physical arguments, offered in physical terms without mathematics. Discussion is based on numerous drawings that introduce the essential three dimensional concepts.

Procedures in Experimental Metallurgy, by A. U. Seybolt and J. E. Burke. *John Wiley & Sons, Inc.* $7.00, 340 pp., 1953—Preparation of metal samples up to the point of making observations on the properties of the metal is the guiding principle or theme of the book. In general, chapter arrangement follows the natural sequence of events in the laboratory; melting, casting, fabrication, and heat treatment. Since, however, most of the operations require the use of high temperature, the book starts with methods for obtaining high temperatures, and methods for controlling them. Powder metallurgy is also covered.

ASME Handbook—Metals Engineering Design, edited by Oscar J. Horger. *McGraw-Hill Book Co., Inc.* $15.00, 405 pp., 1953—The book was prepared to fill what was felt to be an urgent need for a reference manual related to the design engineer's point of view. The volume contains 48 sections contributed by authorities. They cover fatigue characteristics, wear consideration, impact, corrosion, nondestructive testing, elasticity, theories of failure, and many other topics.

FBI Register of British Manufacturers—1954, 26th edition. *Federation of British Industries.* About $6.00, 1953—This is the only standard export reference book to British industry and is the only authorized directory of the Federation of British Industries. There are seven sections to this edition, each with a reinforced index card. A buyers' guide classifies about 6000 FBI member firms under more than 5000 alphabetical trade headings. Full details of all these firms are given in a comprehensive alphabetical directory. Other information is carried in additional sections.

Temperature Measurement in Engineering, by H. Dean Baker, E. A. Ryder, and N. H. Baker. *John Wiley & Sons, Inc.* $3.75, 179 pp., 1953—This is the first of two volumes and discusses temperature accurately in terms of engineering measurement. Facts needed to design, construct, and operate an effective temperature measurement installation are all in this one book. It provides a list of techniques to be employed, the proven methods of analysis, a survey of previous designs, and a procedure of general applicability.

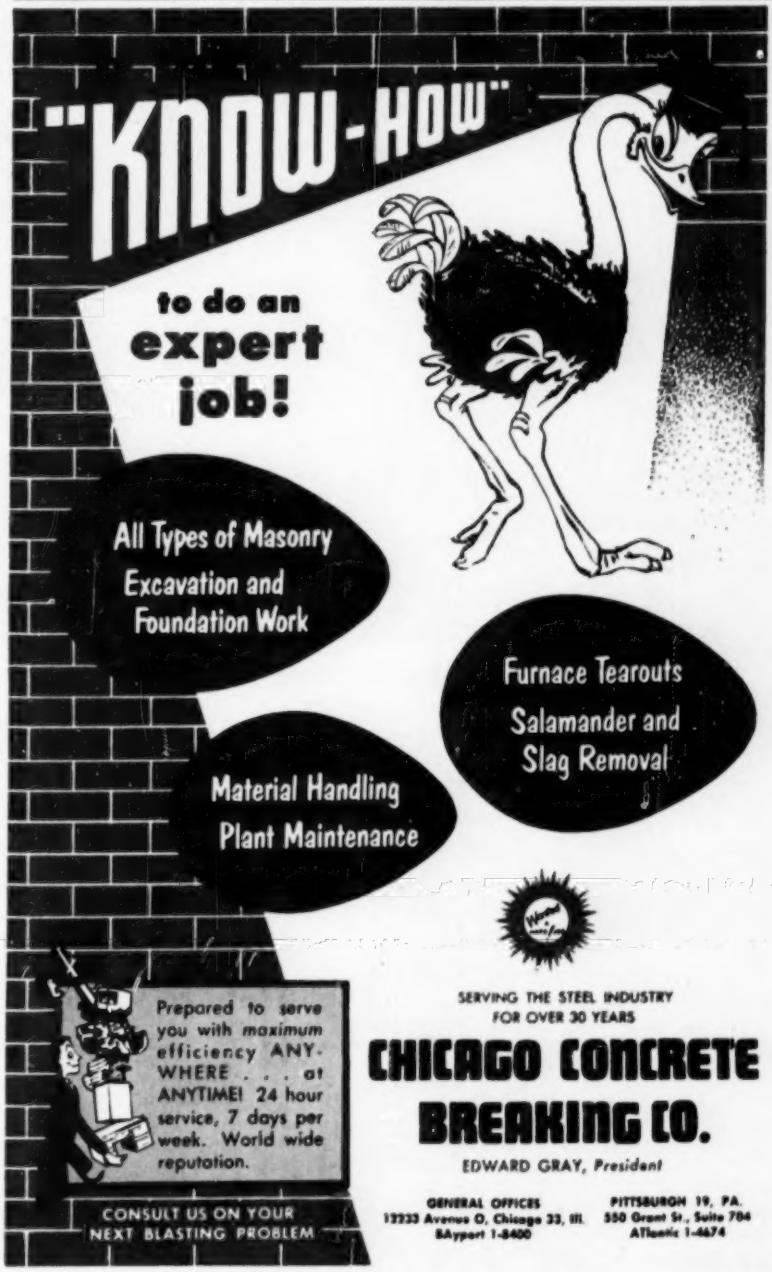

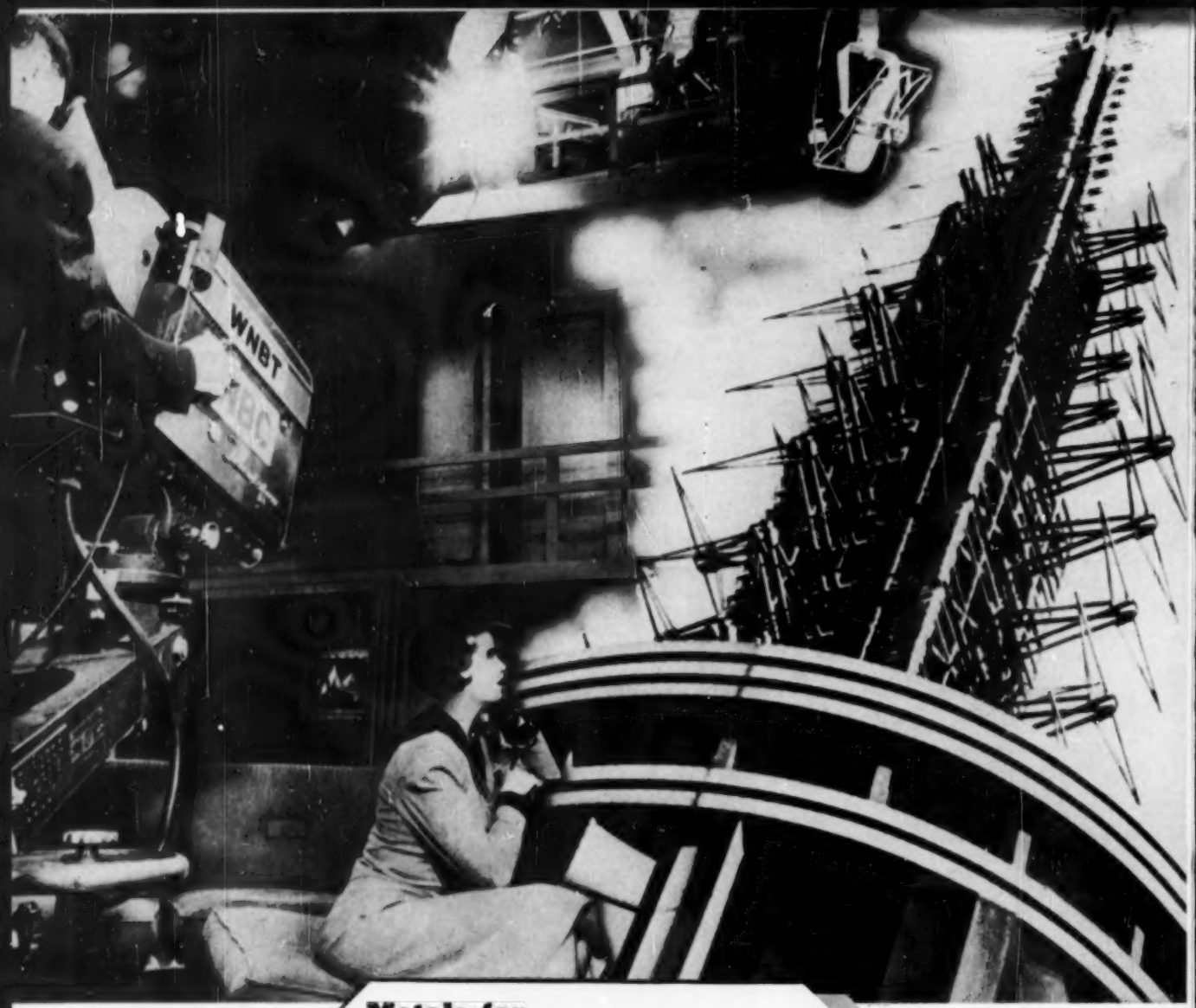

Metals for

Communications...

GLC GRAPHITE ELECTRODES help make a great variety of metals utilized by manufacturers of communications equipment and supplies.

The performance of GLC GRAPHITE ELECTRODES is unsurpassed in the processing of electric steels, foundry metals, ferroalloys and magnesium.

ELECTRODE DIVISION

Great Lakes Carbon Corporation

Niagara Falls, N.Y. GLC Morganton, N. C.

Graphite Electrodes, Anodes, Molds and Specialties

Sales office: Niagara Falls, N. Y. **Other offices:** New York, N. Y., Chicago, Ill., Pittsburgh, Pa.

Sales Agents: J. B. Hayes, Birmingham, Ala., George O'Hara, Long Beach, Cal., Great Northern Carbon & Chemical Co., Ltd., Montreal, Canada.

New Products

New Products | New Literature | New Services

For Further Information or Literature on any Product, Fill in the Coupon and Send to JOURNAL OF METALS
Students are Requested to Apply Directly to Manufacturers for Bulletins and Information

1—FLAME-HARDENING: Flame hardening of cast iron and steel with specially developed hydraulic equipment is being used to service industry by *Columbia Industries*. It is equipped with a 35 ft lift that permits the processing of shafting or tubing up to 35 ft in length.

2—VACUUM GAGE: A new Pirani vacuum gage has been announced by *National Research Corp.* Designed to operate in the pressure range between 1.0 and 0.001 mm Hg (1000 to

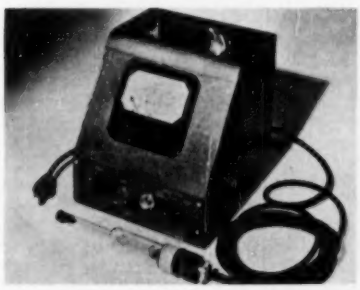

1 microns), the instrument has one meter that is used for both voltage adjustment and pressure reading.

3—DEMINERALIZERS: Mixed bed water demineralizers featuring the latest engineering developments in

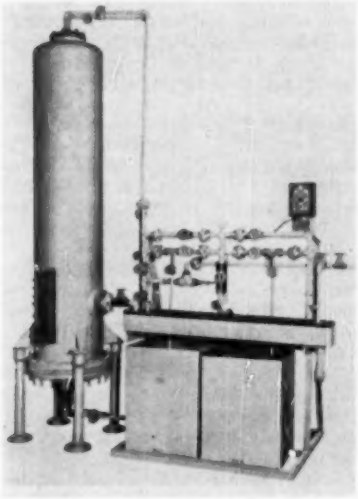

the ion-exchange process of water purification have been announced by *Barnstead Still & Sterilizer Co.* Capacities run from a range of 50 to 2500 gal per hr of mineral free water.

4—PLATING TANK: An improved Mercil-type tank for barrel electroplating has been announced by *Hanson-Van Winkle-Munning Corp.* Some of the key improvements that have been made are: Flanges turned in; overflow trough not needed; and now made of rigid angle-iron.

5—SPECTROGRAPH ATTACHMENT: An attachment for Norelco X-ray Spectrograph units that permits use of helium instead of air in

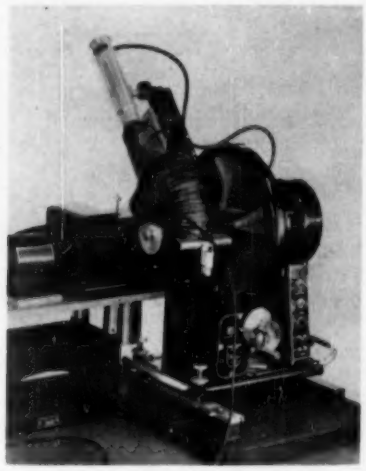

the path of the X-ray beam, is available from the *North American Philips Co., Inc.*

6—HARDNESS TESTER: *Pacific Transducer Corp.*, announced a new precision hardness tester for all types of sheet metal, both ferrous and nonferrous. By use of a calibrated microscope and reticle, readings can be obtained as accurate as the operator can read the scale, well within 2 points in the Brinell scale.

7—BRINE QUENCH: Designed to speed quenching of heat treated metals through automatic cycling, a new brine quench unit has been announced. The compact, welded steel unit is available in load capacities of 300, 400, and 700 lb. *Ipsen Industries, Inc.*

8—CENTRIFUGAL PUMPS: New series of Karbate impervious graphite centrifugal pump sizes and types has been announced by *National Carbon Co.* Several features are: Capacities from 5 to 1500 gpm at discharge pressures up to 1000 psi; mechanical seal with enclosed coolant; and rugged type SN armored connections.

9—HEAT TREATING-UNIT: A new 300 lb per hr automatic heat treating unit is being marketed by *Ipsen Industries, Inc.* The company claims the machine has 100 pct forced convection heating and long life radiant heating tubes. Operating at temperatures up to 1850°F, the new unit also features controlled atmosphere and automatic handling. Another achievement claimed for the Ipsen T-300 is complete automatic straight-through operation from heat through cooling or oil quench.

10—SAFETY DEVICE: The atmosphere safety unit is for use in furnaces for prevention of explosions, according to *Ferguson Equipment Corp.* Basic part of the unit is an electrically heated tube which is maintained at a temperature above that of the ignition point of the fuel gas or protective atmosphere. Of primary importance is the control system which indicates audibly and visually when temperature of ignition unit falls to a point dangerously close to the ignition point of the gas in use.

11—X-RAY: *Andrex's* new 250 kvp industrial X-ray is now available. Like other Andrex units, it features complete portability and weighs less than 350 lb. Small size and light weight results from elimination of all high tension cables, cooling connections, separate transformers, and cooling pumps. The X-ray tube and other high tension parts are combined in a single all-welded steel tank. The manufacturers claim that this 250 kvp unit will penetrate 4 in. of steel. Focal spot is 4 mm, and at a focus-film distance of 24 in. a 17 in. film is covered.

12—HARDNESS TESTERS: Two new pocket size hardness testers marketed by *Kurt Orban Co., Inc.*, are claimed to be the smallest ever made. The testers, known as Sklerografs, operate on the rebound principle. Model M weighs 5¼ oz. including container. Model D, somewhat larger, is designed to withstand the rougher usage encountered in shop practice.

13—TESTING MACHINE: New Baldwin-Emery SR-4 universal testing machine of 50,000 lb capacity is made by *Baldwin-Lima-Hamilton Corp.* Novel weighing system, construction, and automatic operation, as well as an unusual multiplicity of uses are features.

Free Literature

20—SICLONE: New series of silicon carbide wheels for grinding tungsten carbide tools is announced by *Fuller Mierriam Co.* Brochure describes advantages.

21—AC MOTOR: A selection wall chart shows the comparison between old and new NEMA standard dimensions for ac motors from 1 to 30 hp is available from *Westinghouse Electric Corp.*

22—EXTENSION WIRE: Bulletin 5603 issued by *Minneapolis-Honeywell Regulator Co.*, describes premium extension wire for Nobel metal thermocouples. It is designed for applications requiring higher degrees of accuracy and reproducibility than can be obtained with regular grades.

23—CASE HISTORIES: Brochure contains a sampling of cases in which *Arthur D. Little, Inc.*, has participated.

24—PLANT MODERNIZATION: Study published by *Walter Kidde Constructors, Inc.*, is to help guide company management and engineers in dealing with the complex problems of modernizing and expanding plant facilities.

25—ELECTROPOLISHER: Bulletin is offered providing information on the theory and practice of electrolytic polishing of metallurgical samples together with description of the Buehler electropolisher. *Buehler, Ltd.*

26—CORROSION: Bulletin with tables and illustrations covers results from tests which indicate that the more corrosion resistant a steel is, the more enduring the protective value of a paint covering. *International Nickel Co., Inc.*

27—HYDRAULIC CYLINDERS: Descriptions of large, special custom built heavy duty air and hydraulic cylinders are included in bulletin No. 800 issued by *Lindberg Engineering Co.*, air and hydraulic div. Standard line is explained in detail along with features.

28—BATCH FURNACE: Information on Allcase batch type controlled atmosphere furnace has been released by *Surface Combustion Corp.* Equipped with a recirculating fan and an enclosed quench it can be used for all types of controlled atmosphere steel treatments.

29—HOISTS: Two new arm type hydraulic hoists for on or off highway application were recently introduced by *Gar Wood Industries, Inc.* Models 2825 and 2025 are described in bulletin W129.

30—TUBES: Heat exchanger and condenser tubes, seamless and welded, are explained in bulletin TB-329A. Specifications, general application data, and mechanical properties are listed. *Babcock & Wilcox Co.*

31—TEMPERATURE CONTROL: Bulletin 6149 entitled Temperature Control Systems is available from *Barber-Colman Co.* A section will aid in the selection of sensing elements and their correct use for the most satisfactory results.

32—METALBLAST: Complete story of the Metalblast process for controlled surface finishing is available in booklet issued by *American Metaseal Mfg. Corp.*

33—TESTING MACHINES: Folder illustrating current Amsler machines for test in tension, compression, torsion, shear, fatigue, bending and ductility, is available from *Adolph I. Buehler, Inc.*

34—MILLING CUTTER LINE: Complete milling cutter line of the *Do-All Co.*, is described in brochure. Slitting saws, screw slotting saws, shell end mills, and counterbores are just a few of the items described.

35—SOLDERING FURNACES: A new soldering iron furnace capable of heating two 4-lb irons from room temperature to 900°F or one iron to 1200°F, in less than 8 min, with a heat input of only 9100 Btu per hr, is described in bulletin SC-1038. *Selas Corp. of America.*

36—GEAR SPEEDERS: *Michigan Tool Co.* has issued a bulletin covering the complete line of these machines now available. Each gear speeder's operation, control and specifications are covered. Illustrations of the complete line are also included.

37—THAWING PITS: Pamphlet 1041 describes how to solve the winter problem of thawing frozen railroad hopper cars of ores, coal, etc., with radiant heat. These prefabricated thawing pits, oil or gas fired, are designed for easy installation, and avoid direct flame contact and damage. *Hauck Mfg. Co.*

38—MG: Folder entitled *Magnesium Plate and Sheet to Reduce Weight* is available from *Brooks & Perkins, Inc.* Dimensions, tolerances, etc., of the different grades of products are described and gages required for equal stiffness in sheet magnesium, aluminum, brass, and steel are compared.

39—NONFERROUS METALS: Booklet issued by *M. H. Treadwell Co., Inc.* covers the nonferrous metals equipment for a variety of smelting and refining purposes. Illustrations include copper converters, reverberatory furnaces, smelting equipment and accessories, among others.

40—TOOL CHANGE: Four faced tool block and instant change tool holders are described in illustrated folder. How and why Lathemaster cuts tool setup time to a minimum is explained. *Marvic, Inc.*

41—COMBUSTION PROCESS: How too much or too little air can have costly effects in combustion processes is explained in brochure issued by *Arnold O. Beckman, Inc.* It points out that by using oxygen itself as the criterion to proper combustion, greater overall process efficiency and more profits can be realized.

45—NI ALLOYS: New booklet on nickel alloys in railroad equipment contains new illustrations and data on use of alloys to meet requirements of improved design and modern methods of manufacture of Diesel electric locomotives, gas turbines, etc. *International Nickel Co., Inc.*

Journal of Metals
29 West 39th St.
New York 18, N. Y.

January

Please send me { More Information ☐ / Free Literature ☐ / Price Data ☐ } on items indicated.

1	2	3	4	5	6	7	8	9	10
11	12	13	14	15	16	17	18	19	20
21	22	23	24	25	26	27	28	29	30
31	32	33	34	35	36	37	38	39	40
41	42	43	44	45	46	47	48	49	50

Name_____ Title_____

Company_____

Street_____

City and Zone_____ State_____

Products of fame

wherever there's flame...

Keeping flame on the job is the business of brick. Refractory brick to contain the flame and put it to work with efficiency and economy in the furnaces of industry.

Grefco refractory products have long been famed for doing this job reliably. Grefco brick, special shapes, mortars, plastics and castables to hold the heat and help spew out products for the service of industry.

If your operation requires *flame*, here's the name . . . *Grefco!*

A Complete Refractories Service . . .

GREFCO

GENERAL REFRACTORIES COMPANY
Philadelphia

GENERAL REFRACTORIES COMPANY

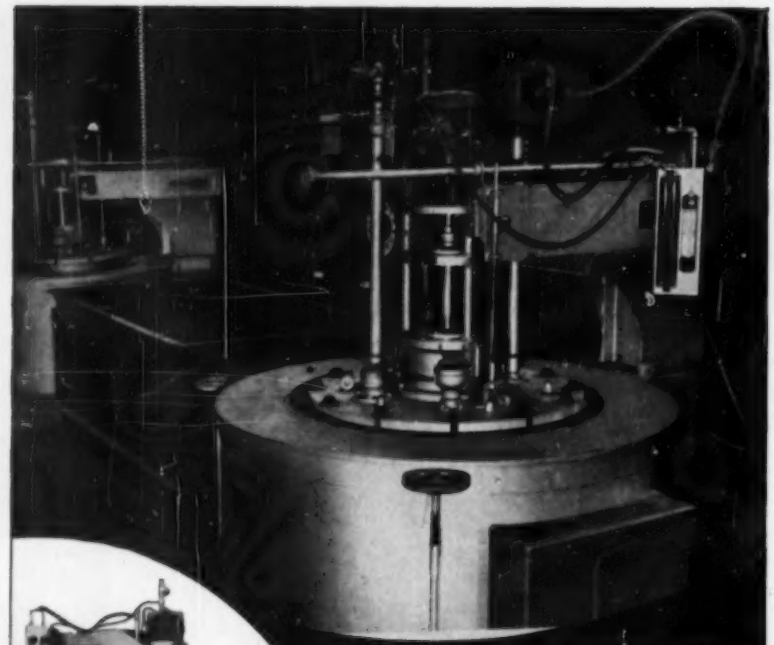

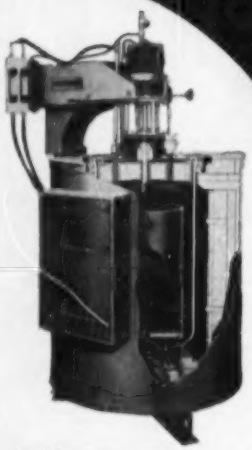

HEVI DUTY

Pressure Carburizing FURNACES

Hevi Duty Construction — Return Bend Heating Coils — Graded layers of insulation.

Simplify Control of the Carbon Case

Carburizing with a positive pressure inside the retort has simplified the obtaining of exact carbon concentrations on the surface of the work and to specified case depths. Close case tolerances and shorter carburizing cycles are additional advantages.

Identical results are assured from heat to heat because conditions in the retort can easily be duplicated. Forced atmosphere circulation assures uniform cases in the densest loads. You, too, can produce consistently uniform results if you specify Hevi Duty Verticle Retort Furnaces for Carburizing, Nitriding, Dry Cyaniding, and Bright Annealing.

Write for Bulletin HD - 646R.

Consult your nearest Hevi Duty Office for more information —

Eastern District, 50 Journal Square, Jersey City 6, N. J.
Cleveland District, 1979 Union Commerce Bldg., Cleveland 14, Ohio
Chicago District, 205 W. Wacker Drive, Chicago 6, Illinois
California District, 15026 Oxnard St., Van Nuys, Calif.

HEVI DUTY ELECTRIC COMPANY

MILWAUKEE 1, WISCONSIN

Heat Treating Furnaces... Electric Exclusively
Dry Type Transformers *Constant Current Regulators*

Industrial Notes . . .

• Inland Steel Co., Chicago has ordered two batteries of soaking pits of improved design, according to Salem-Brosius of Pittsburgh. Each battery will consist of three individual *holes* or furnace chambers, and will be used to reheat steel ingots in Inland's blooming mill and finishing mills. Individual pits are 21 ft long, 8½ ft wide, and 12 ft deep. They will be equipped with Thermal Transfer Corp. metallic needle type recuperators to preheat air used in combustion to reduce the amount of fuel needed. Each of the six end-fired pits are equipped with one of these recuperator units.

• U. S. Steel products div. is expected to start construction soon of a steel container plant on a 26.7-acre plot in Pennsauken Township, Camden County, N. J. The plant will have 168,000 sq ft of floor space. Completion of construction is expected early in 1955.

• *Colorado Fuel & Iron Corp. has organized a new department to coordinate and expand product research and development. Headquarters for the new organization will be in Washington, D. C.*

• Board of directors of Olin Industries has authorized $5.5 million for expansion of fabricating facilities of the metals div. at East Alton, Ill. Products to be manufactured at this plant will require aluminum and copper base alloys. New facilities at East Alton are not related to Olin's entrance into the aluminum industry.

• The H. H. Wills Physical Laboratory of the University of Bristol, in cooperation with the International Union of Pure and Applied Physics, and with the Institute of Crystalline Solids is organizing a conference on Defects in Crystalline Solids. The conference is to be held July 13 to 17, 1954 at Bristol, England. Particular attention will be given to defects such as dissolved atoms, vacancies, and F-centers, to microwave resonance methods of investigating their properties, and to the way in which they react with dislocations.

• *Ferro Corp. of Cleveland has formed Ferro Powdered Metals, Inc., a wholly owned subsidiary at Salem, Ind. Ferro started in the powder metal business last year with the acquisition of Welmet Co. Since that time Ferro has consolidated this division's operations at Salem. Installations at the new plant include presses, sintering furnaces, mixing equipment, precision tools, and inspection devices.*

• Metal Carbides Corp. is completing a million dollar plant at Youngstown, Ohio expected to begin operation this month. It will produce tungsten carbide metal, including tool tips, die nibs, bar stock, rings, bushing, and special shapes.

• Armour Research Foundation of Illinois Institute of Technology established 11 cooperative scholarships for work in metallurgical and mechanical engineering. The scholarships are for students entering IIT February 1954. Four of the awards are in metallurgical engineering. Tuition will be paid and students will receive $90 per month. In June students will be employed by the Foundation doing work related to fields of study. Until degrees are earned students will go to school and work alternate semesters.

• **Westinghouse Electric Corp. plans to build a metals development plant at Blairsville, Pa. The plant is scheduled for completion by late 1955 and is part of the company's $300 million expansion program. While its prime purpose will be metallurgical development, the plant's production will be geared mainly as a feeder of specialty materials within Westinghouse. It will provide wrought alloy and casting facilities to bridge the gap between research laboratories and ultimate commercial use of new metals and new processes.**

• Vanadium Corp. of America plans to consolidate all of its research activities at its new center at Cambridge, Ohio. First unit of the center was dedicated recently. It contains, in some 30,000 sq ft of floor space, complete metallurgical and chemical laboratories for evaluation of metals and alloys.

• Bridgeport Brass Co. has entered a bid with the U. S. Air Force to operate the USAF $25 million aluminum extrusion plant in Adrian, Mich. Bohn Aluminum & Brass Corp. is currently operating the facility, but its contract expires May 1. Eight U. S. firms have been asked to submit bids.

• *Salem Brosius, Inc. of Pittsburgh recently completed construction of a 64-ft long, oil-fired, continuous roller hearth furnace for Winchester Repeating Arms div., of Olin Industries, Inc., at New Haven, Conn. The furnace can heat 24,000 lb of brass slabs per hr from room temperature to 1500°F. Salem Brosius also announced that construction of 10 circular ingot heating furnaces, each 18 ft in diam, has been practically completed for Detroit Steel Corp., in Portsmouth, Ohio.*

• A contract has been awarded to the Selas Corp. of America for a new type, 72 ft overall diam furnace, which is designed and equipped to heat 22 in. diam ingots of about 4 tons each to piercing temperature of 2300°F in less than 2 hr. The furnaces will be built for Phoenix Iron & Steel Co., Phoenixville, Pa., a Barium Steel Corp. subsidiary. The furnace will be used in connection with a new pipe mill.

If Your Product Requires

The Strength of a Panther

But Must be the Size of a Kitten . . .

Use **M H Chromium-Nickel Pre-alloyed Powders**

Very small amounts of Metal Hydrides' chromium-nickel pre-alloyed powders combined with iron powders, can mean volume production of small and intricate parts having high tensile strength.

Write now for complete information on properties of iron powders with alloys of varied chromium-nickel contents. Your inquiries will receive prompt, interested attention. Ask for Bulletin 800-A.

M H

METAL HYDRIDES

INCORPORATED

24 CONGRESS ST., BEVERLY, MASS.

TITANIUM is the sixth most abundant element in the Earth's crust. Its importance has multiplied tremendously with development of jet aircraft and certain military weapons. Army and Air Force spokesmen feel strongly that production is way behind demand. Unless something is done to increase the supply of titanium available for jet aircraft, at least one Air Force general feels U. S. air power won't be strong enough to win a war. This is what Senator George Malone's Subcommittee on Strategic Minerals, Materials, and Fuels heard during recent titanium hearings.

Brig. General Kern D. Metzger, chief of the Aircraft Resources Div., says that the insufficient number of plants for processing ilmenite and other ores offers a "dismal picture." Even when viewed optimistically, the general said, present production outlook shows that titanium for only 2000 fighter planes will be available over the next five years. "That won't win any war," he said. He added that the Office of Defense Mobilization reduced to 22,000 an Air Force recommendation of a 35,000-ton per year goal. Since that time, ODM authorized General Service Administration to contract for 25,000 tons of titanium production.

General Metzger recommended that government offer immediate assistance by guarantees to purchase the entire output of future titanium plants. He further advised that financial aid be given to any processor with knowledge and financial stability to invent quicker and cheaper production methods.

Curtiss-Wright Aircraft will need 72,000 tons of titanium for production requirements in an all-out war, this accordin, to Roy T. Hurley, chief of the Wright Aeronautical Div. Enough titanium could save between 400 to 4000 lb on each aircraft engine, depending upon size. Following testimony before the Subcommittee, Mr. Hurley termed the shortage serious. "We had better get on it quick."

C. I. Bradford, vice-president of Rem-Cru Titanium Corp. told the Senate group that about 36,000 lb of titanium sponge will be needed for the new military planes with speeds of more than 1200 mph. Metallic structure of the planes will be 90 pct titanium, according to Mr. Bradford. Actual present production is about 6½ tons per day or 2300 tons per year. GSA has contracted for about 13 pct of estimated Air Force requirements of 100,000 tons.

Col. Benjamin Mesick, commanding officer of the Watertown, Mass., Arsenal, estimated that Army Ordnance could use a million tons of titanium if the material was in plentiful supply and price was no object. Experiments are currently being made on equipment for the foot soldier, combat vehicles, and airborne artillery. Experiments on "very heavy" artillery are not being made, Colonel Mesick said.

Another witness, E. A. Gee, manager of the plants technical section, pigments dept., E. I. du Pont de Nemours & Co., told the Subcommittee that all the raw material needed for titanium production is available in Canada or in the U. S. His main line of testimony was that at this time development of new processes is more important than raw material availability. Mr. Gee quite frankly said that in view of present production costs it did not seem wise for his company to expand at this time. Efforts should be devoted to devising production methods offering titanium at prices nearer to long range requirements of military and civilian fields. If, however, National Defense interests cannot be met in this way, the Du Pont company will give serious considerations to government expansion proposals. Du Pont gave 303 tons of titanium to a revolving stockpile during 1952 and 1953, according to Mr. Gee. Because of military demand the company is oversold and it is his understanding that the stockpile is depleted. The revolving stockpile is in no way connected with the national stockpile of essential materials.

◆◆◆◆◆◆

A NEW type transistor which can be used at frequencies 10 to 100 times as high as obtainable with older alloy junction transistors has been announced by Philco Corp. "The new unit operates with such economy of power consumption that for the first time a portable military communications receiver operating on very high frequency channels can be powered solely by two flashlight cells. The receiver can be made as small as a pack of cigarettes and has an operating life of many weeks," according to Leslie J. Woods, vice-president, director of Philco research and engineering.

A new method of processing germanium which may result in transistor mass production made the "Surface Barrier" transistor possible. Mr. Woods stated that the method may be precisely controlled. He noted that inability to control production methods has been a limiting factor in transistor production up to this time.

"The process consists of directing two tiny streams of liquid indium salt at opposite sides of a tiny slab of germanium. Electric current is passed through the streams so as to etch away the germanium. This process continues until the two streams almost drill through the slab. When the germanium has been etched down to a few ten thousandths of an inch in thickness, the current is suddenly reversed. The etching is thus instantly arrested and indium is immediately electroplated on the germanium by the reversed current flow to form electrodes on both sides. The resultant assembly, with wires attached to the two electrodes, is hermetically sealed in a metal container."

Mr. Woods, in announcing the new transistor, said that methods have been developed that arrest etching so precisely that remaining germanium thickness is controlled to a tolerance of 10 millionths of an inch, or less than the wave length of visible light. "Such precision has not been possible in producing earlier types of transistors."

The "Surface-Barrier transistor is the result of the research teamwork in the Philco Research Laboratory led by William E. Bradley, technical director, and William H. Forster, research coordinator. Philco anticipates that the new transistor will find application in the near future in military uses. Phil-

co also expects that someday the unit will be employed for civilian electronic equipment. Electronic computors may be one of the areas for utilization. It can quite possibly reduce the need for the many vacuum tubes and cut back the tremendous power loads needed for electronic computors.

◆◆◆◆◆◆

REPORTS from England, via the British Steel Castings Research Assn., tell of the successful development of a rotary metal sampling device based upon a design of the late S. Westberg of Rotherham, England. The sampler enables samples of steel or other metals to be produced in finely granulated or divided form directly from liquid state and without drilling operations.

The liquid sample is poured on to a rotating copper disc, which centrifugally disperses the metal upon the internal periphery of a surrounding metal bowl. Oxidation must be prevented during the sampling operation and a high purity nitrogen or inert gas atmosphere is provided in the dispersion cavity of the machine. Gas is admitted through a chambered cover-plate.

Extended field trials on the Westberg sampling device have demonstrated "the necessary degree of reliability and correlation with analyses performed upon orthodox drilled samples, not only in respect to the normal elements—carbon, sulphur, silicon, phosphorus, and manganese—but to nickel, chromium, molybdenum, and tungsten, over a relatively wide range," reports say. Westberg Developments Ltd., of Rotherham, England are manufacturing and marketing the equipment under patents pending.

HARVEY Aluminum of Torrance, Calif., successfully hot extruded alloy steel shapes for two important military aircraft, recently, and have high hopes that it will lead to "revolutionary developments in the field. . ." The extruded shapes produced by Harvey were used in production of Northrop F-89 Scorpions, and Lockheed's Super Constellation. Until Harvey tried it, this method of shaping steel had not been applied to aircraft components.

Extruded part manufactured for Lockheed is an 8630 steel radome attachment bracket. A flap track was made from 4340 steel for Northrop. Extrusions made for Lockheed were cut into 5 in. lengths, drilled and installed on the Super Constellations without further machining, according to Harvey. Finished product cost was $8.90 each, compared for a cost of $29.40 if the parts had been machined. Harvey points out, however, that the cost-saving factor is not constant, since reductions of cost depend on the configuration of the section and the cost of machining over the cost of extruding.

In making the flap track for Northrop, the steel shape extruded was made in 15 ft lengths and cut into 2 ft lengths. A real saving of almost 3 to 1 was realized in materials over that of machined bar stock.

Extrusion starts by placing billets or ingots in containers of the horizontal presses, ordinarily used for aluminum, next to hard alloy steel dies. Current production calls for billets 6¾ in. diam. Rams, operating under up to 150,000 psi, squeeze hot steel against dies, shooting extruded configurations out the other end. Presses were modified to accommodate metallurgical characteristics of steel ingots, as opposed to aluminum. The company indicates that specially designed dies and lubricants are among the well guarded secrets which made hot extrusion of alloy steel shapes possible.

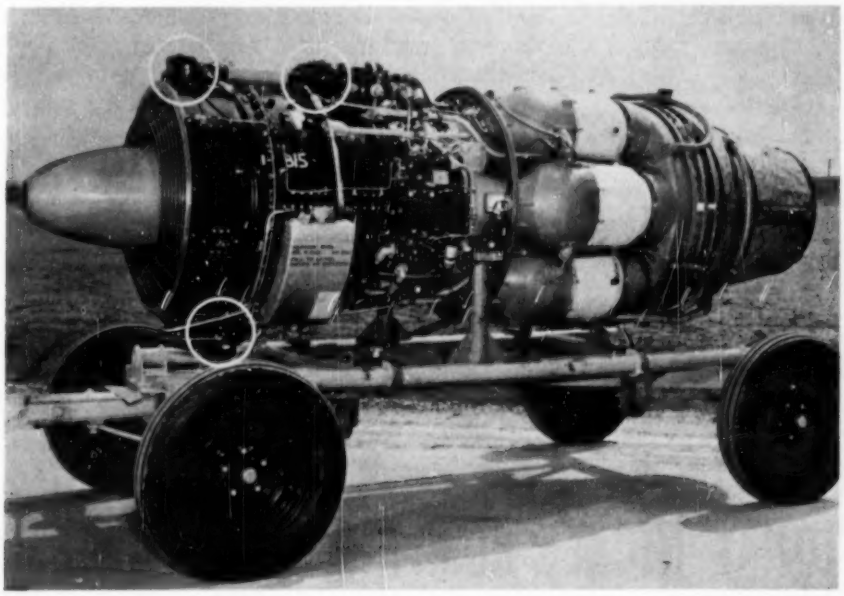

Magnesium gear box castings that will stand up to exacting jet engine operation standards are being delivered to A. V. Roe Canada, Ltd., by York Gears, Ltd., Toronto. The castings are impregnated with Permafil 3255 in vacuum equipment designed and built by F. J. Stokes Machine Co., Philadelphia. Gearbox housings are circled. The jet engine, called the Orenda, is being used to power Canadian built Sabrejets and AVRO's own twin jet all-weather intercepter, the CF-100.

Ingersoll-Rand uses Nickel Alloy Steel Gears

A size 20 Ingersoll-Rand Multi-vane close-quarter drill reaming a one inch hole in a machine bed plate casting. Extremely close quarter operations on much of today's modern machinery has created a demand for powerful tools capable of getting into narrow corners for such operations as drilling and reaming of holes. And it poses the problem of getting gears which are small enough for the job, yet tough enough to transmit high torques. Ingersoll-Rand Company engineers specified a nickel alloy steel for the bevel gears and pinions in that company's pneumatically operated close-quarter drills.

For Increased Strength . . . Heavier Loads . . . Longer Machine Life

Maximum wear resistance . . . greatest surface compressive strength . . . extremely tough cores that withstand shock loads as well as fatigue and bending stresses . . .

These are some of the properties you get in gears fabricated from *nickel alloy carburizing steels.*

Furthermore, distortion that accompanies heat treating . . . a chief cause of noisy gears . . . is inherently resisted by nickel alloy carburizing steels.

Direct hardening nickel alloy steels are used for gears carrying heavy tooth loading in applications where resistance to wear and surface compressive stresses is not quite so vital a factor. Here again, the nickel-containing steels develop the required strength more consistently and in heavier sections than carbon steels, and are generally more resistant to shock, fatigue and multi-axial stresses. Distortion resulting from heat treatment may be minimized by using nickel alloy steels. And, their machinability before final heat treatment is very good.

When you face revised stress analysis due to design changes . . . or changed fabricating methods that demand improved response to heat treating . . . remember that the many standard grades of nickel alloyed steels permit specifying the particular type which provides the best set of properties for any reasonable fabrication and service demands.

Investigate all the benefits nickel alloy steel gears can give you. Send us details of your problems for our suggestions.

INCO

THE INTERNATIONAL NICKEL COMPANY, INC. 67 WALL STREET NEW YORK 5, N.Y.

The only elliptical six electrode electric furnace in existence is some 25 years old, and according to J. K. Preston, Timken Roller Bearing Co., is outproducing the most modern, circular, three electrode furnace in a similar tonnage class. The furnace in point is a 100-ton unit at Timken's Canton facilities. Mr. Preston describes fully the operation of the furnace, starting on page 18 of this month's JOURNAL OF METALS.

Erie Mining Co. announced that it has completed financial arrangements for the initial development of its program for construction of facilities in Minnesota for ultimate production of taconite pellets at the rate of 7.5 million per year. Work has already begun. According to Erie, the program may ultimately lead to production up to 10.5 million tons and an investment of more than $300 million. Erie has arranged to sell $207 million first mortgage 4 1/4 pct bonds, due in 1983 to nine insurance companies and Bethlehem Steel Corp.

Testimony at hearings held by the Subcommittee on Strategic Minerals, Materials, and Fuels, under the Chairmanship of Senator Malone (R-Nev.), disclosed that the use of titanium on DC-7 aircraft has saved some 200 lb valued at $40 per lb. It was also stated that use of titanium on commercial aircraft might increase payload some 30 pct. Future aircraft may be 25 to 30 pct titanium by weight. Plans are already on the boards for planes using 90 pct titanium.

Universal-Cyclops Steel Corp. is working on a special atmosphere process for the melting of steel. Basic features of the process, described by the company as "closed circuit melting," have been employed in experimental laboratories in the U. S. and abroad for several years. However, the Universal-Cyclops operation is expected to be the largest commercial pilot plant.

Nickel expansion goal, 80 pct completed, according to Defense Mobilization Director Arthur Flemming, has been fixed at 190,000 tons of annual production, the General Services Administration announced. It is believed that the 38,000 tons still to be realized may come from expansion of Nicaro and other nickel facilities. Freeport Sulphur Co. recently announced plans for expansion of its Moa Bay, Cuba, operation.

Steel Co. of Canada, Ltd., is scheduled to let subcontracts in the near future for construction of a new sintering plant at its Hamilton works. Approximate cost will be $3.65 million. The new plant will replace the sintering operation now in existence in the basic steelmaking works. Engineering design contracts for the new building have been let. Stelco will handle general contracting. The plant is expected to turn out more than 1500 gross tons and is scheduled for completion late in 1954. The sinter will replace feed ore in the open hearths. The new plant will produce four times as much sinter as the old operation.

Drift of Things

WE have just returned from the AIME Electric Furnace Steel Conference in Cincinnati, and are happy to report that there were no major casualties among registrants despite the close proximity to Covington, Ky. (For those who haven't heard, Covington, in addition to fine food, liquors, and entertainment, offers one the opportunity to part with his money via various games of chance).

There is nothing in the steel industry that can compare to the Electric Furnace, Open Hearth, or Blast Furnace, Coke Oven and Raw Materials Conferences. The opportunity for the exchange of technical information, the personal contacts, and the good will that prevails, set these specialized conferences on a plane by themselves.

That these conferences are successful is evident by the large attendance, the calibre of those attending, and the comments made. Registrants came from Oregon to Alabama; from Texas to Canada. Just about every company of repute in the electric steel industry is represented.

This success is not spontaneous—the various committees spend the better part of a year planning the activities, the authors and discussers work hard filling out the program, and registrants come prepared to be informed, and to inform. Attendance at the technical meetings was very heavy — one session the first morning having over 400 in attendance — and much information changed hands between and after sessions.

As usual, the suppliers filled in their share [of the meeting], and helped to ease the tension of the concentrated technical aspects of the meeting. In addition to supplying solid and liquid refreshment, they provided common meeting places for after session discussions and rendered a great service by helping to introduce registrants to each other.

IT is not often that a young man in the mineral engineering field gets "written up" in a magazine, but that is just what happened to George Albert Parks. George is an AIME Student Associate from the University of California, where he is undertaking graduate work in extractive metallurgy. Kaiser Steel Corp.'s June issue of *Westward*, in an article about engineering graduates *Booked for Tomorrow* by J. A. Hildreth, selected George for its study. It is interesting reading about an interesting person. Incidentally, George is not the only member of his family in AIME — an uncle, Ernie Parks, is a consulting petroleum production engineer, and a member of long standing.

THE burning question is not "to move or not to move" but rather one of where to move. It has been established that we will move out of the present Engineering Societies Building, because the building is no longer adequate in size or facilities. The answer to the question is quite complex. United Engineering Trustees own the present building, and UET is in turn "owned" by AIME, ASME, ASCE, and AIEE. Thus, each individual society must settle the question of where to move, and have it approved through the Board of Directors, before it gets to UET. This individual solution is now in process. However, it is not too unlikely that the individual societies may have different opinions, and some compromise may have to be worked out. In any event, it will be at least two years before any actual move is made. To the cities that are interested in offering us a home, and 't can be considered that these have been narrowed down to New York, Chicago, and Pittsburgh, all we can say is please be patient with us. We personally at this time would welcome an offer from Bermuda or Hawaii. We have never been there, make no claims as to center of industry or population, or convenience, but still would be willing to accept!

TIME was when banks were conducted as rather austere institutions, and maintained an air of sober dignity. Between the dark-suited vice-presidents and their polished desks on one side, and the quiet clerks behind the tall glass and grill work on the other, customers always trod softly and kept their voices lowered. It was somewhat like the air in a museum, hushed and reserved. Banks did little or no advertising, and the small depositor dealt with the neighborhood bank.

Today, banks are undergoing a radical change. Bank architecture is tending to resemble something by Frank Lloyd Wright, and interiors are taking on new magnificence in color and lighting. They just don't look like banks anymore!

An even more startling change is in the manner of doing business. Banks are advertising more, and offering incentives such as grace periods for computing interest, personalized checks, and advice on saving plans. Banks opening new branches are now offering door prizes, souvenirs, and almost everything but dancing girls to bring depositors around to their doors. Now all that is needed is for the banks to tell people where to get the money they expect them to deposit!

FOR almost two weeks last month, New York City was devoid of newspapers because of an engravers' strike. It was the first opportunity many people had to realize the important role that the daily newspaper plays in their lives. There were no stock market reports, world news, bridge columns, help wanted ads, or latest political bickerings to peruse. Hardest hit was the commuter, who had much time left on his hands.

Extra news coverage on radio and TV attempted to fill the gap, but the capsule summaries left much to be desired. Even the New York Central RR pitched in and distributed a one page digest newspaper to its riders. Sales of magazines and paper covered novels soared.

We must admit that we were not too disturbed by the lack of newspapers. Maybe it was a good thing to get away for a few days from routine reading, and the tensions resulting from interpreting the foreign and domestic news, and the ups and downs of the stock market. It may just have been psychological but we imagine we saw more smiling faces going to and from work, and more commuters indulging in the almost lost art of conversation.

A. S. Cohan

Aluminum is Why

you can do what you doodle

In an extruded shape, you can put the metal exactly where you want it.

Almost any cross-section you sketch can be duplicated in metal. Extrusion eliminates design compromises that are required when a part must be built up by riveting or welding, or machined out of solid metal . . . and saves production time.

While extrusion is not a precision process, extruded shapes can be produced to fairly close tolerances. Lengths up to 80 feet or more are possible. Alcoa has a wide selection of standard extrusion alloys, from versatile 63S (excellent for architecture) to high-strength 75S (much used in aircraft).

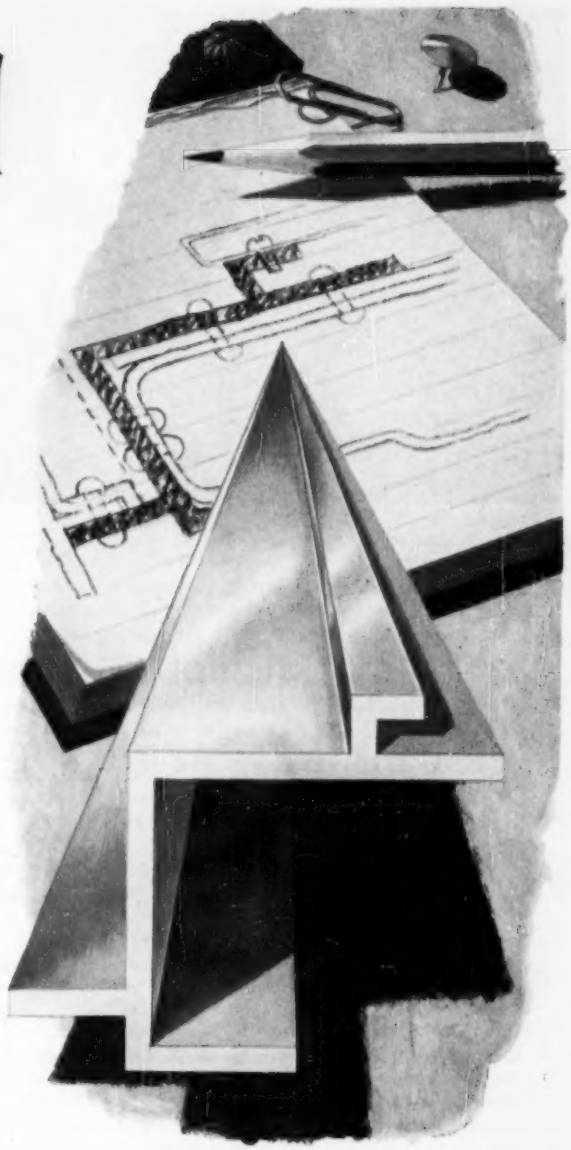

ALCOA is How

Alcoa is the world's largest light metal extrusion facility—operating plants in Lafayette, Ind.; New Kensington, Pa.; Cressona, Pa.; Vernon, Calif., and soon in Vancouver, Wash. Knowledge gained from 50 years in the extrusion business is available to help you use these efficient shapes. The output of 50 extrusion presses is available. Aluminum Company of America, 878-A Alcoa Building, Pittsburgh 19, Pa.

ALCOA ALUMINUM

ALUMINUM COMPANY OF AMERICA

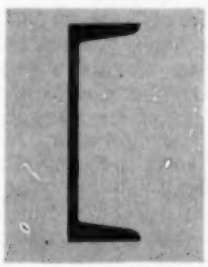

A

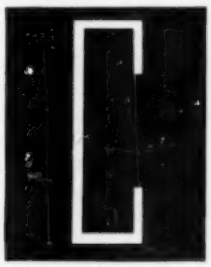

B

EXTRUDED CHANNEL B is designed to distribute the metal where it will resist column loads more effectively than Standard Channel A. As a result, it will support as a long column almost twice as much load as Channel A, though their weight is the same (2.91 pounds per foot).

C

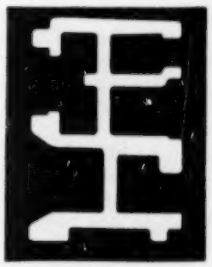

D

FIGURE C is a cross-section of a steel-reinforced wood beam used in a loom. It was desired that it be replaced with lightweight aluminum. Extrusion D offered the only method short of prohibitively expensive machining and required only surface finishing.

On a comparison of similar charges, this 25-yr old, elliptical, six electrode furnace melted faster and with a lower power requirement than the most modern, circular, three electrode furnace in a similar tonnage class. Consequently, the elliptical design can no longer be ignored in the development of larger, faster melting furnaces.

Elliptical Electric Furnace Outperforms Conventional Circular Type

by James K. Preston

THE development of the electric arc furnace in this country has become stabilized around one design, a furnace with a circular hearth and three electrodes. To increase the holding capacity of such a furnace, the shell diameters have been increased so that 20 ft shells are common and 22 and 24½ ft shells will be more frequently encountered as the proportion of carbon steels melted in electric furnaces rises. Bath depths have also increased to raise holding capacities, and while this detracts from the versatility of the furnace for efficient slag-metal reactions it does not have particularly adverse effects on the melting of carbon steel. To obtain the faster melting rates necessary to reduce overall costs, larger and more powerful transformers are being installed. The greater power input has necessitated the decreasing of the diameter of the electrode pitch circle to lessen the damage to refractories by the radiation from the arcs.

At Timken it is believed that in the development of larger, faster melting arc furnaces one of the prototype furnaces has been ignored. This is, of course, Timken's No. 7 furnace which was the first 100-ton arc furnace ever built and for more than 20 years was the only furnace with this rated capacity. This furnace has an elliptical hearth 29 ft on the major axis and 20 ft on the minor axis. It is equipped with two 7500 kva transformers which supply power to two sets of three 18-in. graphite electrodes. The furnace has two doors in the front wall through which it is charged; normally about 215,000 lb.

The unit with which the elliptical furnace is compared is newer and of a well-known type, and has a circular shell 20 ft in diam. It is equipped with one 20,000 kva transformer and has three 20-in. graphite electrodes through which the power is transmitted to the charge. The furnace is top charged with a normal charge of 185,000 lb.

Both of the furnaces to be compared are equipped with rotary type electrode controls, and also have preset power input controls on the melt-down voltage taps. The transformers of the elliptical furnace have four secondary voltage taps and the transformer of the circular furnace has six secondary voltage taps. Data are shown in Table I.

Melting Rates

Several months after the new furnace was installed it became apparent that this unit was not melting as fast as had been anticipated. Further, the furnace was not melting faster than the older

J. K. PRESTON is a Supervisory Trainee, Timken Roller Bearing Co., Canton, Ohio. This paper was presented at the AIME Electric Furnace Steel Conference, Cincinnati, Dec. 2 to 4, 1953.

elliptical unit, although the new installation had a transformer with a 33 1/3 pct higher power rating. A comparative study of melting rates of these two furnaces was then initiated.

To compare the melting rates of these two furnaces, Type 4720 steel which was frequently melted in both furnaces was selected. Factors also taken into consideration were similarity of charge and normal melt carbon level. Fifty heats of Type 4720, melted in each furnace, were selected at random.

Scrap charges for these heats consisted of alloy bloom crops, plain and alloy light and medium scrap, and alloy turnings. The proportions charged for both furnaces were 20 pct bloom crops, 50 to 55 pct light and medium scrap, and 25 to 30 pct turnings. The average carbon melt on this type has usually fallen in the range of 25 to 30 points. Because a higher carbon melt required extensive oreing-down which protracted the melting period abnormally, heats melting above 35 points of carbon were eliminated from the study.

The melting rates were calculated from the metallic charge weight and the net time from *power on* to *slag-off*. Slag-off was elected as the terminus of the melting period since an arbitrary time of clear melt would have been almost impossible to fix. Delay times for back charging, adding and slipping of electrodes, and maintenance were removed from the gross melting time to yield the net.

The mean melting rate for the elliptical furnace calculated in this manner was 24.8 tons per hr, and for the circular furnace it was 22.2 tons per hr. Both figures were computed on a basis of 50 heats. The statistical distribution of melting rates about these means indicated that about 125 heats out of 1000 from the elliptical furnace would melt at a rate equal to or lower than the average for the circular furnace. Similarly 108 out of 1000 heats from the circular furnace might melt at a rate to or higher than the mean of the elliptical furnace.

The divergence of these average rates instigated some speculation as to the reasons for the variations in the speed of melting. It was realized that the components of the charge and their distribution in the furnace was of great importance. In this study the variations in the charge make-up were precluded by the selection of types of steel with completely similar charges. Distribution of the charge was undoubtedly better in the top charged, circular furnace, although distribution has always been carefully controlled in the door charged elliptical furnace. Also, in this study, the unusual delays and the higher than normal carbon melts were eliminated from consideration. This left the power input and heat or energy distribution to be considered.

With regard to energy distribution two points should be kept in mind:

A—The temperature of the arc is probably constant around 6300°F.

B—The intensity of radiation decreases as the fourth power with increasing distance from the source.

Obviously, the temperature of an arc cannot be increased by increasing the power input to the electrodes. Therefore, more efficient distribution of energy in the charge by proper placement of enough radiation sources is the more feasible way to promote faster melting. This placement of energy sources, or electrodes, should probably be such that areas of effective radiation from one arc should not overlap that of others. To demonstrate this point, the elliptical furnace has 32.8 sq ft of bath surface per sq ft of electrode cross-section while the circular furnace has 33.6 sq ft of bath surface per sq ft of electrode cross-section. This inconsiderable difference could not explain the observed variation in melting rates. The explanation most probably is in the better placement of electrodes in the elliptical furnace. In this furnace, the distance between centers of any two electrodes in either set is 4 ft 10 in., while in the circular furnace the comparable dimension is 4 ft 5 in., or a difference of about 8½ pct. However, because of the difference in size of the electrodes used in the two furnaces, the least distance between any two electrodes in the elliptical furnace is 40 in. while in the circular furnace this least distance is 33 in. or a difference of 17½ pct. Also, the greater exposed surface area of the scrap in the elliptical furnace undoubtedly aids in obtaining the faster melting rates.

Power Input Compared

Power input is of great importance in any consideration of melting rates. Energy consumption expressions of the form kilowatt hours per ton are in common use, but power input is usually thought of as a furnace specification, rather than as an operating variable on a per ton basis. Energy input or consumption was discarded in the investigation since the time variation for melting different heats distorted the picture unless time for melting was removed from consideration. The average power input for the 50 heats melted in each furnace was computed on a per ton basis. This was done by dividing the energy use in kilowatt hours from *power on* to *slag-off* by the charge weight and the net melting times. The derived figures in kilowatts per ton when plotted versus the melting rates in tons per hr appeared to yield a straight line relationship.

Since the plotted data did indicate a straight line relationship, calculations of the least squares lines for both sets of data were made. In Fig. 1 these lines have been drawn through their respective groups of points. The greater slope of the line for the circular furnace indicates that for an increase in melting rate the increase in power input for the circular furnace is greater than that for the elliptical furnace. The relative positions of the two straight lines shows that at any given melting rate, above the point of intersection of the two lines, the elliptical furnace requires a lower power input than the circular furnace. It may also be noted that the lower points on

Table I. Characteristics of Elliptical and Circular Electric Furnaces

Furnace Specifications	Six Electrode Elliptical Furnace	Three Electrode Circular Furnace
Shell dimensions	29x20 ft	20 ft diam
Normal charge	215,000 lb	185,000 lb
Electrode diam	18 in.	20 in.
Electrode pitch circle diam	5 ft 7½ in.	5 ft
Transformer ratings		
Capacity	7500 kva (2)	20,000 kva
Voltage taps	1 – 222*	1 – 370*
	2 – 195*	2 – 310*
	3 – 128	3 – 280*
	4 – 113	4 – 231
		5 – 179
		6 – 144
Power factor range (100 pct rheostat)	78 to 83	77 to 84

* Preset power input.

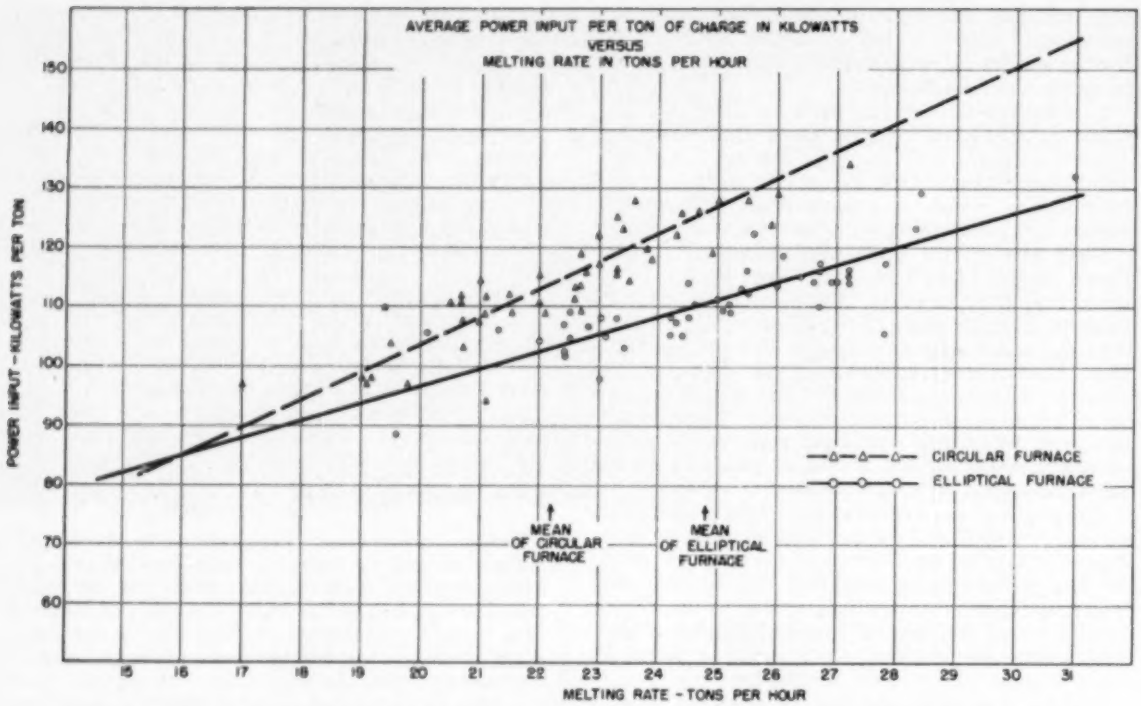
AVERAGE POWER INPUT PER TON OF CHARGE IN KILOWATTS
VERSUS
MELTING RATE IN TONS PER HOUR
POWER INPUT - KILOWATTS PER TON
MELTING RATE - TONS PER HOUR
CIRCULAR FURNACE
ELLIPTICAL FURNACE
MEAN OF CIRCULAR FURNACE
MEAN OF ELLIPTICAL FURNACE

Fig. 1—Calculated least squares lines for the plotted data indicate that for any given melting rate, above the point of intersection, the elliptical furnace requires a lower power input than the circular furnace.

the graphs show more divergence from the straight line than do higher melting rates. This is the effect of short heats and, most likely, the reason for this is that there is a lesser volume of material present for energy absorption, while the area radiating heat to the atmosphere remains unchanged. However, when the optimum charge for each furnace is used, that is the best for fast handling, melting and working, the points are in accord with the lines drawn.

Another point of interest is the intersection of the two straight lines shown at a melting rate well below the operating ranges of both furnaces. If these straight lines are extrapolated to a melting rate of zero tons per hr, the intercepts upon the power input axis should give some indication of the steady state heat loss at a temperature just below melting for a full charge. These intercepts would be 40 kw per ton for the elliptical furnace and 10 kw per ton for the circular furnace. The higher intercept for the elliptical furnace and the lesser slope of its least squares line explain the intersection of the two lines at about 16 tons per hr. The great difference in steady state heat losses may be explained by the greater ratio of surface area to heated volume of the elliptical furnace; this furnace has a flat bottom while the circular furnace has a dished bottom.

Economic Comparison

The data in Fig. 1 show that the elliptical furnace is definitely a faster melting furnace with a lower power requirement. The elliptical furnace which has a partial silica lining has a 13½ pct lower refractory cost on a per ton basis than the completely basic lined circular furnace. Electrode consumption on the circular furnace is 11½ pct less on a per ton basis than on the elliptical furnace. However, this may be due in great part to the longer time that the electrodes are raised for charging of the elliptical furnace. Under the present conditions total energy consumption of the two furnaces is essentially the same, with less than a plus or minus variation of 1 pct from month to month. This does not refute previous statements of lower power input for the elliptical furnace since this furnace is currently melting about 11 pct faster than the circular furnace.

Summary

The conclusions reached in Timken's comparison of the melting rates of elliptical and circular furnaces may be summarized as follows:

A—On a comparison of similar charges, a 25-yr old, elliptical, six electrode furnace has been shown to have a higher melting rate than the most modern, circular, three electrode furnace in a similar tonnage class.

B—The elliptical furnace requires a lower power input than the circular furnace to achieve the same melting rate.

C—These facts seem to indicate that the elliptical, six electrode furnace deserves considerable study as the need for larger, faster melting electric arc furnaces grows. It is believed that such a furnace, equipped for top charging, having automatic electrode clamps, and utilizing higher powered transformers would be faster and more efficient than any circular furnace with the same rated capacity.

Acknowledgment

The author appreciates the advice and help of H. F. Walther, melting superintendent, and D. J. Girardi, metallurgical engineer, Timken Roller Bearing Co. in the preparation of this study.

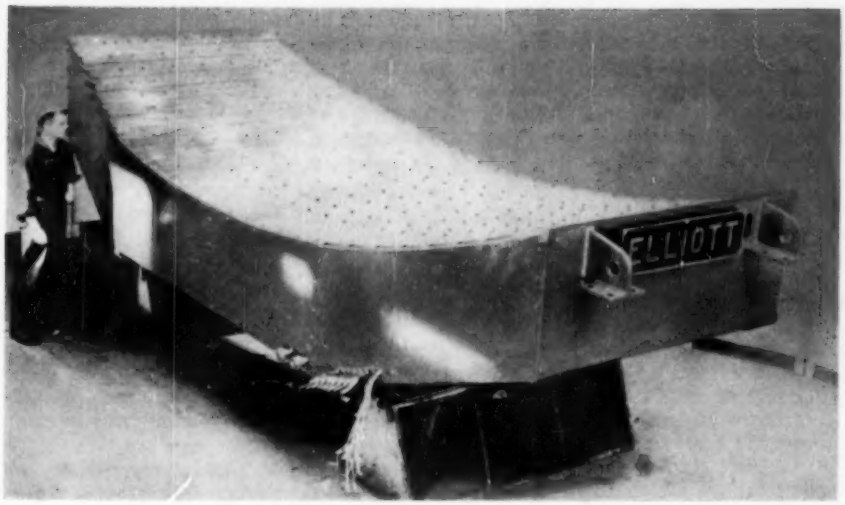

Induction stirrer used on Timken furnace is 12 ft 6 in. long, 7 ft 10 in. wide, and 27 in. thick. The stirrer assembly including coils and container weighs 51,000 lb.

Induction Stirring Provides Better Control of Operating Techniques

by Harry F. Walther

INDUCTION stirring has provided a method for adequately moving an inert molten bath in the arc furnace whereby certain objectives may be accomplished which otherwise are almost impossible. The need for some metal and slag movement in producing high grade alloy steel of accurate chemical content is universally recognized. The problem becomes even more pronounced as furnaces increase in size.

Various manual and mechanical methods are used in most plants to achieve some mixing action in the metal and between the metal and slag; but the beneficial effects of such methods are in the main only temporary. A continuous movement of the bath is obviously more desirable. Many melting troubles may be traced to the tendency of electric baths to stratify thermally and this is often accompanied by chemical inhomogeneity. Thus, bath temperature measurements and samples for chemistry may not be representative, and this frequently results in off temperature and off chemistry heats.

Many high quality steels must be low in sulphur. The usual method of achieving this is to select known low sulphur scrap for charge and/or spend excessive time in the furnace reducing sulphur. In any event, it is still almost impossible to establish proper slag-metal relationships because of sluggish baths. The solution and uniform dispersion of alloying elements in the molten bath can at times be a slow process. Ferrochromium, ferromanganese, and nickel are the chief offenders in this respect. Other ferroalloys with high melting points, such as ferromolybdenum and ferrotungsten, tend to rest on the bottom of the furnace where the bath temperature is lowest. Therefore, solution of these alloys proceeds more slowly. Extensive mechanical or manual rabbling of the bath and the expenditure of time or ladling have been the only means available in trying to correct such situations.

H. F. WALTHER is Superintendent of Melting, Steel and Tube Div., Timken Roller Bearing Co., Canton, Ohio. This paper was presented at the AIME Electric Furnace Steel Conference, Cincinnati, Dec. 2 to 4, 1953.

Installation of Induction Stirrer

Recognizing the need for a better approach to the problem of an inert bath, the Timken Roller Bearing Co. decided in late 1950 to investigate an induction stirring device invented and developed by ASEA in Sweden and installed on two small furnaces at Hagfors and Surahammars. Observations at these two plants confirmed most of the metallurgical data and Timken was convinced that this ingenious tool was practical—particularly in quality alloy steel production. It appeared that the problem of an inert bath, which is a most pressing melting deficiency, could be solved on large furnaces as well as on the small ones by installing a suitably powered stirrer to obtain the desired metal movement.

Subsequently, on Oct. 9, 1952, an ASEA stirrer was placed in operation on one new top-charge, 20-

ft diam furnace equipped with a 20,000 kva transformer. The bath in this furnace is 40 in. deep and the hearth is 31 in. thick at the low point. The stirring device is a water-cooled coil resembling a segment of the stator of a large two-phase induction motor. The stirrer coils are encased in a steel container, or box, which is curved lengthwise to fit the furnace bottom contour. The box is 12 ft 6 in. long, 7 ft 10 in. wide, and 27 in. thick and is suspended beneath the furnace at a distance which may be as little as 2 in. from the stainless bottom plate of the furnace.

The top of the stirrer container is covered with a layer of Kaocast, 1 to 1½ in. thick, which serves as an insulator. The stirrer assembly, including coils and container, weighs 51,000 lb. The coil is protected from possible adverse effects of overheating by a warning system which is temperature actuated. This system consists of resistance type thermometers installed at 14 points in the coils, at 20 positions on the furnace bottom, and at one position which indicates the temperature of the water in the coil cooling system. These temperature measuring devices are set to trip an alarm system if a predetermined maximum safe temperature is exceeded. When the alarm system for the furnace bottom is tripped, a horn sounds and the stirrer is automatically stopped. If the coil or its coolant become overheated, a bell sounds and the stirrer will also stop. Signal lights indicate the nature of the trouble, and the exact hot spot may be found on temperature indicating dials on the panel board that may be connected to any of the resistance thermometers.

Production of Stirred Steel

As of Dec. 1, 1953, a total of 1200 heats, averaging 90 tons, have been tapped from this furnace. All of the heats were made by the conventional two-slag method. No single-slag melting was involved. It was decided that the greatest benefits would be derived in melting high quality alloy steels which would be accurately controlled and contain unusually low sulphur and phosphorus.

The stirrer is usually started about 10 min before slag-off and run on high speed throughout the deslagging operation. High speed is a little more effective in bringing the slag around to the door. However, a slag of low viscosity is more readily managed. Throughout the refining period, the direction of force is reversed occasionally. An average of 10 kwh per ton is consumed in operating the device.

Several outstanding factors concerning the production of induction stirred steel became apparent soon after starting operations:

A—Thermal stratification is practically eliminated. It thus has become possible to refine the metal throughout the heat cycle within the desired temperature range. Immersion thermocouple readings are more truly representative. The metal is tapped at a measured temperature of 10° to 15° less than formerly from the furnace but still is poured into the molds at the desired level. In the case of unstirred heats where, in general, the metal is hotter near the surface of the bath, the measured temperatures are frequently not representative of the average bath temperatures.

B—Bath samples for chemistry on stirred heats are more reliable than for non-stirred heats because the stirred baths are homogeneous in compositions. It becomes possible to produce pin-point analyses.

C—Alloy solution in the molten bath is rapid and uniform. As an example, samples were taken at various points in the bath 5 min after ferrosilicon was added. They were found to check within 0.01 or 0.02 pct, indicating complete silicon diffusion.

D—With a reducing slag composition similar to that used for non-stirred heats, sulphurs can be reduced to extremely low levels with no more effort than a flick of a switch and a little time. Sulphur may be reduced to as low as 0.005 pct if desired. This has been practically impossible to accomplish by usual methods. Ordinarily, sulphur may be expected to consistently finish around 0.008 to 0.011 pct with no increase in furnace time over regular practice in conventional furnaces. There is no need for charging other than ordinary scrap.

An unforeseen side effect of low sulphur heats is worthy of mention: When the crops from the mills are returned and charged into conventional furnaces, the sulphur residuals are quite low and this results in lower finals than normally. The stirrer, thus, indirectly may be used to produce relatively lower sulphur metal in other furnaces by simple scrap manipulation.

E—Experience has shown that inherent grain size is controlled more consistently. It is probable that the downward flow of metal keeps the added aluminum from slag contact when it is poled into the bath. It is also probable that the oxygen content of the bath is uniformly low at this time.

F—Carbide or silicon type slags can be made and controlled more easily. Areas of unfluxed slag components are practically non-existent shortly after the slag mix is added. A sample of slag taken directly inside the door is usually representative of

Details of Induction Stirrer Described

The induction stirrer is best described as a section from the stator of a large polyphase motor and containing the same elementary parts. Thus, it has a magnetic core, a polyphase winding properly insulated, cooling equipment for the winding, and adequate bracing of the winding against mechanical forces.

Because of the low frequency of the current supply (approximately ½ cycle per sec), the eddy current and hysteresis losses are sufficiently low that the usual thinly laminated steel is not required. The core section is made, therefore, from ¾-in. steel plates bolted together, and the teeth and slots for the winding are formed of steel channels welded to the core.

The coils of the stirrer are wound from a hollow rectangular section of copper. Each coil is wound first as a rectangular shaped pancake, and then the ends are bent down to facilitate bracing and finally the whole coil is given a further bend to conform to the curved surface of the core. The coils are taped with mica to meet Class B temperature rises and are inserted in the slots to form a single-layer, concentric-type winding. The connections are such as to form a two-phase winding with two electrical poles. Resistence against mechanical movement is furnished by a series of brass plates laid over the top of the coils and bolted through to the steel core. Movement of the

the whole. This fact is no doubt of great importance in obtaining low sulphur. There were some misgivings at first regarding possible pick-up in carbon under carbide slags. However, it soon became evident that such is not the case as carbon is controlled more accurately and with a minimum of absorption from the slag.

G—Because of lower final sulphur levels in stirred heats, the sulphide type of non-metallics are less frequently encountered.

H—The oxygen content of metal under the reducing slag is somewhat lower than in a comparable furnace without a stirrer. Oxygen drops to a low level in about 40 min after slag-off.

I—Of some importance is the ease of the de-slagging operation. The direction of the slag movement can be controlled so that it may be brought to the vicinity of the door and removed more effectively. This is an advantage and a time saver in large furnaces. Phosphorus may thus be held to a low content.

J—In general, bloom surface is improved. This is believed to be a result of more accurate temperature control in addition to low sulphur content.

K—Employee acceptance of the device is particularly gratifying. The furnace operators may now safely accomplish many objectives in making a heat by pushing buttons, where formerly manual effort and exposure to intense heat were required. This ability to accomplish with ease what previously was practically impossible has given the furnace operators a deep sense of pride and, in general, has resulted in improved job attitudes. The art of making steel in an electric arc furnace is thus more appealing when the equipment includes a stirrer.

L—Furnace time can be saved in several ways: In the case of an unbalanced charge, where scrap is hanging to one side of the furnace, the mass may be undercut and melted off more quickly with the aid of the stirrer. Also, in the event of a bottom skull, the induced bath turnover will easily help to melt it off. Carbon oxidation may be expedited when ore is used. However, the reaction can be very sudden and violent and extreme care must be used at this time. Some furnace time may be saved slagging off, particularly when a clean bath and low phosphorus are desired. The stirrer equipped furnace is far more efficient than the conventional furnace under certain conditions, both before and after slag off.

There has been very little maintenance on this device and all of it has been minor in nature. Daily routine inspection and making adjustments as required keep it in top operating condition.

Hearth Erosion

One aspect of using the stirrer has caused more speculation than any other. This is the effect on the hearth by possible erosion from prolonged use of the device. Experience in actual operation under varying conditions was the only means available to obtain this important information. No one knew just what the optimum point in metal movement in the furnace should be to obtain the maximum benefits metallurgically and avoid undue erosion which was probable should the molten bath be moved too swiftly. The manufacturer, however, built into the device a choice of two speeds: The high speed is calculated to move metal across the bottom at from 3 to 4 fps. The displacement in the metal movement pattern results in a surface motion of about 2 fps. The low speed induces just about half this motion.

The furnace was operated for about six months with the stirrer on high speed most of the time. There was some erosion on the bottom, but there were some mitigating circumstances. In the case of one heat, there were two broken electrodes that became imbedded in the bottom of the charge, which could not be removed and which were responsible for superheated areas in the furnace bottom during melting. Also, the melting personnel had to become familiar with the operating characteristics of a new high-powered top charge furnace as well as the stirrer. As operations improved and some changes in charging practice were introduced, there was very little erosion other than what is experienced in conventional furnaces. In addition, stirrer speed is left to the discretion of the melter in charge.

The fact that a furnace is stirrer equipped does not mean that all the difficulties encountered in making steel in the arc furnace are obliterated. Neither can it be said that metallurgically perfect metal is a natural result. However, on the basis of experience to date, there are some aspects of melting with the stirrer which have most certainly resulted in an improved product. Handling of the molten metal and slag in the furnace may be accomplished in a very desirable and practical manner. Good furnace practice must still be observed to gain the greatest benefits.

Frequently, many undesirable properties in the finished product have been attributed to alleged poor furnace practices such as lack of control of steel making temperatures, too wide a spread in final analyses among heats of a given grade, failure to produce low sulphurs, etc. It now appears possible to control better many of the furnace operating techniques in electric arc steel making by the judicious use of suitable induction stirring devices.

by Quentin Graham

Vice-President, The Elliott Co., Ridgway, Pa.

end windings is prevented by heavy bronze supports bolted through to the sides of the core structure. For protection against dirt an enclosing cover of stainless steel encases each end of the coil extensions.

Cooling of the winding is accomplished by circulating distilled water through the hollow conductors and thence to a heat exchanger, using the plant water supply to carry off the heat. Water connections are made with synthetic rubber tubes which, with the further precaution of using distilled water, prevent an electrical connection between the winding and the water supply system. To keep the water pressure to a reasonable value, parallel circuits are used for the water circuit even though the coils of each phase are in series electrically.

Power for the stirrer is supplied by a commutator type ac generator. This machine has a two-phase stator winding excited by a special ac exciter and supplies two-phase low frequency power at the commutator. The exciter itself is a self-driven converter taking in 60-cycle power at its slip rings and furnishing slip frequency power of approximately ½ cycle per sec at its commutator. Both the main low frequency generator and its 60-cycle driving motor are cooled by closed air systems with air-to-water heat exchangers.

17 Years of Stirring History Shows International Exchange of Ideas

by Eric G. Malmlow

THE development of the induction stirrer started in Sweden in 1936. Dr. Ludwig Dreyfus of the Swedish Electric Co., ASEA, studied the problem of whether the bath in a hot metal mixer could be stirred by some electrical method. He suggested a solution and demonstrated that his principle would work, but the project was abandoned.

It was not until 1939 that a full-scale electric stirrer was constructed. It was tested on a 15-ton arc furnace at Surahammars Bruks AB. Because of the furnace construction, the stirrer had to be placed inside the furnace shell on top of the bottom plate. As a consequence the stirrer was soon damaged mechanically. This experience proved that the electric stirrer must be placed outside the furnace in order to accomplish its purpose under the conditions prevailing in a steel mill.

Investigation showed that a furnace bottom plate made of austenitic steel would permit the passage of an alternating magnetic flux without causing prohibitive eddy current loss. The magnetic flux after penetrating the bottom plate still retained sufficient density to reach the melt through the refractory lining and exert enough force to produce the desired stirring action.

After these fundamental features of the electric stirrer had been demonstrated, the first commercial ASEA induction stirrer was put in operation in the fall of 1947 on a 15-ton furnace at the Hagfors Steelworks, Uddeholm AB. Shortly afterward, in June 1948, a new 12-ton furnace provided with an induction stirrer was put into operation at Surahammars Bruks AB. The principal of the ASEA induction stirrer and the metallurgical results obtained at Hagfors and Surahammar during 1½ years in service were presented in Sweden in May 1949.[1,2,3] The metallurgical results were also discussed before the AIME Electric Furnace Steel Conference in Pittsburgh in 1949.[4]

Since that time, the acceptance of the induction stirrer has been rapid. In Sweden four other steel companies have installed induction stirrers. Stirrers are also to be installed in Spain, France, and Belgium, the last mentioned on a 24-ft furnace. In the United States, one huge induction stirrer has been in operation for more than a year at the Timken Roller Bearing Co. This stirrer, with its converter set, was manufactured in the United States by the Elliott Co. in accordance with ASEA's designs and patents.[5] This was arranged with Aros Electric Inc. which is a wholly owned subsidiary of ASEA (Allmanna Venska Elektriska Aktiebolaget) and represents the Swedish company in the United States.

The application of induction stirrers requires that the bottom of the furnace shell above the stirrer be made of nonmagnetic material having high electric resistivity. This feature is introduced at least expense when the furnace is first constructed or is being rebuilt for some additional reason. The adaption of existing furnaces as well as new ones, with flat or with dished bottoms, is relatively simple because of the development of the highly efficient, static ASEA stirrer. This induction stirrer requires little space under the furnace because of its close concentration of the magnetic flux to the very area above the unit itself.

Induction stirrers have given excellent results and satisfaction to the users, and the economical, metallurgical, and operational advantages[6] of the stirrer warrant close examination by those responsible for the production of quality electric furnace steel. In view of past developments it seems that the time is near when the induction stirrer will be considered an indispensable component of the electric arc furnace whenever quality steel is produced. But the advantages gained with the use of the stirrer have proved it to be economical even when lower grades of steel are made. This trend may gain momentum as more experience is obtained.

It also seems reasonable to anticipate the application of induction stirring to mixers and to open hearth furnaces with special problems. Opportunities can also be found in other industries. In the production of ferroalloys, for instance, the same principles apply. So far, no such applications have been decided upon, but the possibilities do exist.

E. G. MALMLOW is President, Aros Electric Inc., New York. This article is an abstract of the paper presented at the AIME Electric Furnace Steel Conference, Cincinnati, Dec. 2 to 4, 1953.

References

[1] L. Dreyfus: Inductive Stirring in Arc Furnaces. Electrotechnical Aspects. *Jernkontorets Annaler* (1949) **133**, p. 371.

[2] L. Dreyfus: An Induction Stirrer for Arc Furnaces. ASEA *Journal* (1950) **23**, p. 46.

[3] F. Nilsson: Induction Stirring in Arc Furnaces. Metallurgical Aspects. *Jernkontorets Annaler* (1949) **133**, p. 385.

[4] S. Fornander and F. Nilsson: Inductive Stirring in Arc Furnaces. JOURNAL OF METALS (Jan., Feb. 1950) **188**, p. 22, p. 256.

[5] U. S. Patent Nos. 2,256,518; 2,513,082; 2,620,366; and 2,573,319.

[6] P. E. Hammarlund: Induction Stirrers for Arc Furnaces. III° Congres International d'Electothermie (1953) Sec. 1, No. 110.

Tin Increases Strength of Ti-Al Alloys Without Loss in Fabricability

by W. L. Finlay, R. I. Jaffee, R. W. Parcel, and R. C. Durstein

THE alpha type alloy is the oldest titanium alloy type, having first been produced by M. A. Hunter in 1908. This was the first titanium ductile enough to be hot malleable. It was heavily contaminated (or lightly alloyed) with something under 1 pct oxygen. The first commercial titanium, RC-70, was placed on the market in 1948 and has a total interstitial (carbon, oxygen, and nitrogen) content of about 0.2 to 0.3 pct.

During 1953, Rem-Cru Titanium, Inc. has had a substitutional alpha type alloy in trial production. At present its nominal composition is 5 pct Al, 2.5 pct Sn, and a total interstitial content of about 0.2 pct. It is coded A-110AT, and the experimental data show it to be markedly superior to the interstitial alpha type alloys.

This first alpha type alloy has at present a minimum design yield strength of 110,000 psi. With some sacrifice in ductility, the minimum yield strength can be increased to 130,000 psi and the future perhaps holds a 150,000 psi ultimate tensile strength all alpha. However the 200,000 psi ultimate strength titanium alloy with useful low temperature ductility and toughness will probably not be an all-alpha. It will be a beta type or, more likely, a heat-treated alpha-beta type alloy.

Alloying Elements

In contrast to the wealth of beta stabilizing elements for titanium, there are relatively few alpha stabilizers. The interstitials carbon, oxygen, and nitrogen are of only limited utility since they lower toughness and do not contribute much to hot strength.

The beta stabilizing substitutional elements have, with only a few exceptions like zirconium, quite limited solubility in alpha titanium. The alpha stabilizing substitutional elements appear to be non-transitional and with high vapor pressures which preclude fusion alloying with high melting titanium. Aluminum and tin are two of the few such elements that can be used.

Aluminum is an excellent alpha alloying addition for titanium. In addition to its advantages of low density and low cost, it has high alpha solubility so a range of strength levels and good control are in prospect. It raises the alpha-beta transformation range which increases oxidation resistance and permits higher forging temperatures. It preserves weld ductility since it does not cause transformation hardening, and it promotes good hot strength.

W. L. FINLAY, R. W. PARCEL, and R. C. DURSTEIN are Research Manager, Group Leader, and Process Engineer, respectively, Rem-Cru Titanium, Inc., Midland, Pa. R. I. JAFFEE is Supervisor, Nonferrous Physical Metallurgy, Battelle Memorial Institute, Columbus, Ohio. This paper was presented at the AIME Institute of Metals Div. meeting, Cleveland, Oct. 19 to 21, 1953.

The limitation to the use of aluminum is that, outside the laboratory, the titanium-aluminum alloys cannot be fabricated with more than 8 pct Al and can be readily fabricated in the shop only with less than 6 pct Al. This limitation, despite the maximum solid solubility of about 25 pct Al[1,2] has been a major disappointment in titanium alloy development.

To improve the strength of titanium alloys further, one may look toward auxiliary alpha soluble elements added at an aluminum alloy level where satisfactory fabrication characteristics are obtained. Tin appears to be ideally suited to this role. The vapor pressure of tin is even lower than that of aluminum, and it has been found that tin alloys readily with titanium without appreciable evaporation. Moreover, tin has a relatively high alpha solubility[3] as shown in Fig. 1. The effect of tin on the transformation range of beta-quench hardening of titanium is innocuous.

The effect of tin on density might be considered disadvantageous since tin is heavier than titanium with a density of 7.3 compared to 4.5. However, it has been shown by Ogden et al[4] that the measured density of the Ti-5Al alloy is 4.42 compared to 4.52 g per cu cm for pure titanium. The addition of 2.5 pct Sn to Ti-5Al to form A-110AT brings the den-

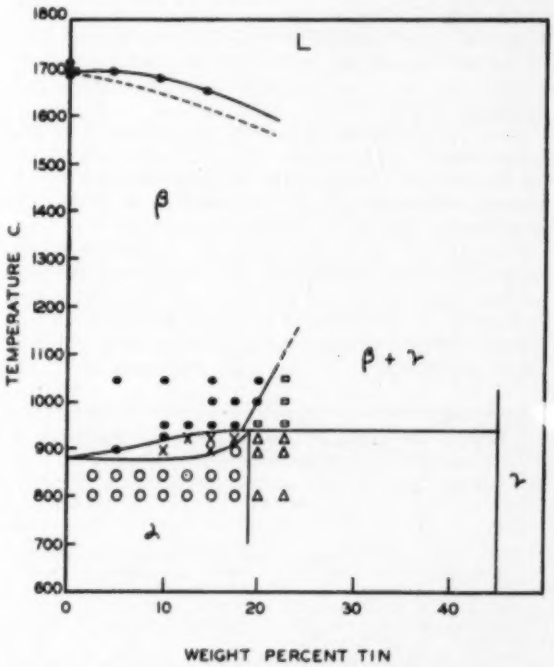

Fig. 1—The relatively high alpha solubility of tin is shown in the titanium-rich region of the titanium-tin system.

Table I. Fabrication Ratings of Titanium-Aluminum-Tin Alloys

Tin Wt-Pct	Aluminum, Wt-Pct 4	5
0	Good	Fair
1	Good	Good to fair
2	Good	Good to fair
3	Good	Good to fair
4	Good	Fair
5	Good	Fair to poor

sity up to 4.44 g per cu cm. This is less than would be indicated by the law of mixtures (4.47) and still less than that of unalloyed titanium.

Fortunately the fabrication characteristics of titanium-aluminum alloys containing several percent of tin were found to be little different from those of the alloys without tin. Thus up to several percent tin could be added to the Ti-5Al alloy (the limiting aluminum content for good fabrication) without suffering any loss in hot fabricability even though the tin addition effects a substantial strength increase in the alloy.

As an example of the innocuous effect of several percent of tin on fabricability, a series of arc-melted ingots were upset forged at 850° to 1000°C, the exact temperature depending upon the alloy. They were then rolled at 850°C to 0.040-in. sheet on a laboratory mill. Fabrication characteristics were rated as good (no cracking), fair (a few light surface and secondary tensile cracks), or poor (heavy cracking). The results are given in Table I.

These ratings must be taken primarily as relative and not necessarily applicable to what might be expected from forging and rolling large-size ingots. They do, however, illustrate that the addition of tin entails no sacrifice in hot fabrication characteristics. It was also noted qualitatively in hand forging experiments that the deformation resistance under the hammer appeared to be primarily a function of the aluminum content and relatively independent of the tin content. This experience was duplicated in trial production comparisons of binary aluminum versus ternary aluminum-tin ingots up to a 9-in. diam and of comparable strength levels.

The specific effect of tin on the tensile and bend properties of the titanium-aluminum alloys is shown by the data for iodide-base alloys plotted in Fig. 2. These properties were determined in 0.040-in. annealed sheet rolled on a laboratory mill.

For clarity, the base-line iodide titanium-aluminum alloy data[a] are shown as curves without data points. The strength of the alloys with over 2 pct Al is seen to be increased 15,000 to 20,000 psi by 2 to 3 pct Sn without any measurable decrease in the ductility parameters. It is also apparent that the

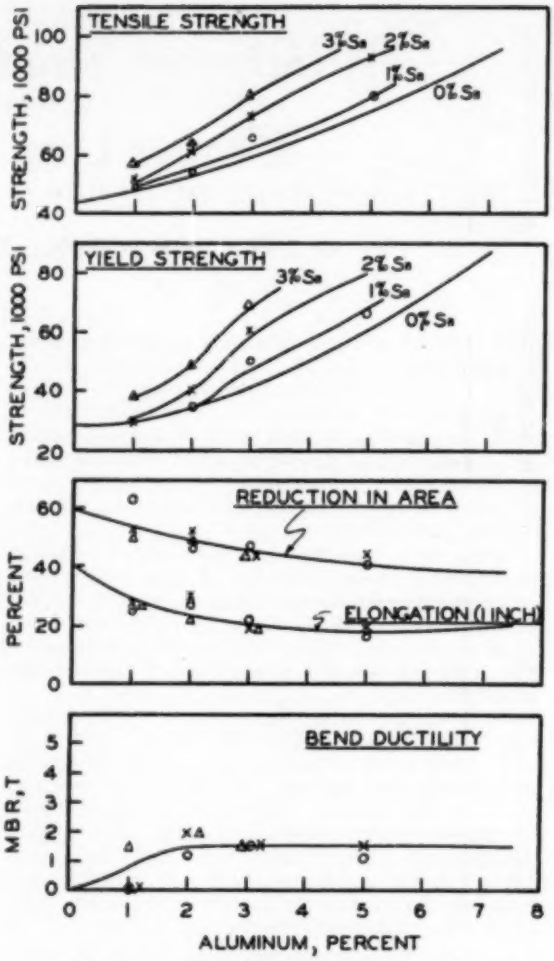

Fig. 2—Specific effect of tin is shown on the tensile and bend properties of the high-purity titanium-aluminum alloys. Properties were determined in 0.040-in. sheet annealed at 850°C.

Table II. Comparison of Laboratory Heats of High-Purity And Commercial-Purity Alpha Alloys*

Property	Ti-5Al High Purity	Ti-5Al Commercial Purity	Ti-5Al-2.5Sn High Purity	Ti-5Al-2.5Sn Commercial Purity
Tensile strength, psi	85,000	105,000	95,000	120,000
0.2 pct offset yield, psi	80,000	85,000	80,000	110,000
Reduction in area, pct	40	40	40	40
Elongation, pct in 1 in.	20	20	20	20
Minimum bend radius, T	1.5	2.0	1.5	2.5

* 0.040-in. sheet, annealed at 850°C.

strengths of the alloys with 5 pct Al and 2 to 3 pct Sn are equivalent to that of the binary titanium-aluminum alloy containing 7 pct Al. This is accomplished with a considerable gain in fabrication characteristics over the 7 pct Al alloy.

In commercially pure alloys, there is present an interstitial content of 0.1 to 0.2 pct combined oxygen, nitrogen, and carbon. This causes the strength of commercially pure alpha alloys to be approximately 20,000 to 25,000 psi higher than that of high-purity alpha alloys although there is little apparent reduction in tensile ductility. Fig. 3 shows the effect of adding up to 5 pct Sn to commercially pure titanium-aluminum alloys in the form of 0.040-in. sheet annealed at 850°C.

The same increase in strength noted previously for the high purity alloys is seen to hold for the commercially pure alloys. Several lots of sponge were involved in making the alloys at the 5 pct Al level, and the scatter in strength values reflects the varying interstitial contents of the sponge. The tensile ductilities of the commercially pure titanium-aluminum alloys are seen to be unaffected by the addition of up to 5 pct Sn although bend ductilities appear to be somewhat poorer.

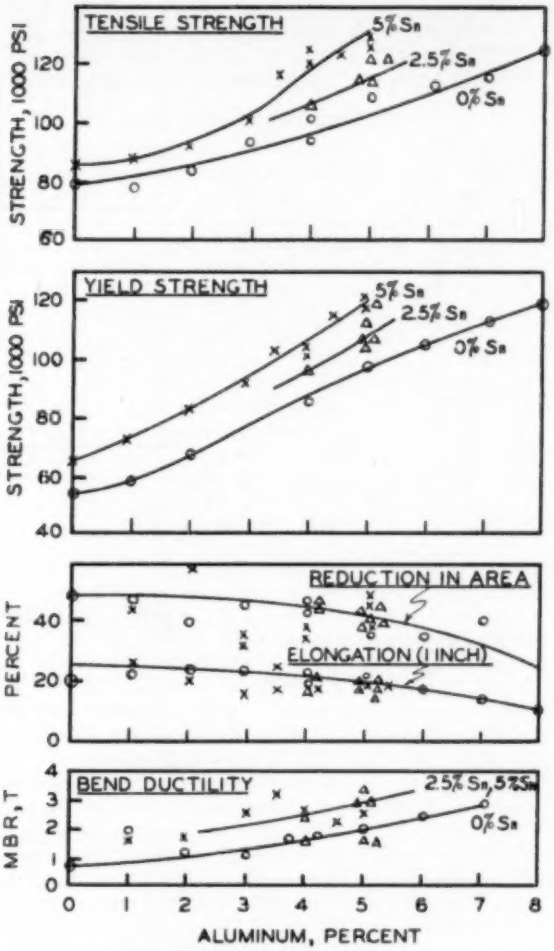

Fig. 3—The effect of adding up to 5 pct Sn to commercially-pure titanium aluminum alloys is shown. The alloys were in the form of 0.040-in. sheet annealed at 850°C.

A comparison of the high-purity and commercial-purity alloy data for Ti-5Al and Ti-5Al-2.5Sn alloys, shown in Table II, emphasizes several facts concerning the effect of tin and an interstitial content corresponding to that in 50,000 psi yield strength sponge. First, the increase in strength caused by the 2.5 pct Sn is less for the commercially pure alloys than for the high-purity alloys, showing a tensile strength increase of 15,000 psi compared to 30,000 psi. Second, there is no difference in the tensile ductility between commercial and high-purity alloys. Such differences appear only with unalloyed or dilute alpha-alloyed titanium. Last, the commercial alloys have poorer bend ductilities by 0.5 to 1 T than the high-purity alloys. Overall, the data show clearly that the ductility of the Ti-5Al-2.5Sn alpha alloy is not decreased by the interstitial level corresponding to 50,000 psi yield strength sponge.

Rem-Cru A-110AT Alloy

Several A-110 ingots of 70, 250, 500 and 1300 lb each have been cast and processed to sheet, plate, bar, and up to 6-in. diam rounds. Before proceeding to the properties of these mill products, it is well to emphasize their single phase alpha alloy nature.

A-110AT is single phase all-alpha up to about 1900°F. It becomes all-beta (at the so-called beta transus temperature) approximately 100°F higher. Suggested forging temperatures are from 1850° to 2150°F. All other fabrication and service temperatures are substantially lower so that, in most experience with A-110 except forging, it will be in the all-alpha condition.

Alpha titanium, particularly when it contains 2.5 pct or more Al[4], is appreciably more resistant to oxidation than beta titanium. Thus the 2000°F beta transus of A-110 permits considerably higher forging temperatures than could be used with other titanium products like RC-130-A, RC-70 and RC-130-B with beta transus points of about 1450°, 1650° and 1750°F respectively.

These higher forging temperatures are necessary because of alpha titanium's high hot strength. This valuable characteristic reflects both the aluminum-tin content of the alpha and its single phase nature. This high hot strength also makes the rolling of sheet and strip thinner than about ⅛-in. much more difficult than that of either unalloyed titanium or the alpha-beta type alloys like RC-130-A. As a result, the rolling of A-110 sheet and strip thinner than ⅛-in. is more experimental than current experimental production of A-110 bar, plate, and forgings.

The aluminum and tin content of the A-110 alloy also raises the recovery and recrystallization temperatures several hundred degrees Fahrenheit. At present this material, regardless of the mill product form, is being supplied in the annealed condition. One hr at 1600°F has been found to be satisfactory. Since the structure is single phase alpha up to about 1900°F, cooling rates from hot fabrication and annealing temperatures can vary without detriment from a furnace cool to a water quench at the convenience of the operator.

Another advantage of the alpha alloy structure appears to be its higher modulus of elasticity. The determination of this property requires rather refined instrumentation and technique and only preliminary data are available. On the basis of these,

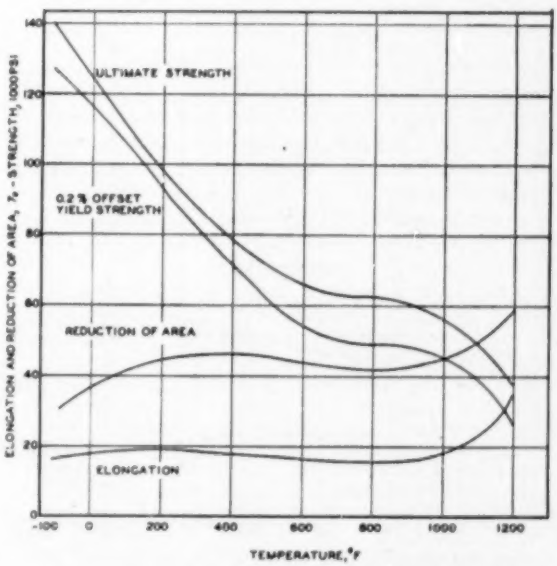

Fig. 4—Most tensile data on A-110AT annealed sheet have been obtained on 1/10 to 1/8-in. material.

however, A-110AT appears to have an elastic modulus of about 16.5 x 10^6 psi relative to one of perhaps 15.5 x 10^6 for unalloyed titanium, 14 to 15 x 10^6 for alpha-beta type alloys and possibly even lower moduli for some beta type candidates.

Weldability

None of the titanium alloys now in routine production, all of which are of the alpha-beta type, are readily weldable, although some can be fusion joined by special techniques. At best, however, the weld zone is distinctly inferior in ductility. Moreover there are few structural materials with strengths above 100,000 psi whose weld metal has comparable ductility and strength with the base metal. One of the major virtues of A-110AT is that, even in the as-fusion-welded condition without the benefit of any post-welding heat treatment, its strength and ductility are quite comparable with that of the base metal.

Weld ductility is excellent because of the persistence of the all-alpha structure to quite high temperatures. Fig. 1 shows that there is no basis for supersaturation on quenching from about the transformation, and whatever composition gradient may be set up by the beta to alpha transformation as the weld metal cools tends to be homogenized by the high temperature of the transformation.

Weldability studies of A-110 to date have been almost entirely limited to fusion heliarc welding. Because of the favorable single phase alpha structure, however, it is anticipated that equally satisfactory results will be obtained with other types of welding such as flash butt, spot, and seam.

A-110AT sheet has been fusion butt-welded with complete success when proper procedures are used. Placid molten weld metal, with no signs of porosity in the solidified weld, is normally obtained with the heliarc method. It appears that a somewhat higher current must be used than is normally employed in welding RC-70. Eighty to 110 amp have proven to be satisfactory at about 0.100-in. thickness using a filler rod of the same composition as the base metal.

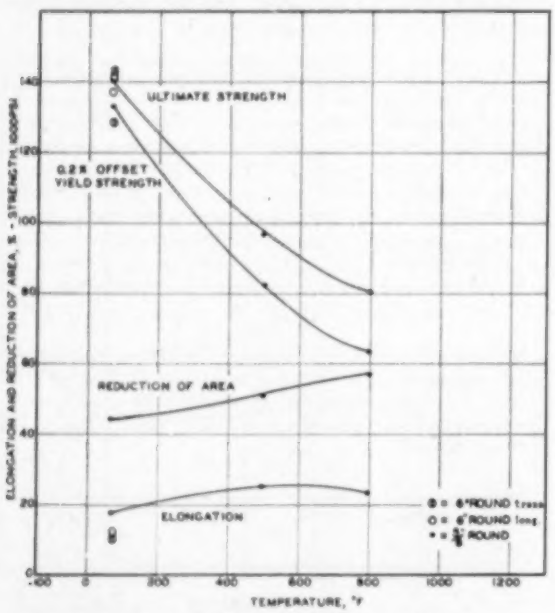

Fig. 5—Tensile properties of A-100AT annealed rounds are plotted against temperature.

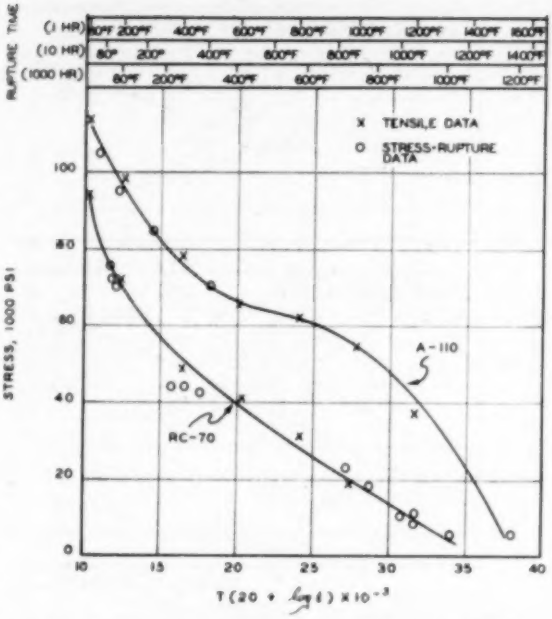

Fig. 6—Master rupture curves of A-110AT and RC-70 plotted from actual tensile and stress-rupture data utilizing the Larson-Miller equation.

Battelle Memorial Institute, several Government laboratories, Rem-Cru, and a number of aircraft plants have tested the mechanical properties of fusion welded A-110 specimens. Bend ductility in both directions of these specimens has equalled that of the base metal, 2½ to 3½ T. Welded tensile specimens show a slight loss in tensile elongation with very little change in the ultimate and yield strengths.

Tensile Properties

As previously mentioned, A-110 sheet and strip thinner than about ⅛-in. is more difficult to produce and at present is not even in trial production. Most tensile data on sheet have been obtained on 1/10 to ⅛-in. material. The room temperature properties of A-110 sheet produced recently average 116,000 psi ultimate tensile strength, 110,000 psi yield strength, 18 pct elongation, and 40 pct reduction of area. Typical tensile properties are plotted as a function of temperature in Fig. 4.

The tensile properties of A-100 bar stock are shown in Fig. 5. The preliminary strengths of forged 6-in. diam rounds are equal to those of ⅝-in. round bar although ductilities are slightly lower.

Bend Ductility and Fatigue

Room temperature bend tests (through 105°F on a V-block) show A-110AT sheet to have a minimum bend radius of 2.5T to 3.5T, there being no consistent difference between longitudinal and transverse directions. The minimum bend radius at −80°F is at least as good as that at room temperature and in many cases is slightly better. Preliminary tests indicate that bend ductility does not improve at elevated temperatures up to 900°F.

Preliminary fatigue results at room temperature with annealed A-110 sheet material indicate an approximate endurance limit of 70,000 psi for complete stress reversal. This value is 58.5 pct of the ultimate and suggests that the unnotched endur-

ance limit of A-110 may prove to be excellent. Tension-tension fatigue tests with S minimum = 0.25 maximum show an endurance limit of 95,000 to 100,000 psi. Notched fatigue tests are being run.

Stress-Rupture and Notch Sensitivity

Larsen and Miller[5] have shown that the stress-rupture characteristics of metals can be correlated well with tensile properties by relating time and temperature. Fig. 6 shows the master rupture curves for A-110 and RC-70 plotted from actual tensile and stress-rupture data. This figure illustrates both the validity of the Larson-Miller equation when applied to alpha titanium and the attractive high temperature properties of A-110AT.

The data graphed in Fig. 7 illustrates the marked notch insensitivity of A-110 sheet. Charpy V-notch impact specimens from forged ⅝-in. A-110AT plate have given encouraging results. Limited data show that the lowest values are obtained when the notch is perpendicular to the forging plane. Typical values obtained on such specimens are 20 ft-lb at room temperature and 16 ft-lb at −40°F.

Forgeability

Metallic elements which stabilize the alpha phase also impart high temperature strength as shown in Figs. 4, 5, 6, and 7. Moreover, unlike steels, there is no conveniently low temperature phase change at which plasticity suddenly increases. The beta transus of about 2000°F coincides approximately with the optimum forging temperature. Fortunately, the metallic alpha stabilizers also impart resistance to hot air corrosion so that these temperatures are practical for moderate thicknesses.

Quantitative forgeability data based on preliminary tests are shown in Fig. 8 for A-110, RC-70 and RC-130-B. Many tons of RC-130-B have been forged to date so that the comparison of the RC-130-B and A-110 forgeability curves is particularly interesting. The data were obtained by cutting ½-in. diam x ½-in. high right cylinders from production ingots or forgings, heating to test temperature, and dropping a 5¼-lb weight 60 in. onto them.

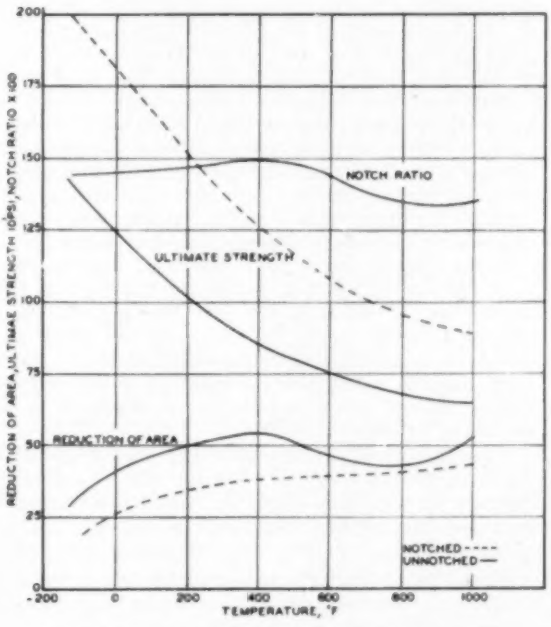

Fig. 7—Notched vs unnotched tensile properties of A-110AT annealed sheet are plotted as a function of temperature (60° notch, 0.012-in. root radius, 0.0118-in. deep, K 3.25).

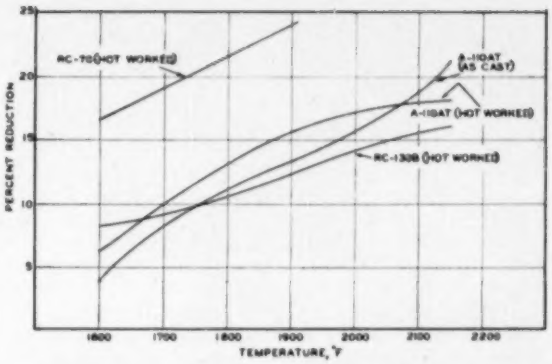

Fig. 8—Data on dropping weight forgeability test were obtained by cutting ½-in. right cylinders and dropping a 5¼-lb weight 60 in. onto them.

RC-130-B is a single phase all-beta alloy above about 1750°F and it contains a total of 8 pct metallic alloy content (4 pct Mn and 4 pct Al) in solid solution. Manganese is a more potent titanium strengthener than tin, so RC-130-B requires more power to forge in the 1800° to 2150°F range than A-110. Below about 1700°F the two-phase nature of the alpha-beta type RC-130-B alloy manifests itself in easier deformability and A-110 is more difficult to forge. Hence the recommended forging range for A-110AT is 1850° to 2150°F.

Creep and Corrosion

Preliminary data indicate that the marine and chemical corrosion resistance of unalloyed titanium and A-110 alloy are comparable. Encouraging results are being obtained from fuming nitric acid tests. Creep tests are also currently underway on A-110AT but sufficient data are not yet available to permit presentation at this time.

Acknowledgments

The laboratory development of titanium-aluminum-tin alloys was initiated at Battelle Memorial Institute under Rem-Cru Titanium, Inc. sponsorship. H. R. Ogden, D. Maykuth and R. Happe particularly contributed to the evaluation of this alloy family there. D. R. Luster and J. P. Catlin contributed to the mechanical testing of A-110 at Rem-Cru.

References

[1] H. R. Ogden, D. J. Maykuth, W. L. Finlay, and R. I. Jaffee: Constitution of Titanium-Aluminum Alloys. *Trans.* AIME (1951) **191**, p. 1150.

[2] E. S. Bumps, H. D. Kessler, and M. Hansen: Titanium-Aluminum System. *Trans.* AIME (1952) **194**, p. 609.

[3] R. I. Jaffee, H. R. Ogden, D. J. Maykuth, and W. L. Finlay: Constitution and Quenching Characteristics of Alpha Titanium Alloys. (paper in preparation).

[4] H. R. Ogden, D. J. Maykuth, W. L. Finlay, and R. I. Jaffee: Mechanical Properties of High-Purity Titanium-Aluminum Alloys. JOURNAL OF METALS (February 1953) **5**, p. 267.

[5] F. R. Larson and J. Miller: A Time-Temperature Relationship for Rupture and Creep Stresses. ASME Paper No. 51-A-36 (1951).

Fig. 1—In the ELKEM rotating hearth furnace (type Ellefsen) the furnace pot slowly rotates or oscillates about 120° while the electrodes remain stationary.

Closed Electric Reduction Furnaces Permit Utilization of Furnace Gas

by M. O. Sem

UTILIZATION of the gas developed by the reduction process has been discussed ever since the establishment of the electric smelting industry. This refers particularly to the open electric reduction furnaces as they are used in the production of calcium carbide and such ferroalloys as ferromanganese, ferrochrome, ferrosilicon, etc. The electric smelting furnaces for these products produce a large amount of gas which carries a heavy burden of dust that is objectionable. In some cases, as in the production of ferromanganese, the fumes also may represent a serious health hazard.

In open furnaces where the gas is allowed to burn over the top of the charge, air is mixed with furnace gas. Since this mixing makes it approximately 100 times the actual volume of the gas produced in the furnace, gas collection and cleaning becomes a very costly problem. If it were possible in a commercial process to collect the carbon monoxide gas in a concentrated form, the gas could then be cleaned by scrubbing with water or by other simple means and used for heating and other purposes.

In the reduction process the carbonaceous material which is used as a reductant ordinarily is oxidized to carbon monoxide and burned over the top of the charge. Roughly one third of the heating value of the coke is utilized in the charge whereas two thirds of the heat value is found in the escaping gas provided it is carbon monoxide. Table I shows that theoretically as much as 88 pct of the heat value can be recovered in the gas in the case of ferromanganese if the smelting is carried out in a closed furnace. This is true even if the gas contains as much as 10 pct CO_2.

It has been one of the aims of Elecktrokemisk, Norway, to develop and put in practice closed electric smelting furnaces where this heat value can be recovered from the gas. The collection of gas started with furnaces for production of electric pig iron and is already well known. Now gas collection from furnaces for calcium carbide, ferromanganese, and similar ferroalloys has been accomplished.

M. O. SEM is Technical Director of Electrokemisk A/S located in Oslo, Norway.

Electric Pig Iron Furnace

The old Elektrometall furnace in Sweden which dates back to before 1910 was equipped with full gas collection equipment. In the 1920's the Tysland-Hole furnace was developed in Norway for the use of Soderberg electrodes and with coke as a reducing agent. The Tysland-Hole furnace soon spread to many other countries with cheap electric power and took the place of most Elektrometall furnaces. At present a total of about 360,000 kw is being developed in closed electric pig iron furnaces which means that more than 1 million metric tons of pig iron yearly may be produced in electric furnaces.

The ordinary size of the electric pig iron furnace is of 6000 to 10,000 kw, producing about 50 to 100 metric tons of pig iron per day. Three larger furnaces of 16,000 to 20,000 kw each are being installed in a government steel plant at Mo in Norway. In this plant alone a total of about 180,000 metric tons of pig iron per year is expected to be produced by electric smelting.

The basic principle for collection of the gas in a Tysland-Hole furnace is that the gas is collected directly around each electrode where the charge is renewed rapidly and regularly so that the charge remains porous. This is very important in a fully enclosed furnace where it is not possible to do any reasonable amount of stoking. Hanging of the charge and eruptions must therefore be avoided.

The actual operating results of the electric pig iron furnaces vary quite a bit according to the raw

materials and local operating conditions. In many cases the Tysland-Hole furnace has been operated with a charge which has not been dried or which does not have a uniform physical composition. In many cases 8 to 15 pct moisture has been found in the coke and the amount of fines (−¼-in.) has often amounted to 30 pct or more. It is fair to say that the electric pig iron furnaces usually have been charged with whatever the blast furnaces cannot accept.

Recently a report was published by Professor Kalling about the results obtained in the Tysland-Hole furnaces at Domnarfvet in Sweden. The company has been using a sintered ore where most of the lime used as a flux has been sintered into the ore. Furthermore the raw materials have been selected so that the screen analysis of the charge is nearly constant all the time. The power consumption in the Tysland-Hole furnaces has thereby been reduced to about 2000 kw-hr per metric ton of pig iron on a yearly basis. The results reported by Professor Kalling are given in Table II.

On the basis of experience with the many electric pig iron furnaces now operating under varying conditions, it is easy to calculate the production costs of electric pig iron under different conditions prevailing in the different countries. One important question, however, is how to evaluate the collected furnace gas. It has a theoretical heat value by combustion of about 2500 calories per cu m (290 Btu per cu ft). In most cases it is used for heating purposes, however, a great deal of work is being carried out today to use the gas for reduction purposes.

Rotating Hearth Furnace

The prerequisite for a covered furnace is that it can be operated without the need of a mechanical stoker. The ELKEM rotating hearth furnace (type Ellefsen) solves the problem of reducing hangings in smelting furnaces without the need of any mechanical stoker. In this furnace shown in Fig. 1 the furnace pot slowly rotates or oscillates about 120° while the electrodes remain stationary. The movement of the furnace is ordinarily so slow that the 120° rotation takes from 18 to 35 hr to complete. As a result of this rotation the crater walls do not become impregnated by dust and slag and stay porous allowing the gas to escape during the operation.

In equalizing the wear and tear on the furnace lining and the bottom, the rotating furnace also makes it possible to develop more power in the same furnace. The furnace bottom stays cleaner and it is possible to clean out the furnace very quickly which greatly facilitates the changeover from one alloy to another. It is interesting to note that a furnace in operation in Switzerland sometimes produces ferrosilicon and sometimes calcium carbide.

A rotating furnace of 7250 kva capacity operated at Riouperoux by the French company, Pechiney, produces 98 pct silicon with a power consumption of 12,000 to 12,500 kw-hr per metric ton of metal. The reductant was then 100 pct charcoal. When the furnace rotation was stopped the company reported that the power consumption increased gradually to about 14,000 kw-hr per metric ton after four days of operation.

Elkem Covered Rotating Furnace

The first covered rotating hearth furnace was designed and built in 1947 with the cooperation of Elektrokemisk by the Tennessee Valley Authority at Sheffield, Ala., for smelting phosphate to produce elemental phosphorus. It was found that the phosphorus furnace could be operated on a charge of −¼-in. material. Later a 7500 kva furnace was built which was started up in 1950.

In the yearly report for 1952 the TVA gives the following statement about the furnace: "TVA's rotating electric furnace, in its second year of demonstration and production, continued to show advantages over the stationary type of furnace. On the average, it used about 10 pct less power to produce the same amount of phosphorus. Experimental tests were made to determine whether the furnace would smelt fine phosphate used in the other furnaces. Satisfactory operation was obtained with phosphate fines, although operation was more difficult and power consumption was higher than with nodules. However, it appeared that in some locations cheaper phosphorus could be obtained by using increased quantities of fines instead of nodules, and a major advantage in a new plant would be elimination of expensive agglomeration equipment."

The operation of the closed rotating hearth carbide furnace has been described by the author in *The Iron Age*, Aug. 28, 1952. Since that time the first two of these furnaces of 24,000 kw each are now in operation at Calvert City, Ky.

Table I. Data on Gases Given Off by Various Types of Electric Reduction Furnaces

Furnace Type	Power Consumption, Kw-hr Per Metric Ton	Gas Vol. Cu Meters Per Metric Ton	Gas Analyses						Temperature of Gas at Outlet	Calorie Value in Pct of Furnace Load	
			CO	CO_2	H_2	O_2	N_2	CH_4		Total	Heat Content of Gas
Pig iron	2400	650 to 700	72*	15	8	—	2	2	350°C	80	4.3
FeMn (80 pct high C)	3000	800 to 950	72*	11	6	—	10	1	350°C	88	4.5
FeCr (high C)	4200	900 to 1050	72**	11	6	—	10	1	350°C	87	4.0
FeSi (75 pct Si)	10,000	1700 to 1800	90**	—	6**	—	—	—	1000°C	65	8.0
Calcium Carbide	3200	330 to 400	90*	1	2	0.33	—	1	500°C	40	5.0
Phosphorus	5200	850 to 950	98**	—	—	—	—	—	400°C	60	4.0
Aluminum Reduction	17,500	850 to 950	62*	30	4	—	—	—	400°C	14.5	6.0

* Actual observation. ** Assumed values.

Closed Furnace for Ferromanganese

Standard high carbon ferromanganese has been produced in Tysland-Hole furnaces by Falck, Milan. Electrometallurgical Co. who have also for years produced high carbon ferromanganese in closed furnaces. The first ELKEM covered rotating furnace for ferromanganese was installed by Wargon A/B, Sweden in the summer of 1952. This furnace is shown in Fig. 2. Because of a restricted power supply in the winter months, the furnace has not yet been in operation sufficiently to be fully tested. However, some information may be given.

The furnace is operated on a blend of Russian and Indian manganese ore containing large amounts of fines. Sintering of the fines would facilitate the smelting but is not very attractive since it requires coke consumption of from 8 to 12 pct. Also the dust losses are appreciable. It was therefore decided to start the operation using the same charge as in open furnaces consisting of lump ore and increasing the addition of fines during rotation so as to consume as much of the fine grained ore as possible. Although the plant has not yet been able to dry the coke which regularly has contained between 10 to 20 pct H_2O, it has been found possible to increase the amount of fine grained ore up to 30 pct in the ore blend. The fine grained ore is all of −5/12 in. (10 mm). Optimum results cannot be obtained until the coke is dried before use.

The furnace load is approximately 4000 kw with a secondary voltage of about 95 v. The furnace is rotated at a speed of one revolution in about 100 hr with a power consumption of approximately 3000 kw-hr per metric ton of ferromanganese with 700 to 800 kg of slag running from 20 to 25 pct Mn. The slag is used in the production of siliconmanganese. Electrode consumption has been about 12 kg Soderberg per metric ton of alloy.

In the process some 850 cu meters of gas is developed per metric ton of alloy, the amount varying with the oxygen content of the ore. The analyses that have been carried out so far show about 72 pct CO, 11 pct CO_2, 6 pct H_2, 1 pct CH_4, and 10 pct N_2. The high content of nitrogen indicates that quite a bit of air is being sucked into the furnace which probably is due to the fact that the company has not yet started utilizing the gas. Heat value of the above gas is about 2400 kilocalories per cu m.

As in all ferromanganese furnaces the gas carries a heavy burden of dust which usually contains from 30 to 40 pct Mn. The recovery of this dust is therefore important both from an economical point of view and also because of the health hazard which this dust brings to the surrounding country. So far the company reports that the first five months of operation shutdowns caused by the furnace accounted for only 0.8 pct of the total operating time.

Table II. Yearly Average of Raw Material Consumption Per Metric Ton of Pig Iron in Tysland-Hole Furnace

Electric power	2050 kw-hr
Coke breeze	115 kg
Pearl coke	165 kg
Blast furnace coke*	105 to 385 kg
Electrode paste	15.5 kg

* Owing to the low consumption of coke, the content of phosphorus in the pig iron is favorable. The pig iron contains approximately 1 pct Si and 0.02 pct S.

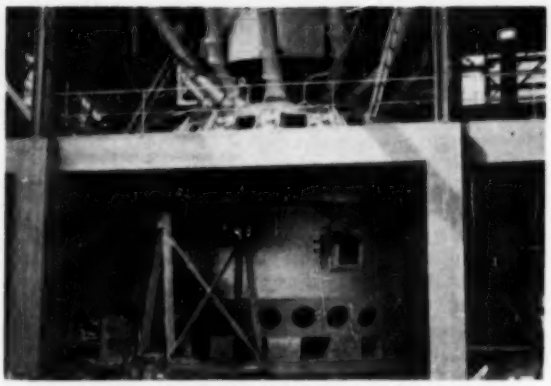

Fig. 2—Closed furnace for ferromanganese develops about 850 cu m of gas per metric ton of alloy. The gas has a heat value of 2400 kilocalories per cu m.

Operation is fully automatic, and there is only one man per shift on the furnace operating floor in addition to two tappers on each shift.

A covered rotating furnace for smelting of ferromanganese has now also been started up in the plant of Porsgrunds Elektrometallurgiske A/S in Norway with a rated capacity of 6000 kw.

Furnace Gas

All reduction furnaces although producing a gas of different analysis give a gas of remarkably high heat value as shown in Table I. It is apparent that the furnaces when working serve as efficient gas generators. Actually a plant that can utilize the gas will be able to credit the reduction process according to the heat value of the produced gas after cleaning. The cleaning of this concentrated gas is ordinarily easy to accomplish in a wet scrubber. Where water is scarce or the produced sludge cannot be disposed of easily a dry cleaning possibly followed by a wet scrubber will do in most cases.

Considerable thought has been given to the use of the gas. It lends itself very well to ordinary heating purposes including drying, sintering, agglomerating, or preheating of the ore to be smelted. It is also used in open hearth furnaces and in the rolling mills. In case of iron or ferromanganese smelting a reduction of the power consumption of about 250 kw-hr per metric ton is obtained when the charge is preheated to about 600° to 700°C. At the same time a saving in electrode consumption of from 15 to 20 pct is realized. This has been fully proven by pilot plant operation.

Because of the high content of carbon monoxide in the gas, it can be used for reduction purposes before finally being burned. Prof. M. Wiberg is well known for his contribution to the Wiberg process for production of sponge iron. Professor Wiberg, in cooperation with Elektrokemisk, Oslo, has patented a process dealing with the use of the gas of an electric pig iron furnace for prereduction of the iron ore to be smelted in the electric pig iron furnace. Thereby an additional saving of from 300 to 400 kw-hr per metric ton of pig iron should be obtained. Accordingly, it would seem possible when using gas to full extent under favorable conditions to arrive at a figure of about 1500 kw-hr per metric ton. Some 4000 metric tons of pig iron have been produced from a prereduced charge in tests at Norbottn Jernverk in Sweden. The results fully sustained the calculations, and tests will be continued.

Optimum Composition of Blast Furnace Slag As Deduced from Liquidus Data for The Quaternary System CaO-MgO-Al_2O_3-SiO_2

by E. F. Osborn, R. C. DeVries, K. H. Gee, and H. M. Kraner

On the basis of liquidus measurements in the system CaO-MgO-Al_2O_3-SiO_2 and previously published data, diagrams have been constructed at 5 pct Al_2O_3 intervals from 5 to 35 pct Al_2O_3. Liquidus temperatures and primary phase fields are shown. The optimum composition of a blast furnace slag for a given alumina content is indicated. At the optimum point, ordinary slags will be entirely liquid and will have maximum desulphurization potential and minimum viscosity. The relation of optimum composition of slags to the "plateau region" of the liquidus surface, and the application of these data on synthetic quaternary slags to actual slag compositions are discussed. Index of refraction of glasses is given as well as composition, temperature, and phase data for each mixture.

THE usual blast furnace slag, as a first approximation, can be considered a mixture of the four oxides, CaO, MgO, Al_2O_3, and SiO_2. Systematic, extensive data for the quaternary system, CaO-MgO-Al_2O_3-SiO_2 is therefore required for the understanding of the properties of such a slag as a function of composition and temperature. With sufficient data, it should be possible to fix unequivocably the relative amounts of lime, magnesia, and silica required for a given alumina content to result in a slag composition having optimum properties. Other constituents, such as FeO, MnO, TiO_2, and S, have an effect on the properties of a slag, but as long as they are present in small and approximately constant amounts they produce only a second-order effect superimposed upon the major changes in properties of slags determined by the relative amounts of the four major components.

Viscosity and desulphurization data have been reported for mixtures approaching blast furnace slags in composition, but systematic liquidus data have not been obtained. Inasmuch as a slag must be all liquid in order to be most effective as well as practicable, clearly the temperature above which a mixture is all liquid (liquidus temperature) is a type of data needed. Such data have been obtained through the study of 446 compositions and are presented in this paper along with a discussion of their bearing on the optimum composition of blast furnace slags.

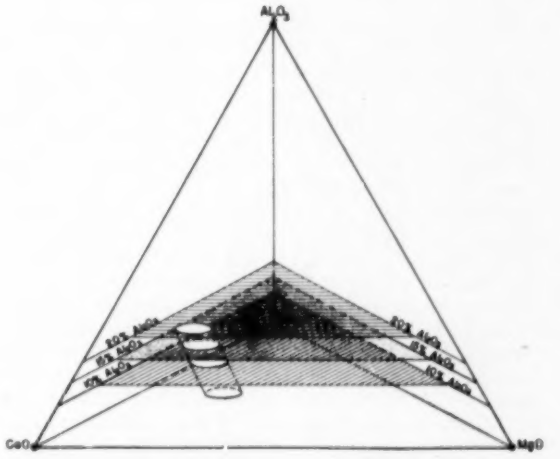

Fig. 1--Representation of the system CaO-MgO-Al_2O_3-SiO_2 as a tetrahedron with one component at each apex. Three triangular planes are shown inserted into the tetrahedron parallel to the base, representing the 10, 15, and 20 pct Al_2O_3 planes. The cylinder intersecting these planes represents the composition volume in which lie optimum blast furnace slags.

For an orderly presentation of the data, the quaternary system is viewed as a tetrahedron with one component at each apex. Fig. 1 shows a tetrahedron representing the system CaO-MgO-Al_2O_3-SiO_2. The base is the ternary system CaO-MgO-SiO_2, Al_2O_3 is the top apex, and the front face, the system CaO-

E. F. OSBORN, Member AIME, is Dean, R. C. DeVRIES is Graduate Fellow, K. H. GEE is Research Associate, College of Mineral Industries, The Pennsylvania State University, State College, Pa., and H. M. KRANER, Member AIME, is Ceramic Engineer, Bethlehem Steel Co., Bethlehem, Pa.

Discussion on this paper, TP 3690C, may be sent, 2 copies, to AIME by April 1, 1954. Manuscript, April 30, 1953. Presented at AIME Blast Furnace, Coke Oven and Raw Materials Conference, Buffalo, N. Y., April 1953.

The Transactions papers appearing in the Journal of Metals during 1954 will subsequently appear in AIME Transactions Volume 200, and may be permanently referenced to that volume.

Table I. Liquidus Data for Mixtures Containing 5 Pct Al_2O_3

	Composition, Wt Pct			Liquidus Temperature, °C	Time, Hr	R.I. of Glass*	Primary Phases
	CaO	MgO	SiO_2				
5-29	27.0	4.0	64.0	1375±15	8	1.578	Tridymite
5-33	27.0	5.0	63.0	1290±3	15	1.572	Tridymite
5-34	26.0	6.0	63.0	1290±3	15	1.574	Tridymite
5-20	29.0	6.0	60.0	1280±5	4	1.584	β-$CaSiO_3$
5-19	30.0	6.0	59.0	1301±3	2	1.586	β-$CaSiO_3$
5-17	32.0	7.0	56.0	1321±3	2	1.598	β-$CaSiO_3$, α-$CaSiO_3$
5-25	34.0	7.0	54.0	1327±2	4	1.592	α-$CaSiO_3$
5-26	31.0	10.0	54.0	1327±2	4	1.600	Pyroxene
5-27	35.0	10.0	50.0	1320±4	4	1.612	β-$CaSiO_3$
5-15	37.0	9.0	49.0	1331±3	2	1.620	α-$CaSiO_3$
5-16	34.0	12.0	49.0	1331±3	2	1.616	Melilite
5-21	31.0	15.0	49.0	1323±4	2	1.616	Pyroxene
5-14	32.0	15.0	48.0	1338±3	2	1.616	Melilite
5-13	40.0	8.0	47.0	1355±5	2	1.620	α-$CaSiO_3$
5-32	45.0	6.0	44.0	1342±3	8	1.632	Melilite
5-2	39.0	12.0	44.0	1397±3	2	1.628	Melilite
5-22	31.0	20.0	44.0	1402±3	2	1.624	Forsterite
5-23	25.0	26.0	44.0	1503±3	2	1.620	Forsterite
5-4	33.0	19.0	43.0	1389±3	2	1.624	Melilite
5-1	49.0	5.0	41.0	1463±3	½	1.640	Ca_2SiO_4
5-7	34.0	20.0	41.0	1435±3	2	1.636	Melilite
5-28	47.0	8.0	40.0	1473±2	1	1.638	Ca_2SiO_4
5-3	42.0	13.0	40.0	1441±3	2	1.640*	Merwinite
5-5	39.0	16.0	40.0	1459±3	2	1.640	Merwinite
5-6	37.0	19.0	39.0	1449±3	2	1.640	Monticellite
5-8	33.0	23.0	39.0	1480±4	2	1.636	Monticellite
5-9	49.0	8.0	38.0	>1584	½	1.644	Ca_2SiO_4
5-11	42.0	15.0	38.0	1495±5	1	1.640*	Merwinite
5-12	38.0	20.0	37.0	1524±1	1	1.640	Periclase
5-10	44.0	16.0	35.0	1589±4	1	1.644*	Periclase

* Refractive index of quenched glasses measured in white light by liquid immersion techniques. In this and succeeding tables, an asterisk follows a figure for refractive index where the mixture was not entirely glass owing to the presence of a small amount of crystals. In these cases the composition of the glass is therefore slightly different from that of the mixture.

MgO-Al_2O_3 has been removed. Horizontal planes in a tetrahedron represent levels of constant alumina content. In Fig. 1 the positions of three such planes are indicated, extending from the back edge part way toward the front face. The cylinder shown intersecting these planes is the volume of optimum slag compositions, as will be discussed. Mixtures made up for study have compositions lying in these horizontal planes, and the latter are designated as the "5 pct Al_2O_3 plane," the "10 pct Al_2O_3 plane," and so on. Data are presented for mixtures containing 5, 10, 15, 20, 25, 30, and 35 pct Al_2O_3. Approximate phase relations for intermediate planes can be derived by interpolation. In applying the data to blast furnace slag problems, it was found that their representation on planes of constant alumina content was of most use, and it was the initial guess that such would be the case that determined the policy of studying series of mixtures where each series contained the same amount of alumina. These data can of course be replotted, if required, on planes of constant MgO, CaO, or SiO_2 content, and can be applied to many other industrial processes.

Method of Investigation

The method of quenching used has been described in many reports from the Geophysical Laboratory, for example, Osborn and Schairer.[3] From the pure ingredients $CaCO_3$, MgO, Al_2O_3, and SiO_2, 10 gram homogeneous mixtures were prepared by repeatedly fusing in a platinum crucible, quenching, and finely crushing. The crushed material, commonly a glass, was completely crystallized at a temperature of the order of 1000°C. A charge of about 20 mg of the powdered crystalline material was enclosed in a platinum envelope, held at a desired temperature for a time sufficient to attain a close approach to equilibrium among the phases, and quenched in mercury. Phases present in the quenched product were identified by means of a petrographic microscope and X-ray diffraction techniques. The Pt-90 pct Pt-10 pct Rh thermocouples were frequently calibrated at standard melting points defined as follows: Au, 1062.5°; $CaMgSi_2O_6$, 1391.5°; and $CaSiO_3$, 1544°.

Inasmuch as the chief objective in the study of each mixture was to obtain its liquidus temperature, it was necessary to examine the quenched product

Table II. Liquidus Data for Mixtures Containing 10 Pct Al_2O_3

	Composition, Wt Pct			Liquidus Temperature, °C	Time, Hr	R.I. of Glass*	Primary Phases
	CaO	MgO	SiO_2				
D97	20.0	8.0	62.0	1277±2	12	1.562	Pyroxene
D75	29.0	2.0	59.0	1295±3	8	1.578	α-$CaSiO_3$
D76	25.0	6.0	59.0	1269±4	2	1.574	Pyroxene
D77	21.0	10.0	59.0	1288±2	2	1.572*	Pyroxene
D78	17.0	14.0	59.0	1292±3	2	1.570	Pyroxene
D93	29.0	4.0	57.0	1268±4	12	1.582	α-$CaSiO_3$
D92	27.0	6.0	57.0	1269±4	2	1.582	Pyroxene
D94	26.0	8.0	56.0	1293±2	2	—	Pyroxene
D55	33.0	2.0	55.0	1353±2	2	1.592	α-$CaSiO_3$
D56	29.0	6.0	55.0	1269±4	2	1.590	Pyroxene
D57	24.0	11.0	55.0	1311±1	2	1.588	Pyroxene
D58	19.0	16.0	55.0	1319±5	3	1.586	Pyroxene
D98	31.0	5.0	54.0	1293±2	2	—	α-$CaSiO_3$
D100	20.0	18.0	52.0	1353±3	3	—	Forsterite
D51	37.0	2.0	51.0	1400±4	3	1.605	α-$CaSiO_3$
D52	33.0	6.0	51.0	1305±3	2	1.604	α-$CaSiO_3$
D53	28.0	11.0	51.0	1309±3	2	1.600	Pyroxene
D54	23.0	16.0	51.0	1324±2	2	1.598	Pyroxene
D79	33.0	8.0	49.0	1273±2	2	1.606	β-$CaSiO_3$
D99	24.0	18.0	48.0	1369±3	2	1.606	Pyroxene
D46	41.0	2.0	47.0	1382±2	2	1.616	α-$CaSiO_3$
D47	37.0	6.0	47.0	1326±6	2	1.614	α-$CaSiO_3$
D80	34.0	9.0	47.0	1293±2	3	1.614	Melilite
D48	32.0	11.0	47.0	1301±3	2	1.612	Melilite
D49	27.0	16.0	47.0	1329±3	2	1.610	Pyroxene
D50	22.0	21.0	47.0	1427±2	3	1.607	Forsterite
D81	35.0	9.0	46.0	1318±1	2	1.616	Melilite
D45	44.0	2.0	44.0	1352±2	2	1.626*	α-$CaSiO_3$
D44	39.0	7.0	44.0	1336±2	2	1.626	Melilite
D43	34.0	12.0	44.0	1351±3	4	1.619	Melilite
D74	31.0	15.0	44.0	1343±3	3	1.620	Melilite
D42	29.0	17.0	44.0	1348±4	3	1.619	Forsterite
D41	24.0	22.0	44.0	1444±2	2	1.614	Forsterite
D85	30.5	16.5	43.0	1335±2	2	—	Melilite
D37	47.0	2.0	41.0	1319±3	2	1.636	Rankinite
D38	42.0	7.0	41.0	1360±4	3	1.614	Melilite
D39	37.0	12.0	41.0	1379±4	2	1.628*	Melilite
D40	32.0	17.0	41.0	1355±3	2	1.626	Melilite
D83	47.0	3.0	40.0	1350±3	2	1.636	Melilite
D73	31.0	19.0	40.0	1395±5	2½	1.630	Forsterite
D84	48.0	3.0	39.0	1420±3	½	1.636	Ca_2SiO_4
D113	45.0	6.0	39.0	1380±3	½	1.638	Melilite
D67	27.0	24.0	39.0	1480±4	2	1.630	Forsterite
D36	46.0	6.0	38.0	1409±3	½	1.640	Merwinite
D35	42.0	10.0	38.0	1407±2	½	1.632	Merwinite
D121	39.0	13.0	38.0	1382±2	½	1.638	Melilite
D34	37.0	15.0	38.0	1384±2	½	1.636	Melilite
D72	34.0	18.0	38.0	1401±3	½	1.634	Monticellite
D59	32.0	20.0	38.0	1407±2	2	1.632	Forsterite
D68	50.0	3.0	37.0	>1600†	2	—	Ca_2SiO_4
D112	47.0	6.0	37.0	1475±3	½	1.642	Ca_2SiO_4
D117	43.0	10.0	37.0	1438±3	½	1.640	Merwinite
D120	40.0	13.0	37.0	1419±3	½	1.640	Merwinite
D125	38.0	15.0	37.0	1409±3	½	1.638	Merwinite
D86	33.0	20.0	37.0	1427±2	2	1.632	Forsterite
D91	28.0	25.0	37.0	1486±4	2	1.632	Forsterite
D111	48.0	4.0	36.0	1545±2	½	1.644	Ca_2SiO_4
D69	46.0	8.0	36.0	1480±3	2	1.642	Merwinite
D116	44.0	10.0	36.0	1463±2	½	1.642	Merwinite
D70	41.0	13.0	36.0	1455±3	½	1.642	Merwinite
D124	39.0	15.0	36.0	1438±3	½	1.640	Merwinite
D71	36.0	18.0	36.0	1427±2	3	1.634	Monticellite
D108	34.0	20.0	36.0	1417±3	½	—	Monticellite
D109	32.0	22.0	36.0	1429±4	1	—	Forsterite
D31	49.0	6.0	35.0	>1600	2	—	Ca_2SiO_4
D115	45.0	10.0	35.0	1495±2	½	1.644*	Merwinite
D32	44.0	11.0	35.0	1470±5	2	—	Merwinite
D119	42.0	13.0	35.0	1481±2	½	1.644	Merwinite
D123	40.0	15.0	35.0	1464±3	½	1.642	Merwinite
D33	39.0	16.0	35.0	1436±1	2	—	Merwinite
D60	34.0	21.0	35.0	1482±1	2	1.638*	Periclase
D66	29.0	26.0	35.0	>1633†	2	1.638*	Periclase
D87	46.0	10.0	34.0	1549±5	½	1.634	Ca_2SiO_4
D118	43.0	13.0	34.0	1505±3	½	1.646	Merwinite
D102	41.0	15.0	34.0	1490±2	2	1.644	Merwinite
D90	37.0	19.0	34.0	1544±5	2	1.638*	Periclase
D114	47.0	10.0	33.0	1595±4	½	1.648*	Ca_2SiO_4
D101	44.0	13.0	33.0	1518±3	2	1.648	Merwinite
D122	42.0	15.0	33.0	1512±2	½	1.646	Merwinite
D61	48.0	10.0	32.0	>1600	2	—	Ca_2SiO_4
D88	45.0	13.0	32.0	1565±2	½	1.650	Ca_2SiO_4
D62	43.0	15.0	32.0	1558±2	½	1.642	Periclase
D89	41.0	17.0	32.0	1608±5	2	1.646	Periclase
D63	38.0	20.0	32.0	>1600	2	1.648*	Periclase
D64	33.0	25.0	32.0	>1600	2	1.642*	Periclase
D65	28.0	30.0	32.0	>1600	2	1.640*	Periclase
D103	47.0	13.0	30.0	>1600	1	—	Ca_2SiO_4
D104	45.0	15.0	30.0	>1600	1	1.648*	Periclase

* See footnote to Table I.

to determine whether it had been all liquid at the temperature of the run or whether crystals coexisted with the liquid. Liquids having a relatively low lime plus magnesia content quench to glasses. Both the liquidus temperature and the crystalline phases in equilibrium with the liquid can be determined easily for such mixtures. Mixtures containing more than about 60 pct lime plus magnesia do not quench to a glass with the experimental techniques used but devitrify during quenching. In these mixtures the crystals formed on quenching must be distinguished from "primary crystals," or those present at the temperature of the run. The "quench crystals" are usually very fine-grained, feathery aggregates, with wavy extinction if birefringent; and with experience these can be distinguished from the primary crystals with very little chance of error.

Assuming that equilibrium was attained during a run, the liquidus temperature lies between the temperature at which the mixture is all liquid and some lower temperature at which crystals are present in the liquid. With the quenching technique, therefore, the liquidus temperature is bracketed, and the precise value can be approached as closely as desired within the limits of error of the temperature measuring and controlling equipment. In the tables of data, each liquidus temperature is followed by a plus or minus value, indicating the closeness of bracketing of the liquidus temperature by runs. Exceptions are some mixtures whose liquidus temperatures are listed only as being greater than a certain value.

For various compositional regions, tests were made of the minimum time required to reach equilibrium at liquidus temperatures. A time of at least twice this length was used for the runs. In general, the greater the percentage of lime plus magnesia and the higher the temperature, the shorter the time required. Two tests indicating attainment of equilibrium were used. In one case, two samples of the same mixture were run together, one as a glass and the other all crystalline. If they gave the same product after quenching, this suggested that the time was sufficiently long and equilibrium among the phases was attained. In the second case, the time of a run was doubled and this procedure repeated until it was found that on doubling the time no further change could be noted in the quenched product.

Liquidus Data

Liquidus data for mixtures are listed in Tables I to VII, arranged according to alumina content. Along with the figure for the liquidus temperature are given the crystalline phase in equilibrium with the liquid at this temperature (primary phase) and the index of refraction for the quenched glass where the liquid cooled to a glass without crystallizing. The data are presented graphically by means of a series of diagrams (Figs. 3 to 9). Included with this series is Fig. 2, showing liquidus relations in the system CaO-MgO-SiO_2 (base of the tetrahedron, Fig. 1) after the recent work of Ricker and Osborn.[2] In these figures, dots represent compositions of mixtures studied, light lines are isotherms of the liquidus surface, and heavy lines represent primary phase field boundaries. These are not ternary systems, except for Fig. 2, but planes through a quaternary system. Consequently, the field boundaries are not univariant lines but intersections of the plane with divariant surfaces. Similarly, the point of intersection of three field boundaries is not an invariant point but rather a "piercing point," which, according to Schairer,[3] is the intersection of the plane with a univariant line along which one liquid and three crystalline phases are in equilibrium. The positions of field boundaries and isotherms are known most precisely in the general area of blast furnace slags because of the greater number of mixtures studied in this region, but the approximate location of lines is shown for the whole triangle in each case, dashed lines indicating that the accuracy of location may be low. Previous studies of parts of the quaternary system CaO-MgO-Al_2O_3-SiO_2 by Andersen,[4] McMurdie and Insley,[5] Osborn and Schairer,[1] Osborn,[6] Prince,[7] and Osborn and Tait[8] were useful in checking the accuracy of liquidus relations along certain lines on some of the planes. Liquidus relations along the edges of the planes are after Rankin and Wright,[9] Rankin and Merwin,[10, 11] Bowen and Greig,[12] Greig,[13] and Keith and Schairer.[14]

A clear picture of the phase volume relationships in the quaternary system CaO-MgO-Al_2O_3-SiO_2 is

Table III. Liquidus Data for Mixtures Containing 15 Pct Al_2O_3

	Composition, Wt Pct			Liquidus Temperature, °C	Time, Hr	R.I. of Glass	Primary Phases
	CaO	MgO	SiO_2				
15A-62	17.0	6.0	62.0	1245±6	100	1.554	Pyroxene
15A-60	13.0	10.0	62.0	1250±5	100	1.553	Pyroxene
15A-61	15.0	10.0	60.0	1235±6	100	1.560	Pyroxene
15A-35	23.0	10.0	52.0	1281±2	1½	1.590	Pyroxene
15A-32	30.0	4.0	51.0	1243±2	10	1.595	Anorthite
15A-37	21.0	13.0	51.0	1283±4	1½	1.591	Pyroxene
15A-23	25.0	10.0	50.0	1274±2	6	1.597	Pyroxene
15A-22	20.0	15.0	50.0	1302±8	2	1.594	Forsterite
15A-33	31.0	5.0	49.0	1243±2	10	1.600	Anorthite
15A-31	29.0	7.0	49.0	1243±2	48	1.599	Anorthite, pyroxene
15A-36	25.0	12.0	48.0	1275±4	6	1.602	Pyroxene
15A-38	23.0	14.0	48.0	1264±3	3	1.598	Forsterite
15A-34	32.0	6.0	47.0	1233±3	12	1.607	Anorthite
15A-48	30.0	8.0	47.0	1238±2	1½	1.605	Pyroxene
15A-16	28.0	10.0	47.0	1248±1	44	1.605	Pyroxene
15A-49	33.0	6.0	46.0	1234±2	19	1.610	Anorthite, melilite
15A-29	26.0	13.0	46.0	1263±1	15	1.607	Pyroxene
15A-39	24.0	15.0	46.0	1307±10	30	1.604	Forsterite
15A-15	35.0	5.0	45.0	1250±4	2	1.614	a-$CaSiO_3$
15A-27	32.0	8.0	45.0	1261±4	17	1.611	Melilite
15A-28	29.0	11.0	45.0	1261±4	17	1.610	Melilite
15A-17	25.0	15.0	45.0	1307±2	1	1.608	Forsterite
15A-30	23.0	17.0	45.0	1355±4	5	1.610	Forsterite
15A-21	20.0	20.0	45.0	1406±6	1½	1.608	Forsterite
15A-26a	37.0	5.0	43.0	1295±2	22	1.620	Melilite
15A-13	31.0	12.0	42.0	1304±6	1	1.618	Melilite
15A-14a	40.0	4.0	41.0	1334±4	1	1.624	Melilite
15A-54	30.0	14.0	41.0	1303±5	3	1.620	Melilite
15A-47	28.0	16.0	41.0	1338±8	17	1.620	Forsterite
15A-18	25.0	20.0	40.0	1421±1	1	1.618	Forsterite
15A-40	23.0	22.0	40.0	1445±6	3	1.621	Forsterite
15A-20	20.0	25.0	40.0	1498±9	2	1.620	Forsterite
15A-7	39.0	8.0	38.0	1421±3	½	1.629	Melilite
15A-6	35.0	12.0	38.0	1373±13	½	1.627	Melilite
15A-5	31.0	16.0	38.0	1406±6	½	1.625	Spinel
15A-24	27.0	20.0	38.0	1458±12	1	1.625	Spinel
15A-41	23.0	24.0	38.0	1472±3	3	1.622	Forsterite, spinel
15A-53	17.0	30.0	38.0	1554±6	2	1.624	Forsterite
15A-8	43.0	5.0	37.0	1427±2	½	1.632	Melilite
15A-12	35.0	14.0	36.0	1405±3	2	1.629	Spinel
15A-19	30.0	20.0	35.0	1490±10	½	1.632	Spinel
15A-1	47.0	4.0	34.0	1478±1	2	1.640	Ca_2SiO_4
15A-2	43.0	8.0	34.0	1453±10	1	1.638	Melilite
15A-69	41.0	10.0	34.0	1437±2	1½	1.641	Melilite
15A-3a	39.0	12.0	34.0	1413±2	1½	1.637	Melilite
15A-44	37.0	14.0	34.0	1408±7	1½	1.640	Spinel
15A-4	35.0	16.0	34.0	1477±5?	½	1.635	Spinel
15A-59	17.0	34.0	34.0	1586±6	½	1.633	Forsterite, periclase
15A-45a	42.0	10.0	33.0	1439±1	2	1.643	Melilite
15A-66	40.0	12.0	33.0	1426±2	1	1.642	Merwinite
15A-9	45.0	8.0	32.0	1477±7	1	1.647	Ca_2SiO_4
15A-68	43.0	10.0	32.0	1450±2	12	1.645	Merwinite
15A-10a	41.0	12.0	32.0	1448±1	1	1.640	Merwinite
15A-11a	38.0	15.0	32.0	1432±1	½	1.640	Merwinite, spinel
15A-43	36.0	17.0	32.0	1446±6	3	1.645	Spinel
15A-42	31.0	22.0	32.0	1515±6	½	1.640	Spinel
15A-58	23.0	30.0	32.0	>1630?	½	1.638	Periclase
15A-67	44.0	10.0	31.0	1472±4	1	1.645	Ca_2SiO_4
15A-65	42.0	12.0	31.0	1460±2	1	1.646	Merwinite
15A-56	49.0	6.0	30.0	1610±9	½	1.651	Ca_2SiO_4
15A-50	43.0	12.0	30.0	1482±3	1	1.649	Merwinite or Ca_2SiO_4
15A-46	38.0	17.0	30.0	1545±15	1	1.646	Periclase
15A-25	35.0	20.0	30.0	>1624?	1½	1.644	Periclase
15A-52	31.0	24.0	30.0	>1650	½	1.646	Periclase
15A-64	44.0	12.0	29.0	1502±2	½	1.648	Ca_2SiO_4
15A-51	41.0	15.0	29.0	1544±14	1½	1.648	Periclase
15A-57	45.0	14.0	26.0	1643±10	2/3	1.657	Periclase

Table IV. Liquidus Data for Mixtures Containing 20 Pct Al_2O_3

	Composition, Wt Pct			Liquidus Temperature, °C	Time, Hr	R.I. of Glass*	Primary Phases
	CaO	MgO	SiO_2				
P72a	4.0	6.0	70.0	1406±2	1	1.516	Tridymite
P73	2.0	10.0	68.0	1412±2	1	1.520	Tridymite
P43	8.0	6.0	66.0	1278±3	3	1.526	Anorthite
P65	6.0	9.0	65.0	1324±3	3	1.536	Tridymite
P46	5.0	12.0	63.0	1320±2	1	1.542	Cordierite
P91	8.0	10.0	62.0	1227±3	17	1.544	Anorthite
P40	10.0	10.0	60.0	1272±2	1	1.548	Anorthite
P90	8.0	12.0	60.0	1225±2	2	1.548	Anorthite
P45	2.0	18.0	60.0	1335±5	1	1.540	Cordierite
P37a	7.0	14.0	59.0	1304	98	1.548	Cordierite
P74	6.0	16.0	58.0	1292±3	5	1.552	Pyroxene
P75	4.0	18.0	58.0	1318±3	1	1.552	Pyroxene
P76	2.0	20.0	58.0	1338±2	1	1.552	Pyroxene, cordierite
P89	8.0	15.0	57.0	1292±7	2	1.556	Pyroxene
P66	7.0	17.0	56.0	1292±3	1	1.560	Pyroxene
P77	4.0	20.0	56.0	1329±3	1	1.556	Pyroxene
P78	2.0	22.0	56.0	1339±1	2	1.556	Pyroxene
P38	14.0	11.0	55.0	1284±3	3	1.554	Anorthite
P44	5.0	20.0	55.0	1334±1	1	1.560	Pyroxene
P67	9.0	18.0	53.0	1317±2	½	1.572	Forsterite
P68	3.0	24.0	53.0	1370±2	1	1.572	Forsterite
P41a	7.0	22.0	51.0	1370±5	1	1.572	Forsterite
P36	18.0	12.0	50.0	1317±4	2	1.588	Anorthite
P35	15.0	15.0	50.0	1279±3	—	1.584	Forsterite
P69	10.0	20.0	50.0	1365±2	1	1.580	Forsterite
P19	30.0	5.0	45.0	1305±4	15	1.600	Anorthite
P20	25.0	10.0	45.0	1305±4	15	1.600	Anorthite
P21	20.0	15.0	45.0	1291±2	2	1.598	Forsterite
P22	15.0	20.0	45.0	1380±5	1	1.598	Forsterite
P23	10.0	25.0	45.0	1443±3	1	1.598	Forsterite
P93	23.0	13.0	44.0	1300±3	1½	1.602	Spinel
P84	28.0	9.0	43.0	1282±2	1	1.602	Anorthite
P34	21.0	16.0	43.0	1353±4	—	1.602	Spinel
P70	31.0	7.0	42.0	1260±1	1	1.609	Melilite
P92	29.0	9.0	42.0	1270±3	1	1.610	Melilite
P33	25.0	13.0	42.0	1336±4	2	1.608	Spinel
P87	36.0	3.0	41.0	1300	1	1.616*	Melilite
P82	33.0	6.0	41.0	1300±3	2	1.612	Melilite
P83	31.0	8.0	41.0	1284±4	1	1.610	Melilite
P14	30.0	10.0	40.0	1290±2	2	1.616	Spinel
P15	25.0	15.0	40.0	1415±3	1	1.608	Spinel
P16	20.0	20.0	40.0	1480±5	1	1.612	Spinel
P17	15.0	25.0	40.0	1525	1	1.612*	Spinel
P18	10.0	30.0	40.0	1575	2	1.612*	Spinel
P71	33.0	8.0	39.0	1327±2	1	1.618	Melilite
P32	35.0	7.0	38.0	1353±4	—	1.620	Melilite
P55	32.0	10.0	38.0	1366±3	1	1.618*	Spinel
P54	33.0	11.0	36.0	1398±2	1	1.624	Spinel
P29	31.0	13.0	36.0	1450±5	½	1.622	Spinel
P7	40.0	5.0	35.0	1454±4	1	1.632	Melilite
P8	35.0	10.0	35.0	1405±5	1	1.630	Melilite
P9	30.0	15.0	35.0	1480±5	1	1.628	Spinel
P10	25.0	20.0	35.0	1592±6	2	1.628	Spinel
P11	20.0	25.0	35.0	>1600	2	1.624*	Spinel
P12	15.0	30.0	35.0	>1597	1	1.624*	Spinel
P53	36.0	11.0	33.0	1456±3	1	1.632	Spinel
P30	34.0	13.0	33.0	1488±2	1	1.630	Spinel
P52	38.0	11.0	31.0	1455±3	1	1.636*	Spinel
P1	45.0	5.0	30.0	1505±5	1	1.642	Melilite
P2	40.0	10.0	30.0	1447±3	1	1.642	Melilite
P31	37.0	13.0	30.0	1484±2	1	1.640	Spinel
P3	35.0	15.0	30.0	1505±5	1	1.640	Spinel
P4	30.0	20.0	30.0	1567±7	2	1.640	Spinel
P5	25.0	25.0	30.0	>1597	1	1.640*	Spinel
P6	20.0	30.0	30.0	>1597	1	1.638	Spinel
P103	39.5	11.5	29.0	1445±3	3	1.640	Spinel
P111	44.5	7.0	28.5	1465±2	2	1.646	Ca_3SiO_5, melilite
P42	48.0	4.0	28.0	>1375	1	1.648*	Ca_3SiO_5
P109	45.0	7.0	28.0	1462±1	2	1.648	Ca_3SiO_5, melilite
P81	43.0	9.0	28.0	1445±1	1	1.645	Melilite
P50a	41.0	11.0	28.0	1440	2	1.646	Melilite, spinel
P81	38.0	14.0	28.0	1474±3	1	1.644	Spinel
P128	44.0	8.5	27.5	1460±4	1	1.647	Ca_3SiO_5
P126	43.0	9.5	27.5	1460±4	1	1.648—	Merwinite
P115	42.0	10.5	27.5	1449±2	1	1.647	Merwinite
P117	41.5	11.0	27.5	1436±3	1	1.647	Merwinite
P120	40.5	12.0	27.5	1460±4	1	1.646	Spinel
P127	44.5	8.5	27.0	1488±3	1	1.648	Ca_3SiO_5
P125	43.5	9.5	27.0	1455±2	1	1.647	Merwinite
P114	42.5	10.5	27.0	1446±4	1	1.648—	Merwinite
P104	38.5	14.5	27.0	1475±5	2	1.644	Spinel, periclase
P113	43.0	10.5	26.5	1450±4	1	1.648	Merwinite
P116	42.5	11.0	26.5	1452±2	1	1.648	Merwinite
P119	41.5	12.0	26.5	1446±3	1	1.648	Merwinite
P110	46.5	7.5	26.0	1536±2	2	1.648*	Ca_3SiO_5
P24a	45.0	9.0	26.0	1522±3	1	1.650	Ca_3SiO_5
P123	44.5	9.5	26.0	1490±4	1	1.651	Ca_3SiO_5
P112	43.5	10.5	26.0	1465±4	1	1.649	Ca_3SiO_5
P80a	43.0	11.0	26.0	1455±4	1	1.649	Merwinite
P86	42.0	12.0	26.0	1454±4	1½	1.649	Merwinite
P131	41.5	12.5	26.0	1476±4	1½	1.648	Periclase
P25	41.0	13.0	26.0	1475±5	1½	1.648	Periclase
P26	37.0	17.0	26.0	>1600	3	1.656*	Periclase
P27	33.0	21.0	26.0	>1600	2	1.644*	Periclase
P28	29.0	25.0	26.0	>1600	2	1.642*	Periclase
P122	43.5	11.0	25.5	1476	1	1.650	Ca_3SiO_5
P118	42.5	12.0	25.5	1477±3	1	1.649	Periclase
P130	43.5	11.5	25.0	1491±5	1	1.652—	Periclase
P121	44.5	11.0	24.5	1508±4	1½	1.653	Ca_3SiO_5
P79a	45.0	11.0	24.0	1531±6	1	1.654	Ca_3SiO_5

Table IV. Continued

	Composition, Wt Pct			Liquidus Temperature, °C	Time, Hr	R.I. of Glass*	Primary Phases
	CaO	MgO	SiO_2				
P47	47.0	10.0	23.0	1552±2	12	1.656	Ca_3SiO_5
P48a	44.0	13.0	23.0	>1620	1	1.644*	Periclase
P49	40.0	17.0	23.0	>1602	1	1.652*	Periclase
P62	48.0	11.0	21.0	1565±5	1	1.656*	Ca_3SiO_5, periclase
P63	46.0	13.0	21.0	>1603	1	1.654*	Periclase
P61	51.0	9.0	20.0	>1602	1	1.660*	Ca_3SiO_5
P64	44.0	16.0	20.0	>1603	½	1.654*	Periclase
P59	50.0	12.0	18.0	>1603	½	1.664*	Periclase
P60	49.0	13.0	18.0	>1602	1	1.664*	Periclase
P108	58.5	5.5	16.0	1600±6	1	1.682	Ca_3SiO_5
P106	56.0	8.0	16.0	>1600	½	1.678*	Ca_3SiO_5
P105	60.0	5.0	15.0	>1600	½	1.682*	Ca_3SiO_5
P132	58.0	7.0	15.0	1600±20	¼		Ca_3SiO_5
P85	62.0	4.0	14.0	>1604	1	1.684*	CaO
P133	59.0	7.0	14.0	1585±15	¼		Ca_3SiO_5
P134	60.0	7.0	13.0	1660±25	¼		CaO
P56	59.0	8.0	13.0	>1602	1	1.684*	Periclase
P57	55.0	12.0	13.0	>1602	1	1.684*	Periclase
P58	53.0	14.0	13.0	>1602	½	1.680*	Periclase

* See footnote to Table I.

obtained if a tetrahedron is constructed of transparent plastic with horizontal planes of the same material fixed at 5 pct Al_2O_3 intervals. On the faces of the tetrahedron and on each plane are sketched the phase equilibrium relations. Liquidus temperatures throughout the tetrahedron, the approximate location of invariant points, and primary phase volume relationships are readily seen. It will be noted, for example, that the volume of the tetrahedron is dominated by the primary phase volumes of a few phases, especially spinel ($MgAl_2O_4$) and periclase (MgO). Two moderately large volumes are occupied by the melilites (solid solutions of akermanite, $Ca_2MgSi_2O_7$, and gehlenite, $Ca_2Al_2SiO_7$) and by the pyroxenes (predominantly solid solutions of clinoenstatite, $MgSiO_3$, and diopside, $CaMgSi_2O_6$). In contrast, the primary phase volume of sapphirine ($Mg_4Al_{10}Si_2O_{20}$) is minute. The volume of monticellite ($CaMgSiO_4$) extends upward from the base as a four sided prism terminating against the spinel volume before reaching the 15 pct Al_2O_3 plane. The merwinite ($Ca_3MgSi_2O_8$) volume extends upward from the base through the 20 pct Al_2O_3 plane before being truncated.

A liquidus surface may be portrayed graphically as a solid model, in which the isotherms become contours separated by a vertical interval proportional to the temperature interval. Such solid models have been constructed of several of the alumina planes to illustrate in three dimensions the liquidus relations. Fig. 10 is a photograph of the model for the 10 pct Al_2O_3 plane. The steep rise of the dicalcium silicate and periclase liquidus surfaces in contrast with the plateau-like form of the merwinite, monticellite, and melilite surfaces is particularly to be noted in connection with blast furnace slag composition problems. This feature, along with the re-entrant angle of the merwinite plateau into the steeply rising liquidus surfaces of dicalcium silicate and periclase, is the key to the position of optimum blast furnace slag compositions.

Optimum Blast Furnace Slag Compositions

For a blast furnace to operate smoothly and with maximum efficiency, the slag should have the following characteristics: 1—It should be a homogeneous liquid, that is, without notable variations in the properties of the liquid and without crystalline

phases present. 2—Its composition should be such that a wide latitude of variation in composition is possible without a troublesome slag developing. Under the best conditions of operation, raw materials vary sufficiently to cause significant variations in slag composition. The slag should tolerate such inevitable variations in composition without notable changes in its properties and performance. 3—It should have a high potentiality for retaining sulphur, or in other words, the distribution ratio of sulphur between the slag and metal phases under conditions of temperature and atmosphere existing in a blast furnace should be high. 4—It should have a low viscosity at the temperatures prevailing in the furnace in order to melt down and move through and out of the furnace quickly and smoothly.

Using a slag of optimum composition will make possible the maximum production of metal containing the minimum amount of sulphur, with the minimum slag volume and fuel costs. With less coke per

Table V. Liquidus Data for Mixtures Containing 25 Pct Al_2O_3

	Composition, Wt Pct			Liquidus Temperature, °C	Time, Hr	R.I. of Glass*	Primary Phases
	CaO	MgO	SiO_2				
Q-74	10.0	3.0	62.0	1400±5	100	1.536	Anorthite
Q-64	6.0	7.0	62.0	1390±8	100	1.534	Cordierite
Q-75	3.0	10.0	62.0	1450±8	100	1.534	Cordierite
Q-32	5.0	10.0	60.0	1382±8	100	1.540	Cordierite
Q-73	8.5	11.5	55.0	1327±3	280	1.560	Anorthite, cordierite
Q-67	7.0	13.0	55.0	1351±5	70	1.556	Cordierite
Q-31	5.0	15.0	55.0	1365±2	18	1.552	Cordierite
Q-72	9.0	14.0	52.0	1315±2	150	1.564	Cordierite, anorthite, spinel
Q-70	5.5	18.5	51.0	1354±5	100	1.568	Spinel
Q-71	3.0	21.0	51.0	1386±5	100	1.568	Spinel
Q-80	1.0	23.0	51.0	1396±3	50	1.568	Spinel
Q-81	9.5	15.0	50.5	1349±5	160	1.568	Spinel
Q-65	7.0	18.0	50.0	1382±5	100	1.572	Spinel
Q-29	5.0	20.0	50.0	1390±10	1	1.556	Spinel
Q-66	3.0	22.0	50.0	1405±5	70	1.574	Spinel
Q-68	10.0	16.0	49.0	1382±5	100	1.574	Spinel
Q-69	6.5	19.5	49.0	1410±5	200	1.576	Spinel
Q-47	22.0	10.0	43.0	1349±5	100	1.598	Anorthite, spinel
Q-46	26.0	8.0	41.0	1315±5	100	1.604	Anorthite, spinel
Q-13	30.0	5.0	40.0	1320±5	1	1.604	Anorthite
Q-63	28.0	7.0	40.0	1336±6	90	1.608	Spinel
Q-14	25.0	10.0	40.0	1405±5	1	1.604	Spinel
Q-15	20.0	15.0	40.0	1494±8	1	1.600	Spinel
Q-16	15.0	20.0	40.0	1542±6	1	1.600	Spinel
Q-79	30.0	6.0	39.0	1316±3	6	1.606	Spinel
Q-45a	29.0	7.0	39.0	1334±4	18	1.604	Spinel
Q-34	30.0	7.0	38.0	1350±1	8	1.610	Spinel
Q-48	31.0	8.0	36.0	1417±3	1	1.614	Spinel
Q-9	35.0	5.0	35.0	1438±3	1	1.616	Melilite
Q-10	30.0	10.0	35.0	1480±5	3	1.616	Spinel
Q-11	25.0	15.0	35.0	1557±6	1	1.610	Spinel
Q-12	20.0	20.0	35.0	>1600?	½	1.612*	Spinel
Q-5	40.0	5.0	30.0	1514±2	1	1.632	Melilite
Q-6	35.0	10.0	30.0	1505±5	1	1.624	Spinel
Q-7	30.0	15.0	30.0	>1600	½	1.638*	Spinel
Q-8	25.0	20.0	30.0	>1600	½	1.628*	Spinel
Q-43	38.0	9.0	28.0	1485±3	2	1.640	Melilite
Q-1	45.0	5.0	25.0	1495±5	1	1.644	Melilite
Q-3	35.0	15.0	25.0	1545±6	1	1.640	Spinel
Q-4	30.0	20.0	25.0	>1600	½	1.632*	Spinel
Q-36	47.0	4.0	24.0	1540±4	1½	1.646	Ca_2SiO_4
Q-82	43.0	8.0	24.0	1477±3	6	1.648—	Melilite
Q91	45.0	6.5	23.5	1477±4	1	1.652—	Ca_2SiO_4
Q83	44.0	8.0	23.0	1449±1	2	1.650	Ca_2SiO_4
Q84	43.0	9.0	23.0	1477±3	6	1.651	Melilite, spinel
Q86	42.0	10.0	23.0	1442±2	1½	1.650	Spinel
Q57	40.0	12.0	23.0	1471±1	3½	1.648	Spinel
Q55	46.0	7.0	22.0	1458±3	2	1.652	Ca_2SiO_4
Q85	44	9.0	22.0	1449±1	2	1.653	Ca_2SiO_4
Q87	43.0	10.0	22.0	1428±2	2	1.652+	Ca_2SiO_4, spinel
Q56	42.0	11.0	22.0	1441±2	1½	1.648	Periclase
Q62	41.0	12.0	22.0	1473±3	4	1.650	Periclase
Q44	36.0	17.5	21.5	>1602	1	1.648	Periclase
Q88	45.0	9.0	21.0	1484±3	6	1.655	Ca_2SiO_4
Q89	44.0	10.0	21.0	1462±4	12	1.655	Ca_2SiO_4, periclase
Q90	43.0	11.0	21.0	1472±3	1	1.656	Periclase
Q22	50.0	5.0	20.0	1585	1	1.656	Ca_2SiO_4
Q23	45.0	10.0	20.0	1465	1	1.652	Periclase, Ca_2SiO_4
Q24	40.0	15.0	20.0	>1600	1	1.648*	Periclase
Q25	35.0	20.0	20.0	>1610	½	1.648*	Periclase
Q20	45.0	15.0	15.0	>1600	½	1.660*	Periclase
Q21	40.0	20.0	15.0	>1600	½	1.656*	Periclase
Q78	52.5	8.5	14.0	1585±10	1	1.670	Periclase
Q77	59.0	3.0	13.0	1590±4	1	1.680	Ca_3SiO_4
Q92	59.0	4.0	12.0	1585±15	2	—	Ca_3SiO_5
Q93	60.0	4.0	11.0	1555±15	2	—	Ca_3SiO_5
Q94	61.0	4.0	10.0	>1600	2	—	CaO
Q17	55.0	10.0	10.0	>1600	½	1.628*	Periclase
Q18	50.0	15.0	10.0	>1600	1	1.668*	Periclase

* See footnote to Table I.

Table VI. Liquidus Data for Mixtures Containing 30 Pct Al_2O_3

	Composition, Wt Pct			Liquidus Temperature, °C	Time, Hr	R.I. of Glass*	Primary Phases
	CaO	MgO	SiO_2				
30-29	10.0	6.0	54.0	1439±8	214	1.552	Mullite
30-30	4.0	12.0	54.0	1425±6	200	1.552	Mullite
30-44	2.0	14.0	54.0	1450±5	100	1.554	Cordierite
30-47	6.0	11.5	52.5	1397±3	80	1.560	Cordierite
30-42	3.5	14.0	52.5	1452±4	100	1.558	Cordierite
30-46	10.0	9.0	51.0	1380±5	100	1.564	Mullite
30-15	8.0	11.0	51.0	1395±5	18	1.558	Spinel
30-41	3.0	16.0	51.0	1416±5	181	1.560	Spinel
30-45	1.0	18.0	51.0	1439±4	150	1.560	Cordierite, spinel
30-31	6.0	14.0	50.0	1433±3	70	1.564	Spinel
30-43	0.5	20.0	49.5	1452±2	120	1.566	Spinel
30-27	11.0	10.0	49.0	1390±4	170	1.568	Spinel
30-40	9.0	12.0	49.0	1420±4	140	1.568	Spinel
30-28	4.0	17.0	49.0	1465±4	190	1.566	Spinel
30-14	2.0	19.0	49.0	1469±5	54	1.564	Spinel
30-35	11.0	12.0	47.0	1446±6	125	1.570	Spinel
30-13	9.0	14.0	47.0	1443±4	18	1.570	Spinel
30-34	7.0	16.0	47.0	1435±5	150	1.576*	Spinel
30-26	8.0	18.0	44.0	1555±4	150	1.582	Spinel
30-12	24.0	6.0	40.0	1397±4	1	1.594	Anorthite, spinel
30-36	27.0	4.0	39.0	1416±4	15	1.600	Anorthite
30-20	22.0	10.0	38.0	1505±2	2	1.600	Spinel
30-37	29.0	4.0	37.0	1342±4	1	1.604	Anorthite
30-19	27.0	6.0	37.0	1423±3	5	1.600	Spinel
30-11	28.0	8.0	34.0	1488±3	1	1.604	Spinel
30-10	34.0	6.0	30.0	1491±4	1	1.624	Melilite
30-25	31.0	9.0	30.0	1546±4	3	1.622*	Spinel
30-9	34.0	10.0	26.0	1567±5	3	1.628	Spinel
30-24	37.0	8.0	25.0	1493±1	22	1.634*	Spinel, melilite
30-17	44.0	6.0	20.0	1455±4	4	1.648	Melilite
40-33	43.0	8.0	19.0	1416±3	48	1.648*	Melilite
30-8	42.0	9.0	19.0	1422±4	4	1.656	Spinel
30-38	43.0	9.0	18.0	1403±2	2	1.656	Ca_3SiO_4, spinel
30-18	40.0	12.0	18.0	1496±4	2	1.652	Spinel, periclase
30-23	45.0	8.0	17.0	1426±2	16	1.652*	Ca_3SiO_4
30-1	50.0	5.0	15.0	1526±6	2	1.658	Ca_3SiO_4
30-2	45.0	10.0	15.0	1520±2	1½	1.659	Periclase
30-7	50.0	8.0	12.0	1511±4	1	1.664	Periclase
30-21	58.0	2.0	10.0	1510±4	4	1.682*	Ca_3SiO_5
30-3	55.0	5.0	10.0	1447±3	2	1.674	Ca_3SiO_4
30-4	50.0	10.0	10.0	>1606	1	1.670*	Periclase
30-22	45.0	15.0	10.0	>1700	½	—	Periclase
30-32	57.0	4.0	9.0	1476±5	2	1.678	Ca_3SiO_5
30-39	55.0	6.0	9.0	1463±3	18	1.681	Ca_3SiO_5
30-16	54.0	7.0	9.0	1487±4	18	1.680	Periclase
30-6	57.0	6.0	7.0	>1600	1	1.684*	CaO
30-5	53.0	10.0	7.0	>1600	1	1.676*	Periclase

* See footnote to Table I.

Table VII. Liquidus Data for Mixtures Containing 35 Pct Al_2O_3

	Composition, Wt Pct			Liquidus Temperature, °C	Time, Hr	R.I. of Glass	Primary Phases
	CaO	MgO	SiO_2				
35-19	6.0	10.0	49.0	1493±4	75	1.557	Mullite
35-20	2.0	14.0	49.0	1486±5	100	1.562+	Mullite
35-17	1.0	16.0	48.0	1496±4	150	1.565	Spinel
35-21	10.0	8.0	47.0	1491±4	75	1.566	Mullite, spinel
35-28	8.0	10.0	47.0	1457±4	150	1.568	Spinel
35-22	6.0	12.0	47.0	1478±4	10	1.567	Spinel
35-23	2.0	16.0	47.0	1508±4	100	1.568	Spinel
35-24	10.0	10.0	45.0	1486±5	100	1.573	Spinel
35-25	6.0	14.0	45.0	1510±4	100	1.572+	Spinel
35-26	10.0	12.0	43.0	1528±5	70	1.578	Spinel
35-27	6.0	16.0	43.0	1555±5	48	1.581	Spinel
35-15	28.0	4.0	33.0	1447±4	24	1.608—	Spinel
35-16	24.0	8.0	33.0	1561±2	2	1.607	Spinel
35-13	32.0	4.0	29.0	1480±3	24	1.618	Melilite
35-14	28.0	8.0	29.0	1597±4	2	1.616	Spinel
35-12	32.0	8.0	25.0	1595±5	1	1.628	Spinel
35-9	40.0	4.0	21.0	1549±2	3	1.640	Melilite
35-10	36.0	8.0	21.0	1550±2	4	1.637	Spinel
35-7	44.0	4.0	17.0	1452±3	24	1.650	Melilite
35-8	40.0	8.0	17.0	1478±3	40	1.649	Spinel
35-5	48.0	4.0	13.0	1436±4	20	1.659	Ca_3SiO_4
35-6	44.0	8.0	13.0	1402±4	2	1.661	Ca_3SiO_4
35-3	52.0	4.0	9.0	1398±2	1	1.659	Ca_3SiO_4
35-4	48.0	8.0	9.0	1452±4	1	1.670	Periclase
35-1	56.0	4.0	5.0	1484±4	1	1.682	CaO
35-2	52.0	8.0	5.0	1529±4	2	1.678	Periclase

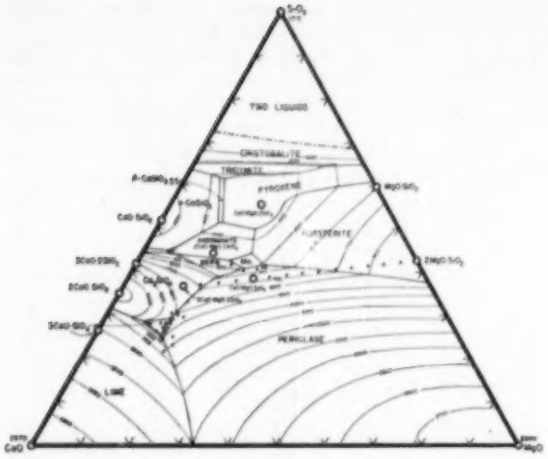

Fig. 2—Liquidus diagram for the system CaO-MgO-SiO_2 as modified by Ricker and Osborn.[6] Light lines are liquidus isotherms in °C, and heavier lines are boundary curves. The primary crystalline phase (crystal in equilibrium with liquid at the liquidus temperature) in each field is indicated by composition or name or both. Merw, merwinite ($Ca_3MgSi_2O_8$); Mo, monticellite ($CaMgSiO_4$).

charge, less sulphur is introduced into the furnace; and with a smoother operation less production time is lost because of malfunctioning of the furnace.

These statements would probably not be questioned seriously by blast furnace operators. The questions are how to determine the optimum slag composition and how to shift the composition of a slag to approach this optimum, given raw materials which permit only relatively small changes in slag composition, without unduly increasing slag volume. Liquidus data for the quaternary system CaO-MgO-Al_2O_3-SiO_2, along with some general considerations, provide an approach to the answer. It will be seen

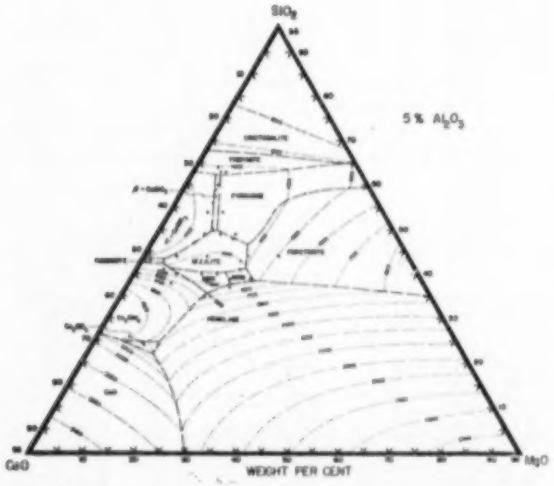

Fig. 3—Liquidus diagram at 5 pct Al_2O_3 in the system CaO-MgO-Al_2O_3-SiO_2. Light lines are isotherms of the liquidus surface, heavier lines are primary phase boundary curves, and dots represent compositions of mixtures studied. Temperatures are in °C. Mer, merwinite ($Ca_3MgSi_2O_8$); Mon, monticellite ($CaMgSiO_4$); rankinite, $Ca_3Si_2O_7$; melilite, solid solution of akermanite ($Ca_2MgSi_2O_7$) and gehlenite ($Ca_2Al_2SiO_7$); pyroxene, solid solution largely of diopside ($CaMgSi_2O_6$) and clinoenstatite ($MgSiO_3$); tridymite and cristobalite are forms of SiO_2; forsterite, Mg_2SiO_4; periclase, MgO.

from an examination of these data that the alumina content of a slag is not critical within broad limits, permitting planes of constant alumina content to serve as a base for estimating direction and amount of change of lime, magnesia, and silica in order to approach the optimum position.

Desulphurization Potential of a Slag: The distribution of sulphur between the slag and metal phases

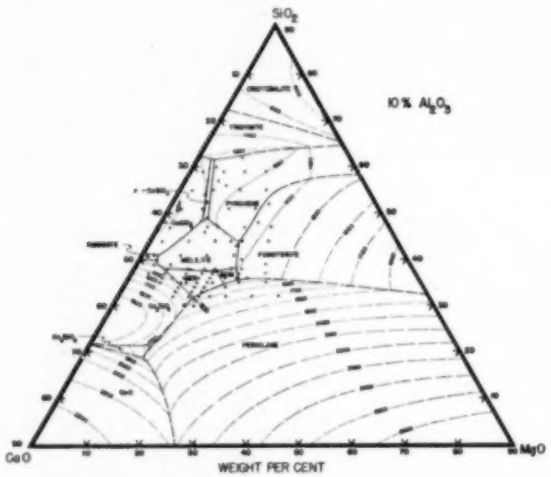

Fig. 4—Liquidus diagram for the 10 pct Al_2O_3 plane. Anorthite, $CaAl_2Si_2O_8$; mullite, $3Al_2O_3 \cdot 2SiO_2$.

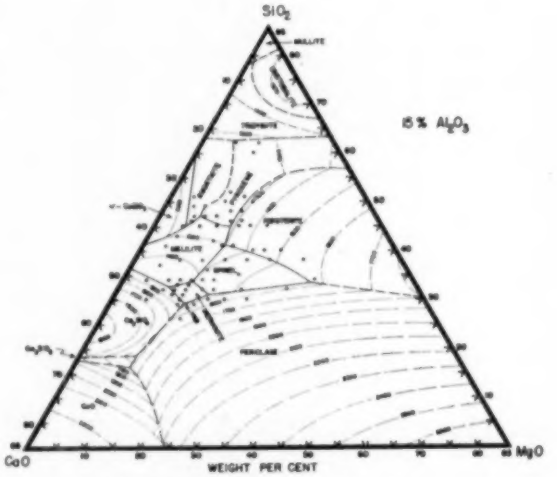

Fig. 5—Liquidus diagram for the 15 pct Al_2O_3 plane. Spinel, $MgAlO_4$.

in a blast furnace is dependent upon many factors, including temperature, degree of attainment of equilibrium among the phases, total sulphur present, and composition of slag, metal, and gas phases. Considering only the variable of slag composition, a slag will retain proportionately more of the total sulphur in the system the greater the tendency of the cations in the slag to form bonds with $S^{=}$ in the presence of abundant $O^{=}$. If this tendency is very weak, as it would be for example if the slag contained only Si^{4+} and Al^{3+} cations, then a very small amount of sulphur could be accommodated in the liquid oxide structure. On the other

hand, if significant amounts of K^+ or Na^+ were present in the slag, sulphur ions could be retained in relatively large proportions.

As a first approximation, the heats of formation of oxides and sulphides may be used as indications of the tendencies of these cations to combine with either O^{2-} or S^{2-} ions. Table VIII gives the heats of formation, which although applicable to 18°C, serve as a basis for judging relative heats of formation at higher temperatures.

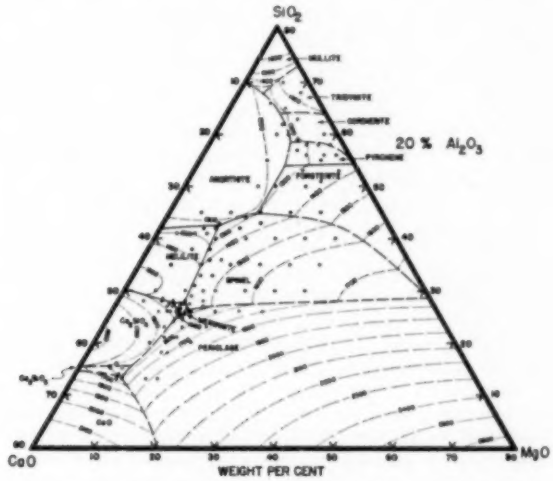

Fig. 6—Liquidus diagram for the 20 pct Al_2O_3 plane. Cordierite, $2MgO \cdot 2Al_2O_3 \cdot 5SiO_2$.

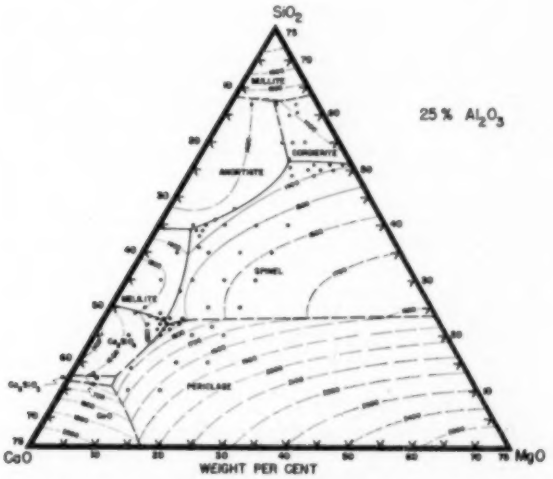

Fig. 7—Liquidus diagram for the 25 pct Al_2O_3 plane.

Potassium and sodium are not practicable as constituents of a blast furnace slag, except as added after tapping, but it will be noted that their heats of formation of oxides and sulphides are of the same order of magnitude and their desulphurizing power therefore high. These data indicate, on the other hand, that the desulphurizing action of Si^{4+} is negligible. If a silicon atom is given the choice of combining with oxygen or sulphur, it will form the oxide because this reaction lowers the free energy of the system far more than by formation of the sulphide. For the four major cations in a blast furnace slag, the tendency for forming bonds with O^{2-} rather than with S^{2-} decreases in the order: $Si^{4+} > Al^{3+} > Mg^{2+} > Ca^{2+}$; or as desulphurizers, the order is $Ca^{2+} > Mg^{2+} > Al^{3+} > Si^{4+}$. Clearly, for the best sulphur retention by the slag in a blast furnace, the "lowest possible" proportions of alumina and silica should be used. Of the two "bases," lime should be preferable to magnesia on a mol percentage basis as the component added to lower the percentage of aluminum and silicon ions present, in view of its better desulphurizing tendencies. On the other hand, on a weight percentage basis magnesia is more effective than lime in lowering the percentage of aluminum plus silicon ions present in the mixture because of the lower molecular weight of magnesia. These two effects, difference in desulphurizing power and difference in number of atoms in a given weight of the oxide, are of the same order of mag-

Table VIII. Heats of Formation of Oxides and Sulphides, Kcal per Gram Atom Oxygen

	K^+	Na^+	Ca^{2+}	Mg^{2+}	Al^{3+}	Si^{4+}
O^{2-}	86	99	152	146	133	101
S^{2-}	88	90	114	82	42	14

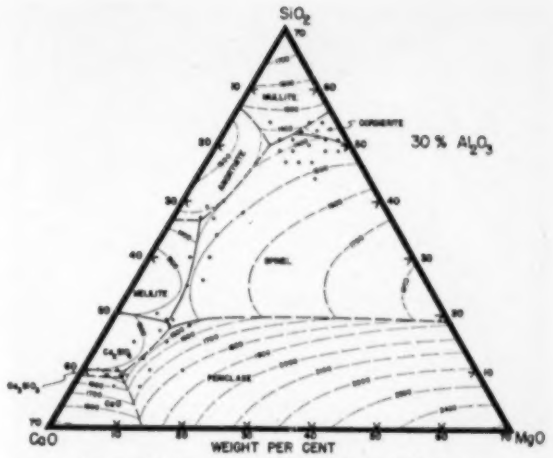

Fig. 8—Liquidus diagram for the 30 pct Al_2O_3 plane.

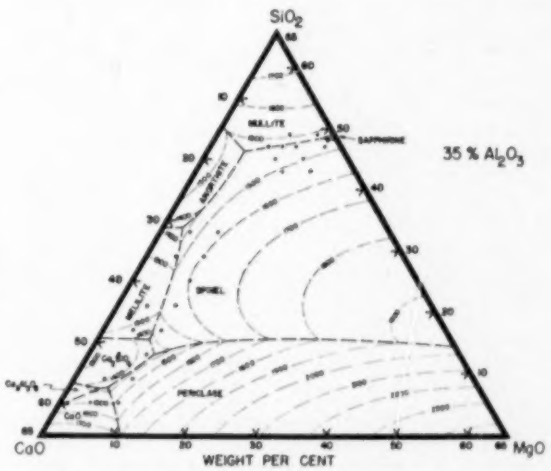

Fig. 9—Liquidus diagram for the 35 pct Al_2O_3 plane. Sapphirine, $4MgO \cdot 5Al_2O_3 \cdot 2SiO_2$.

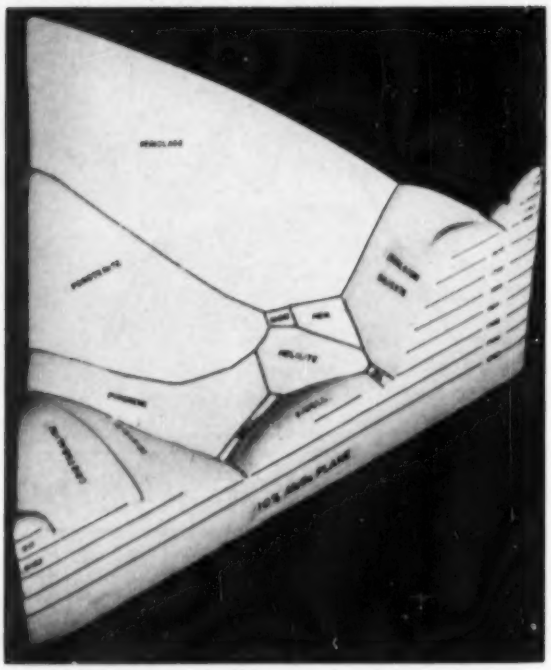

Fig. 10—Photograph of a solid model of part of the liquidus surface of the 10 pct Al_2O_3 plane in the system CaO-MgO-Al_2O_3-SiO_2. The area shown extends from the SiO_2 apex to a base line at 16 pct SiO_2 (74 pct CaO at one corner and 74 pct MgO at the other). Straight lines on front face are at intervals of 100°C. Lines on liquidus surface are boundary curves. Note plateau-like surface of melilite, monticellite, and merwinite fields, which rises gently to the steep slopes of the periclase and dicalcium silicate liquidus surfaces. The optimum position of blast furnace slags at this alumina level lies in the field of merwinite (Mer).

nitude. Therefore, on a weight percentage basis, lime and magnesia should be about equally effective in increasing the desulphurization potential of a slag.

The critical question is, what is the "lowest possible" proportion of alumina and silica, or for a given alumina content, what is the lowest possible silica content which can be used? This question is answered directly by an examination of the liquidus data as soon as one reasonable assumption is made with respect to the temperature of the slag in the furnace. The order of magnitude of this temperature is 1400° to 1500°C. If it is assumed for purposes of illustration that the temperature in a particular furnace is 1500°C and that the slag contains 15 pct alumina with the balance being lime, magnesia, and silica, by referring to Fig. 5, it can be seen that all compositions lying in a large area in the upper left central part of the diagram will be entirely liquid at 1500°C. These of course are compositions having liquidus temperatures less than 1500°C. Compositions having the lowest silica content at 1500°C and which are completely liquid at this temperature are those lying along the 1500°C isotherm where the percentage of silica is the lowest. The minimum silica point is on the dicalcium silicate-periclase boundary curve at approximately 13 pct MgO. At 1500°C and 15 pct alumina, a liquid of lower silica content than this is not possible. If more lime and magnesia are added in order to reduce the silica content of the mixture, the composition then lies in a higher liquidus region where crystals will be present in the liquid at 1500°C, and the composition of the liquid present in the mixture will be no lower in silica. With crystals such as dicalcium silicate, merwinite, monticellite, and periclase coexisting with the liquid, the composition of the latter must still lie along the 1500° isotherm, but the composition of the liquid will no longer be represented by a point on the 15 pct Al_2O_3 plane. This liquid in equilibrium with crystals will contain more than 15 pct Al_2O_3. Clearly, then, from the standpoint of desulphurization, the optimum composition of a lime-magnesia-alumina-silica slag at 1500°C, containing 15 pct alumina, is this point at 13 pct MgO and 28 pct SiO_2.

If the temperature of the slag is lower or higher than 1500°C, its optimum composition with respect to desulphurization is again the point of lowest silica content lying on the liquidus isotherm for this temperature. In an actual slag other constituents such as FeO, TiO_2, and MnO, along with S, are present to a total extent of a few percent, and these all serve to lower the liquidus temperature (and viscosity) of the slag, but their effect on this general picture is small because of the small amounts present, and the effect is in the direction of giving a safety factor in the use of these diagrams; that is, liquidus temperatures of an actual slag, where its composition is recalculated on a basis of 100 pct CaO, MgO, Al_2O_3, and SiO_2, are somewhat lower than those shown in the diagrams for the system CaO-MgO-Al_2O_3-SiO_2, as will be discussed.

If the alumina content of the slag is approximately 10 pct, then the diagram for this plane can be used (Fig. 4) and the optimum composition of the slag from the standpoint of desulphurization is indicated in Fig. 13. Diagrams are presented at 5 pct Al_2O_3 intervals for planes containing for 0 to 35 pct Al_2O_3. For alumina contents other than those for which diagrams have been presented, planes showing the position of liquidus isotherms can be constructed with reasonable accuracy by interpolation of data given.

It has been instructive to replot the data of Holbrook-and Joseph[15] and of Holbrook[16] on the relative desulphurizing powers of blast furnace slags, using as a base these planes of constant alumina content. Taking the 10 pct Al_2O_3 plane as an example, a plot of their data on this plane is shown in Fig. 11. The isodesulphurization lines* are just as would be expected from the considerations discussed above except that the maximum desulphurization instead of being at the lowest silica content on the 1500°C isotherm lies approximately at the lowest silica content on the 1600° to 1700°C isotherm, or in other words it is displaced to a somewhat lower silica percentage. Above this maximum, lines of equal desulphurization are approximately parallel to the base, or in other words they are essentially lines of constant silica content. Below this maximum, desulphurization falls off very rapidly as silica is decreased, as would be expected because of the increasing amounts of crystals present in the liquid as mixtures of higher and higher liquidus temperatures are encountered. The crystals present contain no significant amount of sulphur, and the more crystals present the less liquid there is to do the desulphurizing. Furthermore, as mentioned above, if crystals of a lower SiO_2 content than that of the

* Lines of equal desulphurization ratio, i.e., ratio of sulphur in slag to sulphur in metal.

mixture are present, the coexisting liquid has a higher SiO_2 content than that of the mixture.

These data of Holbrook and Joseph were obtained at 1500°C. Although the correspondence of their data with our conception of desulphurization based on liquidus data is good, their maximum for desulphurization (Fig. 11) is displaced to somewhat lower silica contents than a point on the 1500°C isotherm. This is at least partly explained by the fact that their slags contained FeO and sulphur, inasmuch as their work was done with slags in contact with a metallic phase and sulphur was added. The FeO and S present would lower liquidus temperatures and cause a displacement of the maximum in this direction.

In their study of sulphur equilibria between iron blast furnace slag and metal, Hatch and Chipman[17] concluded that the desulphurization ratio is approximately proportional on a mol percentage basis to $(CaO+2/3MgO)/(Al_2O_3+SiO_2)$; and that on a weight percentage basis, CaO and MgO are approximately equivalent. This is further corroboration of the principle that for a given Al_2O_3 content, maximum desulphurization under equilibrium conditions will occur with the liquid having the lowest silica content.

Viscosity of a Slag: The viscosity of a fused silicate is a function of the degree of polymerization of the silica. The structural element in all silicates (crystals, glasses, and melts) is the SiO_4 tetrahedron. Pure SiO_2 has to form a polymer of infinite molecular weight in order to produce this structure. In SiO_2 each O^{2-} ion is shared by two Si^{4+} ions. Only silicates with an O:Si ratio > 4 can have isolated SiO_4 tetrahedra, and for this reason such fused silicates can have a low viscosity. All other silicates contain polymer silicate units and as a first approximation their viscosity increases with increasing Si^{4+} to O^{2-} ratio.

In fused, complex aluminosilicates, AlO_4 groups form polymer units with SiO_4 groups. Hence, in the system CaO-MgO-Al_2O_3-SiO_2, Al_2O_3 as well as SiO_2 are effective in increasing viscosity. The oxides, CaO and MgO, on the other hand, lower the viscosity of liquids in this system. Therefore, for a given alumina content of a liquid in this system, the lower the silica content, the lower will be the viscosity. Bearing in mind that crystals suspended in a liquid raise the viscosity of the mixture over that of the liquid, compositions of minimum viscosity will be those which are all liquid at the temperature used (above their liquidus temperature) and which for a given alumina content contain the smallest amount of silica. On a weight percentage basis, lime and magnesia should be approximately equivalent in effect on viscosity. From the standpoint of having a slag of minimum viscosity, therefore, the optimum composition of a slag is the same as that for maximum desulphurization, a very convenient arrangement. Accurate viscosity measurements in the region of optimum blast furnace slag compositions will no doubt show that minimum viscosity and maximum desulphurization points do not exactly coincide, but they will undoubtedly be close in composition. The experimental studies of Machin, Yee, and Hanna[18, 19] on viscosity of liquids in the system CaO-MgO-Al_2O_3-SiO_2 are instructive in this connection. Their viscosity data for the system CaO-Al_2O_3-SiO_2 at temperatures from 1350° to 1500°C show clearly that viscosity of liquid decreases regularly with increase of CaO. Furthermore, isokoms are very

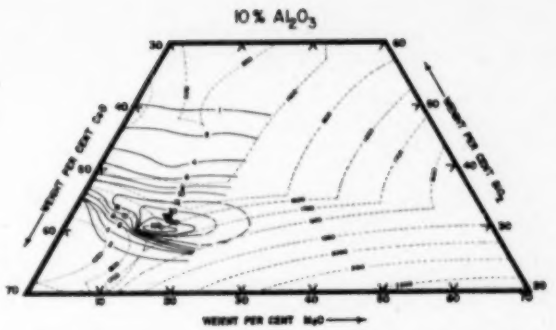

Fig. 11—Diagram of part of 10 pct Al_2O_3 plane showing relation of desulphurization data of Holbrook and Joseph[17] and of Holbrook[16] to liquidus isotherms. Dashed lines are liquidus isotherms, solid lines are isodesulphurization curves. Figures on latter represent the sulphur distribution ratio: sulphur in slag/sulphur in metal, under conditions of experiments at 1500°C. Triangle represents optimum slag region as deduced from the present study, see Fig. 13 and text.

nearly parallel to lines of equal CaO content; in other words, Al_2O_3 and SiO_2 are approximately equivalent, on a weight percentage basis, with respect to effect on viscosity. It is interesting to note from their diagrams of quaternary mixtures that on a weight percentage basis magnesia is slightly more effective than lime in lowering viscosity.

Significance of the Plateau Region: In the earlier discussion of liquidus data, attention was called to a plateau on the liquidus surface. This feature appears in the regions where melilite, merwinite, and monticellite are primary phases and stands out as a region of low liquidus slope because of the contrasting steep slope of the liquidus surfaces of the fields of dicalcium silicate and periclase. For the 10 pct Al_2O_3 plane, this plateau can be seen as a striking feature in the solid model (Fig. 10). The plateau rises gradually and narrows as it approaches the steep fronts of the dicalcium silicate and periclase fields. The optimum slag compositions lie in this upper, narrow part of the plateau where silica contents are lowest and the liquidus temperatures are still below the temperature of a slag in a furnace. Because of the existence of this plateau, considerable latitude with respect to variation in composition of a blast furnace slag is permissible. As long as the slag composition is in the plateau region, the slag will be all liquid at usual operating temperatures and there should be no furnace operational difficulties because of the slag. But if an intended slag composition is close to the steeply rising front of the dicalcium silicate or periclase fields, then trouble may result when the slag, in its normal variation in composition, becomes a little too low in silica and moves into the high liquidus region. As it does this, crystals will appear in the slag, raising the viscosity of the mixture, promoting "gumminess" and other undesirable slag characteristics. In order that a furnace be in a continually smooth working condition, the intended slag composition should be back far enough from the steep liquidus fronts that the inevitable shifts in composition will not carry it into the high liquidus region. Usual slag temperatures are sufficiently high that as long as the slag composition lies in the plateau region with respect to percentages of lime, magnesia, alumina, and silica, the slag will be all liquid.

The existence of this plateau region is highly significant with respect to the effect of increasing or

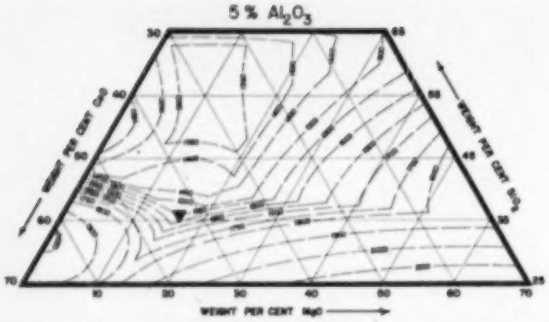

Fig. 12—Diagram of part of liquidus surface of 5 pct Al_2O_3 plane showing location of optimum blast furnace slag composition (triangle).

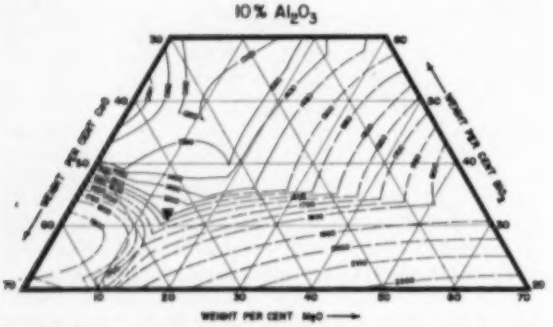

Fig. 13—Optimum blast furnace slag composition (triangle) at 10 pct Al_2O_3.

decreasing the proportion of a component in a slag, e.g., magnesia or lime. Somewhat arbitrary statements to the effect that high magnesia is beneficial or higher lime slags should be used, have little meaning without carefully considering the total composition of the slag. If the slag carries about 10 pct Al_2O_3, as an example, then by plotting the slag composition on Fig. 13, the effect of changing relative amounts of CaO, MgO, or SiO_2 is readily seen. If the slag composition lies on the right side of the plateau close to the periclase liquidus surface, then even a slight increase in MgO may increase viscosity of slag because of the appearance of periclase crystals. On the other hand, if the slag composition lies on the left side, near the dicalcium silicate surface, increase in the magnesia content, by replacing lime by magnesia on a weight percentage basis, will have no particular effect on slag properties. In this latter case, however, a "safer" slag is obtained by substituting MgO for part of the CaO and moving the composition away from the steep liquidus slope. Finally, if the slag composition lies in a central position on the plateau, changing the ratio of lime to magnesia within rather broad limits will have little or no effect on slag properties. Changing the percentage of silica of course will have.

Optimum Slag Composition at Various Alumina Levels: Blast furnace slags commonly contain alumina in the range of 10 to 15 pct, but may, when using certain ores and stone, run as high as 35 pct or lower than 10 pct alumina. The alumina content does not seem to be critical within wide limits, as discussed later, in contrast, for example, to the magnesia content. Therefore, given some particular alumina content, what, in view of the data and principles discussed above, should be the relative amounts of lime, magnesia, and silica? This can be judged by a consideration of Figs. 12 to 18. These diagrams are at 5, 10, 15, 20, 25, 30, and 35 pct alumina levels, depicting liquidus relations in a smaller area of the triangles than Figs. 3 to 9. Curves are liquidus isotherms at 50°C intervals from 1300° to 1800°C, and at 100°C intervals at higher temperatures. Straight lines at 10 pct intervals are included to facilitate estimation of compositions. On each diagram is shown a small triangle in black indicating the optimum composition of a blast furnace slag. This optimum position as shown can serve only as a guide and will be shifted, especially with respect to silica content, if unusual temperatures are used or if amounts of constituents other than lime, magnesia, alumina, and silica are unusual. That is, if temperatures are very high, as indicated for example by a very high silicon content in the metal, slag compositions can be moved to lower silica percentages, but not below the high liquidus fronts of the periclase and dicalcium fields. Or, for example, if large amounts of MnO are present, the significant lowering of liquidus temperatures caused by this component will make possible a shift of the optimum composition to lower silica values.

The optimum zone on the 5 pct Al_2O_3 plane (Fig. 12) is shown to center at 36 pct SiO_2, 16 pct MgO, and 43 pct CaO. Increasing the Al_2O_3 content to 10 pct (Fig. 13) causes an approximately corresponding decrease in SiO_2 as MgO decreases to 14 pct and CaO increases to 44 pct. In passing upward in the tetrahedron (Fig. 1) to the 15 pct Al_2O_3 plane (Fig. 14), this same trend in change of composition of the optimum point is continued as the percentage of SiO_2 changes to 28½. As Al_2O_3 increases, a complementary decrease in SiO_2 occurs for the optimum point as the re-entrant angle of the liquidus plateau shifts to a lower SiO_2 position. Concommitantly, temperatures along the narrow liquidus valley con-

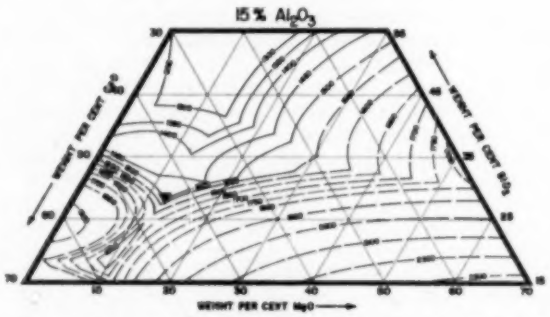

Fig. 14—Optimum blast furnace slag composition (triangle) at 15 pct Al_2O_3.

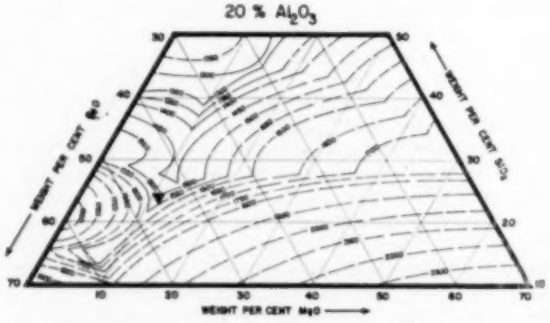

Fig. 15—Optimum blast furnace slag composition (triangle) at 20 pct Al_2O_3.

necting the merwinite plateau region with the tricalcium silicate "sink" are reduced (see Figs. 2 to 6). That is, temperatures along the periclase-dicalcium silicate boundary curve decrease with increasing Al_2O_3. On the 20 pct Al_2O_3 plane (Fig. 6), it will be noted that temperatures along this valley are less than 1600°C. Considering the effect in lowering of liquidus temperatures of the minor constituents in a blast furnace slag, a slag would probably be all liquid under usual furnace conditions if its composition lies in this valley. Hence, a 20 pct Al_2O_3 slag having highly satisfactory desulphurization and viscosity characteristics would be possible with a silica content of only 14 pct (58 pct CaO and 8 pct MgO). However, the optimum point for a slag on the 20 pct Al_2O_3 plane has been placed at 24 pct SiO_2, 11 pct MgO, and 45 pct CaO, in the low silica part of the plateau (Fig. 15), because the valley and sink areas are narrow and may not permit sufficient latitude in variation of slag composition to insure that slag compositions will remain within this liquidus valley. Similarly, on the 25 pct Al_2O_3 plane (Fig. 16), the optimum slag point might be taken at considerably lower SiO_2 and higher CaO contents than is indicated by the upper triangle, for the plateau is now coextensive with the broad valley leading to the tricalcium silicate field. The point shown as the upper triangle is located at 19 pct SiO_2, 8 pct MgO, and 48 pct CaO, but the optimum position might with safety be placed at the point indicated by the lower triangle, where the slag would be expected to have a much higher desulphurization potential and a lower viscosity. This alternate point has the composition, 12 pct SiO_2, 6 pct MgO, and 57 pct CaO. Optimum points for the 30 and 35 pct Al_2O_3 planes are located in the tricalcium silicate sink area (Figs. 17 and 18).

It should be understood that the triangles in Figs. 12 to 18 serve only as an indication of the optimum area, and might have been placed in slightly different positions. This is especially true for the high Al_2O_3 planes.

Table IX gives the compositions of optimum slag points (triangles, Figs. 12 to 18) for the various alumina levels. It will be noticed that for the usual range of alumina in a slag, about 8 to 15 pct, the variation in magnesia or in lime content for the optimum slag composition varies only slightly, centering around 14 pct MgO and 44 pct CaO. As alumina increases, magnesia decreases and lime increases. On the other hand, silica is approximately complementary to alumina, decreasing as alumina increases. If the optimum point is considered to be a circular area on an Al_2O_3 plane, the optimum slag region becomes a cylindrical volume in the tetrahedron, extending upward from the base and tilting

Table IX. Optimum Slag Composition Points Shown on Figs. 12 to 18 in Weight Percent

Al_2O_3	CaO	MgO	SiO_2
5	43	16	36
10	44	14	32
15	44	12½	28½
20	45	11	24
25	48	8	19
	(57)*	(6)	(12)
30	56	5	9
35	54	4	7

* Figures in parentheses are alternate optimum slag composition as shown in Fig. 16.

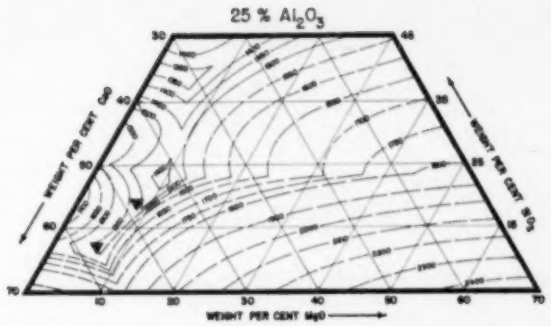

Fig. 16—Diagram of part of liquidus surface of 25 pct Al_2O_3 plane. Upper triangle is a conservative position for optimum blast furnace slag composition. Lower silica slags, however, might be practicable, and if so would be superior. Optimum composition for these latter is indicated by the lower triangle.

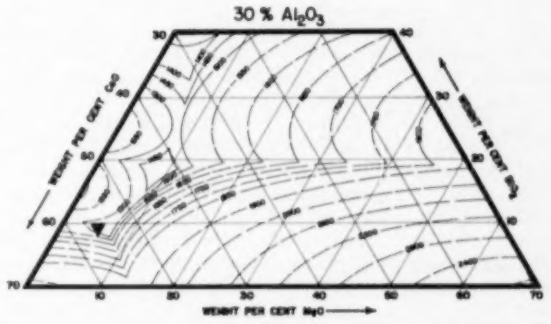

Fig. 17—Optimum blast furnace slag composition (triangle) at 30 pct Al_2O_3.

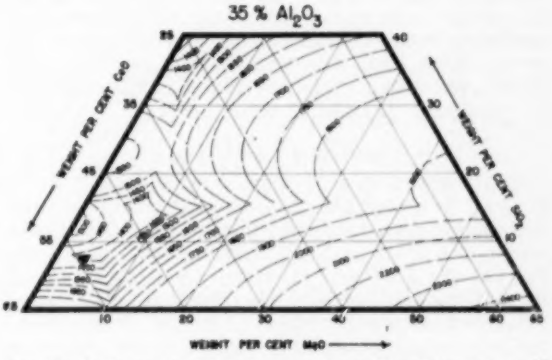

Fig. 18—Optimum blast furnace slag composition (triangle) at 35 pct Al_2O_3.

to the left (Fig. 1). For the whole series of alumina planes, total bases at the optimum points (Table IX) range between 56 and 61 pct, or for an average value the ratio of $(CaO+MgO)/(Al_2O_3+SiO_2)$ is 1:41. It will be noted that ratios in common use, which do not include Al_2O_3, such as $(CaO+MgO)/SiO_2$, have little significance except in comparing slags of similar alumina content.

Optimum Alumina Level for a Blast Furnace Slag

In the preceding discussion only the optimum point on each Al_2O_3 plane has been considered. Is there also an optimum percentage of Al_2O_3 for a blast furnace slag? Or in other words, is the opti-

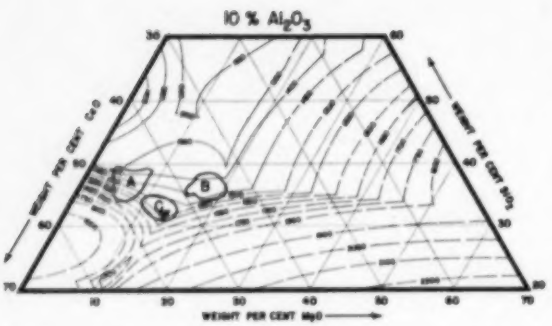

Fig. 19—Diagram of part of 10 pct Al_2O_3 plane showing location of representative blast furnace slags recalculated to 100 pct CaO + MgO + Al_2O_3 + SiO_2. Each area delimited by a heavy line (*A*, *B*, and *C*) includes daily average slag analyses from a particular furnace where Al_2O_3 was 10±1 pct.

mum point on one Al_2O_3 plane preferable to that on other Al_2O_3 planes? Both the desulphurization data of Hatch and Chipman[17] and the viscosity studies of Machin and Yee[15] suggest that Al_2O_3 and SiO_2 are approximately equivalent with respect to desulphurization and viscosity. It would seem, therefore, that as long as the same $(CaO+MgO)/(Al_2O_3+SiO_2)$ ratio is maintained, the Al_2O_3 content is not critical. This ratio at the optimum point is approximately the same on all but the highest Al_2O_3 planes. On the other hand, the incomplete data of Holbrook and Joseph[15] and of Holbrook[16] suggest that for slags of optimum composition with respect to CaO, MgO, and SiO_2, the desulphurization ratio is at a maximum at about 10 pct Al_2O_3. Their data, however, do not extend to sufficiently low SiO_2 percentages at the lower MgO levels to prove that this indication is valid. On the basis of available data, it is possible to conclude that the Al_2O_3 content of a slag is not significant from the standpoint of slag properties, providing the CaO, MgO, and SiO_2 percentages can be adjusted to those of the optimum composition for the particular Al_2O_3 level being used.

Actual Slag Compositions

Blast furnace slags employed during the making of iron for open hearth furnaces contain of the order of 5 pct of minor constituents, or in other words, the total of lime, magnesia, alumina, and silica is about 95 pct. In order to use the diagrams to show the position of a slag, the four major constituents should be recalculated to 100 pct and plotted on the appropriate diagram. A simple, approximate method, whereby the percentage of the minor constituents is roughly apportioned among the four major oxides, requiring no complicated calculation, is sufficient for most purposes in view of the normal variations in slag composition. The alumina content after recalculation will determine the appropriate diagram to use for the plotting. The diagrams are spaced at 5 pct Al_2O_3 intervals (Figs. 12 to 18), and the diagram to use will of course be the one to which the alumina content of the slag most nearly corresponds. (If the alumina content lies about half way between that of two diagrams, a new diagram can be made by interpolation, to use in plotting. There are no abrupt changes in optimum slag composition with changing alumina content, but rather the point changes in position in a regular manner.) Using the 10 pct Al_2O_3 plane as an example, in Fig. 19 daily average slag analyses from three furnaces have been plotted. The slags plotted all contained 10± 1 pct Al_2O_3 on a recalculated basis (analyses which when recalculated contained more or less than this amount of Al_2O_3 were not plotted on this diagram). Slags from each furnace lie within the area included within the heavy line. It will be noted that slags from furnace *C* include and surround the optimum point. These would be expected, from the foregoing, to be excellent slags, and they have been found to be so. Slags from furnaces *A* and *B* lie at some distance from the optimum point and have the expected disadvantages. They cannot be as efficient desulphurizers, and in attempts to increase the desulphurization by increasing the basicity, high liquidus temperatures, and therefore troublesome slags, are encountered.

The actual slags plotted in Fig. 19 show that on a recalculated basis slags are used having a liquidus temperature close to or even above 1600°C. Slag temperatures are of the order of 100°C lower than this. The minor constituents in the slags act as fluxes lowering the liquidus temperature below that which would obtain if the slag were composed only of the four major components. On the basis of measurements of liquidus temperature of actual slags,† this liquidus temperature lowering is estimated to be of the order of 100°C on the steep liquidus slopes of the periclase and dicalcium silicate fields, and somewhat less in the plateau region. The minor constituents act in the main to give a general lowering of the liquidus surface without affecting the overall configuration, or relationship, of slopes. If, however, one or more additional oxides are present in relatively large amounts, for example MnO, then lowering of liquidus temperatures and shifting of positions of liquidus slopes may be of a sufficiently high order that these diagrams can serve as only a very rough guide. In this case, additional liquidus measurements of mixtures approaching these slags in composition should be made to find the order of magnitude of the change in liquidus relationships caused by these large departures of the slag from compositions in the quaternary system CaO-MgO-Al_2O_3-SiO_2. The non-noble gas configuration of Fe^{2+} and Mn^{2+} along with their relatively low field strengths suggest that these two ions are good fluxes. Therefore, for a given alumina content, the percentage of silica can be lower, the greater the amount of these ions present, without moving into high liquidus regions where excessive temperatures are required to melt the crystalline phases.

† Accurate measurement of liquidus temperature on small, laboratory samples of an actual slag are exceedingly difficult owing to the virtual impossibility of maintaining a constant composition, especially with respect to the percentage of FeO and sulphur in the melt.

Summary

Liquidus data are presented for 446 mixtures in the quaternary system CaO-MgO-Al_2O_3-SiO_2, prepared at 5 pct Al_2O_3 intervals over the range of 5 to 35 pct Al_2O_3. The liquidus temperature, primary crystalline phase, and refractive index of the glass are given. On the basis of these data, along with previously published information, liquidus diagrams are presented for the seven triangular joins, or "Al_2O_3 planes," at 5, 10, 15, 20, 25, 30, and 35 pct Al_2O_3. Isotherms for the liquidus surface, and primary phase fields are shown. The diagrams thus show, for a particular Al_2O_3 content, the effect of changes of relative percentages of CaO, MgO, and SiO_2 on the temperature of complete melting of a mixture.

A blast furnace slag to be most effective and practicable must be completely liquid, i.e., its liquidus temperature must be below that of the temperature to which it is heated in the furnace. Assuming as a first approximation that blast furnace slags are composed entirely of CaO, MgO, Al_2O_3, and SiO_2, and assuming a temperature of 1500°C, practical slag compositions lie in those areas on the diagrams where liquidus temperatures are lower than 1500°C. The optimum composition of a slag lying in this area on any particular Al_2O_3 plane is that point of lowest SiO_2 content; for this slag will have maximum desulphurization potential and minimum viscosity. On a second series of diagrams, this point of optimum composition is shown. The point lies on the low silica side of a "plateau region" on the liquidus surface, most clearly shown on three-dimensional models (see Fig. 10). For the usual range of Al_2O_3 in a slag, about 8 to 15 pct, the variation in MgO or CaO for optimum slag composition varies only slightly, centering around 14 pct MgO and 44 pct CaO. SiO_2 is approximately complementary to Al_2O_3, being 32 pct at 10 pct Al_2O_3, and decreasing as Al_2O_3 increases.

Blast furnace slags may be recalculated to 100 pct $CaO+MgO+Al_2O_3+SiO_2$ and plotted on the appropriate Al_2O_3 diagram for comparison of their compositions with that of the optimum point. Where this has been done it was found that slags are used having liquidus temperatures, on the basis of the four components, of 1600°C or slightly higher. Slag temperatures are of the order of 100°C lower than this. The minor components in the slag have the effect of lowering liquidus temperatures about 100°C in the periclase and dicalcium silicate fields.

Acknowledgment

This study represents a research project sponsored by the Bethlehem Steel Co. in the College of Mineral Industries. The authors wish to acknowledge the assistance in this research of the following graduate and research assistants: Ann P. Comer, W. E. Counts, F. P. Glasser, Guy Ervin, Jr., Pasquale Licastro, Elizabeth A. Myers, Bernard Roesch, and Charlotte M. Warshaw.

References

[1] E. F. Osborn and J. F. Schairer: The Ternary System Pseudo-Wollastonite-Akermanite-Gehlenite: *American Journal of Science* (1941) Folio **239**, pp. 715-763.

[2] R. W. Ricker and E. F. Osborn: Additional Phase Equilibrium Data for the System CaO-MgO-SiO_2. Abstract, *Bull.* Amer. Ceramic Soc. (1952) **31**, p. 106.

[3] J. F. Schairer: The System CaO-FeO-Al_2O_3-SiO_2: I, Results of Quenching Experiments on Five Joins. *Journal* Amer. Ceramic Soc. (1942) **25**, pp. 241-274.

[4] Olaf Andersen: The System Anorthite-Forsterite-Silica. *American Journal of Science* (1915) 4th Series, **39**, pp. 407-454.

[5] H. F. McMurdie and H. Insley: Studies on the Quaternary System CaO-MgO-$2CaO \cdot SiO_2$-$5CaO \cdot 3Al_2O_3$. *Journal of Research* Nat. Bur. of Standards (1936) **16**, pp. 467-474.

[6] E. F. Osborn: The System $CaSiO_3$-Diopside-Anorthite. *American Journal of Science* (1942) **240**, pp. 751-778.

[7] A. T. Prince: Phase Equilibrium Relationships in a Portion of the System MgO-Al_2O_3-$2CaO \cdot SiO_2$. *Journal* Amer. Ceramic Soc. (1951) **34**, pp. 44-51.

[8] E. F. Osborn and D. B. Tait: The System Diopside-Forsterite-Anorthite: *American Journal of Science* (1952) Bowen Volume, pp. 413-433.

[9] G. A. Rankin and F. E. Wright: The Ternary System CaO-Al_2O_3-SiO_2. *American Journal of Science* (1915) **39**, pp. 1-79.

[10] G. A. Rankin and H. E. Merwin: The Ternary System CaO-Al_2O_3-MgO. *Journal* ACS (1916) **38**, pp. 568-588.

[11] G. A. Rankin and H. E. Merwin: The Ternary System MgO-Al_2O_3-SiO_2. *American Journal of Science* (1918) **45**, pp. 301-325.

[12] N. L. Bowen and J. W. Greig: The System Al_2O_3-SiO_2. *Journal* ACS (1924) **7**, pp. 238-254.

[13] J. W. Greig: Immiscibility in Silicate Melts. *American Journal of Science* (1927) **13**, pp. 1-44, 133-154.

[14] M. L. Keith and J. F. Schairer: The Stability Field of Sapphirine in the System MgO-Al_2O_3-SiO_2. *Journal of Geology* (1952) **60**, pp. 181-186.

[15] W. F. Holbrook and T. L. Joseph: Relative Desulphurizing Powers of Blast Furnace Slags. *Trans.* AIME (1936) **120**, pp. 99-117.

[16] W. F. Holbrook: Relative Desulphurizing Powers of Blast-Furnace Slags, II. *Trans.* AIME (1938) **131**, pp. 127-138.

[17] G. G. Hatch and J. Chipman: Sulphur Equilibria Between Iron Blast Furnace Slags and Metal. *Trans.* AIME (1949) **185**, pp. 274-284; JOURNAL OF METALS (April 1949).

[18] J. S. Machin and T. B. Yee: Viscosity Studies of System CaO-Al_2O_3-SiO_2. *Journal* Amer. Ceramic Soc. (1948) **31**, pp. 200-204.

[19] J. S. Machin, T. B. Yee, and D. L. Hanna: Viscosity Studies of System CaO-MgO-Al_2O_3-SiO_2; III, 35, 45, and 50 Pct SiO_2. *Journal* Amer. Ceramic Soc. (1952) **35**, pp. 322-325.

Technical Note

Magnetic Transformation of Iron in Copper Matrix At Low Temperatures

by R. E. Cech and D. Turnbull

EXPERIMENTAL studies of precipitation of iron from solid solution in copper by Gordon and Cohen,[1] Bitter and Kaufmann,[2] and Smith[3] revealed that the precipitate particles were initially paramagnetic but could be changed to a ferromagnetic

R. E. CECH, Junior Member AIME, and D. TURNBULL, Associate Member AIME, are associated with the General Electric Research Laboratory, Schenectady.

TN 203E. Manuscript, Oct. 10, 1953.

Table I. Effect of Liquid Nitrogen Quench (from 27°C) on Magnetic Force in Specimens Aged Various Times at 700°C. Homogenization Treatment, 17 hr at 1040°C

Time (in Hr) of Aging at 700°C	Magnetic Force (M.F.) at Room Temperature (300°K)	
	After Aging Treatment	After Quenching Aged Specimens to −196°C
0.67	0.1	0.4
5.0	0.1	0.5
7.75	0.3	0.6
23.	0.5	0.7

form by cold working or by extended aging at elevated temperatures. It was concluded from the results of X-ray diffraction studies[3] that the magnetic change was coincident with the transition from face-centered cubic to body-centered cubic structure in the precipitate.

They also found that an increase in magnetic precipitate could be effected by aging a partially precipitated cold worked specimen. This result was presumed to be due to growth of body-centered cubic iron particles.

The conclusion that these changes in magnetic properties are coincident with the γ to α phase change in the precipitate has sometimes been questioned on the basis that small particles of the α phase may be nonferromagnetic. Also the evidence[3] supporting the conclusion is quite indirect. This note will report some further observations that may have a significant bearing on the interpretation of the magnetic transformation in this system.

An alloy of 2.5 pct Fe, balance copper, was prepared by melting OFHC copper and electrolytic iron under a hydrogen atmosphere and pouring into a 1 in. graphite mold. The iron was added as pressed powder mixed with an equal amount of copper powder. Slices were cut from near the bottom of the ingot for specimens. Chemical analysis of turnings from metal adjacent to the specimens indicated an iron content of 2.54 pct.

The magnetic apparatus measured qualitatively the force of magnetic attraction at a fixed position in a nonuniform magnetic field. In one set of experiments this was simply a scale which measured the force required to pull the sample off a plastic spacer on the pole of a strong permanent magnet. In a series of corroborative experiments,[4] an apparatus patterned after one constructed by Buell and Wulff[5] was used to measure the force of attraction on the specimen exerted by a magnetic field. In both cases the measured force was the sum of the paramagnetic attraction of the matrix and ferromagnetic attraction of the precipitate. The qualitative findings of this investigation would not be altered by the diamagnetism or paramagnetism of the matrix, however.

Several different specimens were aged for various times at 700°C and then cooled to 27°C. The aging times and the resulting magnetic forces (magnetic force = M.F.; all M.F. values measured at 27°C) are shown in Table I. It was discovered that M.F. (see Table I) for these specimens was markedly increased after quenching to −196°C. For example, M.F. increased from 0.1 to 0.5 as a result of the −196°C quench for the specimen aged 5 hr at 700°C. Our interpretation is that the −196°C quench causes transformation of part of the nonferromagnetic (*nf*) "phase" to the ferromagnetic (*f*) "phase." The low temperature treatment did not cause complete transformation of *nf* to *f*, however, since cold working a quenched specimen at room temperature increased M.F. by a factor of 10. The treatment of the specimen that was cold worked and the resulting values of M.F. (shown in parentheses) were as follows:

Homogenized 17 hr at 1040°C → Aged 23 hr at 700°C → Cooled to 27°C (M.F. = 0.5) → After −196°C quench (M.F. = 0.7) → Cold worked at 27°C (M.F. = 5.0) → After −196°C quench (M.F. = 6.2).

A major fraction of the transformation below 27°C takes place upon quenching to −79°C, as the following summary of experiments and results shows:

Homogenized 1 hr at 1020°C → Aged 60 hr at 500°C → Cooled to 27°C (M.F. = 4.75) → After quench to −79°C (M.F. = 8.65) → After quench to −196°C (M.F. = 9.65).

Very short heat treatments at temperatures exceeding the transformation temperature causes reversion of *f* to *nf* but does not effect resolution of the major part of the iron. After cooling to room temperature, most of the iron remains in the *nf* phase but a large fraction of this *nf* transforms to *f* upon quenching to 196°C. The experiments and results on which these conclusions are based are summarized as follows:

Homogenized 1 hr at 1020°C → Aged 60 hr at 500°C → Cooled to 27°C (M.F. = 5.3) → Aged 17 hr at 27°C (M.F. = 6.7) → 1040°C for 40 sec → cooled to 27°C (M.F. = 0.95) → After −196°C quench (M.F. = 4.25).

These results also show that a small amount of *nf* reverts to *f* upon aging at 27°C.

The results of the corroborative experiments by Rocco,[4] using the apparatus of Buell and Wulff, were qualitatively similar to those reported here.

It appears that our results are consistent with the concept that the transformation *nf* → *f* corresponds to the structural transformation $\gamma\ (nf) \rightarrow \alpha\ (f)$. Since partial transformation *nf* → *f* is effected either by quenching to low temperature or by cold working, the transition may be of the martensitic type.

Summary

1—The iron-rich precipitate in a Cu-2.54 pct Fe alloy can be caused to transform by subcooling below room temperature. The extent of transformation is increased as temperature of subcooling is increased.

2—Subcooling after a large fraction of precipitate has been transformed by cold working causes further transformation of residual γ precipitate.

3—Aging at room temperature causes a small amount of γ to α transformation to occur.

Acknowledgment

The authors are indebted to W. A. Rocco for performing a separate set of experiments to check the results reported here.

References

[1] R. B. Gordon and M. Cohen: Age Hardening of a Copper Cobalt and a Copper Iron Alloy. *Symposium Age Hardening of Metals.* (1940) p. 161. ASM.

[2] F. Bitter and A. R. Kaufmann: Magnetic Studies of Solid Solutions. *Physical Review* (1939) **56**, p. 1044.

[3] C. S. Smith: Structure and Ferromagnetism of Cold Worked Copper Containing Iron. *Physical Review* (1940) **57**, p. 337.

[4] W. A. Rocco: Unpublished results.

[5] R. Buehl and J. Wulff: A Simple Magnetic Apparatus for Phase Transformation Studies of Ferrous Alloys. *Review of Scientific Instruments* (1938) **9**, p. 224.

Solidification of Aluminum-Rich Aluminum-Copper Alloys

by Arthur B. Michael and Michael B. Bever

The solidification of aluminum-rich aluminum-copper alloys was investigated for different solidification rates. The measured amounts of nonequilibrium eutectic were compared with the amounts calculated on the assumption of no diffusion in the solid. The morphology of the eutectic was studied and dendritic spacings were measured. Compositions of the cored primary solid solutions were determined by quantitative autoradiography after activation of the solute copper by neutron irradiation.

CONSIDERABLE progress has been made in recent years toward an understanding of the solidification of metals. This is especially true for the factors involved in nucleation, the controlled growth of metal crystals from melts, and various aspects of the freezing of ingots and castings. Many features of the solidification process, however, are not understood adequately and much further work is required.

In the research reported here the solidification of a series of aluminum-rich aluminum-copper alloys was investigated. Different degrees of deviation from the idealized case of equilibrium solidification were attained by varying the rate of solidification. Thermal analysis and microscopic examination were supplemented by lineal analysis and autoradiography. The latter required the use of radioactive tracers and was adapted to the quantitative determination on a microscale of concentrations of copper dissolved in aluminum. The tracers were produced *in situ* by activating the copper with neutrons. These techniques permitted a correlated interpretation of the temperature-time history, the amounts of nonequilibrium eutectic and the general morphology of the alloys, and yielded quantitative data on microsegregation.

Nonequilibrium Solidification

In the general case of the solidification of a solid solution in accordance with the phase diagram, the composition of the coexisting liquid and solid must change continuously. This change requires diffusion, which at best remains incomplete in the solid during solidification. The resulting inhomogeneity of the solid solution crystals is well-known as coring, dendritic segregation, or microsegregation.

The generally accepted analysis of coring assumes that, 1—no diffusion occurs in the solid, 2—diffusion is complete in the liquid, and 3—the composition of the solid formed on cooling through any infinitesimal temperature interval is given by the solidus of the phase diagram. On this basis,

$$\ln \frac{m_L}{m_o} = \int_{x_L}^{x_o} \frac{dx_L}{x_L - x_s} . \qquad [1]$$

In this equation m designates mass, x designates the concentration of solute and the subscripts L and S refer to the liquid and solid phases, respectively; the subscript o indicates the initial state, in which the liquid is identical with the entire system. Eq. 1 or its equivalent has been derived repeatedly[1-7] and an analogous equation, known as Rayleigh's equation, has been used for distillation.[8] The assumptions on which Eq. 1 is based do not include an infinitely fast cooling rate as sometimes stated. In fact, Olsen and Hultgren[6] have shown by experiment that very high solidification rates suppress coring, presumably by preventing diffusion in the liquid and by the effect undercooling has on the composition of the nucleus. Coring thus occurs at rates of cooling which are too fast for a close approach to equilibrium in the solid and too slow to suppress diffusion in the liquid and to cause marked undercooling.

If the liquidus and solidus approximate straight lines, Eq. 1 simplifies to

$$\frac{m_L}{m_o} = \left(\frac{x_o}{x_L} \right)^{(x_L)/(x_L - x_S)} . \qquad [2]$$

The fraction of liquid present at any temperature during nonequilibrium solidification can be calculated from Eqs. 1 or 2. By the lever relation it is

A. B. MICHAEL, Junior Member AIME, formerly Research Assistant at M.I.T., is now associated with the Research Dept., Allis-Chalmers Manufacturing Co., Milwaukee, Wis., and M. B. BEVER, Member AIME, is Associate Professor, Dept. of Metallurgy, Massachusetts Institute of Technology, Cambridge, Mass.

Discussion on this paper, TP 3662E, may be sent, 2 copies, to AIME by April 1, 1954. Manuscript, July 14, 1953. New York Meeting, February 1954.

This paper is based on a thesis by A. B. Michael submitted in partial fulfillment of the requirements for the degree of Doctor of Science to the Massachusetts Institute of Technology.

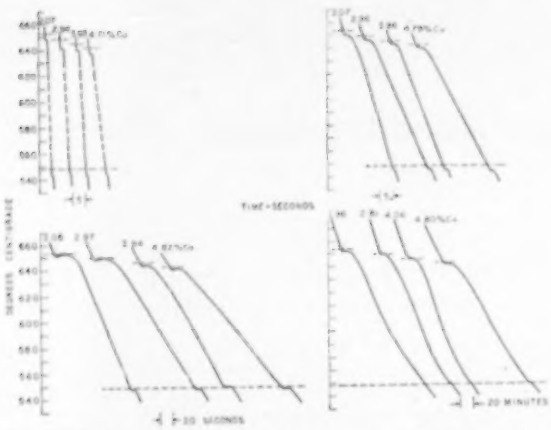

Fig. 1—Cooling curves for aluminum-copper alloys, containing nominally 2, 3, 4, and 5 pct Cu.

possible to determine the average composition $\overline{x_s}$ of the solid. Values of $\overline{x_s}$ for different temperatures constitute the nonequilibrium solidus of an alloy of given composition x_o.

The nonequilibrium solidification of a solid solution terminates in a manner which depends on the type of system. In the case of complete miscibility in the liquid and solid, the final solid forming according to Eq. 1 has the composition of the lower melting component.[4] If the two-phase field for the coexisting solid and liquid solutions is bordered on the low temperature side by an invariant reaction, such as a eutectic, nonequilibrium solidification makes a larger amount of liquid available for that reaction than would be the case under equilibrium conditions. Consequently larger amounts of eutectic form and eutectic is found in alloys of compositions for which the equilibrium diagram indicates only the presence of a terminal solid solution.[4, 10] Corresponding considerations apply to systems in which peritectic reactions occur.

Calculations by Eqs. 1 or 2 represent extreme conditions inasmuch as they are based on the assumption of complete lack of diffusion in the solid. Since the structures originating by a reaction such as a eutectic can be measured by quantitative metallography, it is possible to compare actual with calculated amounts. Some comparative data of this kind have been published.[6]

Gulliver[4] considered the case of solidification of a eutectiferous alloy at a rate permitting partial approach to equilibrium in the solid. His analysis involves a solidification factor Z which is introduced into Eq. 2 as follows:

$$\frac{m_L}{m_o} = \left(\frac{x_o - Z}{x_L - Z}\right)^{(\alpha_L - \beta)/(\alpha_L - \alpha_S)} \quad [3]$$

By determining Z experimentally, nonequilibrium solidus curves for a given alloy can be calculated for various rates of cooling. Z is taken independent of temperature and has the units of concentration. For a eutectiferous alloy Z can vary between zero and the overall composition of the alloy, x_o, provided the latter is less than the maximum solid solubility at the eutectic temperature.

The determination of concentration gradients in cored solid solutions is of interest, but few suitable techniques are available. Brenner and Kostron[11] obtained quantitative data on concentration gradients in the solid solutions of cast aluminum alloys containing 4 pct Cu. They found the distribution of copper within various grains from microhardness readings, which they converted to concentrations by a calibration based on homogeneous standard samples. Microhardness measurements, however, cannot give a continuous indication of the concentration, especially since indentations must not be spaced too closely to each other. Coring in solid solutions has also been studied by microradiography, but no quantitative use of this method appears to have been made.

In addition to altering the phase relations from those of the equilibrium diagram, solidification under various conditions of cooling also produces characteristic grain structures. No attempt will be made here to review the many observations on the morphology of cast metals. For the configuration of eutectics, such as the divorcement of eutectics, observed in the present investigation, the literature should be consulted.[12] The investigation of dendrite formation by Alexander and Rhines will be discussed below.[13]

Aside from their intrinsic interest, coring and the formation of excess constituents in nonequilibrium solidification are of practical importance. If cast alloys require homogenization, the length of the anneal is determined by the severity of microsegregation. If coring results in the presence of lower melting constituents, the safe upper temperature limit for annealing is lowered. For example, the presence of a eutectic may cause partial melting in an alloy which according to the phase diagram should be exclusively a solid solution having a higher solidus temperature. The presence of a second phase also affects mechanical properties and perhaps feeding during solidification. Possible subtle effects of the inhomogeneity of cored solutions on stress conditions, corrosion behavior, and microporosity have not yet been explored.

Table I. Data on the Controlled Solidification of Aluminum-Copper Alloys

Sample	Cu, Wt Pct, x_o	Time of Solidification, Sec	Solidification Index, °C per Sec
a	2.07	~2	53
c	2.07	20	5.3
b	2.08	120	0.87
w	1.96	7440	0.014
k	2.94	6	16.2
m	2.96	22	4.6
l	2.97	156	0.69
v	2.81	6360	0.016
d	3.93	~2	49
f	3.96	20	5.0
e	3.94	110	0.85
u	4.06	5640	0.017
p	4.71	6	15.7
o	4.79	26	3.73
n	4.82	168	0.58
s	4.80	7800	0.012

Procedure of Solidification Experiments

Master alloys of nominally 2, 3, 4, and 5 pct Cu were prepared under controlled conditions from aluminum, containing less than 0.0025 pct analyzed impurities, and copper made by the process of Smart, Smith, and Phillips,[14] which presumably was 99.999 pct pure. Melts of 30 grams of these alloys were made under argon in alumina crucibles. To obtain solidification rates (or solidification indices as defined below) of approximately 50°, 5°, and 0.8°C per sec, the alloys were poured through air into cylindrical steel molds coated with an alumina slurry and preheated to appropriate temperatures. This method

of casting did not cause appreciable oxidation. To obtain a rate (or index) of solidification of the order of 0.01°C per sec, the alloy was made to solidify under argon in the crucible, held in a resistance furnace to which a suitable amount of power was supplied. The liquid alloy was stirred immediately before pouring into the steel mold or before solidification in the crucible. Without this precaution, segregation occurred; for example, an alloy solidified in the crucible and having an overall copper content of 4.5 pct analyzed 8 pct Cu at the bottom and 2 pct at the top of the ingot; stirring reduced the difference in composition of the top and bottom sections to less than one-twentieth of the overall composition.

Continuous records of the cooling curves were obtained by a Leeds and Northrup Speedomax recorder, except for the fastest cooling rate. In the latter case, the liquidus and solidus temperatures were determined separately by setting the recorder in advance to the approximate liquidus temperature and repeating the operation for the solidus under otherwise identical conditions. For the rapid cooling rates a very small thermocouple bead of No. 28 chromel-alumel wire was used without protection to assure rapid response. Separate experiments had shown that protected and unprotected beads gave identical readings during short periods of immersion in liquid aluminum-copper alloys. To prevent possible errors caused by protracted immersion, a coated bead was used for the slowest cooling rate. The beads were placed in the center of the molds or crucibles and all determinations of chemical composition and of structural features were made on samples taken from the adjoining region.

Experiments were conducted to determine the effect of superheating temperatures and times on undercooling. Holding at 720°C up to 14 hr caused no measurable undercooling attributable to that cause. After superheating to higher temperatures undercooling was appreciable; for example, after heating to 920°C for 1 hr, undercooling of 10°C was observed. A maximum temperature of 700°C, therefore, was adopted for the remelting of the master alloys.

Results of Thermal Analysis

Table I gives the exact compositions of the alloys and times of solidification. Cooling curves are shown in Fig. 1, in which the equilibrium liquidus and solidus temperatures are indicated by dashed lines. For the interpretation of the effects of cooling rate, a "solidification index" is defined as the difference between the observed liquidus and solidus temperatures divided by the total time of solidification. This index has the dimensions of a cooling rate, but also reflects any isothermal part of the solidification process. In the discussions which follow the terms "index" and "rate" will be used interchangeably. Values of the solidification index are included in Table I.

All cooling curves, except that for the 2 pct Cu alloy, solidified at the slowest rate (solidification index of 0.014°C per sec) have an approximately horizontal portion, indicating an invariant reaction, at about 548°C which is the eutectic temperature.[16] Metallographic examination of the 2 pct alloy revealed a small amount of eutectic, but this apparently was not large enough for detection by thermal analysis. For a given solidification index the eutectic hold increases with the copper content. However, the length of the hold gives only an approximate indication of the amount of eutectic when comparing different alloys because the size of the melts and other factors were not kept strictly identical.

Undercooling up to 5°C was found for the eutectic reaction with the higher solidification rates. Undercooling below the liquidus temperature was also observed and reached 7°C. The amounts of undercooling decreased with decreasing solidification rates.

Another characteristic of the cooling curves is an approximately horizontal portion near the liquidus; the alloys solidified at slow rates also tended to show recalescence. These observations may be explained by a transient balance at the thermocouple bead between the evolution of the heat of solidification and heat losses to the surroundings.

Determination of Nonequilibrium Eutectic

A detailed examination was made of the amounts and characteristics of the eutectic. In some samples the eutectic was divorced and the secondary κ (aluminum-rich) solid solution could not be distinguished from primary κ. The amount of θ phase rather than the eutectic, therefore, was measured by lineal analysis. Six traverses were made on each sample with a Hurlbut counter[18] at a magnification of 1400X, resulting in standard errors of the mean of 3 pct or less.

The volume percentage of θ was converted into weight percentage using an average value[17, 18] of 4.40 grams per cu cm for its density. The densities of some samples were measured but were not sufficiently reproducible because of a small amount of

Table II. Data on the Amount of Nonequilibrium Eutectic in Cast Aluminum-Copper Alloys

Sample	Density of Alloy, d, Grams per Cu Cm	θ, Vol. Pct, V_θ	θ, Wt Pct, W_θ	Eutectic in Alloy, P_E, Wt Pct	Nonequilibrium Solidus, Pct, Cu at Eutectic Temperature, $x_E{}^\theta$	Calculated Max. Pct Eutectic, $P_E{}^{max.}$	Calculated Nonequilibrium Solidus, Pct, Cu at Eutectic Temperature	Gulliver's Solidification Factor, Z, in Pct Cu
a	2.76	0.99	1.58	2.71	1.21	3.50	0.95	0.55
c	2.76	0.70	1.12	1.92	1.46	3.50	0.95	1.05
b	2.76	0.52	0.83	1.42	1.63	3.52	0.95	1.30
w	2.76	0.34	0.385	0.66	1.76	3.30	0.90	1.60
k	2.78	1.72	2.72	4.67	1.47	5.36	1.24	0.50
m	2.78	1.39	2.20	3.78	1.78	5.40	1.25	1.05
l	2.78	1.36	2.15	3.69	1.82	5.40	1.25	1.20
v	2.78	0.935	1.48	2.54	2.03	5.10	1.19	1.55
d	2.80	2.67	4.19	7.18	1.70	7.60	1.54	0.40
f	2.80	2.58	4.05	6.95	1.78	7.65	1.56	0.55
e	2.80	2.12	3.33	5.72	2.19	7.60	1.54	1.25
u	2.80	1.30	2.04	3.50	3.02	7.90	1.58	2.50
p	2.82	3.60	5.62	9.64	1.70	9.60	1.71	0.05
o	2.82	3.61	5.63	9.66	1.76	9.71	1.76	0.10
n	2.82	3.47	5.42	9.30	1.92	9.72	1.80	0.35
s	2.82	1.88	2.94	5.05	3.30	9.71	1.96	2.60

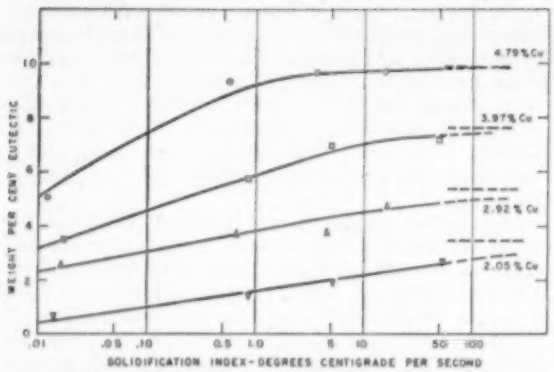

Fig. 2—Weight percent eutectic, P_E, vs solidification index for aluminum-copper alloys. The copper contents stated in the figure are averages of values given in Table I.

unavoidable porosity. The overall density of the samples, therefore, was assumed to be equal to that of a homogeneous solid solution of the same chemical compo ition. The values were computed from published lattice constant data.[20] Since the samples also contain some θ phase, a small error is introduced by this assumption, but can be shown to be less than 2 pct. Table II gives the values of the volume percentage of θ, V_θ, the values of the calculated densities of the alloys, d, and weight percentage of θ, w_θ.

The measured amounts of nonequilibrium eutectic may be compared with the theoretical maximum amounts, P_E^{max}. On the aluminum-rich side of the aluminum-copper system, the liquidus and solidus can be considered as straight lines so that Eq. 2 may be used. The weight percentage of θ phase can be converted to the percentage of eutectic present at the eutectic temperature if it is assumed that for nonequilibrium solidification the compositions of the θ and κ phases in the eutectic are given by the phase diagram, that is, the θ and κ phases contain 52.5 and 5.7 wt pct Cu, respectively. The weight percentage of eutectic, P_E, calculated in this manner is given in Table II. From these values the nonequilibrium solidus $\bar{x}_E^E$ at the eutectic temperature was found and the resulting values are included in Table II.

Fig. 2 is a plot of measured amounts of eutectic, P_E, vs the solidification index. The amount of eutectic increases with increasing solidification index for all compositions investigated. Also for a given solidification index the observed eutectic is a larger fraction of the theoretical amount the higher the copper content of the alloy. The theoretical maximum amount of eutectic, P_E^{max}, shown by dashed lines in Fig. 2, is approached more rapidly the higher the copper content of the alloy and the theoretical maximum amount is almost reached with high solidification indices. A striking feature is that, even for low solidification rates, the cast alloys contain an appreciable quantity of eutectic.

For calculating the nonequilibrium solidus over the entire temperature range of solidification Eq. 3 was used. From the values of the percentage of eutectic, P_E, at the eutectic temperature and the composition of the alloy, x_o, it is possible to find Gulliver's solidification factor Z.[1] This is most readily done by plotting Z as a function of the percentage of eutectic, P_E, for different values of x_o, as shown in Fig. 3. Then using this value of Z and Eq. 3 the nonequilibrium solidus can be found by calculating the fraction of liquid for various values of x_L. Fig. 4 shows the calculated nonequilibrium solidus for the 3 pct Cu alloy for values of Z equal to 0, 0.5, and 1.2. These values of Z correspond to solidification indices represented by a cooling rate which suppresses diffusion in the solid entirely and by solidification indices of 16.2° and 0.69°C per sec, respectively.

Morphology of the Cast Structures

The structures of the samples were studied by examining the grain size, the dendrite spacing, the dispersion of the nonequilibrium eutectic, and the configuration of its constituents.

The grains ranged from almost entirely columnar to almost entirely equiaxed for the highest and lowest solidification indices, respectively. All samples were coarse-grained, but the grain size did not vary systematically with solidification index or alloy content. Because of variations within a single sample, and in some instances, the presence of columnar grains, definite values of grain size could not be assigned. As a rough approximation, the cross-sectional area of a typical grain may be considered to be about 9 sq mm.

The metallographic study of dendrites is complicated as a two-dimensional cross section gives only incomplete information for a three-dimensional structure. The work of Alexander and Rhines[18] demonstrates that it is possible to obtain significant data for dendrites by selecting from any given microsection prominent dendrite formations having maximum spacings. Average values of the dendrite branch spacings obtained in this way are given in Table III. This dendrite spacing is defined as the distance between the center lines of neighboring branches of a dendrite having a prominent axis in the plane of polish.

The measurements show that the dendrite spacing increases with decreasing rate of solidification. This finding agrees with the results of Alexander and Rhines[18] for aluminum alloys containing 5, 10, and 20 pct Cu, solidified at rates that were known only qualitatively. They also observed an increase in

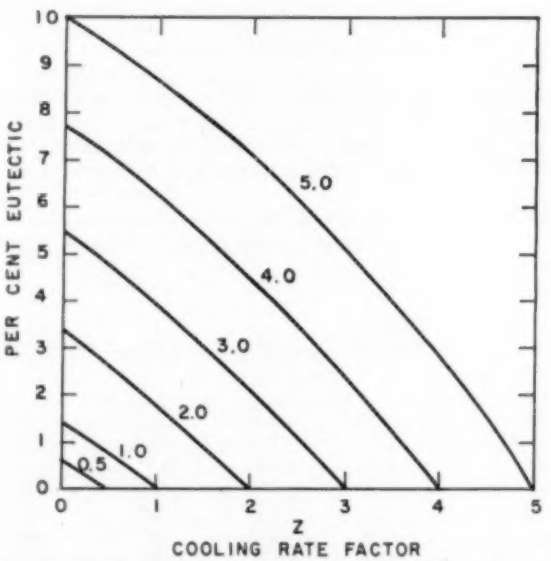

Fig. 3—Weight percent eutectic, P_E, vs calculated values of Gulliver's solidification factor Z (in pct Cu) for aluminum-copper alloys containing 0.5, 1, 2, 3, 4, and 5 pct Cu.

Table III. Data on Morphological Observations

Sample	Dendrite Spacing, Microns	Mean Distance Between θ Particles, Microns	Mean Linear Size of θ Particles, Microns
a	12	175	1.7
c	24	320	3.6
b	63	620	3.2
w	250	1530	3.7
k	23	115	2.0
m	35	198	2.8
l	81	181	2.5
v	220	560	5.2
d	21	85	2.3
f	31	122	3.1
e	60	227	4.7
u	250	615	8.0
p	18	69	2.5
o	27	68	2.5
n	60	54	1.9
s	250	382	7.2

spacing with copper content, but over the range covered in the work reported here there was no appreciable change in spacing with copper content. The spacing also did not vary significantly along the radius from the edge of any sample to its center and in agreement with a similar finding by Alexander and Rhines was independent of grain size in a given sample, if only the prominent dendrites were measured.

Lineal analysis can be used to obtain approximate values of the average particle size and degree of dispersion of a discontinuous phase by counting the number of times this phase appears in a traverse across a sample; the total amount of the phase present is divided by this number and yields an approximate linear measure of particle size. Averages of the mean size of the θ particles and of the mean distance between them are given in Table III.

In some samples the θ phase was uniformly distributed and completely divorced, especially with higher solidification rates, whereas lower rates produced a more normal appearance of the eutectic. In all the alloys investigated the distance between θ particles tended to increase as the rate of solidification decreased. This effect was most pronounced in the alloys with low copper contents. The mean linear sizes of the θ particles are fairly constant except that at the lowest solidification rate a pronounced increase occurs, especially in the alloys of higher copper contents.

Fig. 5a to d illustrates typical configurations of the θ phase and eutectic and Fig. 6a to d shows typical distribution patterns of these constituents. The spheroidal divorced form of individual θ particles (Fig. 5a) was generally associated with a linear arrangement (Fig. 6a); this structure resulted from the highest solidification rates. Fig. 5b shows spheroidal θ particles together with some examples of stringers of the θ phase, which generally tended to form a mixed linear and cellular type of structure, as seen in Fig. 6b; this structure occurred at a somewhat slower solidification rate. When the rate of solidification was further reduced, the irregular form of θ and some lamellar eutectic resulted as shown in Fig. 5c; both of these constituents are also generally associated with the cellular structure shown in Fig. 6c. Low solidification rates lead to an approach to a normal eutectic which is associated with a coarse cellular structure (Figs. 5d and 6d).

The alloy containing 2 pct Cu displayed the same general changes of structure with solidification rate as the 3 pct alloy, but the first evidence of a cellular structure appeared at a slower rate of solidification. In the 4 pct and 5 pct Cu alloy, on the other hand, the cellular structure tended to appear with higher solidification indices than in the 3 pct Cu alloys. The higher copper contents also favor the irregular form of θ particles and the formation of lamellar eutectic. This can be seen by comparing the 3 pct and 5 pct Cu alloys at the same solidification index, Fig. 5c and d.

Summarizing the effects of the rate of solidification on the structures, a linear pattern of spherical, divorced θ particles at high rates changes to a cellular pattern, in which the θ phase occurs in the normal eutectic form, at low rates. For intermediate solidification rates, cellular structures are associated with the normal eutectic or a mixture of spheroidal particles of divorced θ and irregular stringers of divorced θ. At a given solidification index there is a greater tendency to form spheroids of divorced θ, the lower the copper content of the alloy while a cellular structure is favored by higher copper contents.

Microsegregation in the Solid Solution

The presence of nonequilibrium eutectic and the etching response of some of the samples indicated that microsegregation had occurred in the primary aluminum-rich solid solutions. A quantitative technique was developed for determining the concentrations of copper on a microscale in these solutions. This technique was based on rendering copper atoms in the samples radioactive by activation in a flux of thermal neutrons, recording the radioactivity on contact autoradiographs and finding the copper content from the photographic densities of the latter. Details are given in the Appendix.

The autoradiographs were placed in a recording microphotometer and magnified 10X; the dendrites could thus be identified in a manner similar to regular metallographic identification. Prominent dendrites having maximum spacing were chosen, since they most nearly represent the true dendrite spacing, and microphotometer traces were made across them. Since the effective minimum slit size of the microphotometer was 1 by 90 microns, only dendrite branches which were at least 90 microns long could be used. This limitation restricted the measurements to cast alloys solidified at the lowest rates (samples w, v, u, and s). Another limitation results from possible interference by the finely distributed θ phase. Finally, some of the dendrite arm spacings for the

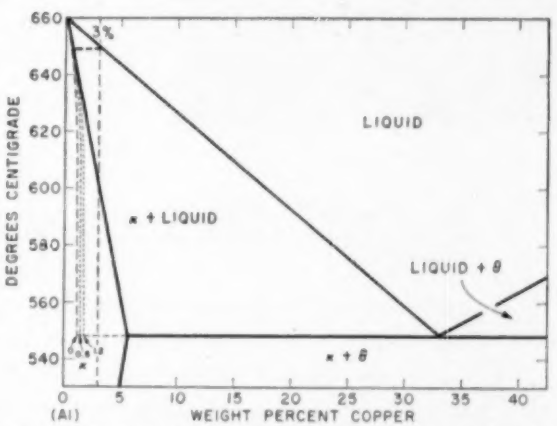

Fig. 4—Aluminum-rich region of the aluminum-copper phase diagram. Calculated nonequilibrium solidus curves for the 3 pct Cu alloy with Gulliver's solidification factors, Z (in pct Cu), of 0, 0.5, and 1.2.

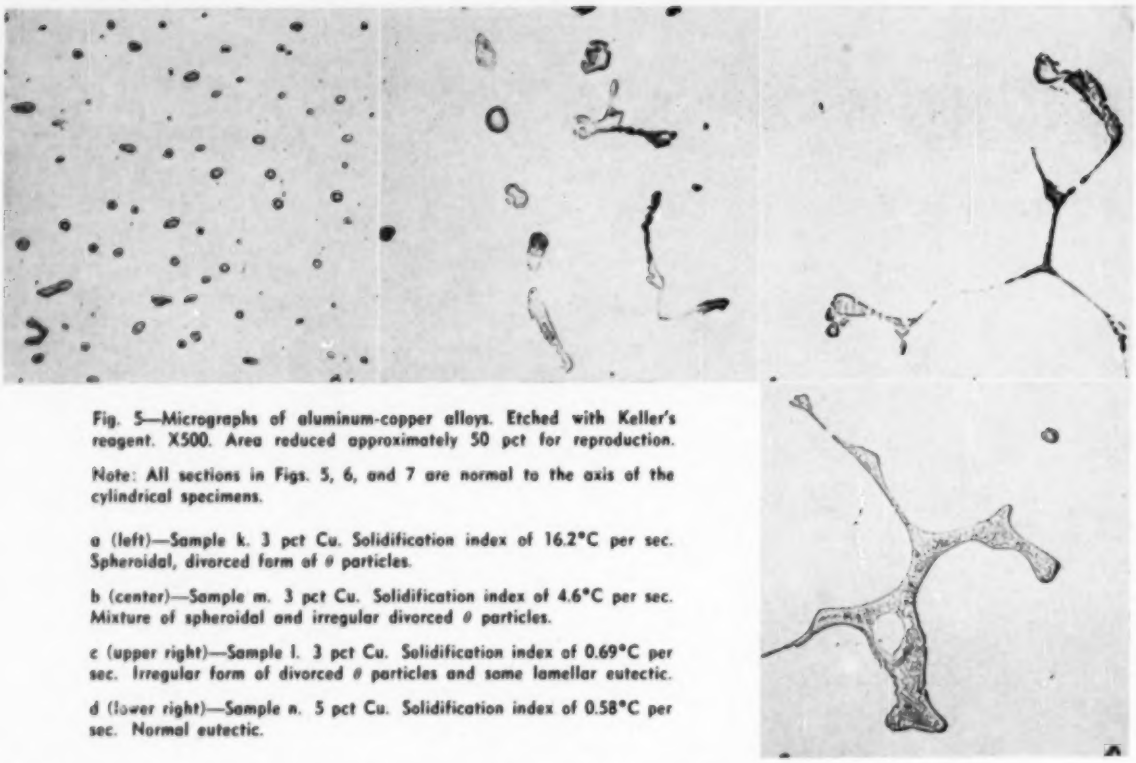

Fig. 5—Micrographs of aluminum-copper alloys. Etched with Keller's reagent. X500. Area reduced approximately 50 pct for reproduction.

Note: All sections in Figs. 5, 6, and 7 are normal to the axis of the cylindrical specimens.

a (left)—Sample k. 3 pct Cu. Solidification index of 16.2°C per sec. Spheroidal, divorced form of θ particles.

b (center)—Sample m. 3 pct Cu. Solidification index of 4.6°C per sec. Mixture of spheroidal and irregular divorced θ particles.

c (upper right)—Sample l. 3 pct Cu. Solidification index of 0.69°C per sec. Irregular form of divorced θ particles and some lamellar eutectic.

d (lower right)—Sample n. 5 pct Cu. Solidification index of 0.58°C per sec. Normal eutectic.

faster cooling rates (as shown by Fig. 6a and Table III) may approach the limit of the inherent resolution of the autoradiographs.

Fig. 7a to c shows micrographs of the autoradiographs of samples w, v, and u. The micrographs were made on a metallograph by light reflected through the autoradiographic plates from a polished piece of iron which served as a mirror. The micrograph was obtained by focusing on the emulsion and illustrates qualitatively the microsegregation in the

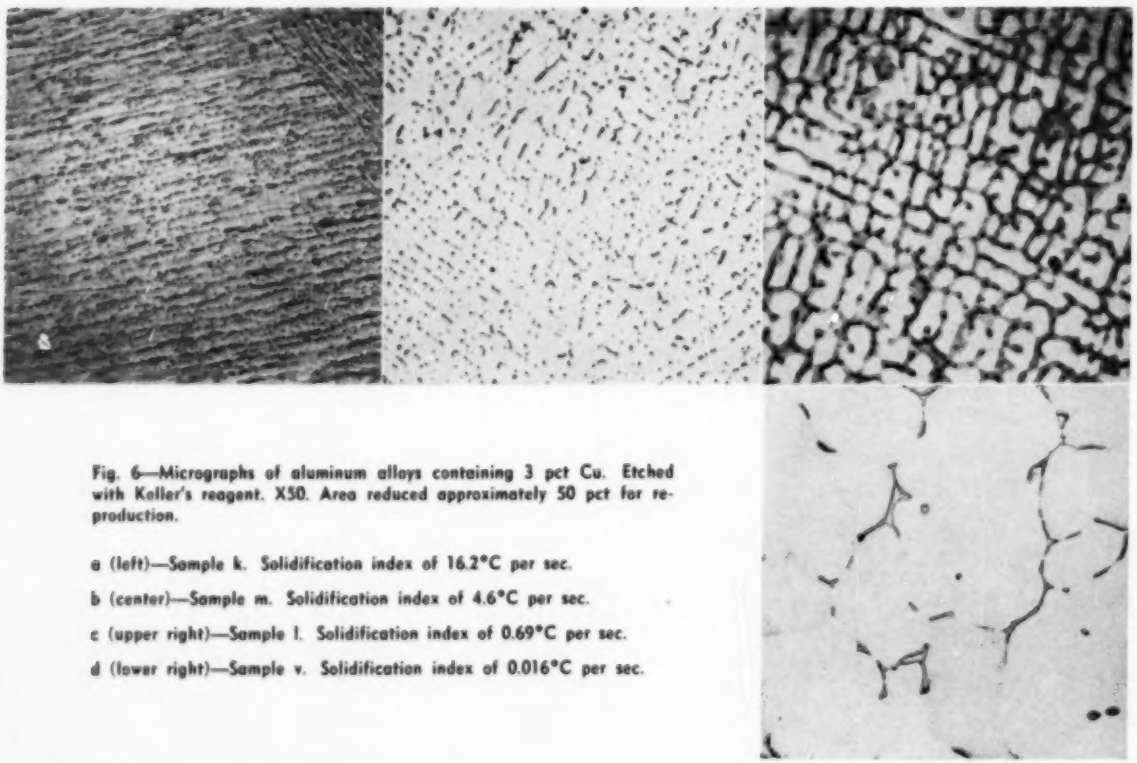

Fig. 6—Micrographs of aluminum alloys containing 3 pct Cu. Etched with Keller's reagent. X50. Area reduced approximately 50 pct for reproduction.

a (left)—Sample k. Solidification index of 16.2°C per sec.

b (center)—Sample m. Solidification index of 4.6°C per sec.

c (upper right)—Sample l. Solidification index of 0.69°C per sec.

d (lower right)—Sample v. Solidification index of 0.016°C per sec.

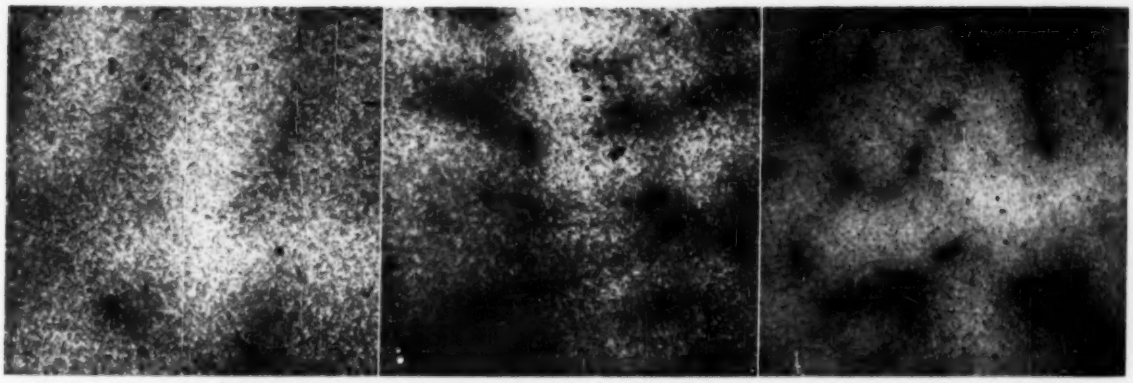

a—Sample w. 2 pct Cu. Solidification index of 0.014°C per sec.

b—Sample v. 3 pct Cu. Solidification index of 0.016°C per sec.

c—Sample u. 4 pct Cu. Solidification index of 0.017°C per sec.

Fig. 7—Micrographs of autoradiographs. X50. Area reduced approximately 50 pct for reproduction.

alloys. The dark areas represent the regions of high copper content. A comparison shows that as the copper content of the alloy increases, there is greater difference between the areas of high and low copper concentration indicating qualitatively that the spread in copper concentration due to microsegregation increases with the copper content.

A typical microphotometer trace of an autoradiograph, given in Fig. 8 for sample v, shows how the copper concentration varies across the dendrite branches. The double arrow in Fig. 8 marks the point where the trace was repeated by reversing the direction of the traverse. The trace was symmetrical about this point and thus checked the reproducibility of the instrument. The average dendrite spacing was 220 microns in this sample, obtained from measurements on the metallographic sample and from the autoradiograph trace. Similar values were found for the other slowly cooled samples.

Table IV summarizes the concentration measurements which refer to the κ solid solution. The samples also contained small amounts of θ phase but these areas were recorded on the microphotometer traces as regions of very low transmission and were disregarded. The results are expressed as the maximum microsegregation, S, that is, the maximum difference between the highest copper concentration, $C_{max.}$, in the interdendritic material and the lowest copper concentration, $C_{min.}$, in the skeleton of the adjoining dendrite branch. The corresponding minimum microsegregation S' is the minimum difference between concentrations $C'_{max.}$ and $C'_{min.}$ in adjoining interdendritic regions and dendrite branches. Values of S and S' are listed in Table IV and in each case are based on several photometer traces across a large number of dendrite branches. This table also includes values of $C_{max.}$, $C'_{max.}$, and $C_{min.}$, and $C'_{min.}$.

Table IV also gives the maximum and minimum concentration gradients in the dendrite branches expressed in percent change of copper per micron. The maximum concentration gradient does not necessarily occur in the branch having the maximum amount of microsegregation, S, and correspondingly the minimum concentration gradient does not neces-

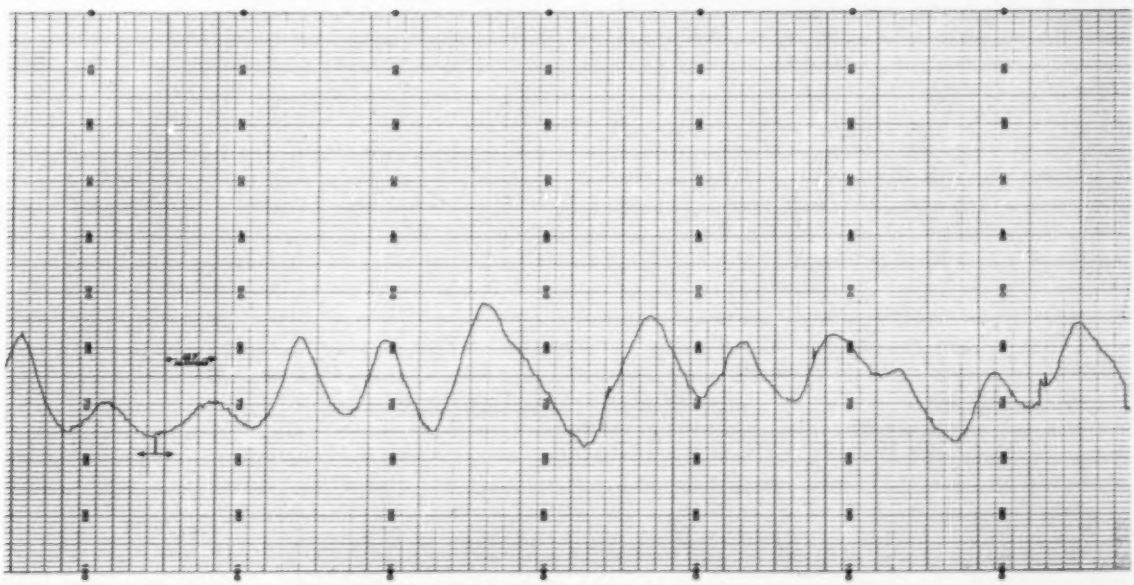

Fig. 8—Microphotometer trace of autoradiograph obtained across the arms of a dendrite in a cast 3 pct Cu alloy. Sample v. Solidification index of 0.016°C per sec. Arrows indicate point of reversal. Increasing vertical distance from the base line indicates increasing light transmission and decreasing concentration of copper.

sarily occur in the arm having the minimum amount of microsegregation, S'. The concentration gradients increase with the copper content of the alloy; this change is most pronounced in the low range of copper contents.

The maximum and minimum microsegregation S and S' increase as the copper content of the alloy increases. The highest and lowest copper concentrations for the dendrite branches having the maximum amount of microsegregation, S, also show an increase with increasing copper content of the alloy. The lowest copper concentration in the branches of the dendrite is considerably higher than the copper concentration of the first solid to form as given by the equilibrium diagram. The latter values are included in Table IV. This difference arises because the first solid is too minute an amount for detection and also some diffusion may occur in the original small particle to reduce concentration differences.

Brenner and Kostron[11] observed a maximum microsegregation of 1.70 pct and a minimum of 0.85 pct Cu in a continuously cast 4 pct Cu alloy. This maximum microsegregation is less than the value of 2.7 pct Cu found in this investigation for a 4 pct Cu alloy, but the values for the minimum microsegregation found in the two investigations were approximately the same, 0.85 and 0.9 pct Cu.

It is of interest to consider whether a row of neighboring dendrite branches exhibits any systematic variation in copper concentration. The microphotometer trace reproduced in Fig. 8 suggests that high and low values of microsegregation are interspersed and this tendency was found in all traverses. Starting from the double arrow and moving to the right, a sequence of low and high values of microsegregation is observed as the dendrite branches are traversed. Also, the branches showing low microsegregation do not have as low a minimum copper concentration associated with them as the branches showing a higher degree of microsegregation. The interpretation of these observations is necessarily speculative, especially since the orientation of the dendrite systems in relation to the plane of observation is an important factor. By choosing from any section only prominent dendrite systems having maximum spacing, the orientation relation can be made more definite, but is still not known precisely.

The following growth sequence is consistent with the observations, but is advanced here only tentatively. A set of parallel branches is first formed along an axis or trunk at comparatively large distances from each other and, at a later stage, additional dendrite branches form between the original ones. It seems significant that the branches having the higher degrees of microsegregation are in general wider than those having a lower microsegregation and lower maximum copper concentration. This difference in width suggests that the branches with the higher microsegregation in addition to being the first to form, grow for a longer time, which is consistent with the suggested growth sequence.

Summary and Conclusions

The nonequilibrium solidification of aluminum alloys containing nominally 2, 3, 4, and 5 pct Cu was investigated at rates of solidification ranging from approximately 50° to 0.01°C per sec. Thermal analysis, metallographic examination, lineal analysis, and quantitative autoradiography on a microscale led to the following conclusions:

1—Nonequilibrium eutectic is present in the alloys at all rates of solidification investigated.

2—The amount of nonequilibrium eutectic increases with the rate of solidification over the composition range investigated. The theoretical maximum amount is approached more rapidly with increasing rate of solidification, the higher the copper content of the alloy.

3—The dendrite spacing of the alloys increases with decreasing rates of solidification, but does not change appreciably with copper content over the composition range investigated. The spacing also does not depend on grain size.

4—As the rate of solidification decreases, the θ phase in the nonequilibrium eutectic remains fairly constant in particle size, but the distance between the particles increases. When the rate of solidification becomes very small, however, the particles show an appreciable increase in size and also in the distance between them.

5—The structures of the cast alloys change from a linear arrangement of spherical, divorced θ particles at high rates of solidification to a cellular pattern, in which the θ phase occurs in the normal eutectic form, at low rates of solidification. At a given rate of solidification there is a greater tendency to form spheroids of divorced θ particles, the lower the copper content of the alloy, while higher copper contents favor a cellular structure.

6—Aluminum-rich aluminum-copper alloys lend themselves to autoradiography after activation of suitable thin samples by irradiation *in situ* with thermal neutrons. This technique can be made quantitative by means of densitometry of the autoradiographs.

7—The amount of microsegregation in prominent dendrite branches of the alloys investigated (that is, the difference between the maximum and minimum copper concentrations in adjoining regions) measured by quantitative autoradiography increases as the copper content of the alloy increases. The concen-

Table IV. Concentration Variations in Dendrites of Cast Aluminum-Copper Alloys

Sample	Chemical* Analysis of Sample	Maximum* Microsegregation, S	Minimum* Microsegregation, S'	Copper* Concentrations for Max. Microsegregation		Copper* Concentrations for Min. Microsegregation		Maximum† Concentration Gradient	Minimum† Concentration Gradient	Equilibrium* Composition of First Solid to Form
				$C_{max.}$	$C_{min.}$	$C'_{max.}$	$C'_{min.}$			
w	1.96	1.7	0.3	2.8	1.1	2.2	1.9	0.0054	0.0012	0.30
v	2.81	2.4	0.6	4.2	1.8	3.5	2.0	0.013	0.0056	0.50
u	4.06	2.7	0.9	4.7	2.0	4.0	3.1	0.019	0.013	0.75
s	4.80	3.3	1.2	5.5	2.2	5.0	3.8	0.019	0.016	0.90

* Weight percent of copper.
† Weight percent of copper per micron.

tration gradients (expressed as the difference in copper concentration per unit distance) in the dendrite branches also increase with copper content of the alloy.

8—The observations suggest, but do not prove conclusively, that the first dendrite arms form along a major dendrite axis at a greater distance than the final dendrite spacing and that additional dendrite arms grow between the original arms.

Acknowledgments

The authors are greatly indebted to the Aluminum Co. of America for making this investigation possible. Thanks are also due to the Cyclotron Group at the Massachusetts Institute of Technology for the activation of alloy samples, and to Jarrell-Ash Co. for the use of a high resolution recording microphotometer.

Appendix

Details of the quantitative determination of copper concentrations in solution in aluminum by autoradiography on a microscale follow. For a discussion of the use of radioactive tracers in physical metallurgy research and especially of autoradiography, reference is made to a recent review.[20]

The radioactive isotope Cu^{64} was produced by activation *in situ*. Sections, 20 microns thick, of the cast alloy were prepared by a procedure described elsewhere[21] and irradiated for about 4 hr in a cyclotron with thermal neutrons at a flux of approximately 10^7 neutrons per sq cm per sec. Selective activation of the copper could be achieved because Al^{28} has a half-life of only 2.4 min compared to 12.8 hr for Cu^{64}. Calculations show that after activation under the above conditions and a decay period of 1 hr, the ratio of the activity of Cu^{64} to that of Al^{28} in a 2 pct Cu alloy is 9000 to 1. High purity of the alloys is essential to exclude activation of contaminants.

Eastman NTB-2 type emulsions 10 microns thick on 1x3 in. glass plates were used. The exposure time for the autoradiographs was based on a cumulative total of 10^6 disintegrations per square centimeter. Because of the small amount of radioactivity present in the samples it was necessary to use exposure times of approximately 48 hr.

The concentration gradients were determined by measuring the photographic density of the autoradiographs and converting this density to weight percent copper. A recording high resolution microphotometer, designed and built by the Jarrell-Ash Co., was used. This instrument records the transmission fraction I/I_o and gives readings reproducible to ± 0.2 pct in the region of 30 to 70 pct transmission. The minimum size of the adjustable slit was used; this is equivalent to 1 by 90 microns at the autoradiographic plate. This instrument projects an enlarged (10X) image of the autoradiograph on a viewing screen so that the exact area could be viewed during scanning and defects in the emulsion could be avoided.

The quantitative use of autoradiographs for measuring concentrations by densitometry requires a method of accurately converting photographic densities to concentrations. The response of emulsions to radiation depends on so many variables that it is necessary to calibrate the emulsion. The following calibration procedure was developed and applied to each batch of plates.

The characteristic response of the emulsion to the radiation emitted from Cu^{64} was obtained in successive exposures to a source consisting of a cylinder of high purity copper activated by thermal neutrons. It can be shown that when the calibrating source is placed in contact with the emulsion, the number of disintegrations, D_n, to which the emulsion is exposed for the nth period of calibration in successive steps is given by the following equation, in which k is the fraction of disintegrations reaching the emulsion, N_o is the number of radioactive atoms at time zero, λ is the decay constant, and t is the time:

$$D_n = kN_o \left[\exp\left(-\lambda \sum_{i=1}^{n-1} t_i\right)\right] \left[1-\exp(-\lambda t_n)\right].$$

If the time for each period of exposure is known, the relative number of disintegrations reaching the emulsion can be found. From the photographic density and values of D_n the characteristic curve of the emulsion with Cu^{64} radiation can be established.

The photographic density, log I_o/I, was plotted vs D_n; the resulting curve may be considered a modified *H-D* curve and gives linear relations in the density region of interest in this investigation. The calibration curve for NTB-2 emulsions with radiation from Cu^{64} is shown in Fig. 9.

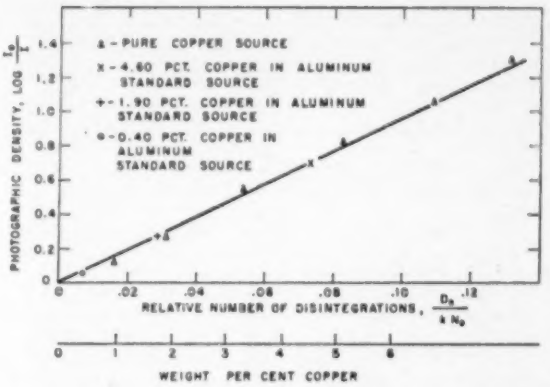
Δ - PURE COPPER SOURCE
X - 4.60 PCT. COPPER IN ALUMINUM STANDARD SOURCE
+ - 1.90 PCT. COPPER IN ALUMINUM STANDARD SOURCE
o - 0.40 PCT. COPPER IN ALUMINUM STANDARD SOURCE
PHOTOGRAPHIC DENSITY, LOG $\frac{I_o}{I}$
RELATIVE NUMBER OF DISINTEGRATIONS, $\frac{D_n}{k N_o}$
WEIGHT PER CENT COPPER

Fig. 9—Calibration curve for NTB-2 emulsion with Cu^{64} radiation.

The conversion of densities to copper concentrations by means of a single calibration curve requires that one point be obtained with a standard source activated together with the unknown. The standard must have a uniform known copper content. In this investigation the standard sources were prepared from solution-treated aluminum-copper alloys. The density of the autoradiograph of the standard source is measured and locates a point on the calibration curve. It is then possible to replace the scale of disintegrations, D_n, by one of copper content, since these two scales have a linear relation to each other. One point on the scale in terms of concentration of copper is that of the standard source and the other is the origin.

The accuracy of this method was checked by using three standard sources of 0.40, 1.90, and 4.60 pct Cu, all 20 microns thick. The scale of photographic density vs copper was established using one of these standard sources and the densities obtained with the other standard sources were checked on the scale. The results gave good agreement, as can be seen in Fig. 9. The use of a linear scale of copper content is not exact, because of the slight change in the density of the alloys with copper content, but the error introduced is very small in the range of composition covered.

The microphotometer must be used under identical conditions for establishing the calibration curve and measuring the autoradiographs of the standard sources and cast alloys.

References

[1] G. H. Gulliver: The Quantitative Effect of Rapid Cooling Upon the Constitution of Binary Alloys. *Journal* Inst. Metals (1913) **9**, p. 120; (1914) **11**, p. 252; (1915) **13**, p. 263. Also: *Metallic Alloys* (1921) 4th Edition. Appendix, p. 397. London.

[2] E. Scheuer: Zum Kornseigerungsproblem. *Ztsch. Metallkunde* (1931) **23**, p. 237.

[3] A. Hayes and J. Chipman: Mechanism of Solidification and Segregation in a Low-Carbon Rimming Steel Ingot. *Trans.* AIME (1938) **135**, p. 85.

[4] E. Scheil: Bemerkungen zur Schichtkristallbildung. *Ztsch. Metallkunde* (1942) **34**, p. 70.
[5] K. Mathieu and H. Neerfeld: Die Form der Umwandlungskurve bei erschwerter Diffusion. *Arch. Eisenhüttenwesen* (1942) **15**, p. 389.
[6] M. J. Luneau: Ce que l'on peut déduire d'un diagramme de solidification. *Revue de Métallurgie* (1942) **39**, p. 218.
[7] W. G. Pfann: Principles of Zone Melting. *Trans.* AIME (1952) **194**, p. 747; JOURNAL OF METALS (July 1952).
[8] Rayleigh (Lord): On the Distillation of Binary Mixtures. *Philosophical Magazine* (1902) (6) **4**, p. 521.
[9] W. T. Olsen, Jr. and R. Hultgren: Effect of Rate of Freezing on Degree of Segregation in Alloys. *Trans.* AIME (1950) **188**, p. 1323; JOURNAL OF METALS (November 1950).
[10] R. M. Brick: Fundamental Principles Involved in Segregation in Alloy Castings. *Trans.* AIME (1945) **161**, p. 65.
[11] P. Brenner and H. Kostron: Macro- and Microsegregation in Ingots of Two Aluminum Alloys. *Metallurgia* (1950) **41**, p. 209.
[12] E. Scheil: Uber die eutektische Kristallisation. *Ztsch. Metallkunde* (1946) **37**, p. 1.
[13] B. H. Alexander and F. N. Rhines: Dendritic Crystallization of Alloys. *Trans.* AIME (1950) **188**, p. 1267; JOURNAL OF METALS (October 1950).
[14] J. S. Smart, Jr., A. A. Smith, Jr., and A. J. Phillips: Preparation and Some Properties of High-purity Copper. *Trans.* AIME (1941) **143**, p. 272.
[15] G. V. Raynor: The Equilibrium Diagram of the System Aluminum-Copper. Annotated Equilibrium Diagram No. 4. Inst. Metals (1944).
[16] R. T. Howard and M. Cohen: Quantitative Metallography by Point-counting and Lineal Analysis. *Trans.* AIME (1947) **172**, p. 413; METALS TECHNOLOGY (August 1947).
[17] J. B. Friauf: The Crystal Structure of Two Intermetallic Compounds. *Journal* ACS (1927) **49**, p. 3107.
[18] E. R. Jette, G. Phragmén, and A. Westgren: X-ray Structure of the Copper-Aluminum Alloys. *Journal* Inst. Metals (1924) **31**, p. 193.
[19] A. Phillips and R. M. Brick: Grain Boundary Effects as a Factor in Heterogeneous Equilibrium of Alloy Systems. *Journal* Franklin Inst. (1933) **215**, p. 557.
[20] M. B. Bever: Radioactive Tracers in Physical Metallurgy Research. In *Modern Research Techniques in Physical Metallurgy.* (1953) p. 278. Cleveland. Also: *Trans.* ASM (1953) **45A**, p. 278.
[21] A. B. Michael, W. Z. Leavitt, M. B. Bever, and H. R. Spedden: Beta Ray Autoradiography of Metals and Minerals. *Journal of Applied Physics* (1951) **22**, p. 1403.

Technical Note

Effect of Repeated Tensile Prestrain on the Ductility of Some Metals

by Edmund C. Franz

IN an effort to understand high cycle fatigue, as well as to study the mechanism of fracture in general, a number of researches have been undertaken whereby the fracture properties of a metal have been determined under conditions of repeated cyclic prestrain employing high strains with relatively few cycles. Liu, Lynch, Ripling, and Sachs[1] showed the effect of a definite strain history consisting of small increments of tensile or compressive prestrain upon the flow and fracture characteristics of metals after a limited number of repeated loadings. Liu and Sachs[2] demonstrated by cyclic straining of the aluminum alloy 24S-T4 that the least reduction in ductility was obtained when the compressive stress was nearly equal to the tensile stress.

Attempts have been made to correlate the reduction in ductility under such prestraining with conventional fatigue data, as was done by Liu and coworkers.[1] The following research was conducted to determine if such reduction as has been noted could be correlated with conventional fatigue data or whether the effect resulted from causes extraneous to the basic mechanism of fatigue failure such as strain aging. It might be pointed out in this connection that the reduction in ductility has occurred in alloys that might be susceptible to strain aging or similar behavior, such as alloy 24S-T4. In the present investigation, the test specimens were prepared from the aluminum alloy 75S-T6 and annealed electrolytic copper. Alloy 75S-T6 is a complex precipitation hardenable alloy, whereas electrolytic copper would not be expected to exhibit strain aging effects, particularly at room temperature.

The experimental procedure consisted of prestraining test specimens repeatedly by increasing tension in small increments to various total prestrain values, followed by testing to failure in a tension test. The prestraining as well as the final testing was performed on a tensile machine using special fixtures[3] to maintain concentricity of the specimens. After prestraining, the specimens were unloaded as rapidly as possible and immediately reloaded so that the total time lapse between strains was held to a few seconds. Logarithmic or true natural strain was used in all calculations.

The results are presented in Figs. 1 and 2. In Fig. 1, the retained ductility,

$$\epsilon_R \left(\ln \frac{\text{area after prestrain}}{\text{area at fracture}} \right)$$

is plotted against the tensile prestrain,

$$\epsilon_P \left(\ln \frac{\text{initial area}}{\text{area after prestrain}} \right),$$

as abscissa with the number of stress reversals executed to attain the required prestrain plotted as parameter. Several specimens that fractured during

E. C. FRANZ is Research Metallurgist, Cleveland Research Div., Aluminum Company of America, Cleveland.
TN 198E. Manuscript, Sept. 11, 1953.
This paper is based on a thesis by E. C. Franz submitted in partial fulfillment of the requirements for the degree of M.S. in Physical Metallurgy to Case Institute of Technology.

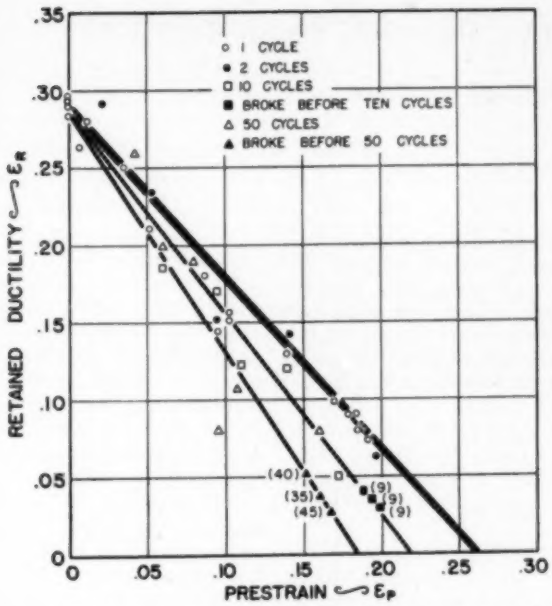

Fig. 1—Retained ductility of 75S-T6 repeatedly prestrained in tension.

prestraining were plotted with the number of cyclic prestrains completed prior to fracture indicated in parentheses. Although some scatter in the data for the individual test specimens is shown in the graph, average curves drawn through the values reveal a significant loss in mean ductility after repeated tensile prestraining of several cycles. In Fig. 2, the retained ductility of the annealed electrolytic copper specimens is plotted against tensile prestrain, with the strain history of each specimen recorded. All the values fall approximately on the line sloping down under 45° from the value at zero prestrain. Small repeated prestrains, at least to the limits of this investigation, have no apparent effect on the ductility of annealed electrolytic copper.

A distinct yield point arrest, which was absent in the unstrained material, was observed with each repeated prestrain in the stress-strain curves of the

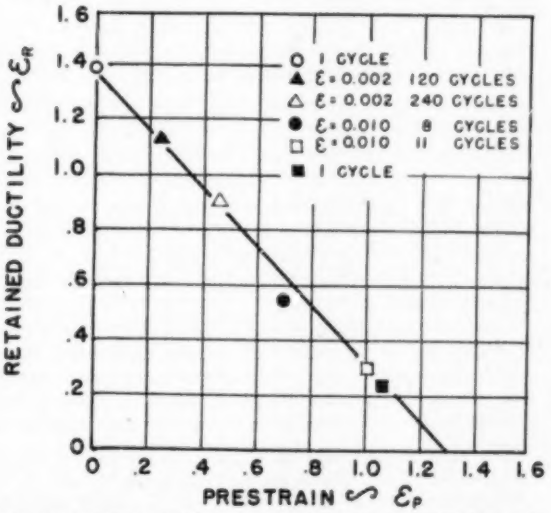

Fig. 2—Retained ductility of annealed copper repeatedly prestrained in tension.

Fig. 3—Microstructure of 75S-T6 specimen subjected to 50 repeated tensile prestrains of 0.003 prior to fracturing in a tension test. Numerous slip lines are delineated presumably by preferential precipitation along certain crystallographic planes. Note microcracks along slip planes. Etched with Keller's reagent. X100.

alloy 75S-T6 when the total strain value exceeded $\epsilon_p = 0.05$. The occurrence of such an arrest, well established for mild steel, has been observed previously by several investigators in nonferrous metals, including several aluminum alloys. Such phenomena have been associated with strain aging effects and explained theoretically by Cottrell[4] on the basis of the dislocation theory. The possibility of strain aging was suggested further by metallographic evidence of certain markings preferentially along the crystallographic planes as shown in Fig. 3, which is a micrograph of a specimen subjected to 50 tensile prestrains of approximately $\epsilon_p = 0.003$ prior to fracture in a tension test. Such markings might be interpreted as an indication of precipitation on slip planes, although the possibility that the lines represent mechanical damage to certain slip systems cannot be overlooked. It should be noted that microcracks are visible along certain slip planes. No indication of strain aging effects was observed with any of the annealed electrolytic copper specimens.

It would appear that the reduction in ductility reported in low cycle prestrain studies may be due to extraneous causes, and that extrapolation of low cycle data in an effort to obtain correlation with conventional fatigue values should not be attempted without due caution. On the other hand, the fact still remains that between a one cycle tensile test and the usual fatigue test, which generally represents millions of cycles, a substantial reduction in ductility occurs even in those metals and alloys that exhibit no known susceptibility to strain aging behavior.

References

[1] S. I. Liu, J. J. Lynch, E. J. Ripling, and G. Sachs: Low Cycle Fatigue of the Aluminum Alloy 24ST in Direct Stress. *Trans.* AIME (1948) **175**, p. 469; METALS TECHNOLOGY (February 1948).

[2] S. I. Liu and G. Sachs: Flow and Fracture Characteristics of the Aluminum Alloy 24ST after Alternating Tension and Compression. *Trans.* AIME (1949) **180**, p. 193; METALS TECHNOLOGY (June 1948).

[3] G. Sachs, D. Lubahn, and L. J. Ebert: Notched Bar Tensile Test Characteristics of Heat Treated Low Alloy Steels. *Trans.* ASM (1944) **33**, p. 340.

[4] A. H. Cottrell: The Yield Point in Single Crystal and Polycrystalline Metals. Symposium on Plastic Deformation of Crystalline Solids, Mellon Institute, Pittsburgh (1950) p. 60.

Mechanism of Plastic Flow in Titanium: Manifestations And Dynamics of Glide

by F. D. Rosi

The slip and twinning behavior in extended titanium crystals were studied in some detail. The formation and appearance of coarse kink bands are discussed. Their crystallographic geometry was determined by X-ray analysis. A phenomenological interpretation of the complexities in kink band development is also presented. The critical resolved shear stress, coefficient of shear hardening, and plane of fracture were determined for several crystals extended at room temperature.

THE slip and twinning elements observed in the room-temperature deformation of titanium were enumerated in a previous paper[1] in which considerations were advanced regarding the nature and selection of these elements and their effect on the known mechanical properties of this metal. The present study concerns the crystallographic, microscopic, and mechanical aspects of flow in relation to the slip and twinning elements, and includes a prediction of slip systems, nature of slip and twin markings, inhomogeneities of plastic flow, and stress-strain characteristics.

Unless otherwise noted, arc-melted titanium sponge (99.77 pct) was used in these experiments. The method of production of crystals, their dimensions, and the surface preparation for micrographic examination have been reported.[1]

For obtaining stress-strain characteristics, only those crystals which traversed the entire width of the specimen and were at least 8 mm in length were used. Tensile deformation of the crystals was performed with conventional grips for sheet specimens and a constant-stress loading beam, designed after the method of Andrade and Chalmers.[2] The specimens were loaded by allowing sand to flow from a reservoir into a bucket suspended from the longer end of a balanced 6:1 lever arm at a rate controlled to load the specimen approximately 2 kg per min. Strain measurements were made using the Baldwin SR-4, bonded, resistance-wire strain gage, Type A-8, which permitted a reading accuracy of 2 microinches per inch.

The formulas used in the evaluation of shear stress and shear strain, as in deriving the coefficient of shear hardening, are given by Schmid and Boas[3] in terms of the original orientation and change in length of the crystal. For calculating the critical resolved shear stress, the standard equation was used.

The crystallographic nature of the unpredictable slip observed in a number of specimens was determined by the single-surface X-ray method of analysis as described in ref. 1.

Experimental Results

Prediction of Slip System: It was reported[1] that room temperature slip in titanium takes place predominantly on $\{10\bar{1}0\}$ and in a $<11\bar{2}0>$ direction, giving three potential slip systems. Hence, it should be possible to predict the operative primary system in the manner used by Taylor and Elam[4] for aluminum (i.e., the one with the greatest component of shear stress in the direction of slip). The stereographic construction in Fig. 1 shows that this is true. In all cases, slip was found to occur initially on the $(01\bar{1}0)$ plane and, in a number of cases, in the $[2\bar{1}\bar{1}0]$ direction. (The direction of slip was not determined for all orientations.)

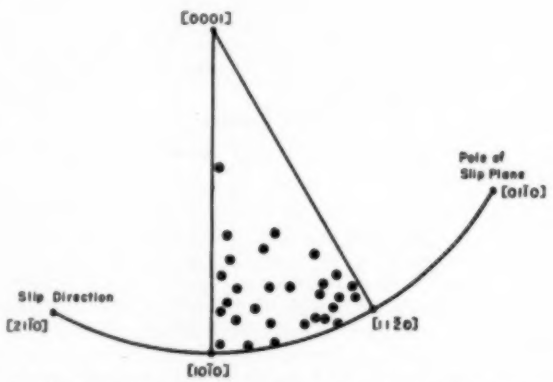

Fig. 1—Prediction of slip system in titanium from crystal orientation. Solid circles indicate original orientations of crystals studied in tension.

It follows that duplex slip can be expected when two slip systems are geometrically equally favorable for slip, as demonstrated in Fig. 2. In both crystals slip took place simultaneously on the $(1\bar{1}00)$ and $(01\bar{1}0)$ prismatic planes, as indicated by Fig. 2a and b. In the case of crystal B the movement of the specimen axis with increasing extension was toward the $(10\bar{1}0)$ direction, which represents the stable end orientation resulting from alternate slip on the $[2\bar{1}\bar{1}0]$ and $[11\bar{2}0]$ directions. This is analogous to the duplex slip process in face-centered cubic metals.[5]

Unpredictable Slip: In a number of crystals whose orientations were well within the operation of a single slip system, secondary slip occurred on planes not predicted by the criterion of maximum shear stress. Examples are shown in Fig. 3. In addition to

F. D. ROSI, Junior Member AIME, is associated with the Metallurgical Laboratories, Sylvania Electric Products Inc., Bayside, N. Y.

Discussion on this paper, TP 3685E, may be sent, 2 copies, to AIME by April 1, 1954. Manuscript, June 18, 1953. New York Meeting, February 1954.

primary slip on the $(1\bar{1}00)$ planes, slip has taken place in isolated regions of the crystal on the $(10\bar{1}0)$ and $(01\bar{1}0)$ prismatic planes.

From observations of unpredictable slip in other specimens, it was found that for orientations near the [0001] $[2\bar{1}\bar{1}0]$ boundary (see Fig. 3) secondary slip invariably occurred on the $(10\bar{1}0)$ planes, while for orientations approaching the [0001] $[10\bar{1}0]$ boundary the secondary slip was on the $(01\bar{1}0)$ planes. Thus, of the two possible prismatic planes secondary slip occurred on that for which the resolved shear stress was greater. It would appear, therefore, that in some cases, at least, the secondary slip plane could be predicted from crystal orientation.

The appearance of unpredicted cross slip in its typically step-like character was observed in only one crystal. X-ray analysis showed that the cross-slip plane approximated a $(10\bar{1}0)$ plane, which did not coincide with that responsible for conjugate slip. Thus, like primary slip, cross slip in titanium occurs on a $\{10\bar{1}0\}$ prismatic plane.

Nature of Slip Bands: It was reported[1] that a striking feature of prismatic slip markings in crystals of different orientation is the considerable variation in their appearance. To determine whether this variation was dependent on orientation, crystals of selected orientations were deformed similar amounts and examined metallographically. The results of this study are summarized in Fig. 4. For those orientations near the [0001] $[11\bar{2}0]$ zone, the slip band formation is of the coarse, widely spaced type. On the other hand for orientations approaching the [0001] $[10\bar{1}0]$ symmetry position for duplex slip, the slip bands are finer and closely spaced. Thus, it may be stated that for decreasing values of the angle, χ, which the slip plane makes with the specimen axis, the slip bands become progressively finer, resulting in a more widespread distribution of deformation by slip. This orientation dependence appears to be similar to that for basal slip band development in cadmium and zinc.[6] A comparison of this orientation effect with those of temperature and loading rate suggests than an increase in the value of χ has the same effect as an increase in the temperature of testing and a decrease in the rate of loading.

Occurrence of Twinning: $\{10\bar{1}2\}$ Twinning: Profuse twinning occurred in those specimens which were deformed by bending, compression in a vice, or a combination of these; but was rarely observed in the extended crystals. In general, the twinning took place predominantly on the $\{10\bar{1}2\}$ or $\{11\bar{2}1\}$ planes simultaneously with, or after, deformation by slip on the $\{10\bar{1}0\}$ planes. Only in one instance was the deformation observed to occur solely by twinning. In this crystal, whose orientation and twinning habit are shown in Fig. 5, twinning took place on those $\{10\bar{1}2\}$ planes (I, Fig. 5) which resulted in an extension in the direction of the tension axis. For this particular crystal, twinning on any $\{10\bar{1}2\}$ plane would give an extension.[5] Consequently, all planes could operate, and this offers some basis for speculation on the choice of twinning planes. Of many arguments advanced, that proposed by Gough[5] is the most attractive. He stated that twinning occurs on those planes which do not contain the slip direction. From the orientation of the crystal (Fig. 5) it may be seen that either $[11\bar{2}0]$ or $[2\bar{1}\bar{1}0]$ can

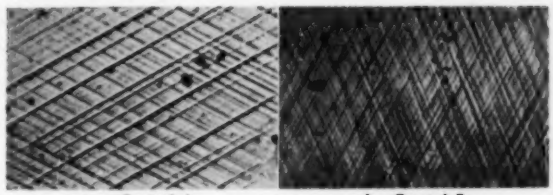

a—Crystal A. b—Crystal B.

X100. Area reduced approximately 50 pct for reproduction.

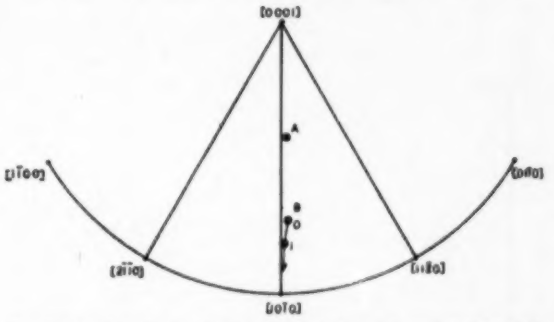

Fig. 2—Duplex slip in titanium. Orientations of crystal B indicate movement of specimen axis with extension.

be considered the slip direction. Consequently, the planes designated II, III, V, and VI would not be expected to operate, as was found to be the case. Of the two remaining possibilities, twinning occurred preferably on plane I, probably because the shear stress on this plane was greater.

The apparent lack of twinning, principally of the $\{10\bar{1}2\}$ type, in those crystals deformed in tension may be explained by Fig. 6. A portion of the standard stereographic triangle in the figure has been subdivided into two orientation fields, *A* and *B*, where very little twinning on $\{10\bar{1}2\}$ planes can be expected in titanium. Superimposed on these two fields is a shaded region which represents the spread in orientation for the crystals deformed in simple

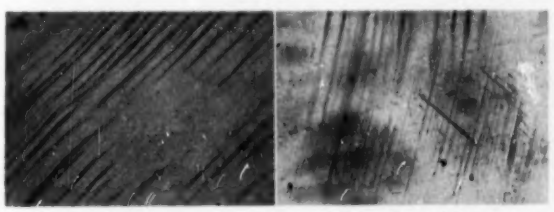

a—Crystal A. b—Crystal B.

X50. Area reduced approximately 30 pct for reproduction.

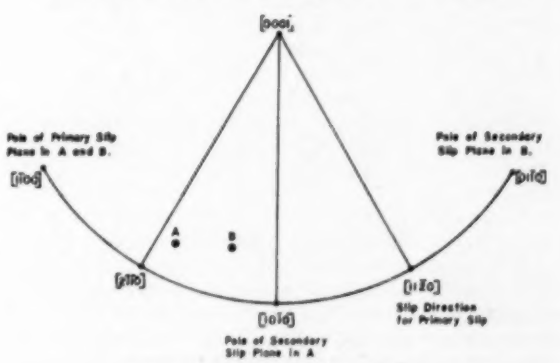
Pole of Primary Slip Plane in A and B.
Pole of Secondary Slip Plane in B.
A
B
Slip Direction for Primary Slip
Pole of Secondary Slip Plane in A

Fig. 3—Unpredicted slip in titanium.

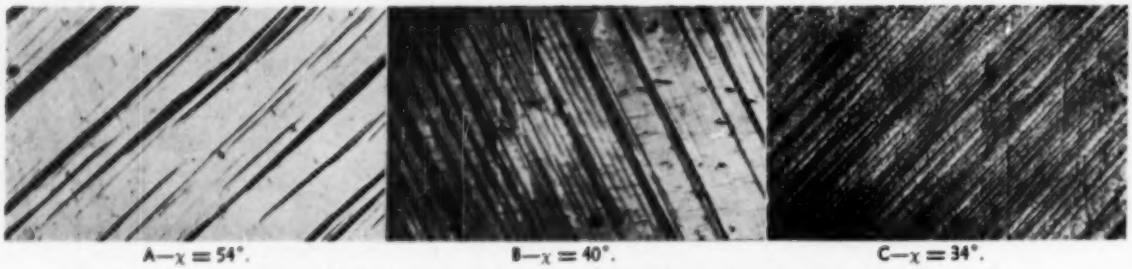

A—$\chi = 54°$. B—$\chi = 40°$. C—$\chi = 34°$.

X100. Area reduced approximately 20 pct for reproduction.

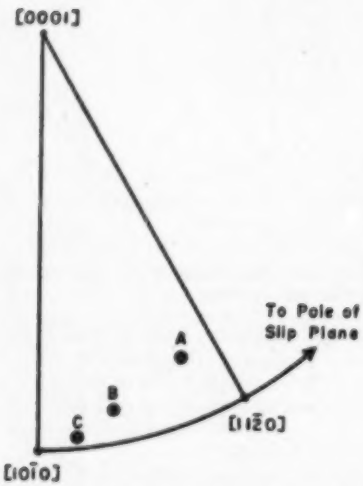

Fig. 4 (above and to left)—Effect of crystal orientation on nature of slip bands. χ is angle which slip makes with specimen axis. The letters in the drawing correspond to the micrographs.

tension (see Fig. 1). For orientations which fall in region *A*, {10$\bar{1}$2} twinning cannot occur because the twinning operation would result in a compression along the tension axis. Similarly, for the orientations of region *B*, twinning on four of the possible six sets of {10$\bar{1}$2} planes could not occur. Therefore, it is apparent from the position of the shaded region that {10$\bar{1}$2} twins could rarely be expected to occur in the tensile specimens.

{11$\bar{2}$1} Twinning: Extensive twinning on {11$\bar{2}$1} planes was observed in a number of crystals whose orientations are indicated in the stereographic triangle of Fig. 7, and it would appear from the extent of the orientation field that their occurrence is orientation dependent. In all cases the twinning occurred on the ($\bar{2}$111) planes, while limited slip took place on the (1$\bar{1}$00) planes, as would be predicted from the crystal orientation. From the general appearance of intersecting slip and twin markings, it seems that the slip preceded the twinning.

Regarding the peculiar selection of the ($\bar{2}$111) twinning planes in these crystals (see Fig. 7), it can be said that: 1—these planes do not contain the slip direction, 2—they make an angle of 40° to 50° with the direction of applied stress, and 3—they intersect the slip plane at an angle between 55° to 60° to the active slip direction. The first of these characteristics loses its singular significance in the selection of twin types, since there are nonoperating {11$\bar{2}$1} planes which also do not contain the slip direction. The second characteristic may be important, since it does suggest that the resolved shear stress is greatest for this plane. The third observation is also significant, since it is in support of Andrade's[7] generalized conclusion that in hexagonal metals the operative twinning planes are those which intersect the slip plane at 60° to the slip direction. Thus, it would appear from these unique criteria that no single one is wholly responsible for the crystallographic selection of twins. Moreover, the paucity and limitations of the data make it difficult to determine their relative importance.

In two of the crystals of Fig. 7 whose orientations are reproduced in the stereographic plot of Fig. 8

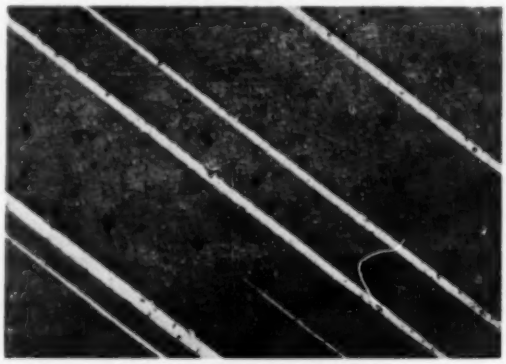

Direction of tension axis → X300.

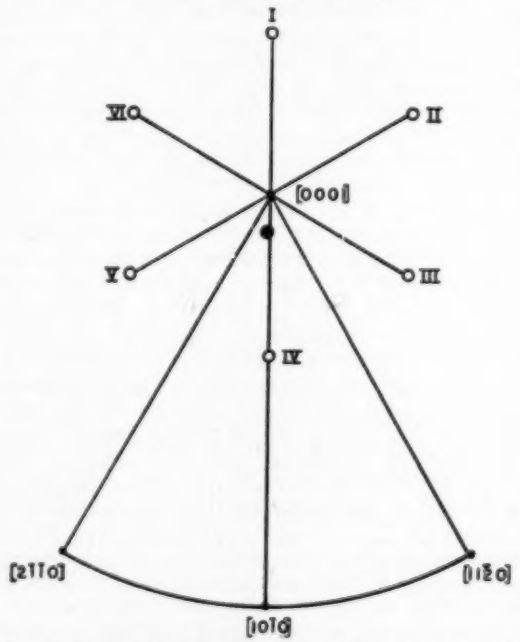

Fig. 5—Orientation of crystal where deformation occurred solely by twinning on a {10$\bar{1}$2} plane. The numerals, I to VI, indicate poles of twinning planes of the form {10$\bar{1}$2}; solid circle represents position of tension axis.

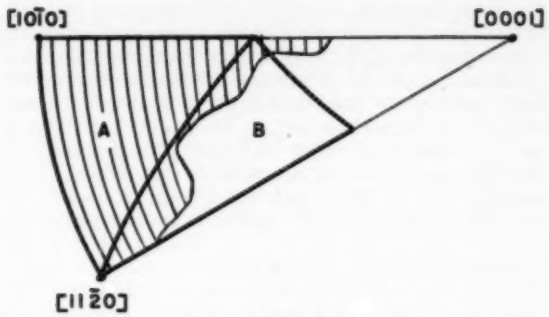

Fig. 6—Orientation regions (A and B) where the occurrence of {10$\bar{1}$2} twinning is unlikely. Shaded region indicates orientation field of crystals studied in tension.

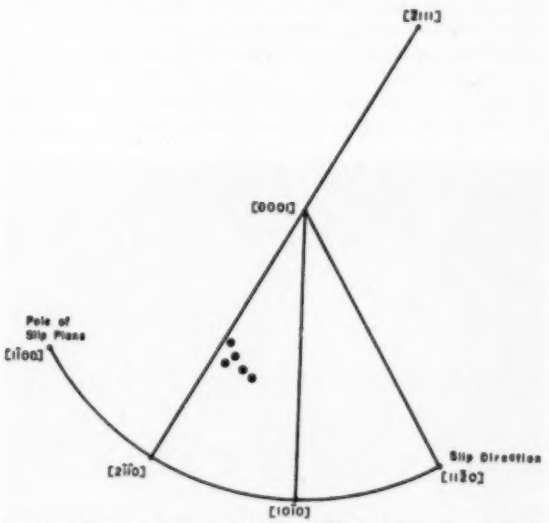

Fig. 7—Orientations of crystals where {11$\bar{2}$1} twinning was observed.

(A and B), it was found that the ($\bar{2}$111) twins exhibited stepped discontinuities, as shown in the accompanying micrograph for crystal B. This twinned discontinuity, characteristic only of {11$\bar{2}$1} twinning, corresponds to twinning on another set of {11$\bar{2}$1} planes whose indices are indicated in the stereographic plot. In both crystals secondary slip occurred on a prismatic plane which bore the same crystallographic relation to the stepped ($\bar{1}$12$\bar{1}$) twins as did the primary (1$\bar{1}$00) slip to the ($\bar{2}$111) twins.

It is further interesting to note that twin discontinuities were not observed in the deformation of crystal C (see Fig. 8), where secondary slip had occurred on the (10$\bar{1}$0) planes. From the crystallographic relationship of the stepped twins to the secondary slip plane in crystals A and B, it might be anticipated that stepped twinning in crystal C would occur on the ($\bar{2}$111) planes. However, since this plane is also the primary twinning plane for this crystal orientation, it indicates that stepped twins in crystal C would occur on the primary twinning plane but in another direction not distinguishable in the experiments; and this could account for the observed absence of stepped discontinuities in the primary twins of the crystal.

Inhomogeneities of Plastic Flow: Kink Bands: Frequent observations of kink bands were made in extended crystals in which extensive slip and no twinning had occurred. These bands were very similar in appearance to those reported in a number of metals by various investigators,[9-14] in that they represent disoriented regions of the crystal which are bounded by parallel bend planes making an angle of approximately 90° with the active slip planes. It may be noted that kink bands were never observed in crystals deformed by bending; and it is significant that the deformation in bent crystals occurred, in part, by twinning on {10$\bar{1}$2} and {11$\bar{2}$1} planes.

Kink bands could be observed in some crystals extended approximately 5 pct. However, at these low deformations the small difference in orientation associated with the bands and their thinness made their micrographic detection difficult.

With increasing deformation (up to 20 pct elongation) the kink bands became more pronounced and are frequently wavy and variable in width in their path across the crystal, as shown in Figs. 9 to 11. Optical examination of as-deformed crystals revealed that the {10$\bar{1}$0} slip line pattern suffered a small discontinuity at the two bend planes defining the band, and that the angular displacement of these lines did not appear to vary along a given band. From the relative angles which the prismatic slip markings made with the tension axis, it is apparent that the lattice reorientation due to slip within the band lagged behind that of the matrix material.

At the higher deformations the density of the primary slip markings in the crystal matrix frequently was greater than that in region of the kink band (see Figs. 9 to 11). This behavior suggests that, once a kink band is formed in the crystal, it can obstruct the propagation of slip developed in later stages of deformation. Some of the slip lines, which were deflected into the band, become discontinuous or fade out in crossing the band (see Figs. 10 and 11).

Most of the features associated with kink band formation in titanium have been described by one investigator or another in a number of metals of different structural class. In particular, the work of

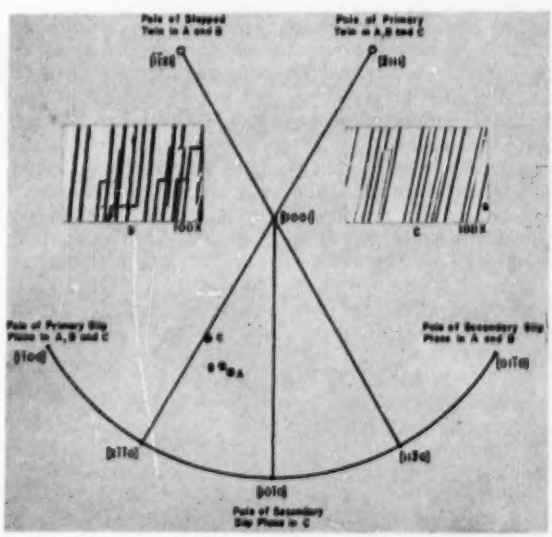
Pole of Stepped Twin in A and B
Pole of Primary Twin in A,B and C
B
100X
C
100X
Pole of Primary Slip Plane in A,B and C
Pole of Secondary Slip Plane in A and B
Pole of Secondary Slip Plane in C

Fig. 8—Occurrence of {11$\bar{2}$1} twinning. Crystals A and B exhibited stepped twin discontinuities. Area reduced approximately 80 pct for reproduction.

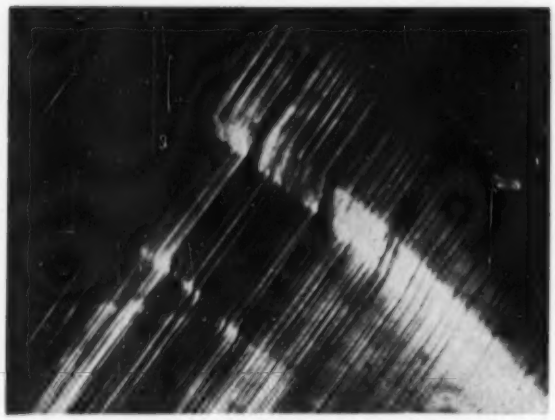

Fig. 9—Appearance of kink bands in crystal extended approximately 20 pct. X100. Area reduced approximately 10 pct for reproduction.

Fig. 10—Stepped kink band formation in the vicinity of an included grain. Crystal extended approximately 18 pct. X250. Area reduced approximately 60 pct for reproduction.

Cahn[9] and Honeycombe[14] in extended aluminum crystals supports the findings of the present study.

In the moderately deformed crystals of Figs. 9 to 11, slip has occurred on a different set of planes within the disoriented region of the kink band. Thus, it would appear that these regions have rotated to positions where duplex slipping can occur. In some bands, deformation appears to have occurred to a greater extent on the second slip system than on the deflected primary slip system of the matrix material (see Figs. 10 and 11). This suggests that at the heavier deformations the lattice of the kink band has effectively rotated to a position which favors increased deformation by slip on the second system.

The kink bands of Fig. 11 are much more pronounced and variable in direction in the vicinity of an unabsorbed grain; and in the regions of the crystal directly below and above the grain, the kink bands appear to suffer a stepped discontinuity whose direction is not well defined and varies from one band to another. The direction of the two sets of slip markings within the band does not appear to be appreciably altered by the stepped discontinuity. This indicates that the orientation of the lattice in the stepped regions is similar to that along the rest of the band, and, consequently, the occurrence of the steps are simply a result of a change in the crystallographic nature of the bend planes outlining the band. On either side of the small grain, increased slip activity has occurred, as evidenced by the degree of blackening. This localized inhomogeneity in the flow pattern could account for the stepped discontinuities, as may be inferred from the relationship of the steps to the regions of varying slip intensity.

Recent evidence[13, 15, 16] has indicated that the occurrence of kink bands in aluminum is orientation dependent in that for certain critical orientations where complex slipping can be expected, kink band formation is not necessary to the glide process. This orientation dependency is also supported by the present data which are summarized in the stereographic triangle of Fig. 12. This plot shows the initial position of the tension axis for a number of moderately deformed crystals. In agreement with Laleouf and Crussard,[15] it may be seen that kink bands were not optically detected in those crystals whose stress axis lay near the $[10\bar{1}0]$ [0001]

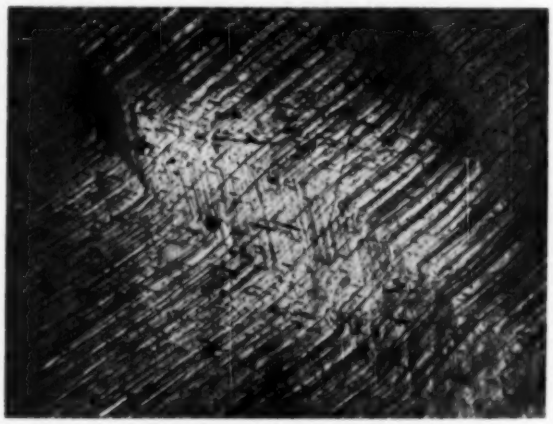

Fig. 11—Slip band pattern associated with kink band formation in crystal extended approximately 16 pct. X500. Area reduced approximately 50 pct for reproduction.

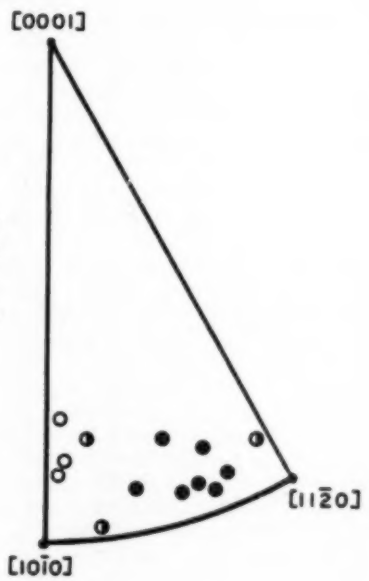

Fig. 12 — Effect of orientation on kink band formation.
○—No kink bands.
◑ —Fine kink bands
●—Coarse kink bands.

symmetry position for duplex slip. Furthermore, it may be noted that kink band formation was most prevalent in crystals whose orientations fell in the central region of the orientation field of Fig. 12. It would appear from this that, even in crystals where a high probability exists for the occurrence of unpredictable slip (e.g., for orientations near any one of the triangle boundaries, as pointed out in an earlier section), there is a tendency for kink bands either to appear so thin as to be optically undetectable or to disappear.

The bend planes of the kink bands in moderately deformed crystals were found by X-ray analysis to coincide with {11$\bar{2}$0} planes, the normal to which corresponded to the active slip direction. Moreover, from the appearance of the slip line pattern in the as-deformed unetched crystal the lattice rotation at the bend plane is about an axis in the slip plane, normal to the slip direction. The axis corresponds to the [0001] direction, which represents the intersection of the {11$\bar{2}$0} bend planes with the {10$\bar{1}$0} slip planes. These data are summarized in the standard projection of Fig. 13 which indicates, in addition to the rotation axis, the positions of the

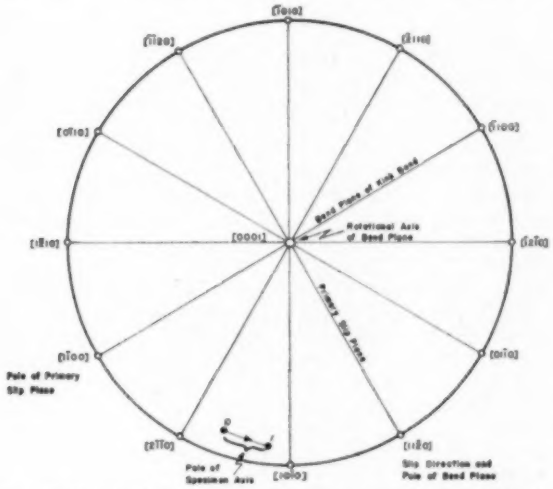
Best Plane of Kink Band
Rotational Axis of Bend Plane
Primary Slip Plane
Pole of Primary Slip Plane
Pole of Specimen Axis
Slip Direction and Pole of Bend Plane

Fig. 13—Standard projection indicating crystallography of bend plane defining kink band formation in crystal extended approximately 18 pct.

slip plane, slip direction, and bend plane in the crystal of Fig. 10. Thus, the crystallographic geometry of kinking in titanium is the same as that reported in aluminum[8, 10, 11, 13, 16] and in a number of hexagonal[9, 12, 17, 18] metals.

It has already been pointed out that in severely deformed crystals the operation of a second slip system was frequently observed in the lattice of the kink band. In order to determine the crystallographic nature of this system, it was necessary to obtain the orientation of the lattice inside the band. Since, in accordance with the geometrical features of kinking, the orientations of the regions inside and outside the band are similar and related by a rotation about the [0001] axis, it was possible to approximate the orientation of the band from an estimate of the angular deflection of the slip markings at the bend planes in the as-deformed crystal. From such stereographic constructions it was found that, in all cases of duplex slip within a band, the second slip plane corresponded to a {10$\bar{1}$0} plane

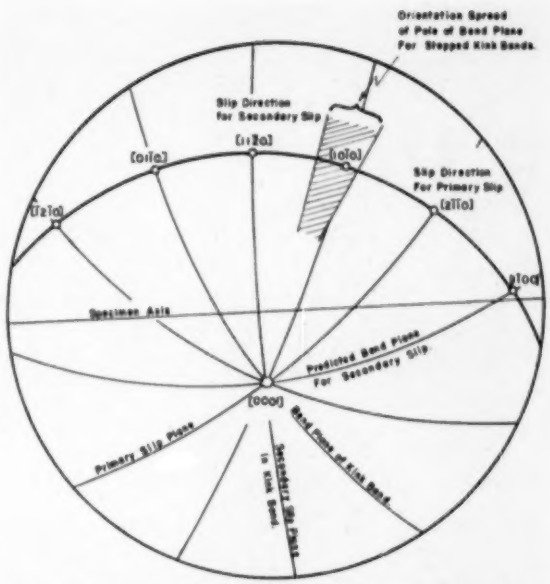
Orientation Spread of Pole of Bend Plane For Stepped Kink Bands
Slip Direction for Secondary Slip
Slip Direction For Primary Slip
Specimen Axis
Predicted Bend Plane For Secondary Slip
Primary Slip Plane
Secondary Slip Plane in Kink Band
Bend Plane of Kink Band

Fig. 14—Stereographic projection indicating crystallography of stepped kink bands in crystal of Fig. 10.

which did not coincide with the conjugate plane of slip for the particular crystal orientation. For example, in the stereographic plot of Fig. 13, this second slip plane corresponded to the (10$\bar{1}$0) plane, which is the predicted plane of slip for orientations in the triangle, [0001] [2$\bar{1}\bar{1}$0] [1$\bar{1}$00].

It would be interesting to know whether the stepped discontinuity of the kink band in Fig. 10 has any crystallographic significance. From the orientation of the crystal after deformation, it was found that the pole of the bend planes associated with the best defined steps fell within a few degrees of the [10$\bar{1}$0] direction, indicated in the stereographic plot of Fig. 14. The coincidence of the bend planes of these steps with a rational plane suggests that their occurrence is a result of the operation of a secondary type of kink plane. This suggestion, however, does not appear valid in view of the apparent variation in the direction of these steps along a given band and from one band to another. Instead, it would be more pertinent if the steps were a result of the cooperative movements of two distinct bend planes, for with such a mechanism it can readily be seen that the direction of the steps will vary with the relative extent of participation of the two cooperating planes. In this connection, it is significant that: 1—the [10$\bar{1}$0] direction is symmetrically positioned between the [11$\bar{2}$0] and [2$\bar{1}\bar{1}$0] directions,

Fig. 15—Kinking phenomenon showing development of secondary kink bands within a primary band in a crystal extended to fracture. X100. Area reduced approximately 40 pct for reproduction.

Fig. 16—Displacement of primary kink band along bend planes of secondary kink bands. X100. Area reduced approximately 80 pct for reproduction.

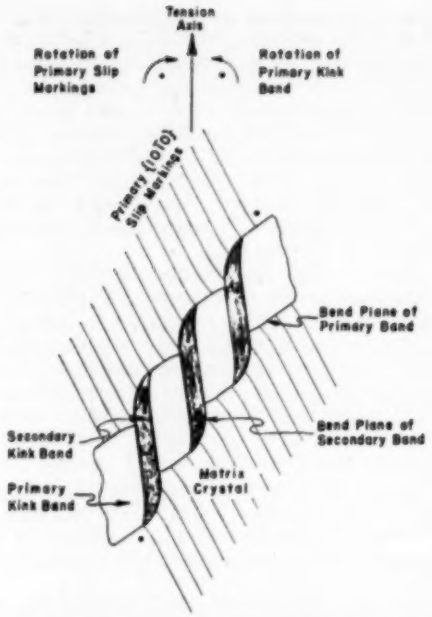

2—[$2\bar{1}\bar{1}0$] is both the slip direction and the pole of the bend plane for slip on the ($01\bar{1}0$) plane, and 3—[$11\bar{2}0$] corresponds to the slip direction and the predicted pole of the bend plane for slip on the ($1\bar{1}00$) plane which is the plane of secondary slip observed inside the kink bands after heavy deformations. Thus, the stepped discontinuities of the bands in Fig. 11 may be considered a result of kinking occurring alternately on the ($11\bar{2}0$) and ($2\bar{1}\bar{1}0$) planes. This cooperative movement could account for the variable direction of these steps and, perhaps, the wavy character of the bands in their path across the crystal. A similar analysis has been made on the appearance of ill-defined cross slip in aluminum.[9, 10]

One other observation of interest with regard to kink band formation has been reserved, in view of its complexity, for final discussion. This kinking phenomenon, shown in the micrograph of Fig. 15, was observed in a crystal which was extended to fracture. Secondary kink bands have developed within a primary band in such a manner as to break up the primary band at its bend planes in a saw-toothed or stepped configuration. This unique displacement of the primary bend planes occurred along the bend planes of the secondary bands in the manner shown in Fig. 16. It appears from the angular relationship of the tension axis to the primary band that these stepped displacements represent, in effect, block movements of the lattice of the primary band in its rotation toward the stress axis with increasing extension. As was demonstrated by Chen and Mathewson[11] in their work on aluminum, this rotation is in an opposite sense to that of the active primary slip planes. Close examination of the micrographs in Fig. 16 reveals the interesting phenomenon of overlapping between the secondary kink bands.

Bend Plane of Secondary Kink Band
Bend Plane of Primary Kink Band
Rotational Axis of Bend Planes
Secondary Slip Plane in Primary Kink Band
Pole of Bend Plane of Secondary Kink Band
Pole of Primary Slip Plane
Primary Slip Plane
Axis of Undeformed Crystal
Pole of Bend Plane of Primary Kink Band
Pole of Secondary Slip Plane in Primary Kink Band

Fig. 17—Standard projection indicating crystallographic topography of kink band formation where secondary bands have formed within a primary band.

The slip line pattern in the as-deformed crystal of Fig. 16 suggests that the geometry of kinking associated with the secondary bands is identical to that of the primary band, involving a rotation about an axis in the slip plane, normal to the slip direction (i.e., the [0001]). The pole of the bend planes defining the secondary bands corresponds approximately to the active slip direction for the secondary slip occurring within the primary band. For purposes of clarification, the crystallographic data pertaining to this complex kink band formation is summarized in the standard stereographic plot of Fig. 17.

It is noteworthy from the micrographs in Figs. 15 and 16 that the secondary slip has concentrated for the most part in the regions of the secondary kink bands. This indicates that, once formed, these bands serve as preferential sites for secondary slip. Moreover, since the secondary slip planes, like the primary kink bands, rotate during deformation toward the tension axis in an opposite sense to the primary slip planes, then the same rotation must apply to the lattice of the secondary kink bands.

The slip line pattern in Fig. 16 further shows that the primary slip markings inside the primary kink

band undergo further rotation about the [0001] axis on passing through the secondary bands. Furthermore, the sense of rotation indicates that the reorientation of the lattice of the secondary bands during extension has lagged behind the lattice of the primary band. Thus, this unusual kinking phenomenon presents a succession of lags in lattice reorientation due to slip in going from the crystal matrix to the regions of primary and then secondary kink bands. The rotational relationships for the crystal of Fig. 16 are schematically illustrated in the kink band formation of Fig. 18. It may be added that the variation in direction of some of the primary slip lines in their path through the secondary bands rules out the possibility that these bands are twins.

Fig. 19 shows another region of this complex band formation where the secondary bands seem to originate at the bend planes of the primary band and then propagate across the band with increasing deformation. This could account for the observed overlapping of the secondary bands. The figure also demonstrates clearly the discontinuous nature of the primary $\{10\bar{1}0\}$ slip markings on passing through the primary band, as well as the opposite sense of rotation of the lattice about a common axis at the bend planes of the primary band.

Fig. 20 shows still another region, where this complex kinking phenomenon crosses a jagged boundary between similarly oriented grains, as evidenced by the directional continuity of both the secondary kink bands and slip markings across the boundary. The density of the secondary bands has increased in the vicinity of the grain boundary, as well as the slip activity within these bands. Somewhat similar behavior was associated with primary band formation in the vicinity of included grains of orientation similar to the matrix crystal. Thus, it would appear that any factor which locally upsets the regularity of the stress pattern in the crystal will tend to promote a complex kink band formation.

Finally, it may be noted that in the general vicinity of fracture it was quite common to find corrugated arrays of closely spaced, fine kink bands, as shown in Fig. 21. These arrays appeared to form preferentially in regions where the complex, coarse band formation described above had not occurred.

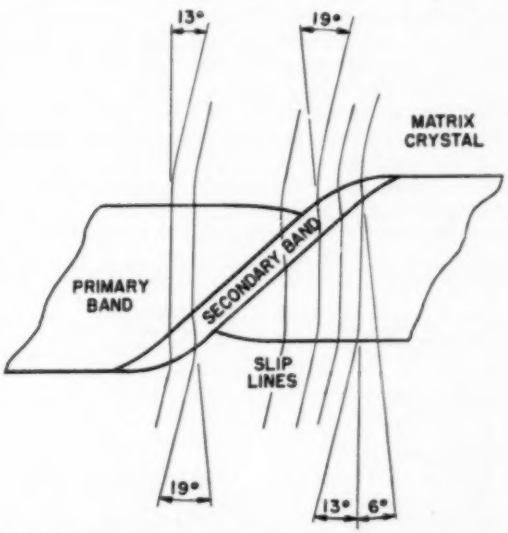

Fig. 18—Rotational relationships of slip markings with primary and secondary kink bands.

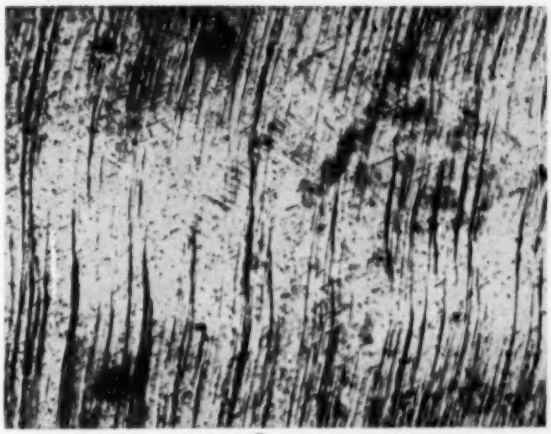

Fig. 19—Nature of primary $\{10\bar{1}0\}$ slip markings on passing through primary kink band. Note faint secondary kink bands. X200. Area reduced approximately 50 pct for reproduction.

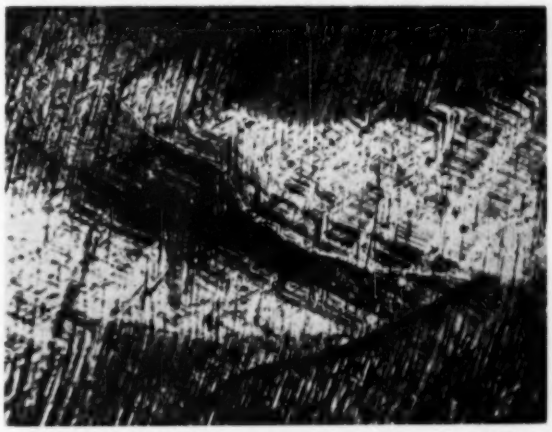

Fig. 20—Kink band formation across low energy grain boundary. X200. Area reduced approximately 30 pct for reproduction.

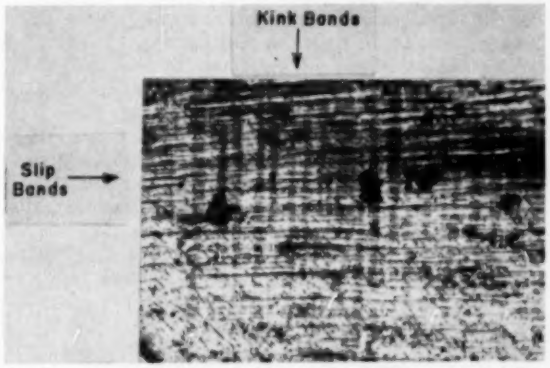

Fig. 21—Arrays of fine kink bands in the vicinity of fracture. X200. Area reduced approximately 50 pct for reproduction.

Lueders' Bands: Lueders' bands, which are also a kind of deformation band characterized by a localized and discontinuous yielding, were observed in a number of extended crystals in the vicinity of the gripped ends. The nature of their occurrence was described in a previous report,[20] which revealed that the bands consist of clusters of fine $\{10\bar{1}0\}$ slip markings.

Two examples are reproduced in Figs. 22 and 23, for the purpose of illustrating the close association

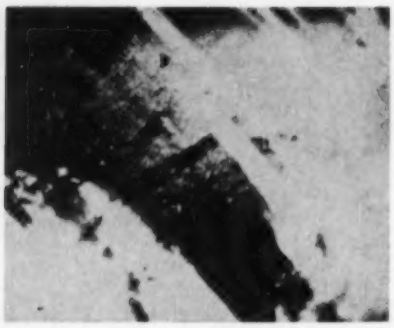

Tension axis → . X7.

Fig. 22 (above)—Appearance of Lueders' bands near gripped end of crystal.

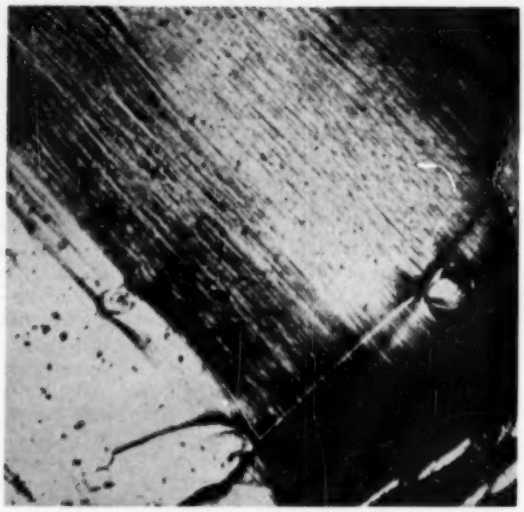

Fig. 23 (right)—Appearance of Lueders' bands at higher magnification. Note complex kink band formation in lower right corner. X350.

of kink bands with the discontinuous yielding of Lueders' deformation. Fig. 22 shows a number of coarse kink bands forming preferentially across a Lueders' deformation at approximately right angles to its advancing edge. Fig. 23 illustrates the complex kink band formation, described in the preceding section. Two primary kink bands, appearing in the lower right corner of the micrograph, have suffered displacements through the formation of secondary kink bands.

Stress-Strain Characteristics: The stress-strain diagram for a crystal extended 2 pct at room temperature is shown in Fig. 24, which also includes a stereographic triangle indicating the original orientation of the crystal. There is a smooth and gradual transition from the elastic to the plastic region of the curve, which makes it difficult to assign a single value to the yield point. For this reason two values of the critical shear stress, S_s, are given in the figure. The value 4900 grams per sq mm represents the shear stress at the point of deviation from linearity in the elastic range; whereas the value 6800 grams per sq mm represents the shear stress for the onset of extensive flow. As indicated in the figure, this latter value was obtained from the extrapolated point representing the intersection of the elastic range and the straight line portion of the plastic region. A comparison of this value of critical shear stress with those reported by Anderson and Jillson[20] for prismatic slip in arc-melted iodide titanium shows reasonable agreement.

Table I contains the data pertinent to the evaluation of the critical resolved shear stress for three crystals of different orientation. The variation between the extreme values is somewhat greater than that which can be attributed to experimental error, but there is good reason to believe that the gaseous impurities (oxygen and hydrogen) in this metal vary in amounts which could account for the variations.

Fig. 24 also indicates a significant and approximately linear increase in the resistance to glide over the extension range of the test. The value of the coefficient of shear hardening, τ/a, was calculated to be 25,900 grams per sq mm, which is considerably higher than that for the other common hexagonal metals (magnesium, zinc, and cadmium) at room temperature.

Two crystals were extended to fracture at a strain rate of 0.003 min^{-1}; and, in both cases, the fracture occurred along a plane which closely approximated the observed $\{10\bar{1}0\}$ slip plane. It would appear from this, therefore, that the fracture plane in titanium has the same crystallographic significance as that observed in a number of other metals.[18, 23-28]

Discussion of Results

Slip and Twin Behavior: The occurrence of unpredictable cross slip in titanium is the first reported in a metal of the hexagonal close-packed type. In α-brass[29] and copper,[27] the cross slip is confined to octahedral planes, which are also the planes of primary slip. In aluminum, where it has been reported that cross slip can occur on several different families of planes,[5] octahedral cross slip is still the most prevalent. This suggests that a definite preference exists for cross slip to take place on planes of the same type as primary slip. Hence, the occurrence of cross slip in titanium on a type I prismatic plane might be attributed to the existence of three possible prismatic slip planes in contrast to the single basal slip plane in the other common hexagonal metals. Unlike the face-centered cubic metals, however, the slip direction is not the same for primary and cross slip.

The results on $\{11\bar{2}1\}$ twinning definitely suggest that the main operative twinning plane bears a definite crystallographic relationship with the primary slip plane and can, therefore, be predicted from crystal orientation. Moreover, it was found that the stepped $\{11\bar{2}1\}$ twinning plane bears a similar relationship with the observed secondary slip plane. Since it has been shown that the secondary slip plane can be predicted from crystal orientation, the same prediction applies to the stepped twinning

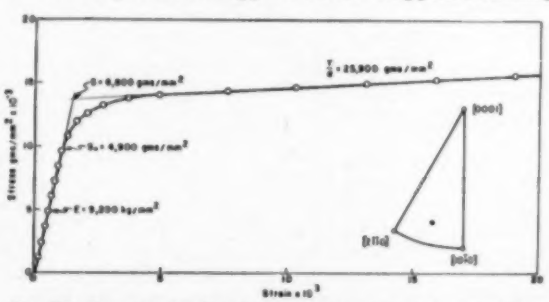

Fig. 24—Stress-strain diagram for titanium crystal extended at room temperature.

plane. The general behavior indicates that, as in the case of slip, the selection of the $\{11\bar{2}1\}$ twinning plane in titanium is determined by a resolved shear stress law. According to the work of Davidenkov et al.,[28] this is also true in the case of $\{10\bar{1}2\}$ twinning in zinc.

Kink Band Formation: The remarkable consistency in the crystallographic geometry of kinking from metal to metal of different slip habit and structural class suggests that this deformation phenomenon is as fundamental a property of the metal as the slip process itself. Moreover, since kink bands are generally observed only after extensive deformation by slip, it is possible that the reasons for their occurrence are related in some manner to the nature of the slip process. In this connection it is significant that kinking in extended titanium crystals was frequently associated with flow inhomogeneities in the vicinity of grain boundaries and included grains, with Lueders' deformation, and with crystals whose orientation suggested a slip pattern of coarse, widely spaced bands. In each case, the deformation by slip was discontinuous in that large contiguous regions of the crystal had undergone markedly different degrees of deformation. On the other hand, in crystals whose orientation predicted duplex slip at the onset of plastic flow, kink bands were microscopically undetectable. The slip band pattern in these crystals consisted of intersecting fine, closely spaced lines, which suggest a uniform, widespread deformation by slip.

Since discontinuous yielding represents a flow pattern which can lead to large bending stresses similar to those associated with the gripped ends of the specimen,[29] it is believed that the formation of kink bands relieves such stresses when other mechanisms of flow are not available. This view is supported by the apparent absence of kink bands in deformed crystals where unpredictable secondary slip or twinning had occurred; and, presumably, these latter mechanisms could relieve those stresses which otherwise would necessitate kink band formation. This reasoning could also explain the absence of kink bands in α-brass crystals exhibiting profuse cross slip, as well as the infrequent occurrence of kinking in extended hexagonal metals as compared to those of the face-centered cubic type where twinning is not regarded as a flow mechanism. By the same argument, the frequent appearance of kink bands in the extended crystals of titanium is probably due to the fact that their orientation prohibited twinning of the $\{10\bar{1}2\}$ type. The inference that twinning is a stress-relief mechanism is not new, and was recently suggested by Burke and Hibbard[16] and Cahn[17] in their work on the deformation processes in magnesium and uranium, respectively.

In view of these considerations, it is possible to conclude that there are available at least three

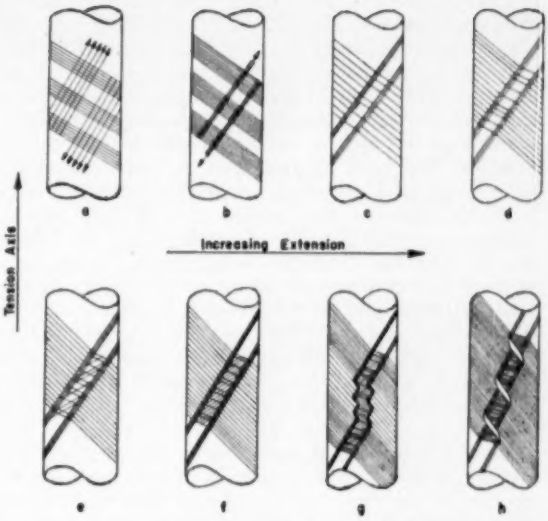

Fig. 25—Schematic representation of coarse kink band formation in extended titanium crystals. With increasing extension: a—Formation of individual bend planes of opposite sign at flow inhomogeneities. b—Grouping of individual bend planes to form bands of bend planes of opposite sign. c—Disorientation of region between bands of bend planes with crystal matrix to form coarse kink band. d—Increasing disorientation as a result of more effective trapping of dislocations by bend planes. e—Formation of secondary slip system within kink band in order to permit rotation of kink band toward the stress axis in an opposite sense to primary slip markings. f—Increasing density of secondary slip within kink band. g—Appearance of stepped discontinuities along the parallel bands of bend planes as a result of wide differences in primary slip band density. h—Formation of secondary kink bands within the primary kink band, and the resulting displacement of the primary band along the bend planes of the secondary bands in order to permit further rotation of primary kink band.

stress-relief mechanisms associated with the accommodation of lattice bending resulting from either a marked heterogeneous flow process or constraints imposed by grips in the conventional method of testing. These are secondary slip, twinning, and kinking. Moreover, it is apparent that the selection of any one, or a combination, of these mechanisms will depend to a large extent upon such factors as crystal structure, crystal orientation, temperature of testing, and alloying; since it is apparent that these factors can have a pronounced effect on the availability of these mechanisms as well as the development of slip bands.

In connection with the orientation dependence on the formation of kink bands, it should be emphasized that failure to detect their presence in crystals exhibiting multiple slip does not necessarily indicate their absence, for it is conceivable that the kink bands in these crystals are so fine as to be undetectable by ordinary light microscopy. This view is supported by the very recent work on aluminum by Honeycombe,[18] who employed X-ray micrography to detect the presence of very fine kink bands which were optically invisible even after heavy deformations. Thus, if the observed orientation dependence of kink band formation is not a true one as regards the occurrence of kinking, such a dependence surely exists in relation to the nature and distribution of kink bands.

From the data of the present investigation, it is believed that the nature of the formation and development of coarse kink bands, along with their com-

Table I. Critical Shear Stress Data for Room Temperature Tests

Crystal No.	χ_o, Degrees	λ_o, Degrees	Sin χ_o Cosλ_o	Critical Shear Stress, Grams per Sq Mm: Deviation from Hooke's Law	Critical Shear Stress, Grams per Sq Mm: Plastic Flow at Constant Rate
1	35	46	0.491	4900	6800
2	52	50	0.472	5600	6400
3	47	47	0.498	4500	5900

plexities, occurs in accordance with the sequence of events depicted in Fig. 25. As a function of increasing deformation, these may be described as follows:

1—In the initial stage, Fig. 25a, it is postulated that a number of bend planes of opposite sign originate in regions associated with large bending stresses as a result of inhomogeneities in the flow process. The bend planes then propagate through the crystal in a direction perpendicular to the slip direction because dislocations of one sign possess minimum energy in such an orientation.[8] As deformation proceeds, Fig. 25b, bend planes of one sign migrate to form narrow bands or groupings of individual bend planes, which are fixed because of their effectiveness in trapping dislocations moving along the active slip planes. It is believed that two such bands of bend planes of opposite sign outline the off-oriented regions defining the coarse kink bands.

2—The number of dislocations trapped by the parallel bands of bend planes increases with deformation so that the density of slip lines within the region bounded by the bend planes is less than that in the crystal matrix (see Fig. 25c). This accounts for the lag in lattice reorientation within the kink bands, which can be expected to increase with deformation as a result of the increased effectiveness of the highly curved bend planes to trap additional moving dislocations (see Fig. 25d). In effect, this is to say that the kink band is rotating toward the stress axis in an opposite sense to the slip lines.

3—With an increased lag in lattice reorientation, secondary slip occurs within the kink band on a type I prismatic plane (Fig. 25e), which would be expected to operate in view of the apparent rotation of the kink band. With increasing extension, slip occurs within the kink band on the secondary planes more often than not, so that at higher deformations the secondary slip system is more predominant and, hence, can no longer be considered secondary (see Fig. 25f). At this stage, the kink bands frequently appear wavy in their path across the crystal. This characteristic is probably due to variations in the degree of deformation along the crystal, which result in the formation of stepped discontinuities along the bend planes (see Fig. 25g). The bend planes corresponding to these steps are related to the secondary slip within the kink band in a manner consistent with the established geometry of kinking.

4—In the final stage, continued rotation of the kink band toward the stress axis is accomplished through the formation of secondary kink bands in the manner depicted in Fig. 25h. The secondary bands originate in the highly stressed regions of the primary bend planes, and are crystallographically related to the secondary slip system, appearing in the lattice of the primary kink band, in the same manner as the primary kink band is related to the primary slip system of the crystal matrix. With increased deformation, extensive secondary slip occurs within the secondary bands (not shown in Fig. 25h, for purposes of clarity), and this results in a rotation of the lattice of the secondary bands toward the stress axis in the same sense as that of the primary kink band. This rotation could account for the observed displacement of the primary kink band along the bend planes of the secondary bands — a gross flow feature not unlike the block movements generally thought of in regard to the process of slip.

Conclusions

1—In conformity with the law of maximum shear stress, type I prismatic slip in titanium can be predicted from crystal orientation, and duplex slip occurs when two slip systems are geometrically favorable for glide.

2—Unpredictable cross slip occurs on the same crystallographic family of planes which define primary slip; i.e., $\{10\bar{1}0\}$.

3—Unpredictable, secondary slip occurs on that $\{10\bar{1}0\}$ plane for which the resolved shear stress is next to the maximum.

4—The development of $\{10\bar{1}0\}$ slip bands is orientation dependent, in that for a given shear the slip band density varies inversely with the angle, χ, which the slip plane makes with the stress axis.

5—$\{11\bar{2}1\}$ twinning can be predicted from crystal orientation, which suggests that its occurrence is determined by a resolved shear stress law.

6—The crystallographic and geometrical features of kink band formation in titanium are very similar to those reported in a number of hexagonal and face-centered cubic metals.

7—The formation of microscopically detectable kink bands appears orientation dependent, and is associated with heterogeneities in the flow process. Kink bands were never observed in crystals which exhibited duplex slip or twinning.

8—The kink band rotates in an opposite sense to the primary slip markings, and this rotation is accommodated by the following phenomena: (a)—appearance of secondary slip within the region of the kink band, (b)—the formation of stepped discontinuities along the bend planes, and (c)—the formation of secondary kink bands within the region of the primary kink bands.

9—The values of critical resolved shear stress and coefficient of shear hardening were determined in several crystals extended at room temperature, and fracture took place on the operative $\{10\bar{1}0\}$ slip plane.

Acknowledgment

The author wishes to express his indebtedness to Mr. F. C. Perkins for his skillful assistance in carrying out various aspects of the experimental program. He is further obliged to Mrs. A. Van Riper for the X-ray orientation determinations; to various members of the metallography department for their work in preparing specimens for optical micrography; and, finally, to Dr. H. P. Kling for his constructive comments on various phases of this study. The work reported herein was supported by the Office of Air Research, Contract No. AF-33-038-16031.

References

[1] F. D. Rosi, C. A. Dube, and B. H. Alexander: Mechanism of Plastic Flow in Titanium. Determination of Slip and Twinning Elements. *Trans.* AIME (1953) **197**, p. 257; JOURNAL OF METALS (February 1953).

[2] E. N. da C. Andrade and B. Chalmers: The Resistivity of Polycrystalline Wires in Relation to Plastic Deformation, and the Mechanism of Plastic Flow. *Proc.* Royal Soc. (1932) **A138**, pp. 348-352.

[3] E. Schmid and W. Boas: *Kristallplastizitat* (1935) Berlin. J. Springer.

[4] G. I. Taylor and C. F. Elam: The Plastic Extension and Fracture of Aluminum Crystals. *Proc.* Royal Soc. (1925) **A108**, p. 28.

[5] G. I. Taylor and C. F. Elam: The Distortion of an Aluminum Crystal During a Tensile Test. *Proc.* Royal Soc. (1923) **A102**, p. 643.

[6] H. J. Gough: *Proc.* ASTM (1933) **33**, Part II, p. 3.
[7] E. N. da C. Andrade and P. J. Hutchings: Behavior of Single Crystals of Mercury. *Proc.* Royal Soc. (1935) **A148**, p. 120.
[8] R. W. Cahn: Slip and Polygonization in Aluminum. *Journal* Inst. Metals (1951) **19**, p. 129.
[9] J. B. Hess and C. S. Barrett: Structure and Nature of Kink Bands in Zinc. *Trans.* AIME (1949) **185**, p. 599; JOURNAL OF METALS (September 1949).
[10] J. A. Collins and C. H. Mathewson: Plastic Deformation and Recrystallization of Aluminum Single Crystals. *Trans.* AIME (1940) **137**, p. 150.
[11] C. Crussard: *Bulletin*, Soc. Franc. Mineral (1945) **68**, p. 174.
[12] D. C. Jillson: An Experimental Survey of Deformation and Annealing Processes in Zinc. *Trans.* AIME (1950) **188**, p. 1009; JOURNAL OF METALS (August 1950).
[13] R. W. K. Honeycombe: Inhomogeneities in the Plastic Deformation of Metal Crystals. *Journal* Inst. Metals (1951) **80**, p. 45.
[14] L. B. Pfeil: *Carnegie Scholarship Memoirs* of the Iron and Steel Inst. (1926) **15**, p. 319; (1927) **16**, p. 153.
[15] A. Lalouef and C. Crussard: Relation Between the Deformation and Recrystallization of Monocrystals of Aluminum. *Revue Metallurgie* (1951) **48**, p. 462.
[16] N. K. Chen and C. H. Mathewson: Structural Studies of Plastic Deformation in Aluminum Single Crystals. *Trans.* AIME (1951) **191**, p. 653; JOURNAL OF METALS (August 1951).
[17] R. W. Cahn: Plastic Deformation of Alpha-Uranium. *Acta Metallurgica* (1953) **1**, p. 49.
[18] E. C. Burke and W. R. Hibbard, Jr.: Plastic Deformation of Magnesium Single Crystals. *Trans.* AIME (1952) **194**, p. 295; JOURNAL OF METALS (March 1952).
[19] F. D. Rosi and C. H. Mathewson: A Study of the Plastic Behavior of High-Purity Aluminum Single Crystals at Various Temperatures. *Trans.* AIME (1950) **188**, p. 1159; JOURNAL OF METALS (September 1950).
[20] F. D. Rosi and F. C. Perkins: Mechanical Properties and Strain Aging Effects in Titanium. *Trans.* ASM (1953) **45**, p. 972.
[21] E. A. Anderson and D. C. Jillson: Progress Report No. 10 (April 1-April 30, 1952) of New Jersey Zinc Co., Palmerton, Pa. Contract No. DA-36-034-ORD-278RD., RAD No. ORDTB-1-12045-2.
[22] E. Schmid: Normalspannungsgesetz. *Proc.* Internat. Congr. Appl. Mech. Delft (1924) p. 342.
[23] W. Boas and E. Schmid: Widenspruch mit Normaldilatationsgesetz. *Ztsch. Physik* (1929) **56**, p. 516.
[24] M. Georgieff and E. Schmid: Uber die Festigkeit und Plastizitat von Wismitkristallen. *Ztsch. Physik* (1926) **36**, p. 759.
[25] E. Schmid and G. Wassermann: Uber die Festigkeit von Tellukristallen. *Ztsch. Physik* (1927) **46**, p. 653.
[26] R. Maddin, C. H. Mathewson, and W. R. Hibbard, Jr.: Unpredicted Cross-Slip in Single Crystals of Alpha Brass. *Trans.* AIME (1948) **175**, p. 86; METALS TECHNOLOGY (February 1948).
[27] F. D. Rosi: Unpublished work on formation of slip bands in metal crystals.
[28] N. N. Davidenkov, A. F. Kolesnikov, and K. N. Fedorov: On the Twinning of Zinc. *Journal of Experimental and Theoretical Physics* (1933) **3**, p. 350.
[29] R. F. Miller: Influence of a Grain Boundary on the Deformation of a Single Crystal of Zinc. *Trans.* AIME (1934) **111**, p. 135.

Technical Note

Reaction of Oxygen and Nitrogen with Titanium from 700° to 1050°C

by Lee S. Richardson and Nicholas J. Grant

REACTIONS of oxygen and nitrogen at low pressures with titanium have recently been studied by a number of investigators.[1-6] Gulbransen and Andrew[1] noted that the reaction with nitrogen followed the parabolic rate law whereas the reaction with oxygen deviated slightly from this law in the temperature range 300° to 800°C.

In the work reported here, commercial titanium (75 A) was used as the test material. Cylinders 2.5 in. long and 0.25 in. in diameter were machined from heavier bar stock. The test pieces were given a metallographic finish, immersed for 30 min in cold concentrated HCl, washed in water, then acetone, and dried with lint-free cloth.

Reaction rates were determined in a modified Sieverts type apparatus by measuring the decrease in gas pressure of the reacting gas contained in a constant volume. The amount of gas added could be measured in a calibrated gas burette to an accuracy of 0.01 mm. During the course of a run the temperature never varied by more than 10°C and then only for brief moments.

After placing the specimen in the furnace, the system was first evacuated for 12 hr at room temperature, and then flushed with purified argon five times, adsorbed gases being discharged during this period from the glass system with a high frequency spark coil. The flushing and discharging were repeated at 400°C. This rather involved procedure was found necessary after a number of trial runs indicated extraneous effects traceable to the system.

Reaction periods up to 2 hr were used, at initial gas pressures of 0.2 to 0.5 atm.

L. S. RICHARDSON, Junior Member AIME, is Research Assistant, and N. J. GRANT, Member AIME, is Associate Professor, Dept. of Metallurgy, Massachusetts Institute of Technology, Cambridge, Mass.

TN 201E. Manuscript, Aug. 31, 1953.

Experimental Results

Fig. 1 shows the decrease in oxygen pressure for tests at 0.5 atm at various temperatures as a function of the square root of the time. Deviations from linearity are minor and the parabolic rate law is obeyed. Fig. 2 shows the same plot for the nitrogen reaction. A definite deviation from linearity is noted; however, it is probable that the higher initial rates are caused by the presence of small amounts of oxygen contamination, the initial faster rate changing to the slower rate after about 5 to 10 min.

Calculations of the rate constants were made on the basis of the latter portion of the curves.

The parabolic rate law constants calculated from these curves are shown for oxygen and nitrogen in Fig. 3. In spite of some scatter the average curves are quite definite. Changes in gas pressure of the order of 20 pct did not result in a measurable change in the rate law constants.

The activation energy for the oxygen reaction was calculated to be 47,400 cal per mol (above 700°C), which is not in agreement with the value quoted by Gulbransen and Andrew[1] for lower temperatures, their value being 26,000 cal below 600°C.

The activation energy for the nitrogen reaction was calculated to be 45,400 cal per mol above about

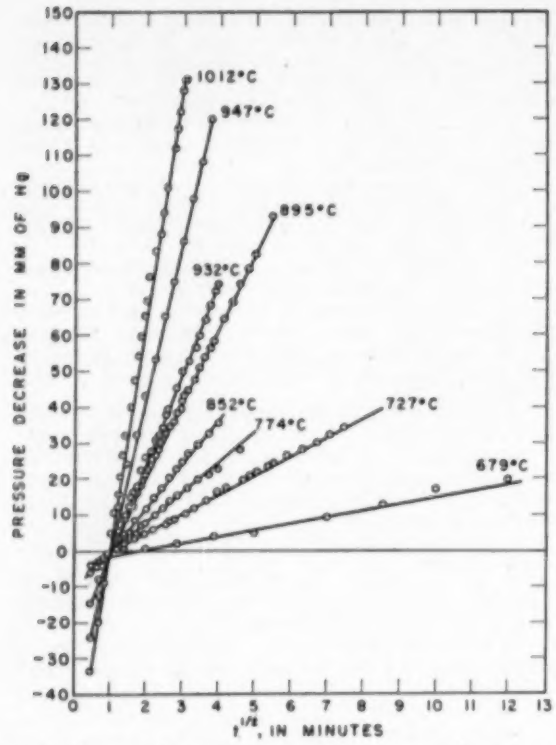

Fig. 1—Decrease of oxygen pressure with time at specimen temperatures shown.

800°C, which is only in fair agreement with the value given by Gulbransen and Andrew, whose value was 36,300 cal below 800°C.

It is evident from Fig. 3 that the reaction rate of titanium with oxygen is nearly 50 times as large as that with nitrogen.

Extensive X-ray studies of the surfaces of the specimens reacted with oxygen showed the presence of TiO_2 (rutile), TiO, and Ti. Presumably any

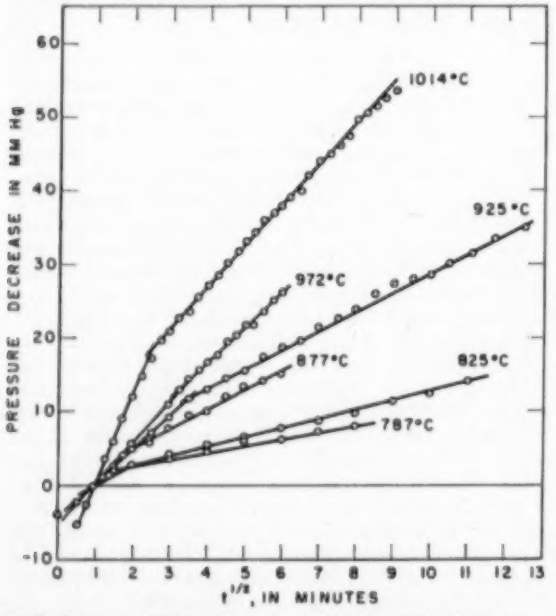

Fig. 2—Decrease of nitrogen pressure with time at specimen temperatures shown.

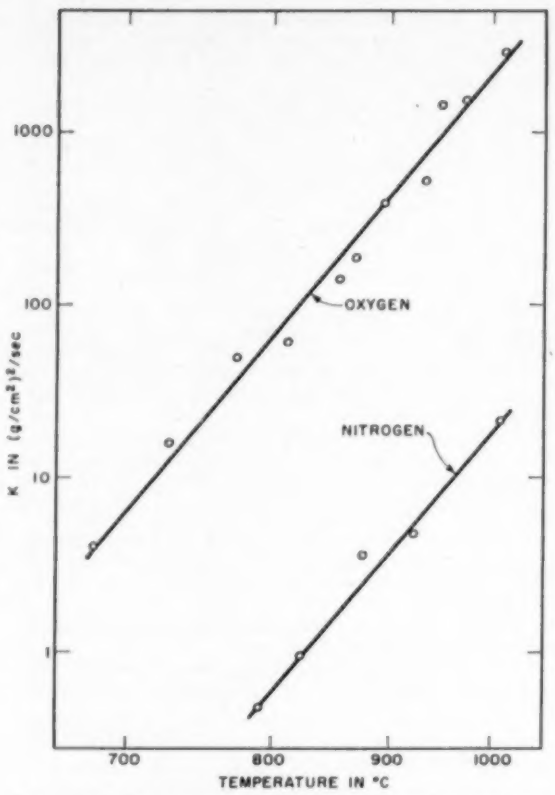

Fig. 3—The change of the parabolic rate law constant with temperature for the reaction of oxygen and of nitrogen with titanium.

coating of Ti_2O_3 was too thin to yield a diffraction pattern, although Davies and Birchenall[3] reported its existence when using sensitive techniques. At 650°C, the oxide thickness was found to be extremely thin. The 800°C test had an appreciable oxide layer. TiO was found when the outermost scale was removed by abrasion.

Based on X-ray diffraction studies of the nitrogen reacted specimens, only the patterns of titanium and TiN were found.

Acknowledgments

The authors acknowledge the support of the Wright Air Development Center, Dayton, Ohio, whose support permitted the initiation of this work, under Contract No. AF 33 (038)-8754.

References

[1] E. A. Gulbransen and K. F. Andrew: Kinetics of the Reaction of Titanium with Oxygen, Nitrogen, and Hydrogen. *Trans.* AIME (1949) **185**, p. 741; JOURNAL OF METALS (October 1949).

[2] L. G. Carpenter and F. R. Reavell: Some Experiments on the Reaction of Titanium with Oxygen and Nitrogen. *Metallurgia* (1948) **39**, p. 63.

[3] M. H. Davies and C. E. Birchenall: The Oxidation of Titanium. *Trans.* AIME (1951) **191**, p. 877; JOURNAL OF METALS (October 1951).

[4] J. W. Hickman and E. A. Gulbransen: Oxide Films Formed on Titanium, Zirconium, and Their Alloys with Nickel, Copper, and Cobalt. *Analytical Chemistry* (1948) **20**, p. 158.

[5] E. A. Gulbransen and K. F. Andrew: Reaction of Tantalum, Columbium, Zirconium, and Titanium with the Gases, Oxygen, Hydrogen and Nitrogen at Elevated Temperatures. *Trans.* Electrochem. Soc. (1946) **96**, p. 364.

Creep Correlations of Metals at Elevated Temperatures

by Oleg D. Sherby, Raymond L. Orr, and John E. Dorn

Creep data for pure metals at temperatures above those at which rapid recovery occurs (above about 0.45 the melting temperature) are correlatable by means of the equations $\epsilon = f(te^{-\Delta H/RT}, \sigma)$ and $\sigma = f(\dot{\epsilon}e^{\Delta H/RT})$. These correlations were applied successfully to data for aluminum, iron, nickel, copper, zinc, platinum, gold, and lead as well as for simple alloys. For a given metal, ΔH is a constant about equal to the activation energy for self-diffusion.

THE early recognition that creep is stimulated by thermal activation prompted numerous investigators[1, 2] to apply the same laws that are valid for the viscous behavior of liquids to analyses of creep data. To a good first approximation these laws are summarized by the equation

$$\dot{\epsilon} = S' e^{-\Delta H/RT} \sinh \frac{B'\sigma}{RT} \qquad [1]$$

where $\dot{\epsilon}$ is the creep rate; T, the absolute temperature; R, the gas constant in cal per degree per mol; σ, the applied stress; ΔH, the activation energy in cal per mol; S', a constant dependent on the entropy of activation, the frequency of activation, and the contribution of each activation to the strain; and B', a constant dependent upon the size of the flow unit that is activated.

Although Eq. 1 describes the flow of viscous fluids very accurately, its application to the creep of solids has been disappointing. Two reasons for the failure of Eq. 1 for creep are now known: First, the decelerating creep rates during primary creep demand that the internal structures of the metals are changing and that these changes might be reflected by changes in one or more of the three creep parameters S', ΔH, and B'. Consequently when the conventional methods of evaluating these parameters are employed by comparing the secondary creep rates at a series of temperatures and at a series of stresses, the true effects of temperature and stress are masked because of simultaneous changes in one or more of the creep parameters. Second, as will be illustrated more fully later, three distinctly different types of investigations have shown that the stress term for high temperature creep enters the analysis as σ and not as σ/T. This rather unexpected result points sharply to a significant fundamental difference between the mechanisms for the viscous behavior of fluids and the high temperature creep of metals.

O. D. SHERBY, Junior Member AIME, and R. L. ORR are Research Engineers, and J. E. DORN, Member AIME, is Professor of Physical Metallurgy, University of California, Berkeley, Calif.

Discussion on this paper, TP 3683E, may be sent, 2 copies, to AIME by April 1, 1954. Manuscript, May 8, 1953. New York Meeting, February 1954.

More recent extensive investigations[3, 4] on the creep of high purity aluminum and several of its dilute α solid solutions have shown that

$$\epsilon = f(\theta, \sigma_c) \qquad [2]$$

where ϵ is the total creep strain; $\theta = \int_0^t e^{-\Delta H/RT}\, dt$ = temperature compensated time $= te^{-\Delta H/RT}$ for a constant temperature test; σ_c is the initial stress in a *constant* load test or the *constant* true stress in a constant stress test;* and t is the duration of test.

* Eq. 2 is valid for either constant stress or constant load tests; but the total creep curve is different (i.e. the function, f, is different) for each test.

The fundamental origin of the validity of Eq. 2 is thought to arise from some equivalence of substructures in constant load creep tests at equal values of θ or ϵ. Both X-ray and metallographic examination revealed that practically identical lattice distortions and subgrain sizes are obtained for the same creep strain under the same load over wide ranges of test temperature.[4] Furthermore the room temperature tensile properties following equal creep strains at different temperatures under constant loads were also identical, illustrating that identical substructures were indeed obtained.[4, 5]

A second type of correlation was obtained by differentiating Eq. 2 with respect to time, giving

$$\dot{\epsilon} = \left(\frac{\partial f}{\partial \theta}\right) \frac{d\theta}{dt} = f'(\theta, \sigma_c)\, e^{-\Delta H/RT}. \qquad [3]$$

For the secondary creep rate, denoted by $\dot{\epsilon}_s$,

$$\dot{\epsilon}_s = f'(\theta_s, \sigma_c)\, e^{-\Delta H/RT}.$$

But Eq. 2 reveals that θ_s is a function of σ_c alone because the secondary creep rate in a given constant load test is always reached at a fixed value ϵ_s.

Therefore

$$\sigma_c = f(\dot{\epsilon}e^{\Delta H/RT}) = f(Z) \qquad [4]$$

where Z is the function that was introduced a number of years ago by Zener and Hollomon.[6] Eq. 4 is not only valid for creep but will permit correlations between constant load creep and tensile data where $\dot{\epsilon}_c$ is the rate of tensile straining and σ_c is the engineering ultimate tensile strength.

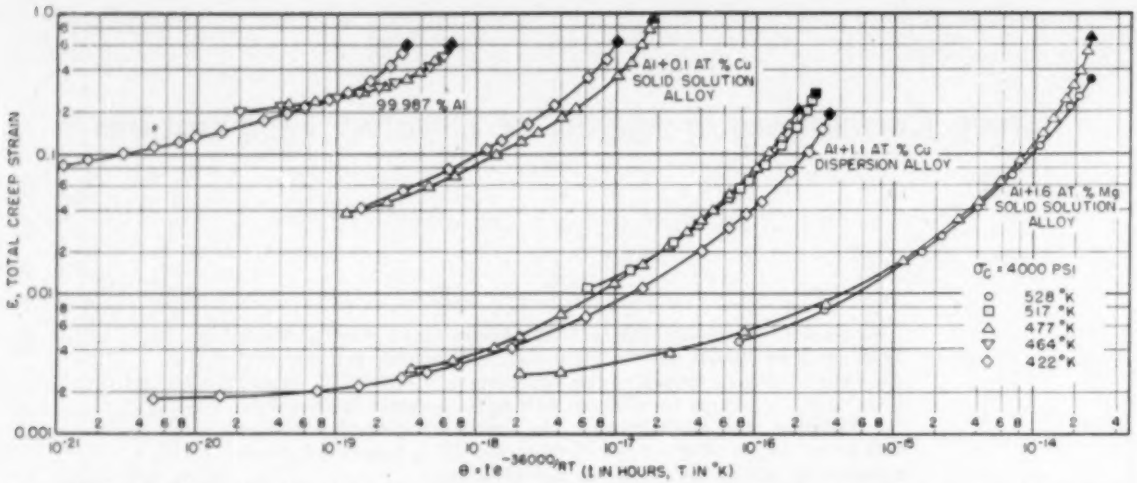
ε, TOTAL CREEP STRAIN
99.987 % Al
Al+0.1 AT % Cu SOLID SOLUTION ALLOY
Al+1.1 AT % Cu DISPERSION ALLOY
Al+1.6 AT % Mg SOLID SOLUTION ALLOY
σc = 4000 PSI
528 °K
517 °K
477 °K
464 °K
422 °K
θ = te^-36000/RT (t IN HOURS, T IN °K)

Fig. 1—Correlation of creep strain-time data for aluminum and dilute aluminum alloys by means of the relation $\epsilon = f(\theta)$ for a stress of 4000 psi. Data of Sherby and Dorn[3, 4] and Giedt, Sherby, and Dorn.[5]

Investigations on the effect of stress on the creep rate at constant substructures[7] have shown that Eq. 3 reduces to

$$\dot{\epsilon} = Se^{-\Delta H/RT} \sinh B\sigma \qquad [5]$$

where B is independent of temperature and substructures generated during creep but does depend on alloying.

The evaluation of the activation energy, ΔH, for the creep of aluminum alloys by means of Eqs. 2 and 4 gave the following conclusions:

1—ΔH is practically a universal constant for aluminum; it is independent of temperature over wide ranges of temperature (above that at which rapid recovery occurs, which is about 0.45 the melting temperature, Tm), creep stress, creep strain, grain size, substructures developed during creep and small alloying additions,[3, 4] as well as cold work[8] and dispersions of $CuAl_2$.[9†]

† For some as yet unknown reasons the creep behaviors of some commercial aluminum alloys such as 24S-T are not analyzable by these methods.

2—Although creep takes place at temperatures below about 0.45 Tm, the correlations suggested by Eqs. 2 and 4 are valid only above 0.45 Tm for aluminum. Perhaps no special meaning can be ascribed to the number 0.45 Tm above which the creep laws given previously are valid. But it is significant to note 0.45 Tm is that temperature at which the tensile strength of aluminum and its dilute alloys begin to decrease rapidly with increase in temperature due to rapid recovery rates.[10] Evidently these proposed

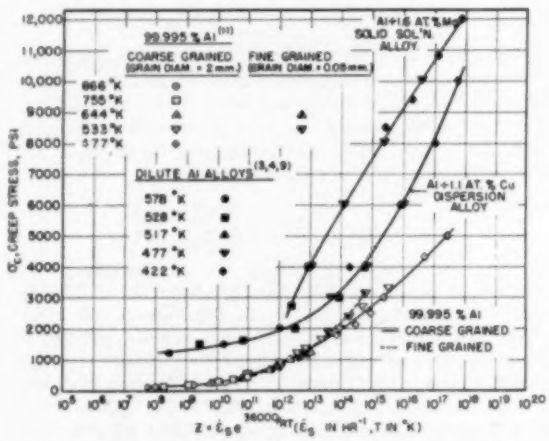

Fig. 2—Correlation of stress-secondary creep rate data for aluminum and dilute aluminum alloys by means of the relation $\sigma_c = f(\dot{\epsilon}, e^{\Delta H/RT})$. Data of Sherby and Dorn,[3, 4] Giedt, Sherby, and Dorn,[5] and Servi and Grant.[11]

Table I. Metals and Alloys Investigated

Atomic No.	Metal or Alloy	Melting Temperature, °K	Crystal Structure	Chemical Composition	Reference
13	Al	933	fcc	99.987% Al	Sherby and Dorn[3,4]
				99.995% Al	Servi and Grant[11]
	Al-Mg solid sol'n. alloy	—	fcc	High purity Al plus 1.6 atomic % Mg	Sherby and Dorn[3,4]
	Al-Cu solid sol'n. alloy	—	fcc	High purity Al plus 0.1 atomic % Cu	Sherby and Dorn[3,4]
	Al-Cu dispersion alloy	—	fcc	High purity Al plus 1.1 atomic % Cu	Giedt, Sherby and Dorn[5]
26	Fe	1812	bcc	99.93% Fe	Tapsell and Clenshaw[12]
28	Ni	1728	fcc	98.7% Ni	Hazlett, Parker and Nathans[13]
29	Cu	1356	fcc	—	Nadai and Manjoine[14]
	Cu-Ni alloy (Constantan)	—	fcc	55% Cu, 45% Ni (traces of Mn and Fe)	Dushman, Dunbar and Huthsteiner[6]
30	Zn	693	cph	99.0% Zn	Pomp and Länge[15]
				99.99% Zn	Graeser, Hanemann and Hofmann[16]
78	Pt	2047	fcc	99.98 + % Pt	Carreker[17]
79	Au	1336	fcc	—	Dushman et al.[2]
82	Pb	601	fcc	High purity	Alexander, Dawson and Kling[18]
				99.9998% Pb	Smith[19]
				99.997% Pb	McKeown[20]
				99.92% Pb	Smith and Howe[21]
				—	Andrade[22]

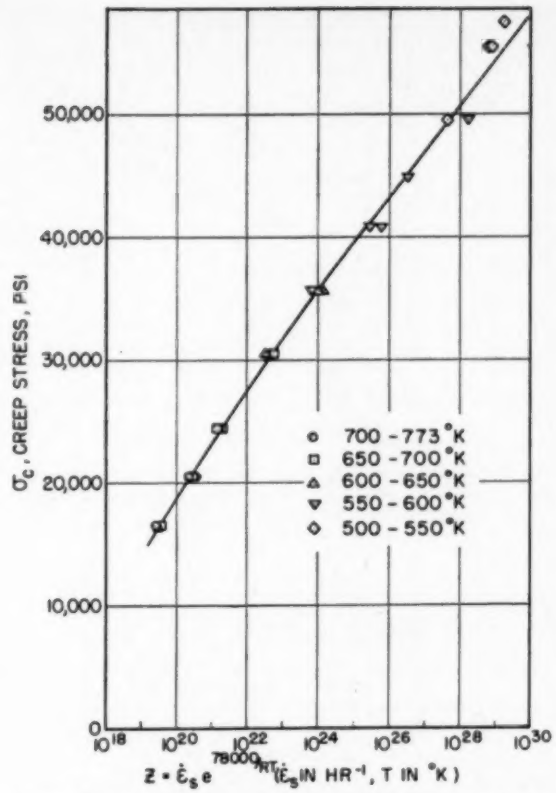

Fig. 3—Correlation of stress-secondary creep rate data for iron by means of the relation $\sigma_c = f(\dot{\epsilon}, e^{\Delta H/RT})$. Data of Tapsell and Clenshaw.[10]

laws are only valid in the temperature range where reasonably rapid recovery can occur.

3—Furthermore, the experimentally established validity of Eqs. 2, 4, and 5 proves that the stress and not the stress divided by the absolute temperature enters the creep equation for high creep temperatures. Since the stress does not enter the creep equation as stress divided by temperature, the stress term cannot enter the free energy of activation term. Consequently the mechanism for creep cannot be that of thermal activation wherein the free energy of activation includes the work term arising from the applied stress as is assumed in the derivation of Eq. 1.

The success achieved by applying Eqs. 2 and 4 to the creep of aluminum suggests that they should also be valid for other systems. Since ΔH appears to be rather insensitive to structural variables and minor alloying additions, it appears to be a fundamental property and should therefore be correlatable with other fundamental properties. It is the purpose of this paper to review creep data of various metals already reported in the literature in an attempt to test the general validity of Eqs. 2 and 4. Furthermore the activation energies for the elements studied will be evaluated in a preliminary attempt to uncover additional correlations.

Materials Investigated

Although the literature on the creep of metals is voluminous, only a few investigations have been conducted on relatively pure metals covering the ranges of variables that are required for unambiguous checks on either Eqs. 2 or 4. In order to avoid complications arising from simultaneous phenomena such as precipitation hardening, phase changes, etc., only data for relatively pure metals or simple alloy systems have been analyzed in this study. These metals are listed in Table I together with the melting temperature, crystal structure, and purity, insofar as these data were available. In view of the fact that Eqs. 2 and 4 were found to be invalid below the temperature for rapid recovery (about 0.45 Tm) for pure aluminum and its dilute alloys, an attempt was made to limit the present analyses to the high temperature range of reported test data.

Separate sets of creep data, obtained by different investigators, were found for aluminum, zinc, platinum, and lead as shown in Table I. The metals used by each group of investigators differed in chemical composition, method of preparation, and other details. The correlations of such data serve as excellent checks on the insensitivity of the activation energy for creep to small differences in alloy content, metallographic structure, and pretreatment history.

Results

Aluminum (Atomic No. 13): The various examples of analyses of creep data on high purity aluminum and its dilute alloys[3, 4, 11] including effects of grain size[11] and dispersions of $CuAl_2$[9] are reproduced here to illustrate the two alternate analytical procedures. The data recorded in Fig. 1 reveal the validity of Eq. 2 for high purity Al, high purity Al-Mg, and Al-Cu solid solution alloys, and an alloy consisting of a dispersion of $CuAl_2$ in a saturated solution of copper in aluminum. In spite of minor alloying additions in the solid solution alloys and the dispersion of $CuAl_2$ in the Al-Cu alloy, the acti-

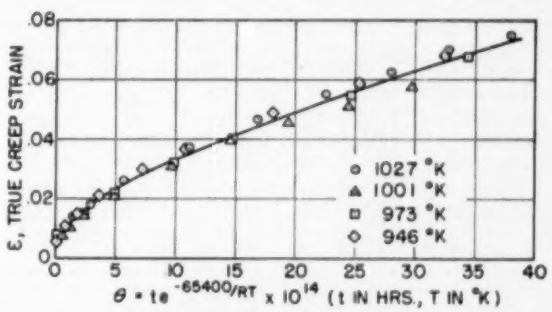

Fig. 4—Correlation of creep strain-time data for nickel by the relation $\epsilon = f(\theta, \sigma_c)$ at a constant stress of 5750 psi. Data of Hazlett, Parker, and Nathans.[10]

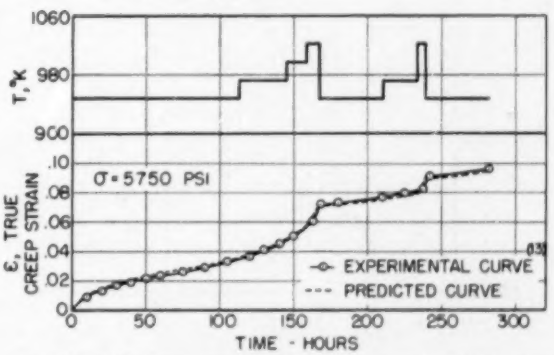

Fig. 5—Predicted and experimental creep curves for nickel when the temperature is changed as a function of time under constant stress condition.

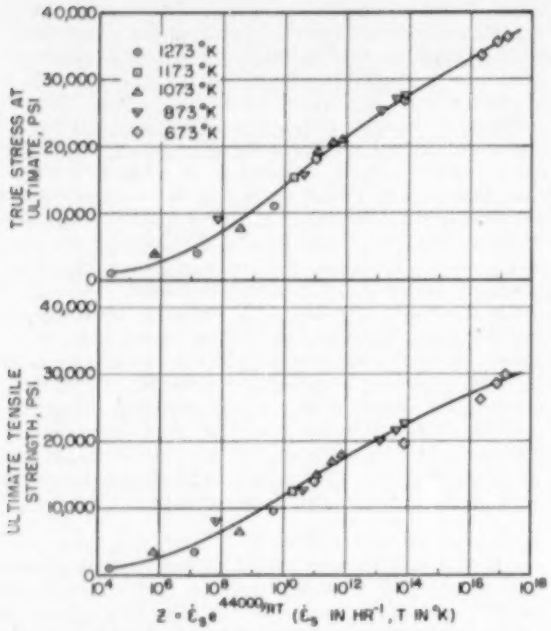

Fig. 6—Correlation of tensile data for copper at various strain rates and temperatures by means of the relation $\sigma_c = f(\dot{\epsilon}_s e^{\Delta H/RT})$. Data of Nadai and Manjoine.[14]

vation energy for creep is about the same as that for pure aluminum, namely 36,000 cal per mol. Differences in both B and S of Eq. 5 for the various alloys account for the different ϵ-θ curves shown in Fig. 1.

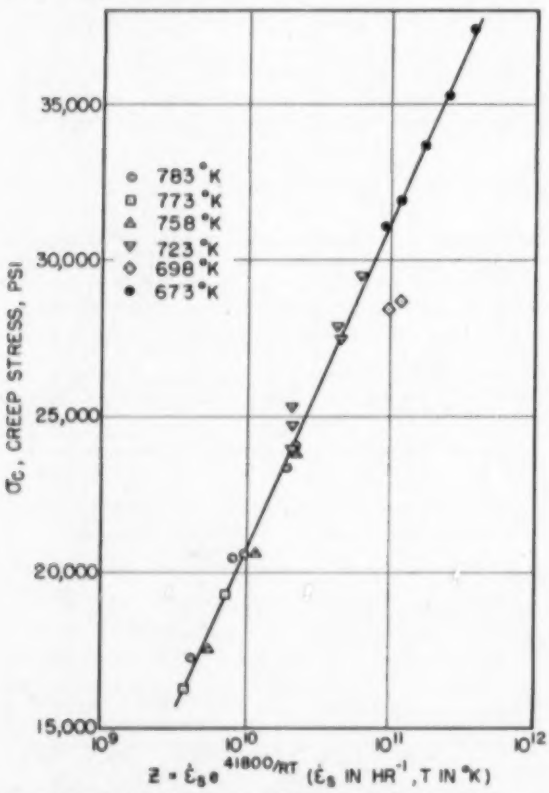

Fig. 7—Correlation of stress-secondary creep rate data for constantan (45 pct Ni, 55 pct Cu) by means of the relation $\sigma_c = f(\dot{\epsilon}_s e^{\Delta H/RT})$. Data of Dushman, Dunbar, and Huthsteiner.[3]

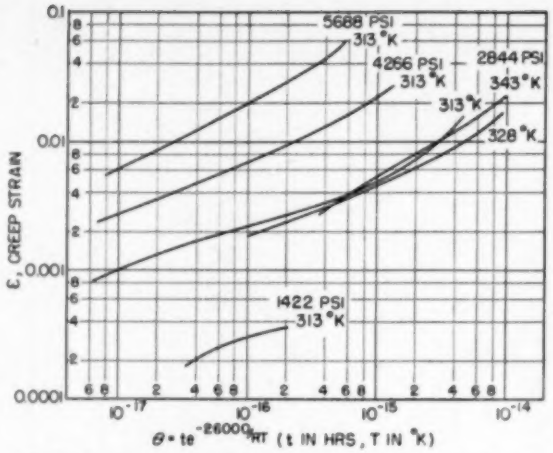

Fig. 8—Correlation of creep strain-time data for zinc by the relation $\epsilon = f(\theta, \sigma_c)$ at various stresses. Data of Pomp and Lange.[15]

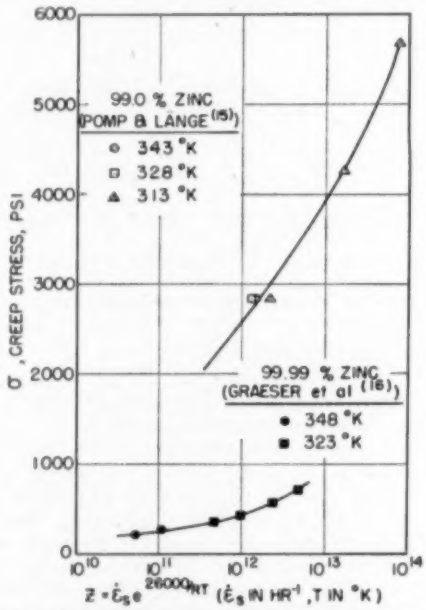

Fig. 9—Correlation of stress-minimum creep rate data for zinc by means of the relation $\sigma_c = f(\dot{\epsilon}_s e^{\Delta H/RT})$. Data of Pomp and Lange[15] and Graeser, Hanemann, and Hofmann.[16]

The data recorded in Fig. 2 reveal the application of Eq. 4 to the creep of simple aluminum alloys. Again the same activation energy is obtained independent of alloying, grain size, dispersions, or other test variables. The differences in the curves for the various alloys are again attributable to differences in B and in the values of S that are obtained at the secondary stage of creep.

Iron (Atomic No. 26): Tapsell and Clenshaw's data[13] for the creep of Armco iron from 500° to 773°K were analyzed by means of Eq. 4 which yielded an activation energy for creep of about 78,000 cal per mol. Although this range of temperature falls below 0.45 Tm, excellent correlations were achieved as shown in Fig. 3. The validity of Eq. 4 for pure iron at these temperatures suggests that for this material rapid recovery occurs at tempera-

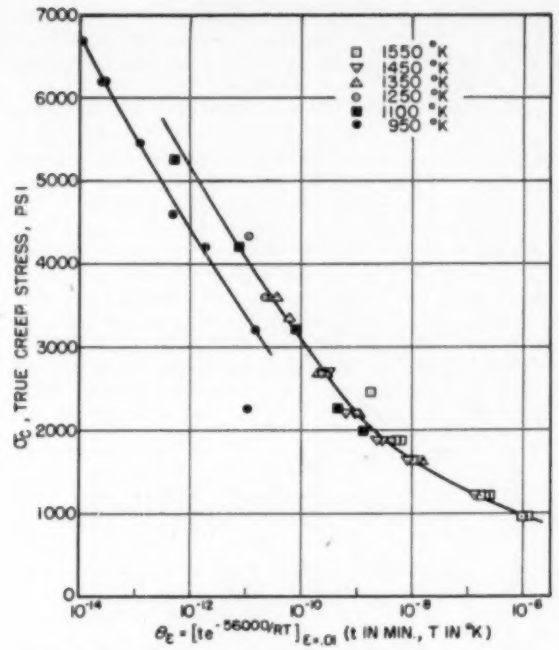

Fig. 10—Correlation of creep data for platinum by the relation $\theta = f(\epsilon, \sigma_c)$. Data of Carreker.[17]

tures considerably below 0.45 *Tm*. This deduction is given further justification by the tensile data of Tapsell and Clenshaw[18] which show the tensile strength to decrease rapidly with increase in temperature at about 500°K.

Nickel (Atomic No. 28): Hazlett, Parker, and Nathans[19] in an unclassified AEC Technical Report presented creep data under constant true stress of 5750 psi for nickel over the range from 946° to 1027°K. Their data correlated very well by means of Eq. 2 as shown in Fig. 4, wherein an activation energy, ΔH, of 65,400 cal per mol was obtained. These investigators also studied the creep behavior of nickel under the constant stress of 5750 psi for changing temperature conditions shown in the upper half of Fig. 5. They obtained the creep curve shown in the lower half of Fig. 5. Actually this experimental curve can be predicted from the ϵ-θ data of Fig. 4. Thus, when the temperature history of the test is known, a value of θ can be obtained for a given time (the area under an $e^{-\Delta H/RT} - t$ curve), following which the creep strain ϵ can be predicted from the ϵ-θ master curve of Fig. 4. In this manner the predicted curve was obtained as shown by the dotted creep curve of Fig. 5. The actual and predicted curves superimpose extremely well, further justifying the general validity of Eq. 2.

Copper (Atomic No. 29): As far as is known to the authors, there are no data available on the creep of high purity copper above 610°K, that is, above 0.45 *Tm*. Nadai and Manjoine,[14] however, studied the effect of strain rate on the tensile strength of commercially pure copper over the range 300° to 1273°K. The testing rate at high temperatures was at speeds ranging from $\dot{\epsilon}_s = 3.6 \times 10^6$ per hr to $\dot{\epsilon}_s = 3.6$ per hr. In order to correlate all of Nadai and Manjoine's data, Eq. 4 was used where σ_s refers to the ultimate tensile strength or true stress at ultimate and $\dot{\epsilon}_s$ refers to the rate of straining of the specimen. The good correlation by this equation is shown in Fig. 6. ΔH was found to be a constant of about 44,000 cal per mol for copper over the wide temperature range from above 0.45 *Tm* to almost the melting point.

45 Pct Ni-55 Pct Cu Solid Solution Alloy (Constantan): Dushman, Dunbar, and Huthsteiner[3] creep tested constantan at temperatures from 673° to 783°K. The lower limit of creep test temperature used is just equal to 0.45 *Tm*. The creep specimens were pre-annealed for 10 min at 773°K before creep testing. Their data which were analyzed by means of Eq. 4 are replotted in Fig. 7 whereby an activation energy of $\Delta H = 41{,}800$ cal per mol was obtained.

Zinc (Atomic No. 30): The investigation of the creep of zinc under constant load conditions by Pomp and Länge[15] includes data at three temperatures above 0.45 *Tm:* 313°, 328°, and 343°K. The complete creep curves correlate well by means of Eq. 2 as is shown in Fig. 8, yielding an activation energy of 26,000 cal per mol. The minimum creep rates obtainable from these data were also analyzed by means of the relation $\sigma_s = f(\dot{\epsilon}, e^{\Delta H/RT})$ as shown in the upper curve of Fig. 9. Both methods of analysis give the same activation energy for creep.

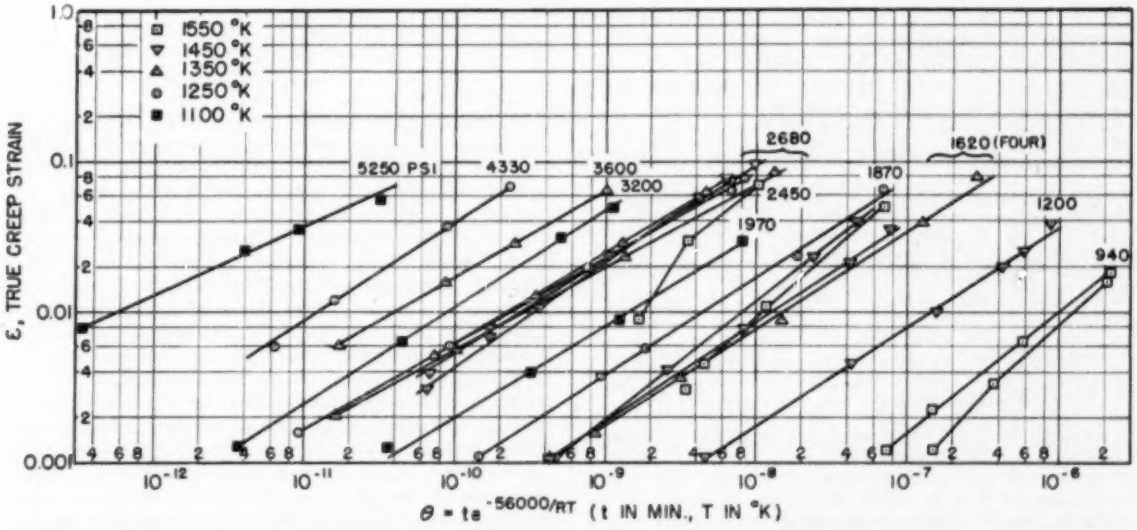

Fig. 11—Correlation of creep strain-time data for platinum by the relation $\epsilon = f(\theta, \sigma_c)$ at various stresses. Data of Carreker.[17]

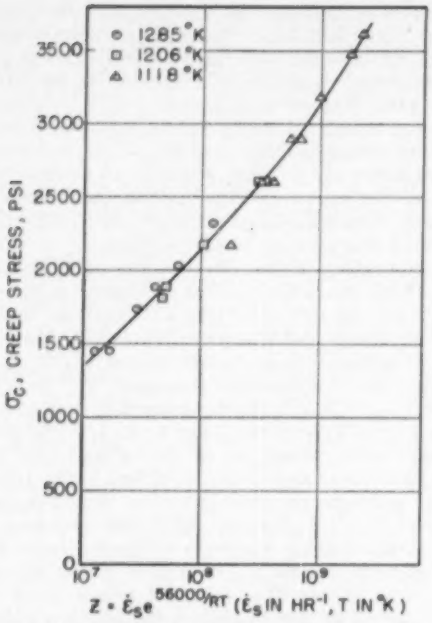

Fig. 12—Correlation of stress-secondary creep rate data for platinum by means of the relation $\sigma_c = f(\dot{\epsilon}, e^{\Delta H/RT})$. Data of Dushman, Dunbar, and Huthsteiner.[3]

Graeser, Hanemann, and Hofmann[16] studied the creep of zinc, pre-annealed at 473°K, under constant load conditions at two temperatures above 0.45 Tm, 323° and 348°K. Their data, presented in the form of minimum creep rates observed under various stresses at each temperature, have been correlated by means of Eq. 4 as is shown in the lower curve of Fig. 9. These data also suggest that the activation energy for the creep of zinc is approximately 26,000 cal per mol.

Platinum (Atomic No. 78): Carreker[37] investigated the creep properties of 99.98+ pct Pt wire under constant true stress conditions at temperatures ranging from 78° to 1550°K. In order to cover all the creep data above 0.45 Tm it was first decided to use Eq. 2 and attempt to correlate the constant stress σ_c with $\theta = te^{-\Delta H/RT}$ at a given strain. These results are shown in Fig. 10 for a given strain of 1 pct, wherein an activation energy of 56,000 cal per mol was found to be valid for all the data above 0.45 Tm with the exception of those obtained at 950°K. It therefore appears that the correlation by means of Eq. 2 is valid for platinum only somewhat above about 0.50 Tm.

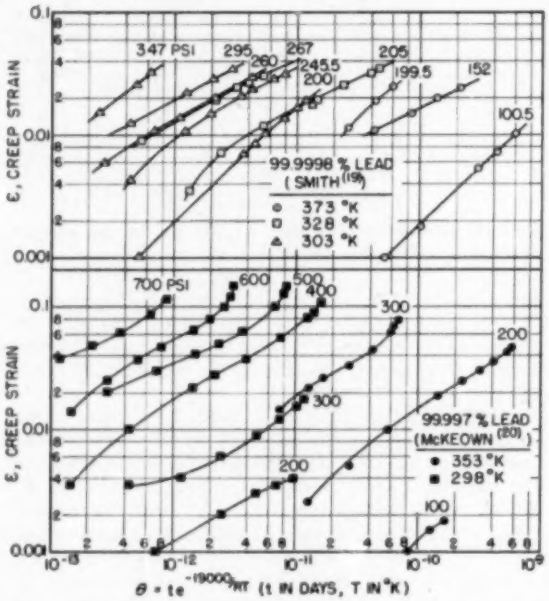

Fig. 14—Correlation of creep strain-time data for high purity lead by the relation $\epsilon = f(\theta, \sigma_c)$ at various stresses. Data of Smith[19] and McKeown.[20]

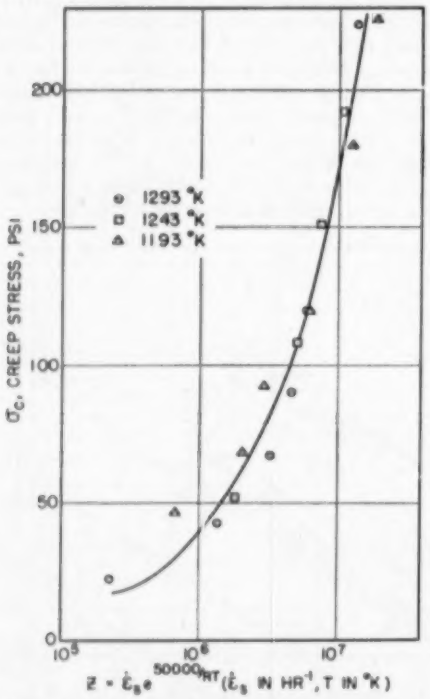

Fig. 13—Correlation of stress-initial creep rate data for gold by means of the relation $\sigma_c = f(\dot{\epsilon}, e^{\Delta H/RT})$. Data of Alexander, Dawson, and Kling.[38]

A second analysis based on Eq. 2 was also made for three representative stresses at each temperature as shown in Fig. 11. These results further justify the validity of Eq. 2.

Dushman, Dunbar, and Huthsteiner[3] investigated the secondary creep rate characteristics of pure platinum at temperatures of 1118°, 1206°, and 1285°K under constant load conditions. Their results are plotted in terms of Eq. 4 as shown in Fig. 12. The correlation obtained was quite good using the same activation energy of 56,000 cal per mol obtained from the more extensive data of Carreker.

Gold (Atomic No. 79): Alexander, Dawson, and Kling[38] performed creep tests on pure gold near the melting point. Unfortunately, they were primarily interested in the so-called microcreep range wherein an apparent viscous behavior of the metal was obtained. The data are therefore quite limited; furthermore, at very low stresses they obtained negative creep rates due to surface tension effects. If these very low stress tests are eliminated their data can be correlated by means of the Z parameter of Eq. 4. Fig. 13 is a plot of this correlation wherein an acti-

vation energy of 50,000 cal per mol was found valid for the creep of gold.

Lead (Atomic No. 82): Only limited data are available on the creep of lead at elevated temperatures. Smith[19] studied the creep of 99.9998 pct Pb at 303°, 328°, and 373°K under constant load. McKeown[20] also studied the creep of a high purity (99.997 pct) lead at 298° and 353°K under constant load. The correlations of Smith's and McKeown's data as based on Eq. 2 are shown in Fig. 14. In spite of differences in purity, the same activation energy for creep was obtained for Smith's and for McKeown's lead. The creep resistance, however, was found to be greater for the less pure lead used by McKeown. These differences are attributable to differences in B and S resulting from impurities and perhaps other factors.

Smith's and McKeown's data were also analyzed by means of Eq. 4 as shown in Fig. 15. Three low stress tests of McKeown were deleted from this

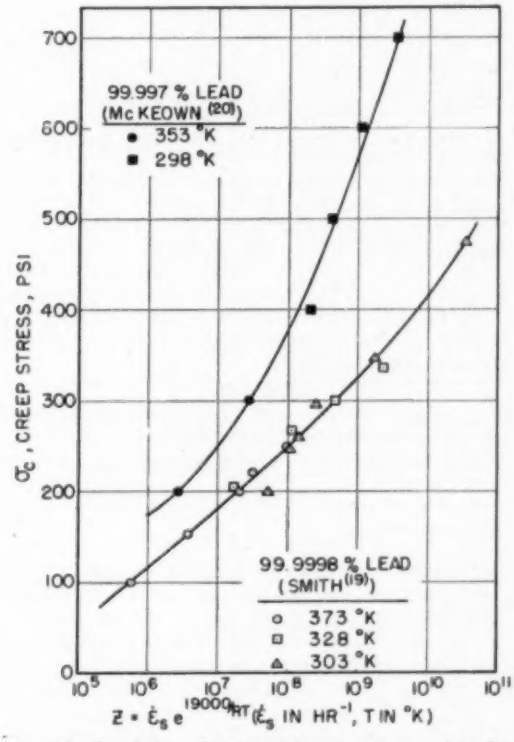

Fig. 15—Correlation of stress-minimum creep rate data for high purity lead by means of the relation $\sigma_s = f(\dot{\epsilon}, e^{\Delta H/RT})$. Data of Smith[19] and McKeown.[20]

analysis because the secondary creep rate had not been reached in these tests. Again an activation energy of 19,000 cal per mol was obtained from both sets of data, and again the less pure lead was found to be more creep resistant than that of higher purity.

The only other usable data on the creep of relatively pure lead at various temperatures are those presented by Smith and Howe[21] and Andrade.[22] These investigators studied commercially pure lead. Smith and Howe creep tested 99.92 pct Pb at 303° and 373°K under constant load, whereas Andrade tested lead of unreported composition at 290° and 433°K under constant stress. The data are too limited to make an exact determination of ΔH and therefore are not reproduced here; the most reasonable value

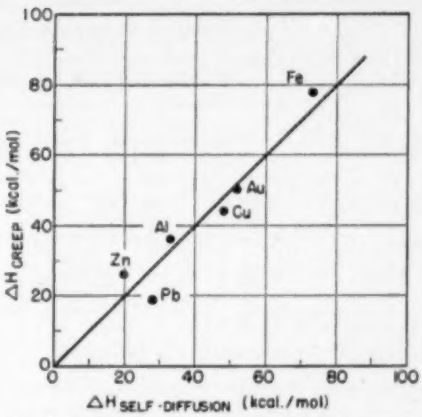

Fig. 16—Correlation between the activation energy for creep and the activation energy for self-diffusion.

(primarily based on Smith and Howe's data) was 23,000 cal per mol.

Discussion of Results

The previously outlined analyses of all pertinent data currently available in the literature confirm the general validity of Eqs. 2 and 4 for the creep of simple metal systems at temperatures above about 0.45 of the melting temperature. Since this is probably the temperature at which recovery first becomes pronounced for most metals, it appears as if Eqs. 2 and 4 are valid only at temperatures of rapid recovery.

The good agreement obtained for the activation energies from data by different investigators for a given metal confirms that the rate-controlling process is rather insensitive to minor differences in metal preparation, purity, and structure. Thus, the activation energies determined in the context of this paper for relatively pure metals should approach those of the elements.

The confirmation of the general validity of Eqs. 2 and 4 further emphasizes the previously discussed suggestion that the free energy of activation term for the rate-controlling process in high temperature creep cannot be stress dependent; for if this were the case the stress would enter the equations as the stress divided by the absolute temperature which is contrary to the facts. Consequently high temperature creep appears to occur due to removal of barriers to the motion of dislocations by means of some recovery processes. Perhaps once a barrier is removed the dislocations (or other deformation units)

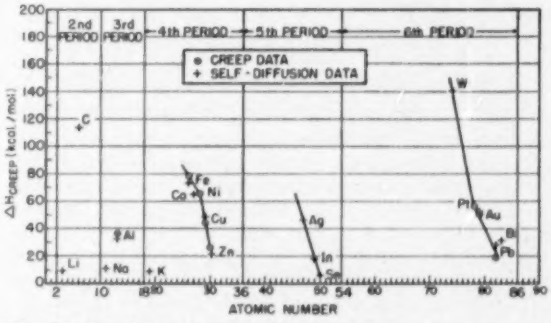

Fig. 17—Correlation between the activation energy for creep and atomic number.

Table II. Data on Activation Energies for Self-Diffusion of Metals

Metal (Atomic No.)	ΔH Self-Diffusion, Cal per Mol: Reported Values (Source Indicated)		Best or Average Value	Remarks (Data Are for Polycrystals Unless Otherwise Noted)
Lithium (3)	9,800	(a)		Deduced from nuclear resonance data
	9,300	(b)		Deduced from electrical resistance data
			9,500	
Carbon (6)	114,000	(c)	114,000	
Sodium (11)	10,450	(d)		
	9,500	(e)		Deduced from nuclear resonance data
	9,100	(b)		Deduced from electrical resistance data
			10,450	
Aluminum (13)	33,000	(f)	33,000	Estimated from diffusion data of other metals in aluminum
Potassium (19)	9,100	(b)		Deduced from electrical resistance data
			9,100	
α-Iron	77,200	(g)		
(26)	73,200	(h)		Extensive data, 720° to 900°C
	59,700	(i)		800° to 900°C
			73,000	
γ-Iron	48,000	(g)		Superseded by later work (h)
(26)	74,200	(h)		
	67,900	(i)		
			71,000	
Cobalt	67,000	(j)		
(27)	61,900	(k)		
			65,000	
Copper	45,100	(l)		
(29)	49,000	(i)		Single crystal
	46,800	(m)		
	44,000	(n)		Based on diffusion data for copper in copper alloys extrapolated to zero concentration of alloying element
	37,200	(o)		
	61,400	(p)		Incomplete work, based on complete data at two temperatures only
	47,000	(f)		Based on reinterpretation of published data
			48,000	
Zinc	20,400 $\parallel c$	(q)		Single crystal, $\Delta H \parallel c$ used in correlations with creep data
(30)	31,000 $\perp c$	(q)		
Silver	45,950	(r)		Large grained polycrystals
(47)	45,950	(s)		Single crystal
	45,500	(t)		Large grained polycrystals
	46,000	(f)		Based on reinterpretation of published data
			46,000	
Indium (49)	17,900	(u)	17,900	
Tin	10,500 $\parallel c$	(v)		Single crystal, $\Delta H \parallel a$ used in correlations with creep data
(50)	5,900 $\parallel a$	(v)		
Tungsten (74)	140,000	(w)	140,000	Diffusion of Fe in W extrapolated to 100 pct W
Gold	51,000	(x)		Extensive data, 721° to 966°C
(79)	62,900	(y)		Data at three temperatures only
	53,000	(z)		
			52,000	
Lead	27,900	(a′)		Single crystal
(82)	27,000	(f)		Based on reinterpretation of published data
			28,000	
Bismuth	31,000 $\parallel c$	(b′)		Single crystal, $\Delta H \parallel c$ used in correlations with creep data
(83)	140,000 $\perp c$	(b′)		

a. H. S. Gutowsky and B. R. McGarvey: *Journal of Applied Physics* (1952) **20**, p. 1472.
b. D. K. C. MacDonald: *Journal of Chemical Physics* (1953) **21**, pp. 177-178.
c. L. Green, Jr.: *Journal of Applied Mechanics* (1952) **19**, pp. 320-326.
d. N. H. Nachtrieb, E. Catalano, and J. A. Weil: *Journal of Chemical Physics* (1952) **20**, pp. 1185-1188.
e. H. S. Gutowsky: *Physical Review* (1951) **83**, p. 1073.
f. A. S. Nowick: *Journal of Applied Physics* (1951) **22**, pp. 1182-1186.
g. C. E. Birchenall and R. F. Mehl: *Journal of Applied Physics* (1948) **19**, p. 217.
h. C. E. Birchenall and R. F. Mehl: *Trans.* AIME (1950) **188**, pp. 144-149; JOURNAL OF METALS (January 1950).
i. F. S. Buffington, I. D. Bakalar, and M. Cohen: *Trans.* AIME (1950) **188**, pp. 1374-1375; JOURNAL OF METALS (November 1950).
j. F. C. Nix and F. E. Jaumot, Jr.: *Physical Review* (1951) **82**, pp. 72-74.
k. R. C. Ruder and C. E. Birchenall: *Trans.* AIME (1951) **191**, pp. 142-146; JOURNAL OF METALS (February 1951).
l. M. S. Maier and H. R. Nelson: *Trans.* AIME (1942) **147**, pp. 39-47.
m. C. L. Raynor, L. Thomassen, and L. J. Rouse: *Trans.* ASM (1942) **30**, pp. 313-325.
n. R. N. Rhines and R. F. Mehl: *Trans.* AIME (1938) **128**, pp. 185-221.
o. J. Steigman, W. Shockley, and F. C. Nix: *Physical Review* (1939) **56**, pp. 13-21.
p. B. V. Rollin: *Physical Review* (1939) **55**, p. 231.
q. P. H. Miller, Jr. and F. R. Banks: *Physical Review* (1942) **61**, pp. 648-652.
r. W. A. Johnson: *Trans.* AIME (1941) **143**, pp. 107-111.
s. R. E. Hoffman and D. Turnbull: *Journal of Applied Physics* (1951) **22**, pp. 634-639.
t. L. Slifkin, D. Lazarus, and T. Tomizuka: *Journal of Applied Physics* (1952) **23**, pp. 1032-1033.
u. R. E. Eckert and H. G. Drickamer: *Journal of Chemical Physics* (1952) **20**, pp. 13-17.
v. P. J. Fensham: *Australian Journal of Scientific Research* (1950) **3A**, pp. 91-104.
w. J. A. M. Van Liempt: *Rec. Trav. Chim.* (1945) **64**, pp. 239-249.
x. H. A. C. McKay: *Trans. Faraday Soc.* (1938) **34**, pp. 845-849.
y. A. M. Sagrubskij: *Phys. Zeit. Sowjet Union* (1937) **12**, pp. 118-119.
z. A. M. Sagrubskij: *Bull. Acad. Sci., U.S.S.R.* (1931) p. 903.
a′. G. von Hevesy, W. Seith, and A. Keil: *Ztsch. Physik* (1932) **79**, pp. 197-202.
b′. W. Seith: *Ztsch. Elektrochem.* (1933) **39**, pp. 538-542.

migrate under the stress to a new barrier which the stressed dislocations cannot surmount. The extent of this motion would therefore depend on the substructure and also the magnitude of the applied stress. This would suggest that the activation energy for creep obtained herein is the activation energy for removal of barriers to the motion of dislocations. It might be supposed that the removal of these barriers is controlled by atomic diffusion processes and therefore the activation energy for creep might be closely associated with the activation energy for self-diffusion. Table II lists for various metals the values of the activation energy for self-diffusion that have been published in the literature. The average or "best" value is listed for each metal using only data that appear reliable, and this value is used for comparison with the activation energy for creep as shown in Fig. 16. The correlation appears exceptionally good. In fact, the almost exact equality between these two activation energies suggests that

the rate-controlling process for self-diffusion might also be the rate-controlling process for creep.

It might be anticipated that the activation energy for creep of the elements should be a periodic function of atomic number. The activation energy data for creep and self-diffusion recorded in Fig. 17 begin to reveal a periodic variation. Undoubtedly the first members of each period, i.e., the alkali and alkaline earth elements, possess low activation energies for creep as indicated by the available self-diffusion data for lithium, sodium, and potassium. The data of Fig. 17 thus suggest that the intermediate elements in each period have the highest activation energies for creep and self-diffusion. The possible effects of crystal structure on the activation energies for creep, however, are neglected in this periodic correlation. Consequently, the data of Fig. 17 are yet too incomplete to select those elements that exhibit the highest activation energies and therefore might be most creep resistant for this reason.

The suspected periodic variation of the activation energy for creep and self-diffusion with atomic number suggests that the activation energy should correlate with other properties that exhibit periodic variation. The activation energy for creep and self-diffusion correlates quite well with the melting temperature as shown in Fig. 18.

It should be noted that although the activation energy for creep is insensitive to most metallurgical factors, the σ_s vs Z curves obtained from separate investigations on a given metal reveal sensitivity to composition, structure, etc. These effects have been shown to be due to the sensitivity of B of Eq. 5 to composition[7] and the sensitivity of S of Eq. 5 to structure.[8] High values of activation energy, ΔH, and low values of B and S favor creep resistance.

Conclusions

1—Creep and tensile data of pure metals at temperatures above about 0.45 of their melting points can be correlated by means of simple equations:

$$\epsilon = f(\theta, \sigma_s)$$

and

$$\sigma_s = f(Z) = f(\dot{\epsilon}, e^{\Delta H/RT})$$

where ϵ is the creep strain; $\theta = te^{-\Delta H/RT}$, where t is the time, T is the absolute temperature, R is the gas constant, and ΔH is the experimental energy of activation for creep in cal per mol; σ_s is the creep stress (or ultimate tensile strength); and $\dot{\epsilon}_s$ is the secondary creep rate (or strain rate of tensile test).

2—Since the equations given in conclusion 1 do not contain the stress divided by the absolute temperature, the stress does not enter the free energy of activation for the rate-controlling process for high temperature creep.

3—ΔH was found to be a constant for a given metal at temperatures above those at which rapid recovery occurs (above about 0.45 Tm). It was shown that the energy of activation for creep is approximately equal to the best known value for the activation energy of self-diffusion. These results suggest that the rate-controlling process for high temperature creep might be similar to the rate-controlling process for self-diffusion.

4—For the elements investigated the activation energy for creep, ΔH, appears to be a periodic function of the atomic number.

Acknowledgments

This investigation was sponsored by the Office of Naval Research. The authors wish to thank the O.N.R. staff for their continued interest and full cooperation throughout the conduct of this and related studies on the plastic properties of metals. In addition, the authors wish to thank Dr. C. Dean Starr for his interest in and contribution to this study, and to Mrs. G. Pelatowski sincere appreciation is extended for her preparation of the figures to this report.

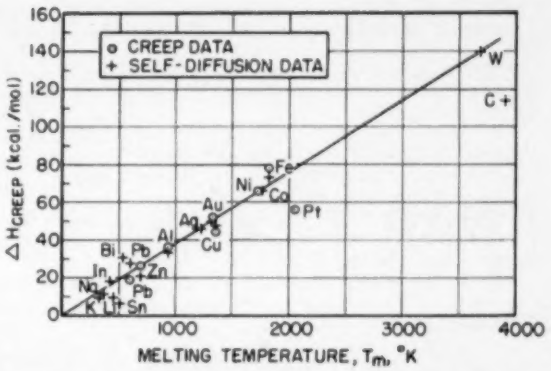

Fig. 18—Correlation between the activation energy for creep and the melting temperature.

References

[1] W. Kauzman: Flow of Solid Metals from the Standpoint of the Chemical Rate Theory. *Trans.* AIME (1941) **143**, pp. 57-83.

[2] S. Dushman, L. W. Dunbar, and H. H. Huthsteiner: Creep of Metals. *Journal of Applied Physics* (1944) **15**, pp. 108-124.

[3] O. D. Sherby and J. E. Dorn: Creep Correlations in Alpha Solid Solutions of Aluminum. *Trans.* AIME (1952) **194**, pp. 959-964; JOURNAL OF METALS (September 1952).

[4] O. D. Sherby and J. E. Dorn: Some Observations on Correlations between the Creep Behavior and the Resulting Structures in Alpha Solid Solutions. *Trans.* AIME (1953) **197**, pp. 324-330; JOURNAL OF METALS (February 1953).

[5] O. D. Sherby, A. Goldberg, and J. E. Dorn: Effect of Prestrain Histories on the Creep and Tensile Properties of Aluminum. ASM Preprint No. 15W (1953).

[6] C. Zener and J. H. Hollomon: Plastic Flow and Rupture of Metals. *Trans.* ASM (1944) **33**, pp. 163-235.

[7] O. D. Sherby, R. E. Frenkel, J. Nadeau, and J. E. Dorn: Effect of Stress on the Creep Rates of Polycrystalline Aluminum Alloys. Inst. of Engineering Research Report, Univ. of California, Berkeley, Series No. 22, Issue No. 24, February 15, 1953.

[8] Robert E. Frenkel, Oleg D. Sherby, and John E. Dorn: Effect of Cold Work on the High Temperature Creep Properties of Dilute Aluminum Alloys. Inst. of Engineering Research Report, Univ. of California, Berkeley, Series No. 22, Issue No. 29, August 1, 1953.

[9] W. H. Giedt, O. D. Sherby, and J. E. Dorn: The Effect of Dispersions on the Creep Properties of Aluminum-Copper Alloys. To be published in *Trans.* ASME.

[10] O. D. Sherby, R. A. Anderson, and J. E. Dorn: The Effect of Alloying Elements on the Elevated Temperature Plastic Properties of Alpha Solid Solutions of Aluminum. *Trans.* AIME (1951) **191**, pp. 643-652; JOURNAL OF METALS (August 1951).

[11] I. S. Servi and N. J. Grant: Creep and Stress-Rupture Behavior of Aluminum as a Function of Purity. *Trans.* AIME (1951) **191**, pp. 909-916; JOURNAL OF METALS (October 1951).

[12] H. J. Tapsell and W. J. Clenshaw: Properties of Materials at High Temperatures—I. Great Britain Dept. of Science and Industrial Research, Special Report No. 1, 1927.

[13] T. H. Hazlett, E. R. Parker, and M. W. Nathans: Determination of Activation Energies for Secondary

Creep. Inst. of Engineering Research Report, Univ. of California, Berkeley, Series No. 28, Issue No. 8, May 1950.

[14] A. Nadai and M. J. Manjoine: High Speed Tension Tests at Elevated Temperatures. *Trans.* ASME (1941) **63**, pp. A-77 - A-91.

[15] A. Pomp and W. Länge: On the Variation with Time of Strain and Strain Rate of Metals Under Static Stress. *Mitt. Kaiser-Wilhelm Institut Eisenforschung zu Düsseldorf* (1936) **18**, pp. 51-63.

[16] W. Graeser, H. Hanemann, and W. Hofmann: The Creep Resistance of Zinc and Zinc Alloys. *Ztsch. Metallkunde* (1943) **35**, pp. 1-13.

[17] R. P. Carreker: Plastic Flow of Platinum Wires. *Journal of Applied Physics* (1950) **21**, pp. 1289-1296.

[18] B. M. Alexander, M. H. Dawson, and H. P. Kling: The Deformation of Gold Wire at Elevated Temperatures. *Journal of Applied Physics* (1951) **22**, pp. 439-443.

[19] A. A. Smith, Jr.: Creep and Recrystallization of Lead. *Trans.* AIME (1941) **143**, pp. 165-171.

[20] J. McKeown: Creep of Lead and Lead Alloys. *Journal* Inst. Metals (1937) **60**, pp. 201-228.

[21] A. A. Smith, Jr. and H. E. Howe: Creep Properties of Some Rolled Lead-Antimony Alloys. *Trans.* AIME (1945) **161**, pp. 472-477.

[22] E. N. daC. Andrade: The Flow in Metals Under Large Constant Stresses. *Proc.* Royal Soc. (1914) **90**, pp. 329-342.

Technical Note

Structure of Some Iridium-Osmium Alloys

by H. C. Vacher, C. J. Bechtoldt, and E. Maxwell

IN the course of an investigation of the properties of metals at low temperature there was occasion to determine the constitution of four iridium-osmium alloys. There is very little information in the literature[1] on the constitution of synthetic Ir-Os alloys. Zvyagintzev[2,3] has made a comprehensive study of different natural Ir-Os alloys and concludes that alloys containing more than 32 pct Os have the close-packed hexagonal structure of osmium, whereas those containing less than 32 pct Os have the face-centered cubic structure of iridium.

The alloys studied in this work were prepared by the American Platinum Works, Newark, N. J., and were received in the form of fragments approximately 1.5 mm average diameter. The fragments had been obtained by crushing ingots made by fusing charges of iridium and osmium under an arc and air cooling. The ingots were not given a homogenizing heat treatment. Sample fragments of the iridium and osmium used in making the alloys also were included.

Several fragments of each metal and alloy were examined microscopically and by X-ray diffraction. For the X-ray method the fragments were crushed further to pass a 270-mesh screen, then sealed in evacuated fused-silica tubes, heated to 1100°C for 18 hr, and allowed to cool in the furnace. Powder X-ray diffraction patterns were obtained from the annealed fragments by means of a Norelco camera having a diameter of 114 mm, and unfiltered cobalt radiation. For the microscopic examination several fragments in the as-received condition were mounted in Melmac, (American Cyanamid Co.) and ground using the conventional series of abrasive papers. The polishing was done with 0-2 diamond abrasive on a Microcloth (Buehler Ltd.) lap, wet with xylene. After polishing, the surface was etched electrolytically in a 10 pct solution of chromic acid or in a 10 pct solution of potassium cyanide. Both reagents attacked the osmium-rich constituent, whereas the iridium constituent was attacked slightly by the chromic acid reagent and not noticeably by the potassium cyanide reagent. The results of the X-ray diffraction and microscopic examinations are summarized in Table I. Fig. 1 shows the microstructure of a 21 pct Ir-79 pct Os alloy.

Table I. Results of X-Ray Diffraction and Microscopic Examinations

Alloy		Phases Present as Determined by X-ray Diffraction		
Osmium, Wt Pct	Iridium, Wt Pct	Osmium Close-Packed Hexagonal Structure	Iridium Face-Centered Cubic Structure	Microscope
0	99.9	None	Present	1
23.6	76.4	None	Present	1
38.7	61.3	Present	Present	2
59.4	40.6	Present	Present	2
79.0	21.0	Present	Not detected	2
99.9	0	Present	None	1

Note: Chemical analyses of the iridium, osmium, and alloys were furnished by the American Platinum Works.

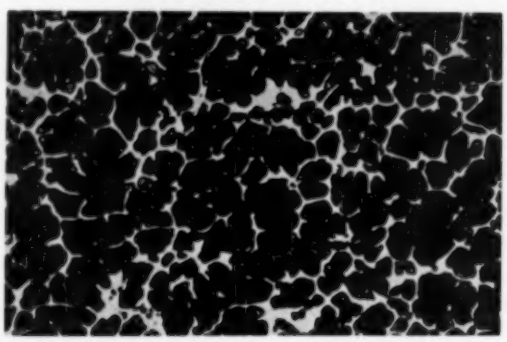

Fig. 1—Microstructure of a 21 pct Ir-79 pct Os alloy. The iridium-rich phase is white. Etched electrolytically with 10 pct potassium cyanide solution. X100.

The results indicate an appreciable solid-solubility range of osmium in iridium as was reported by Zvyagintzev.[3] The solid-solubility range of iridium in osmium is more restricted, apparently less than 21 pct Ir. This implies a large range of composition in which two phases can coexist that was not reported by Zvyagintzev.

H. C. VACHER, Member AIME, C. J. BECHTOLDT, and E. MAXWELL are associated with the National Bureau of Standards, Washington, D. C.

TN 200E. Manuscript, Sept. 18, 1953.

References

[1] *Gmelins Handbuch der Anorganischen Chemie.* System-number 68. Platin Teil A Lieferung 6, Die Legierungen der Platinmetalle: Osmium, Iridium, Platin. (1951) p. 741.

[2] O. E. Zvyagintzev: *Comp. Rend. Acad. Sci., URSS* (1938) **18**, pp. 295-297 (in English).

[3] O. E. Zvyagintzev: *Ann. Sect. Anal. Phys.-Chim.* Inst. Chim. Gén (U.S.S.R.) (1943) **16**, No. 1, pp. 220-228.

AIME OFFICERS:
President—Andrew Fletcher
Vice-Presidents—T. B. Counselman, L. E. Elkins, O. B. J. Fraser, J. L. Gillson, A. B. Kinzel, J. B. Morrow
President-Elect—L. F. Reinartz
Treasurer and Controller—G. I. Brigden
AIME STAFF:
Secretary—E. H. Robie
Ass't. Secretaries—J. B. Alford, H. N. Appleton, E. J. Kennedy, Jr., Ernest Kirkendall, R. E. O'Brien
Ass't. Treasurer—P. J. Apol

aime NEWS

Joint Session EMD and MBD, Latin Quarter Show Promise Stimulating Annual Meeting

Registration for the 1954 Annual Meeting in New York, February 15 to 19, will be on the mezzanine of the Hotel McAlpin. Prospective registrants can look forward to a technical program which appears to be one of the most unusual and interesting ever presented by the AIME.

Without exception, program committees for the three Metals Branch Divisions have evolved a program of well rounded sessions and social functions. One of the most outstanding this year will be the Joint Session on Hydrometallurgy to be held at the Statler Hotel with the Extractive Metallurgy Div. and the Minerals Beneficiation Div. joining forces.

One of the features of the Annual Meeting program of the EMD is always the Stag Luncheon and Business Meeting. Simon Strauss, vice-president, American Smelting & Refining Co., will be the speaker. R. R. McNaughton, manager of the metallurgy div., Consolidated Mining & Smelting Co. of Canada, is scheduled to handle the duties of toastmaster.

Howe Memorial Lecturer for the Iron and Steel Div. will be C. D. King, chairman of engineering committees, U. S. Steel Corp. He will speak on *Steelmaking Processes—Some Future Prospects.* ISD has also scheduled a comprehensive program of technical sessions dealing with blast furnaces, open hearth combustion, use of rare earths, ingot examination and new European practices, and physical chemistry.

Institute of Metals Div., leads off its share of the Annual Meeting program with a Symposium on Semi-Conductors. Sessions dealing with deformation high temperature properties, solidification, and titanium are on the list of technical meetings. Two constitution sessions have also been scheduled. A joint session with EMD on Physical Chemistry of Extractive Metallurgy will be held; and final sessions on Thursday will deal with steel and powder metallurgy.

First social event of the program will take place Sunday, February 14, when the Minerals Industry Education Div. holds its Reception and Buffet Supper. Dr. Grayson Kirk, president of Columbia University will address the traditional Welcoming Luncheon Monday, 12 noon, at the Statler Hotel. A cocktail party is scheduled for 6 pm, while at 8 pm, the Dinner-Smoker will get underway. Feature of the stag affair this year will be the Latin Quarter show. Advance reports on the show say that this is one of the best ever put together by the night club —for years one of New York's most famous.

Metals Branch cocktail party and dinner will start at 6:00 pm that evening. G. L. Mehta, Ambassador from the Republic of India to the U.S.A., will be guest speaker at the Metals Branch Annual Dinner. K. C. McCutcheon will be toastmaster. Informal dancing will cap the evening. The Annual Banquet and President's Reception will take place at Park Avenue's Waldorf Astoria, starting at 7 pm. Leo F. Reinartz will take over as AIME President succeeding Andrew Fletcher, 1953 Institute head.

EXTRACTIVE METALLURGY DIV.

MONDAY, FEBRUARY 15

9:45 am

Aluminum

H. W. Sinclair and P. T. Stroup, Associate Chairmen

Production of Aluminum-Silicon Alloys from Smelting of Clays and Other Aluminum Silicates: W. F. Hergert, L. H. Banning, U. S. Bureau of Mines, Albany, Ore.

Operation of Experimental Plant for Recovery of Alumina from Anorthosite: H. W. St. Clair, U. S. Bureau of Mines, Laramie, Wyo.

9:45 am

Symposium on Arc-Furnace Copper Melting

J. G. Leckie and J. H. Schloen, Associate Chairmen

Electric Furnace Melting Practice at Canadian Copper Refiners, Ltd.: W. Sheaffer, Canadian Copper Refiners, Ltd., Montreal, Canada.

Round Table Discussion

10:00 am

Metals Branch Council Meeting

K. C. McCutcheon, Chairman

2:30 pm

Aluminum

H. W. Sinclair and P. T. Stroup, Associate Chairmen

Cost Factors in Utilization of Foreign Bauxite: A. F. Johnson, consultant, Alton, Ill.

General Prospects and Technology of Using Processed Low Rank Fuels for Electric Power: V. F. Parry, U. S. Bureau of Mines, Denver, Colo.

Direct Reading Spectrograph in Aluminum Smelting: D. L. Colwell, O. Tichy, Apex Smelting Co., Cleveland, Ohio.

Effect of Phosphate in Alumina on the Current Efficiency During Electrolysis of Aluminum: A. C. Byrns, Kaiser Chemical Co., Oakland, Calif.

2:30 pm

Symposium on Arc-Furnace Copper Melting

J. G. Leckie and J. H. Schloen, Associate Chairmen

Continuation of morning session.

TUESDAY, FEBRUARY 16

7:30 am

Executive Committee Breakfast Meeting

R. R. McNaughton, Chairman

9:00 am

Lead - Zinc

P. C. Feddersen and W. T. Isbell, Associate Chairmen

Desilverizing of Lead Bullion: T. R. A. Davey, The Broken Hill Associated Smelters Pty. Ltd., Port Pirie, S. Australia.

Thoughts on Lead Blast-Furnace Practice: L. B. Haney, R. J. Hopkins, The Broken Hill Associated Smelters Pty. Ltd., Port Pirie, S. Australia.

Operation of the Midvale Dwight-Lloyd Sintering Plant and Lead Blast-Furnaces on a Two-Shift Basis: H. L. Johnson, C. A. Nelson, Midvale plant, U. S. Smelting, Refining & Mining Co., Salt Lake City, Utah.

9:00 am

Hydrometallurgy - Physical Chemistry

R. D. MacDonald and D. M. Kentro, Associate Chairmen

Kinetics of the Oxidation of Galena in Ammonium Acetate Solution Under Oxygen Pressure: D. P. Seraphim, C. S. Samis, University of British Columbia, Vancouver, Canada.

Treatment of Uranium Ores by Basic Pressure Leaching Methods: J. Halpern, F. A. Forward, University of British Columbia, Vancouver, Canada.

Fundamentals of Agitation and Applications to Extractive Metallurgy: J. H. Rushton, Illinois Institute of Technology, Chicago, Ill.

Some Factors Affecting the Structure of Zinc Electrodeposits: J. H. Nicholson, G. H. Turner, J. A. Brown, Consolidated Mining & Smelting Co. of Canada, Trail.

2:00 pm

Lead - Zinc - Cadmium

R. E. Lund and T. I. Moore, Associate Chairmen

Additional Information Regarding the Conditioning of Vapors from Electrothermic Zinc Furnaces: F. A. Poland, Revere Copper & Brass, Inc., Rome, N. Y.

Roasting Metallic Sulphides in a Fluid Column: Part I—Experimental Development: H. M. Cyr, C. W. Siller, T. F. Steele, New Jersey Zinc Co., Palmerton, Pa. *Part II—Commercial Development:* A. J. Myhren, C. W. Siller, S. I. Hammond, New Jersey Zinc Co., Palmerton, Pa.

Fluidity of Some Lead Blast-Furnace Slags: T. D. de Souza Santos, Institute de Pesquisas Tech., Sao Paulo, Brazil.

An Important Byproduct of Zinc Recovery—Cadmium in Review: J. R. Musgrave, A. P. Thompson, Eagle-Picher Co., Joplin, Mo.

2:00 pm

Hydrometallurgy Joint Session with MBD, Statler Hotel

A. W. Schlechten and W. L. Dowdy, Chairmen

Electrolytic Production of Hydrometallurgical Reagents for Processing Manganese Ores: J. B. Clemmer, C. Rampacek, P. Churchward, U. S. Bureau of Mines, Salt Lake City, Utah.

Chemistry of the Ammonia Leaching Process for Nickel, Copper, and Cobalt Sulphide Ores: F. A. Forward, V. N. Mackiw, University of British Columbia, Vancouver, Canada.

Specific Data on Ion-Exchange in the Metallurgical Industry: A. B. Mindler, Permutite Co., New York.

Continuous Ion-Exchange with Modified Ore Dressing Jigs: R. McNeil, E. A. Swinton, D. E. Weiss, Commonwealth Scientific & Industrial Research Organization, Melbourne, Australia.

A Practical Determination of Residence Time and Short Circuiting of Dry Solids or Solids in Slurries in Continuous Systems: R. B. Coleman, J. D. Moore, Vitro Chemical Co., Salt Lake City, Utah.

6:00 pm

Metals Branch Cocktail Party

7:00 pm

Metals Branch Annual Dinner

K. C. McCutcheon, Toastmaster

Speaker: G. L. Mehta, Ambassador from the Republic of India to the U. S. A.

WEDNESDAY, FEBRUARY 17

9:00 am

Physical Chemistry of Extractive Metallurgy Joint Session with IMD

T. B. King and H. H. Kellogg, Associate Chairmen

Improved Vacuum-Fusion Method for the Determination of Oxygen and Nitrogen in Metals: N. A. Gokcen, Michigan College of Mining and Technology, Houghton, Mich.

Theoretical Analysis of Diffusion of Solutes During the Solidification of Alloys: C. Wagner, Massachusetts Institute of Technology, Cambridge, Mass.

Diffusion in Liquid Lead-Bismuth Alloys: R. E. Grace, G. Derge, Carnegie Institute of Technology, Pittsburgh, Pa.

Vapor Pressure of Zinc Sulphide from 680° to 825°C: G. L. McCabe, Carnegie Institute of Technology, Pittsburgh, Pa.

Determination of the Standard Free Energy of Formation of Zinc Sulphide and Magnesium Sulphide: W. Curlook, L. M. Pidgeon, University of Toronto, Toronto, Canada.

9:00 am

Titanium

J. Morgan and N. C. Fick, Associate Chairmen

Inherent Problems in the Extractive Metallurgy of Titanium by Chloride Processes: W. R. Opie, National Lead Co., South Amboy, N. J.

Smelting of Titaniferous Ores: D. L. Armant, National Lead Co., South Amboy, N. J.

Commercial Titanium Metal Production: P. J. Maddex, Titanium Metal Corp., Henderson, Nev.

Production and Purification of Titanium Tetrachloride: L. W. Rowe, National Lead Co., South Amboy, N. J.

12:15 pm

Annual EMD Stag Luncheon and Business Meeting

R. R. McNaughton, Toastmaster

Speaker: Simon Strauss, Vice-President American Smelting & Refining Co., New York

2:00 pm

Physical Chemistry of Extractive Metallurgy

E. Michal and L. M. Pidgeon, Associate Chairmen

System Ag_2O-B_2O_3: Its Thermodynamic Properties as a Slag Model: G. M. Willis, University of Melbourne, Melbourne, Australia; F. L. Hennessy, Mt. Morgan Ltd., Mt. Morgan, Queensland, Australia.

Liquid System $NaCl$-$ZrCl_4$: Vapor Pressure and Liquidus: L. Howell, J. T. Benedict, H. H. Kellogg, Columbia University, New York.

Exchange of Antimony Between Molten Antimony and Fused Antimony Oxide: D. Cubicciotti, F. J. Keneshea, North American Aviation, Downey, Calif.

Fuming of Zinc from Lead Blast Furnace Slags—A Thermodynamic Study: R. C. Bell, G. H. Turner, E. Peters, Consolidated Mining & Smelting Co. of Canada, Trail, B. C.

Activities in the Lime-Silica-Iron Oxide System: J. F. Elliott, Inland Steel Co., E. Chicago, Ind.

2:00 pm

Copper

G. H. Weis, Chairman

Hydrometallurgy of Copper-Zinc Concentrate at the Kosaka Smelter: H. Kurushima, S. Tsunoda, Dowa Mining Co., Japan.

Casting 3000-lb Vertical Cast Copper Slabs at Rariton Copper Works: C. D. Pearce, International Smelting & Refining Co., Perth Amboy, N. J.

THURSDAY, FEBRUARY 18

9:00 am

Uncommon Metals

D. W. Lillie and T. G. Diggs, Associate Chairmen

Calcium Metal: Laboratory Preparation by Vacuum Metallurgy: C. R. Couch, C. L. Mantell, Newark College of Engineering, Newark, N. J.

Methods for Separating Rare-Earth Elements in Quantity as Developed at Iowa State College: F. H. Spedding, J. E. Powell, Iowa State College, Ames, Iowa.

Methods of Producing Rare-Earth Metals and Alloys as Developed at Iowa State College: F. H. Spedding, A. Daane, Iowa State College, Ames, Iowa.

New Techniques in Extractive Metallurgy of Vanadium: H. Mason, U. S. Atomic Energy Commission, Washington, D. C.

Production of Zirconium Boride from Zirconia and Boron Carbide: C. T. Baroch, T. E. Evans, U. S. Bureau of Mines, Boulder City, Nev.

IRON AND STEEL DIV.

MONDAY, FEBRUARY 15

9:45 am

Surface Quality of Bars

T. B. Winkler and J. E. Stukel, Associate Chairmen

Factors Affecting Surface Quality of Bar Mill Products: C. V. Klimas, J. V. Florchak, U. S. Steel Corp., Duquesne, Pa.

Controlled Atmosphere Annealing of Cold Drawn Bars: Samuel Beckman, Jones & Laughlin Steel Corp., Pittsburgh, Pa.

Origin and Elimination of Ingot Cracks in C-1020 Steel: M. A. Orehoski, N. R. Arant, J. Pusateri, U. S. Steel Corp., Pittsburgh, Pa.

10:00 am

Metals Branch Council Meeting

K. C. McCutcheon, Chairman

2:30 pm

Open Hearth Combustion

D. L. McBride and George Burrier, Associate Chairmen

Regenerator Efficiency and Air Preheat in the Open Hearth: B. M. Larsen, U. S. Steel Corp., Kearny, N. J.

Prepared Discussion of Mr. Larsen's Paper: John S. Marsh, Bethlehem Steel Co., Bethlehem, Pa.

Prepared Discussion of Mr. Larsen's Paper: Michael Tenenbaum, Inland Steel Co., E. Chicago, Ind.

Prepared Discussion of Mr. Larsen's Paper: R. A. Lambert, Jones & Laughlin Steel Corp., Pittsburgh, Pa.

TUESDAY, FEBRUARY 16

9:00 am

Use of Rare Earths

C. B. Post and J. V. Russell, Associate Chairmen

Study of Desulphurization of Steel by Rare Earths: J. A. Berger, M. G. Snellman, dept. of metallurgical engineering, University of Pittsburgh, Pittsburgh, Pa.

Operating Facts on the Use of Rare Earths: Earl W. Pierce, U. S. Steel Corp., South Works, Chicago, Ill.

Conversion of Stainless Steel Ingots to Slabs: Robert W. Henke, Allegheny-Ludlum Steel Corp., Brackenridge, Pa.

11:00 am

Howe Memorial Lecture

L. F. Reinartz and T. J. McLoughlin, Associate Chairmen

Steelmaking Processes—Some Future Prospects: C. D. King, chairman of engineering committees, U. S. Steel Corp., Pittsburgh, Pa.

2:00 pm

Ingot Examination and New European Practices

H. B. Emerick and W. O. Philbrook, Associate Chairmen

Examination of a High Sulphur Free-Machining Ingot, Bloom and Billet Sections: D. J. Carney, E. C. Rudolphy, U. S. Steel Corp., South works, Chicago, Ill.

The Development of Oxygen Steelmaking: Otwin Cuscoleca, Oesterreichisc-Alpine, Montangesellschaft, Vienna.

Recent Improvements in European Basic Bessemer Practice: Pierre Coheur, National Institute of Metallurgical Research, Liege, Belgium; Hans Kosmider, Hutenwerk Haspe A.G., Hagen-Haspe, Westfalia, Germany.

6:00 pm

Metals Branch Cocktail Party

7:00 pm

Metals Branch Annual Dinner

K. C. McCutcheon, Toastmaster

Speaker: G. L. Mehta, Ambassador from the Republic of India to the U. S. A.

WEDNESDAY, FEBRUARY 17

7:30 am

ISD Executive Committee Breakfast Meeting

9:00 am

Physical Chemistry

D. W. Murphy and Shadburn Marshall, Associate Chairmen

Chromium Distribution Between Liquid Iron and Molten Basic Slags: Nicholas J. Grant, Earl C. Roberts, John Chipman, Massachusetts Institute of Technology, Cambridge, Mass.

Activities of Fe, FeO, Fe_2O_3 and CaO in Simple Slags: John Chipman, Massachusetts Institute of Technology, Cambridge, Mass.; Hugo Larson, American Brake Shoe Co., Mahwah, N. J.

Activities in the Iron-Silicon Alloys: N. A. Gokcen, Michigan College of Mining and Technology, Houghton, Mich.

Manganese Modification of the Fe-O-S System: D. C. Hilty and W. Crafts, Electro Metallurgical Co., Niagara Falls, N. Y.

2:00 pm

Blast Furnace

Solid Phase Identification in Partially Reduced Iron Ore: Gust Bitsianes, T. L. Joseph, University of Minnesota, Minneapolis, Minn.

Wustite Phase in Partially Reduced Hematite: Gust Bitsianes, T. L. Joseph, University of Minnesota, Minneapolis, Minn.

Further Studies of the Tuyere Zone of the Blast Furnace: J. B. Wagstaff, U. S. Steel Corp., research laboratory, Kearny, N. J.

Exchange of Iron Between Liquid Metal and Iron Silicate Slag: G. Derge, Carnegie Institute of Technology, Pittsburgh, Pa.; C. E. Birchenall, Princeton University, Princeton, N. J.

Manganese as an Indicator of Blast Furnace Slag Oxidation and Desulphurizing Power: N. J. Grant, J. W. Dowding, Jr., R. J. Murphy, Massachusetts Institute of Technology, Cambridge, Mass.

Silicon Reduction and the Activity of Silica in Blast Furnace Type Slags: John Chipman, James Fulton, Massachusetts Institute of Technology, Cambridge, Mass.

INSTITUTE OF METALS DIV.

SUNDAY, FEBRUARY 14

2:30 pm

Collaborating with the Mineral Industry Education Div., the Education Committee of the Institute of Metals Div. has arranged a program of two sessions on Sunday simultaneous with those of the MIED. Six papers concerned with techniques of laboratory instruction in physical metallurgy together with discussion will be presented on the afternoon session. At 5:00 pm there will be a short joint session with the Mineral Industry Education Div. Immediately following this joint session the IMD and MIED will again combine for cocktails and a $2.50 buffet supper. The IMD program in the evening will feature an address by an outstanding speaker dealing with broad issues bearing on metallurgical education and metallurgy as a profession. Prepared discussion of this address by invited speakers will present the viewpoint of representatives of government research, industrial research, and industrial operations. These two Sunday sessions will be held at the Men's Faculty Club of Columbia University, Morningside Drive & 117th St., New York, N. Y.

5:00 pm, Men's Faculty Club, Columbia University.

IMD Program Committee Meeting

R. S. Busk, Chairman

MONDAY, FEBRUARY 15

9:45 am

Symposium on Semi Conductors

An Historical Survey of Semi-Conductor Application: E. W. Herold, RCA Laboratories, Princeton, N. J.

Effect of Imperfections on the Properties of Semi-Conductors: Harvey Brooks, Harvard University, Cambridge, Mass.

Semi-Conductor Metallurgy: William Pfann, Bell Telephone Laboratories, Murray Hill, N. J.

10:00 am

Metals Branch Council Meeting

K. C. McCutcheon, Chairman

2:30 pm

Symposium on Semi Conductors (cont)

Contributions from Semi-Conductor Studies to Diffusion in Solids: W. C. Dunlap, Jr., General Electric Co., Schenectady, N. Y.

Analogies Between Lattice Defects and Current Carriers in Semi-Conductors: J. Rothstein, Signal Corps Engineering Laboratories, Fort Monmouth, N. J.

Conversion of Solar Energy to Electrical Energy by Silicon P-N Junction Cells: D. M. Chapin, Bell Telephone Laboratories, Murray Hill, N. J.

Properties of Germanium-Silicon Alloys: C. C. Wang, B. H. Alexander, Sylvania Electric Products, Inc., Ipswich, Mass.

Dislocations in Germanium: S. G. Ellis, RCA Laboratories, Princeton, N. J.

Factors Affecting the Growth of Single Crystals of Silicon: D. C. Jillson, A. C. Scheckler, General Electric Co., Schenectady, N. Y.

Solidus Curves of Indium Tin and Antimony in Germanium: C. D. Thurmond, Bell Telephone Laboratories, Murray Hill, N. J.

2:30 pm

Deformation I

F. D. Rosi and M. A. Steinberg, Associate Chairmen

Bending of Molybdenum Single Crystals: K. T. Aust, Robert Maddin, N. K. Chen, The Johns Hopkins University, Baltimore, Md.

Plasticity of Molybdenum Single Crystals at High Temperatures: Robert Maddin, N. K. Chen, The Johns Hopkins University, Baltimore, Md.

Annealing of a Cold Rolled Aluminum Single Crystal: A. H. Lutts, P. A. Beck, University of Illinois, Urbana, Ill.

On the Torsional Deformation and Recovery of Single Crystals: S. S. Hsu, B. D. Cullity, University of Notre Dame, Notre Dame, Ind.

Torsional After-Effect Measurement and Applications to Aluminum: C. S. Barrett, University of Chicago, Chicago, Ill.; P. M. Aziz, Aluminum Laboratories, Ltd., Kingston, Ontario; I. Markson, Glasgow, Scotland.

3:00 pm

JOURNAL OF METALS Editorial Advisory Board Meeting

J. S. Smart, Jr., Chairman

IMD Membership Committee Meeting

J. P. Nielsen, Chairman

TUESDAY, FEBRUARY 16

7:30 am

IMD Titanium Committee Breakfast Meeting

J. H. Jackson, Chairman

9:00 am

Deformation II

J. S. Smart, Jr. and Bruce Chalmers, Associate Chairmen

Mechanism of Plastic Flow in Titanium: Manifestations and Dynamics of Glide: F. D. Rosi, Sylvania Electric Products, Inc., Bayside, N. Y.

Effects of Temperature on the Flow and Fracture Characteristics of Molybdenum: J. H. Bechtold, Westinghouse Electric Corp., E. Pittsburgh, Pa.

Mechanical Properties of Beryllium Copper at Subzero Temperatures: J. T. Richards, Beryllium Corp., Reading, Pa., R. M. Brick, University of Pennsylvania, Philadelphia, Pa.

12:15 pm

IMD Executive Committee Luncheon Meeting

Morris Cohen, Chairman

2:00 pm

Constitution I

B. D. Cullity and A. H. Geisler, Associate Chairmen

Viscosity of Liquid Lead-Tin and Antimony-Cadmium Alloy Systems: H. J. Fisher, Dept. of Mines and Technical Surveys, Ottawa, Ont.; A. Phillips, Yale University, New Haven, Conn.

Uranium-Titanium Alloy System: M. C. Udy, F. W. Boulger, Battelle Memorial Institute, Columbus, Ohio.

System Zirconium-Oxygen: R. F. Domagala, D. J. McPherson, Armour Research Foundation of Illinois Institute of Technology, Chicago, Ill.

Neptunium-Aluminum Intermetallic Compounds: O. J. C. Runnalls, Atomic Energy of Canada Ltd., Chalk River, Ont.

Cursory Investigation of Intermediate Phases in the Systems Ti-Zn, Ti-Hg, Zr-Zn, Zr-Cd and Zr-Hg by X-ray Powder Diffraction Methods: Paul Pietrokowsky, California Institute of Technology, Pasadena, Calif.

2:00 pm

High Temperature Properties

D. N. Frey and G. V. Smith, Associate Chairmen

Effect of Stress on the Creep Rates of Polycrystalline Aluminum Alloys Under Constant Structure: O. D. Sherby, R. Frenkel, J. E. Dorn, University of Cali-

fornia, Berkeley, Calif.; J. Nadeau, General Electric Co., Erie, Pa.

Creep Correlations of Metals at Elevated Temperatures: O. D. Sherby, R. L. Orr, J. E. Dorn, University of California, Berkeley, Calif.

Aging Characteristics of Nickel-Chromium Alloys Hardened with Titanium and Aluminum: Rolf Nordheim, N. J. Grant, Massachusetts Institute of Technology, Cambridge, Mass.

6:00 pm

Metals Branch Cocktail Party

7:00 pm

Metals Branch Annual Dinner

K. C. McCutcheon, Toastmaster

Speaker: G. L. Mehta, Ambassador from the Republic of India to the U. S. A.

WEDNESDAY, FEBRUARY 17

9:00 am

Solidification

J. H. Frye and B. Lement, Associate Chairmen

Solidification of Aluminum-Rich Aluminum-Copper Alloys: A. B. Michael, Allis-Chalmers Mfg. Co., Milwaukee, Wis.; M. B. Bever, Massachusetts Institute of Technology, Cambridge, Mass.

Redistribution of Solutes by Formation and Solidification of a Molten Zone: W. G. Pfann, Bell Telephone Laboratories, Murray Hill, N. J.

Orientation Relationships in Cast Germanium: W. C. Ellis, Jacqueline Fageant, Bell Telephone Laboratories, Murray Hill, N. J.

9:00 am

Physical Chemistry of Extractive Metallurgy
Joint Session with EMD

Improved Vacuum-Fusion Method for the Determination of Oxygen and Nitrogen in Metals: N. A. Gokcen, Michigan College of Mining and Technology, Houghton, Mich.

Theoretical Analysis of Diffusion of Solutes During the Solidification of Alloys: C. Wagner, Massachusetts Institute of Technology, Cambridge, Mass.

Diffusion in Liquid Lead-Bismuth Alloys: R. E. Grace, G. Derge, Carnegie Institute of Technology, Pittsburgh, Pa.

Vapor Pressure of Zinc Sulphide from 680° to 825°C: G. L. McCabe, Carnegie Institute of Technology, Pittsburgh, Pa.

Determination of the Standard Free Energy of Formation of Zinc Sulphide and Magnesium Sulphide: W. Curlook, L. M. Pidgeon, University of Toronto, Toronto, Canada.

11:00 am

Annual Lecture, IMD

Andrew Fletcher and Morris Cohen, Associate Chairmen

Melting and Freezing: Bruce Chalmers, Harvard University, Cambridge, Mass.

2:00 pm

Constitution II

L. A. Carapella and W. D. Robertson, Associate Chairmen

Diffusion and Solubility of Boron in Iron and Steel: P. E. Busby, Cyril Wells, Carnegie Institute of Technology, Pittsburgh, Pa.; Mary E. Warga; University of Pittsburgh, Pittsburgh, Pa.

Constitution and Properties of Silver-Copper-Zinc Brazing Alloys: Karl M. Weigert, Goldsmith Bros. Smelting & Refining Co., Chicago, Ill.

Sigma Phase in Binary Alloys: Peter Greenfield, P. A. Beck, University of Illinois, Urbana, Ill.

Constitution of Iron-Boron Alloys in the Low Boron Range: M. E. Nicholson, University of Chicago, Chicago, Ill.

Investigation of the Systems Formed by Chromium, Molybdenum, and Nickel: D. S. Bloom, Naval Ordinance Test Station, China Lake, Calif.; N. J. Grant, Massachusetts Institute of Technology, Cambridge, Mass.

2:00 pm

Titanium

O. T. Marzke and W. Finlay, Associate Chairmen

Influence of Oxygen Nitrogen and Carbon on the Phase Relationship of the Titanium-Aluminum System: R. J. Van Thyne, H. D. Kessler, Armour Research Foundation, Chicago, Ill.

Titanium-Chromium-Oxygen System: C. C. Wang, Sylvania Electric Products, Inc., Ipswich, Mass.; N. J. Grant, Massachusetts Institute of Technology, Cambridge, Mass.

System Titanium-Chromium-Molybdenum: R. P. Elliott, W. Rostoker, Armour Research Foundation of Illinois Institute of Technology, Chicago, Ill.; B. W. Levinger, Tung-Sol Electric Inc., Bloomfield, N. J.

System Titanium-Manganese-Molybdenum: R. P. Elliott, W. Rostoker, Armour Research Foundation of Illinois Institute of Technology, Chicago, Ill.; B. W. Levinger, Tung-Sol Electric Inc., Bloomfield, N. J.

Heat Treatment of Commercial Titanium Base Alloys: L. Luini, E. Lee, Curtiss-Wright Corp., Wood-Ridge, N. J.

Heat Treatment, Structure and Mechanical Properties of Ti-Mn Alloys: F. C. Holden, H. R. Ogden, R. I. Jaffee, Battelle Memorial Institute, Columbus, Ohio.

THURSDAY, FEBRUARY 18

9:00 am

Steel

W. J. Harris, Jr. and L. D. Jaffee, Associate Chairmen

Hydrogen Embrittlement of Steels: J. T. Brown, Westinghouse Research Laboratories, Pittsburgh, Pa., W. M. Baldwin, Jr., Case Institute of Technology, Cleveland, Ohio.

Quantitative Measure of Temper Embrittlement: Norman Brown, University of Pennsylvania, Philadelphia, Pa.

475°C Embrittlement in Stainless Steels: A. J. Lena, Allegheny Ludlum Steel Corp., Brackenridge, Pa., M. F. Hawkes, Carnegie Institute of Technology, Pittsburgh, Pa.

9:00 am

Powder Metallurgy

F. N. Rhines and A. Shaler, Associate Chairmen

Mechanical Properties of Beryllium Fabricated by Powder Metallurgy: W. W. Beaver, K. G. Wikle, Brush Beryllium Co., Cleveland, Ohio

Study of the Effect of Carbon Content on the Structure and Properties of Sintered WC-Co Alloys: Joseph Gurland, Firth Sterling Inc., Pittsburgh, Pa.

Solid State Bonding of Aluminum to Nickel: S. Storchheim, J. L. Zambrow, H. H. Hausner, Sylvania Electric Products, Inc., Bayside, N. Y.

High Temperature Strength of Wrought Aluminum Powder Products: Eric Gregory, N. J. Grant, Massachusetts Institute of Technology, Cambridge, Mass.

Resistance Sintering Under Pressure: F. V. Lenel, Rensselaer Polytechnic Institute, Troy, N. Y.

12:15 pm

IMD Powder Metallurgy General Luncheon

J. F. Kuzmick, Chairman

2:00 pm

Powder Metallurgy Seminar

Claus Goetzel, Chairman

The Contribution of Powder Metallurgy to the High Temperature Materials Problem: G. M. Ault, G. C. Deutsch, Materials Research Section, Lewis Flight Propulsion Laboratory, NACA, Cleveland, Ohio.

Plans Progress For Pacific Conference

The Oregon Section AIME will be host to the Pacific Northwest Metals and Minerals Conference to be held Apr. 29 through May 1, 1954. Present plans call for four sessions on metals which will include iron and steel and both extractive and physical metallurgy. Two sessions are planned on industrial minerals, one on geology and one on ground water. The meeting will be held at the Multnomah Hotel, Portland.

Arrangements for the meeting are being made by Frank Cappa, General Conference Chairman; Don W. Johnson, General Activities Chairman; Hal Seykota, Finance Chairman; and Bill Wiltschko, Program Chairman—Metals Branch. Publicity is being handled by A. O. Bartell.

Blast Furnace Group Nominates Officers

The Nominating Committee of the Blast Furnace, Coke Oven and Raw Materials Committee has presented the following slate of officers to fill open positions in the 1954 elections to be held at the spring conference. **Chairman:** Kurt Neustaetter, assistant superintendent, blast furnace, Inland Steel Co., East Chicago, Ind. **Vice-Chairman** (2 years): Leonard Tofft, superintendent, blast furnace, Columbia-Geneva div., U. S. Steel Corp., Geneva, Utah. **Secretary:** James W. Duncan, secretary, blast furnace committee, central operations, steel, U. S. Steel Corp., Pittsburgh, Pa. **Members of Executive Board** (4 years): Carl F. Hoffman, superintendent, blast furnace, Bethlehem Steel Co., Sparrows Point, Md.; J. J. Cavett, superintendent, coke plant, Jones & Laughlin Steel Corp., Aliquippa, Pa.

Students' Night Held By Connecticut Section

The annual Students' Night session of the Connecticut Section AIME was held November 11 at the Hammond Metallurgical Laboratory, Yale University. Leon Thelin, Chairman of the Section, and William Goering, Chairman of the Yale Metallurgical Society (Student Affiliated Chapter, AIME), were Co-Chairmen. Walter D. France, Scovill Mfg. Co., the new Counsellor and liaison between the Yale Metallurgical Society and the Connecticut Section AIME gave a short talk emphasizing the role played by the National and Connecticut Sections and suggested various methods to aid and assist the student activities.

R. W. Christine, Vice-Chairman of the Section, introduced D. W. Kaufmann the guest speaker of the evening. Mr. Kaufmann, assistant sales manager, Rem-Cru Titanium, Inc., presented an illustrated lecture on titanium in which he traced the growth of the metal as an engineering material.

J. I. Mueller Speaks Before Columbia Section

James I. Mueller of the University of Washington was the guest speaker at the Columbia Section's meeting on November 20 at Spokane. Dr. Mueller described X-ray diffraction and spectroscopy and their application to geological and metallurgical problems. Elements present in amounts of one part per ten million can be identified by these methods.

M. E. Volin, Program Chairman of the Spokane Subsection, arranged the meeting and entertainment was provided by the Scientific Supplies Co. of Seattle through the courtesy of W. C. Johnson, the Spokane representative. Mr. Volin announced that F. L. LaQue, who is in charge of the corrosion engineering section of International Nickel Co., would be the speaker for the February meeting.

Howe Memorial And IMD Lecturers Named

John S. Marsh, assistant manager of research for the Bethlehem Steel Co., has been named Howe Memorial Lecturer for 1955. Dr Andre Guinier, Conservatoire des Arts et Metiers, University of Paris, has been selected to present the Institute of Metals Div. Lecture in 1956.

Metallurgical Meeting Will Be Held in Europe

An invitation has been received by AIME from six European technical societies to take part in a joint metallurgical meeting in Europe in June 1955. The societies issuing the invitation are: The Iron and Steel Institute and the Institute of Metals in the United Kingdom; the Société Française de Métallurgie, the Verein deutscher Eisenhüttenleute (acting also on behalf of the Deutsche Gesellschaft für Metallkunde), and the Swedish Jernkontoret.

Subjects proposed for coverage include, in the ferrous field, ironmaking and raw materials(including coke and ore preparation but excluding mining), steelmaking, mechanical working (including hot and cold rolling, forging, and wire-drawing, surface treatment (including metallic coatings), and steel properties and quality control, including heat treatment. In the nonferrous field, discussion would cover light metals, low melting point metals, copper and copper alloys, and precious metals and metals melting at high temperatures. Education and training, and research and development would also be given attention.

Provisionally, the time will be Sunday, June 1, through Sunday, June 19. Plant visits will be made in England, Germany, and France; possibly Sweden as well. Other countries may also be visited, as it is understood that European metallurgists are all anxious to return some of the hospitality that they have enjoyed in the United States.

Institute Meetings Now Self-Supporting

As a result of action of the AIME Board of Directors in 1949, all AIME meetings have become substantially self-supporting. In prior years, expenses in a year for these gatherings ran as high as $13,000, which was met out of income supplied by the dues of many Members who could not attend. Through the simple expedient of setting up an income and expense budget, registration or convention fees can be set at such a figure that will balance income and expense. The cost is placed solely on those who get the benefit. If an Annual Meeting is going to cost an estimated $13,000 for instance, and 2000 Members and 400 nonmembers are expected to attend, a registration fee of $5 for Members and $8 for nonmembers is indicated. Experience has shown about what income and expenses are likely to be. No attempt is made to have income enough greater than expected expense to accumulate a fund for unexpected contingencies. Expense for the social features of a meeting is a responsibility of the host Local Section; tickets are sold on a self-sustaining basis.

1954 Officers Declared Elected

At the meeting of the AIME Board of Directors on Nov. 18, formal announcement was made of the election of the following "official" slate of officers for 1954, to take office Feb. 16: President-Elect, H. DeWitt Smith; Vice-Presidents, T. B. Counselman and Harold Decker; Directors, Ralph E. Kirk, Carleton C. Long, P. J. Shenon, George Dub, Earl R. Marble, and E. C. Babson. All the above serve as Directors for three-year terms. Directors ex officio, as Division Chairmen, for one-year terms: J. R. Van Pelt, MIED; J. H. Scaff, IMD; P. T. Stroup, EMD; John R. McMillan, PD; R. C. Stephenson, Ind. Min. Div.; M. D. Cooper, CD; J. S. Marsh, I&SD; J. D. Forrester, MGGD; S. D. Michaelson, MBD; and J. K. Richardson, MED. Leo F. Reinartz, currently President-Elect, will be President in 1954. One other Director is to be named for a one-year term.

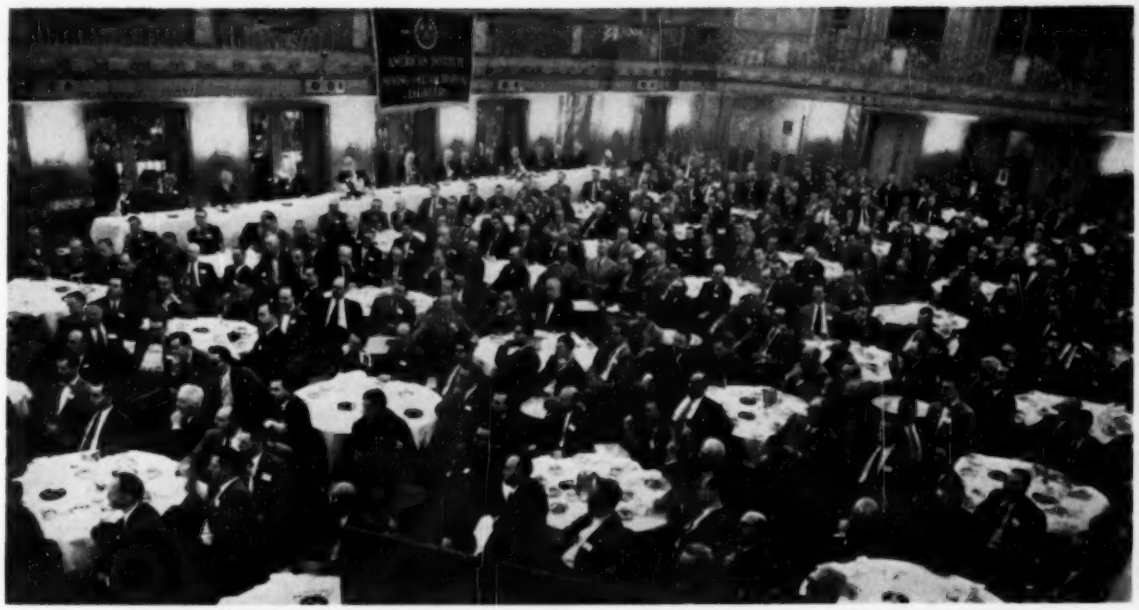

At the Annual Dinner Thursday evening electric furnace men give their attention to H. N. Alyea's topic "Atomic Energy: Weapon for Peace."

Rapid Development of Electric Furnace Steelmaking Reflected in Conference Attendance

Cincinnati, the Queen City, was the locale of the Eleventh Annual Electric Furnace Steel Conference from Dec. 2 to 4, 1953. Nearly 750 persons joined in the technical sessions and took advantage of the opportunity to renew friendships and exchange ideas on steelmaking.

Wednesday was highlighted by a trip through Armco Steel Corp.'s Middletown plant. The formal technical sessions opened Thursday morning with remarks by W. M. Farnsworth, Executive Committee Chairman, and F. O. Lemmon, Chairman of the Conference Committee. Papers were presented on induction stirring in arc furnaces and on jet engines steels and related electric furnace operating problems. On Friday simultaneous sessions were held which included papers on inclusions in steel, the metallurgy of electric furnace steel, mechanical aspects of

Vernon Jones, Armco Steel Corp., Middletown, Ohio, and Frank Weir, Harbison-Walker Refractories Co., discuss the technical session program.

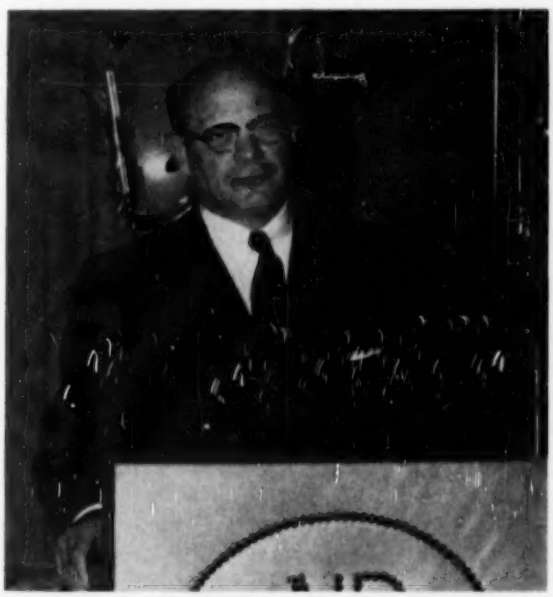

Leo Reinartz, President-Elect of AIME and Vice-President of Armco Steel Corp., summarized the development of the electric furnace.

Walter Farnsworth of Republic Steel Corp., Chairman of the Executive Committee, and Ray Frank of the Bonney-Floyd Co., Past-Chairman, display the AIME certificates presented by Floyd Lemmon, Conference Committee Chairman.

electric furnace operation, and the design of the modern high powered arc furnace.

At the Annual Dinner, Thursday evening, F. O. Lemmon introduced the toastmaster, W. Beckjord, president, Cincinnati Gas & Electric Co. Mr. Beckjord then called upon AIME President-Elect Leo Reinartz, T. J. McLoughlin, past Chairman of the Executive Committee, and E. H. Robie, Secretary of the AIME, to say a few words. R. H. Frank and W. M. Farnsworth were presented with 400-day clocks, permanent AIME registration, and certificates for their service to the Electric Furnace Steel Conference and to the Institute.

The speaker of the evening was Professor H. N. Alyea of Princeton University. Dr. Alyea gave his famous talk on "Atomic Energy: Weapon for Peace."

Norman Tisdale, Molybdenum Corp. of America, explains a few points to his colleagues Worley Albaugh, Miller & Co., Cincinnati, Norman, Jr., and Adam Textor, Firth-Sterling, Inc., McKeesport, Pa.

The interchange of ideas at the meeting went on continuously. From left to right are Sam Arnold, III, consulting engineer, Pittsburgh, Walter Farnsworth, Republic Steel Corp., Clarence Sims, Battelle Memorial Institute, and Vic Zang, Unicast Corp., Toledo.

Among those seated at the head banquet table were A. P. Miller of Newport Steel Co., Ken McCutcheon of Armco Steel Corp., Past-Chairman of the AIME Iron and Steel Div., and Clyde Wyman of Burnside Steel Foundry Co., Electric Metalmakers Guild President.

The general session opened Thursday morning in the Pavilion Caprice. On Friday simultaneous sessions were held to cover the widest possible range of subjects related to electric steelmaking.

J. E. Harrod, U. S. Steel Corp., C. F. Staley, Armco Steel Corp., V. J. Nolan, National Carbon Co., and R. J. McCurdy, Republic Steel Corp. confer before the Electric Furnace Steel Committee meeting Wednesday evening.

Another group at the head table during the banquet included E. H. Robie, Secretary AIME, T. J. McLoughlin of U. S. Steel Corp., Chairman of the AIME Iron and Steel Div., and AIME President-Elect Leo Reinartz.

H. F. Walther of the Timken Roller Bearing Co. presented the lead-off paper on the performance of the induction stirrer. He displays with W. F. Farnsworth the *new look* in electric furnace shop apparel.

WILLIAM E. WRATHER

William E. Wrather Wins Fritz Medal

William Embry Wrather, Past President of the AIME and director of the U. S. Geological Survey, has been awarded the John Fritz Medal by unanimous choice of a 16-man board. Mr. Wrather will receive the Fritz Medal at a dinner to be held on Feb. 4, 1954 in the LePerroquet Suites, Waldorf-Astoria, New York.

The medal is given annually for notable scientific or industrial achievement. In awarding the medal to Dr. Wrather, the board cited him as:

"A geologist of worldwide experience and fame; an outstanding scientist and historian; a wise leader distinguished for his service to the nation."

Selection of Dr. Wrather was made by a board consisting of four members each from the four founder national engineering societies: American Institute of Mining and Metallurgical Engineers; American Society of Civil Engineers; American Society of Mechanical Engineers; and American Institute of Electrical Engineers.

Dr. Wrather has been throughout the world in pursuit of geological knowledge. He has traveled the Balkans, Africa, South America, and Asia in his professional status. In 1933 he helped organize the 16th International Geological Congress in Washington. Four years later he attended the 17th Congress in Moscow, Russia.

In the past Dr. Wrather has been a member of the Texas Historical Society and once served as president.

G. Holt Nominating Committee Chairman

Grover Holt, general manager, Cleveland-Cliffs Iron Co., Ishpeming, Mich., is the Chairman of the Nominating Committee for 1955 AIME Officers. Members of the Institute are invited to write to him or any other Member of the Committee, suggesting the name of a candidate for President-Elect for 1955, a Vice-President, or Director. One President-Elect is to be named, two Vice-Presidents, and six Directors.

Denver Petroleum Section Recognized

First of the recently authorized "overlaying" Local Sections to be recognized by the AIME Board is the Denver Petroleum Section. Its area is to include the entire state of Colorado, the same territory that is included in the Colorado Section, but it will serve only Petroleum Branch Members. Any AIME Member in Colorado may be affiliated with either or both of the Sections.

UPADI Meeting To Be Held During August

The Pan American Federation of Engineering Associations (UPADI) has announced preliminary plans for its next meeting, which will be held in São Paulo, Brazil. Tentative dates are Aug. 3 to 13, 1954. A diversified program of technical papers and social events, combined with a liberal mixture of sightseeing, is being planned. A sectional meeting of the World Power Conference is being held in Brazil at about the same time, so an effort is being made to avoid overlapping dates.

Coming Events

Jan. 6, 1954, AIME, Chicago Section, Chicago Bar Assn., Chicago.

Jan. 8, AIME, St. Louis Local Section, York Hotel, St. Louis.

Jan. 12-14, National Constructors Assn., annual meeting, Hotel Commodore, New York.

Jan. 13, AIME, Connecticut Section, Bridgeport Brass Co., Bridgeport.

Jan. 13, AIME, Bessemer Committee, annual meeting, Duquesne Club, Pittsburgh

Jan. 20, AIME, National Open Hearth Steel Committee, Western Section, Rodger Young Auditorium, Los Angeles.

Jan. 20-22, Conference on Operations Research in Production and Inventory Control, Wade Park Manor, Cleveland.

Jan. 25-27, Plant Maintenance & Engineering Show and Conference, Hotel Conrad Hilton and International Amphitheatre, Chicago.

Feb. 2, AIME, Chicago Section, Chicago Bar Assn., Chicago.

Feb. 15-18, AIME, annual meeting, Metals Branch, Hotel McAlpin; Mining and Petroleum Branches, Hotel Statler, New York.

Mar. 3, AIME, Chicago Section, Chicago Bar Assn., Chicago.

Mar. 8-10, American Institute of Chemical Engineers, Statler Hotel, Washington, D. C.

Mar. 10, AIME, Connecticut Section, American Brass Co., Torrington, Conn.

Mar. 15-19, National Assn. of Corrosion Engineers, Municipal Auditorium, Kansas City.

Mar. 17, AIME, National Open Hearth Steel Committee, Western Section, Rodger Young Auditorium, Los Angeles.

Mar. 24-26, American Power Conference, annual meeting, Sherman Hotel, Chicago.

Apr. 5-7, AIME, Blast Furnace, Coke Oven, Raw Materials Conference, Palmer House, Chicago.

Apr. 5-7, AIME, National Open Hearth Conference, Palmer House, Chicago.

Apr. 5-7, American Society of Lubrication Engineers, annual meeting and exhibit, Cincinnati.

Apr. 7, AIME, Chicago Section, Chicago Bar Assn., Chicago.

Apr. 21-23, Southern Industrial Wastes Conference, Hotel Shamrock, Houston.

Apr. 26-28, Canadian Institute of Mining and Metallurgy, annual meeting, Mount Royal Hotel, Montreal.

Apr. 27, Assn. of Consulting Chemists and Chemical Engineers, Hotel Belmont Plaza, New York.

Apr. 26-30, American Society of Tool Engineers, industrial exposition, Convention Center, Philadelphia.

Apr. 29-May 1, Pacific Northwest Metals and Minerals Conference, Portland, Ore.

May 2-6, Electrochemical Society, La Salle Hotel, Chicago.

May 4-7, American Welding Society, national meeting, Hotel Statler, Buffalo.

May 8-14, American Foundrymen's Society, Cleveland Auditorium, Cleveland.

May 16-17, American Institute of Chemical Engineers, Kimball Hotel, Springfield, Mass.

June 20-23, Chemical Institute of Canada, Toronto, Canada.

PROFESSIONAL SERVICES

Limited to AIME members, or to companies that have at least one AIME member on their staffs. Rates $40 per year per inch.

MAX STERN
Consulting Engineer
Expert for Scrap Recovery and Shipwrecking — Modernization of Plants and Yards for Ferrous and Nonferrous Metal Scrap
149 Broadway New York 6, N. Y.

S T & CO.
SCIENTISTS
CONSULTANTS
METALLURGISTS
Small Jobs Welcomed
SAM TOUR & CO., INC.
Laboratories and offices
44 Trinity Place, New York 6, N. Y.
Testing—Certifying
American Standards
Testing Bureau, Inc.

Personals

H. E. JOHNSON

Hugo E. Johnson has been appointed a vice-president of the Lake Superior Iron Ore Assn. Mr. Johnson has been assistant manager of the project development group of the Battelle Memorial Institute, Columbus for the last five years. Previously, he was associated with the Youngstown Sheet & Tube Co., and the U. S. Steel Corp.

Julius F. Sachse, vice-president and works manager of the Elizabeth plant, Metals Disintegrating Co., Inc., has been appointed vice-president in charge of research and development for the company.

Alton W. Bardeen, formerly chief metallurgist of the Ohio Brass Co., succeeds the late R. W. Parsons as technical director of the Mansfield, Ohio plant.

Joseph J. Constantino has joined the Hooker Electrochemical Co., as a design engineer. **Jacob B. Hufford** has become associated with the company as a chemical engineer in the process study group, and **Frank W. Long** has joined the firm as a chemist in the plastics and resins group in the research and development dept.

Kenneth W. Horsman has been appointed general manager of the Worthington Corp., Plainfield works. **Paul J. Foley** was appointed general sales manager for all Plainfield works products and **John F. Weissert** was named general superintendent of plant operations at Plainfield.

A. M. Neumann has been appointed chief engineer of the Evans lead div., National Lead Co.

Steve Yacus has been elected secretary-treasurer of Metal Finish, Inc., Newark, N. J.

Cecil W. Humphreys has been appointed vice-president in charge of manufacturing for Shell Chemical Corp., New York.

Jack E. Griffin has resigned from the Western Machinery Co. and is now employed as a production engineer for Kaiser Aluminum & Chemical Corp. at the Tacoma smelter.

Robert S. Macfarlane, president, Northern Pacific Railway Co., and **James A. Woods,** president, Commercial Solvents Corp., were elected directors of the American Smelting & Refining Co.

Hugh G. Bain has been elected to honorary membership in the Australasian Institute of Mining and Metallurgy, in recognition of his many services to the mining and metallurgical industries and as honorary treasurer of the Fifth Empire Mining and Metallurgical Congress.

Harry E. Miller has been named manager of the aluminum extrusion plant of Reynolds Metals Co., Grand Rapids, Mich. Mr. Miller was transferred from the Phoenix, Ariz., plant where he was plant superintendent.

John A. Matousek, formerly vice-president of manufacturing, Baker-Raulang Co., has been named vice-president and general manager.

Fred N. Eaton was appointed works manager of the foundry div., of Aluminum Industries, Inc., Cincinnati. Prior to joining Aluminum Industries, Inc., Mr. Eaton was manager of the foundry div. of Bohn Aluminum & Brass Corp.

Jerome C. McCarthy has been appointed to the newly created position of general manager of by-product and metallurgical sales, Island Creek Coal Sales Co.

Herbert A. Morrissey has joined the staff of the filtration dept. of the H. H. Thoerner Co., Pittsburgh. Mr. Morrissey was formerly junior fellow on the American Iron and Steel Institute's research fellowship on iron ore agglomeration at Mellon Institute, Pittsburgh.

H. A. MORRISSEY

N. C. FICK

Nathaniel C. Fick, director of the metals and minerals panel, Office of Assistant Secretary of Defense for Research and Development, has been named chairman of the speakers' bureau for the District of Columbia Council of Engineering and Architectural Societies and the Washington Academy of Sciences.

Henry W. Franz is associated with the Nickel Processing Corp., Nicaro, Oriente, Cuba, as chief metallurgist.

A. M. Talbot has joined the microcast div. of the Austenal Laboratories, Inc., Dover, N. J. as technical director. He had been associated with the International Nickel Co., Inc., as head of the iron alloys section in the research laboratory, Bayonne, N. J.

Lance H. Cooper, chairman of the Mond Nickel Co., Ltd., London, has been elected a vice-president of the International Nickel Co., of Canada, Ltd.

Harold W. Sweatt, president of Minneapolis-Honeywell Regulator Co., was recently elected chairman of the board, succeeding **Mark C. Honeywell,** who was named honorary chairman. **Paul B. Wishart,** vice-president and general manager was elected president.

J. P. Gill has been elected president of Vanadium-Alloys Steel Co., Latrobe, Pa. Mr. Gill joined the firm in 1920 as chief metallurgist. He was elected vice-president in 1943 and in 1945 was made chairman of the executive committee of Vanadium-Alloys and subsidiaries.

Samuel Frankel has resigned as president and director of Foundry Services, Inc., New York and **Herbert A. Frankel** has resigned as secretary and director. They will both remain in a consulting capacity.

G. G. ZIPF

George G. Zipf was recently appointed superintendent of the steel plant of the tubular products div., Babcock & Wilcox Co. Prior to his promotion, Mr. Zipf was assistant superintendent of the steel plant in charge of melting and blooming.

J. S. Robbins, Vulcan Mold & Iron Co., has been transferred from Latrobe, Pa., to Lansing, Ill.

Harold E. Collins has been elected a vice-president of Metals Disintegrating Co.

Sidney F. Kaufman, has joined the Carboloy dept., General Electric Co., as an engineer in the carbide processing and fabrication development unit.

William E. Shoupp has been appointed assistant div. manager in charge of development, atomic power div., Westinghouse Electric Corp.

B. E. Marquis has joined the Mallory-Sharon Titanium Corp., Niles, Ohio. He recently resigned from the Vanadium Corp. of America, Cambridge, Ohio.

Marvin Pesses is with the Alloy Metal Products, Inc., Davenport, Iowa.

Harold B. Emerick, formerly general technical dept., is assistant director, technical services, Jones & Laughlin Steel Corp., Pittsburgh, Pa.

Louis W. Cole was reelected chairman of the board of directors for Federal Electric Products Co., Newark, N. J.

Clement K. Chase has accepted a position as chief metallurgist with the Utex Exploration Co., Moab, Utah.

Raymond M. Fuoss has joined the research staff as a consultant for the U. S. Testing Co., Inc., Hoboken. He will be responsible for research activities in the firm's Boston laboratories.

A. L. Foscue has been appointed president of Electro Metallurgical Co. and U. S. Vanadium Co., divs., Union Carbide & Carbon Corp. Mr. Foscue joined UCC in 1924. He was appointed a vice-president of Electro Metallurgical Co. in 1951.

Obituaries

Richard W. Parsons (Member 1924), until recently technical director of the Ohio Brass Co.'s main plant at Mansfield, Ohio, died on Oct. 5, 1953. A native of Mansfield, he was educated at Ohio State University, graduating in 1925 with a degree in metallurgical engineering. In 1927 he joined the Ohio Brass Co. as metallurgist and later was appointed technical director. Prior to joining Ohio Brass, he had been associated with the Republic Iron & Steel Co., and the Central Steel Co. He also held membership in the ASM, ASTM, and American Foundrymen's Assn.

Necrology

Date Elected	Name	Date of Death
1947	William R. Allen	Oct. 31, 1953
1932	Christian Anderson	Dec. 1, 1953
1948	Littleton Barkley	Unknown
1948	H. R. Bennett	Unknown
1952	Serge Bogroff	Sept. 24, 1953
1941	Alexander Bonnyman	May 14, 1953
1935	H. Cayford Burrell	Nov. 9, 1953
1951	J. B. Donnelly	May 7, 1953
1945	Louis J. Ensch	Sept. 9, 1953
1944	Harry S. Gay	March 1953
1920	William B. Greenlee	Unknown
1934	David Porter Hale, Jr.	Nov. 3, 1953
1937	Leroy G. Hetrick	Oct. 23, 1953
1935	F. D. Howell	Sept. 10, 1953
1914	William J. Jenkins	Jan. 12, 1953
1903	Frank G. Jewett	May 1953
1950	James K. Kent	1951
1943	Sherwin P. Lowe	Oct. 18, 1953
1948	Eero Makinen	Oct. 27, 1953
1935	Emmett McFarland	Oct. 23, 1953
1946	John L. McNulty	Aug. 22, 1953
1914	Donald Miller	July 27, 1953
1896	Carl Scholz	Nov. 15, 1953
1902	Hoval Arnold Smith	Oct. 29, 1953
1945	Owen F. Thornton	July 15, 1953
1899	Harold A. Titcomb	Nov. 26, 1953
1948	Russell F. Wilford	Aug. 6, 1953
1946	J. J. Zorichak	Aug. 6, 1953

Proposed for Membership

— Metals Branch AIME —

Total AIME membership on Nov. 30, 1953 was 19,562; in addition 2067 Student Associates were enrolled.

ADMISSIONS COMMITTEE

O. B. J. Fraser, Chairman; Philip D. Wilson, Vice-Chairman; F. A. Ayer, A. C. Brinker, R. H. Dickson, Max Gensamer, Ivan A. Given, Fred W. Hanson, T. D. Jones, G. W. Lutjen, E. A. Prentis, Sidney Rolle, J. T. Sharman, F. T. Sisco, R. L. Ziegfeld.

The Institute desires to extend its privileges to every person to whom it can be of service, but does not desire as members persons who are unqualified. Institute members are urged to review this list as soon as possible and immediately to inform the Secretary's office if names of people are found who are known to be unqualified for AIME membership.

In the following list C/S means change of status; R, reinstatement; M, Member; J, Junior Member; A, Associate Member; S, Student Associate.

Arizona
Hayden—Henry, Joe A. (J)

California
Glendora—Funk, Campbell, W. F. (M) (C/S—J-M)
Pasadena—Bacon, Loren E. (M)
Walnut Creek—Hazlett, Thomas H. (M)

Colorado
Denver—Drake, Curtis C. (M)

Connecticut
Waterbury—Russell, Richard E. (M) (C/S—J-M)

Idaho
Kellogg—Burgess, Lamar W. (M) (R. C/S—J-M)
Silverton—Thompson, Virgil N. (A)
Wallace—Minshall, William E. (A)

Illinois
N. Pekin—Calton, Marion R. (J)
Park Forest—Morey, Woodruff A. (M)
Pekin—Drake, Justin R. (M)
Peoria—Loyd, Calvin D. (J) (R. C/S—S-J)
Washington—McKloskey, Ambrose S. (M) (R. C/S—S-M)
Washington—Van Pelt, Richard H. (M) (R. C/S—S-M)

Indiana
Elkhart—Conley, Clyde M. (A)

Kentucky
Louisville—Brennan, Bruce E. (A)

Maryland
Silver Spring—Doughton, Richard, Jr. (M)

Massachusetts
Beverly—Carlson, Kenneth A. (M)
Cambridge—Comerford, Matthias F. (J)
Lynnfield—Gruber, Bernard A. (M)
Melrose—Steck, Alfred B. (M) (C/S—J-M)
Salem—Gordon, Emanuel (M)
Swampscott—Frazier, Loring R. (M) (R. C/S—S-M)

Michigan
Birmingham—Kropf, Richard B. (M)

Missouri
Kansas City—Howard, Robert T. (M) (C/S—J-M)

New Jersey
Paramus—Mott, Lambert H. (M)

New York
Lido—Hershcopf, William (M) (C/S—J-M)
New York—Holmes, John G. (M)
Niagara Falls—Gate, Alfred D. (M)
Pleasantville—Macurda, Donald B. (A)

Ohio
Canton—Mravec, Joseph G. (A)
Cincinnati—Crowe, John W. (A)
Columbus—Barth, Vincent D. (M)
Columbus—Ogden, Horace R. (M) (C/S—J-M)
Columbus—Rengstorff, George W. P. (M) (C/S—J-M)
East Liverpool—Porter, Winston A. (A)
Euclid—Toensing, Clarence H. (M) (R. C/S—S-M)
Poland—Phillips, D. Gordon (A)
Willoughby—Zook, John J. (A)

Pennsylvania
Allison Park—Clokey, George V. (A)
Bethlehem—Blickwede, Donald J. (M) (C/S—J-M)
Johnstown—Owens, Gerald L. (M)
Johnstown—Shafer, William M. (M)
McKeesport—Barker, Fred A. (A)
Palmerton—Griffith, William A. (M) (C/S—J-M)
Philadelphia—Hughes, Peter J. (M) (R. C/S—J-M)
Pittsburgh—Beeghly, Hugh F. (M)
Pittsburgh—Findley, Roger S. (A)
Pittsburgh—Fitzmier, Robert E. (A)
Pittsburgh—Lawson, Harry W., Jr. (A)
Pittsburgh—McCabe, Charles L. (A)
Pittsburgh—Weiblen, Carl F. (A)
Sewickley—Lawrence, George D. (A)
Sharon—McClintick, Richard J. (J)

Texas
Corpus Christi—Lister, Thomas R. (M)
El Paso—Davenport, James D. (M) (C/S—J-M)
Midland—Price, William G. (J)

Utah
Salt Lake City—Gudmundsen, Stanley A. (M)

Virginia
Richmond—Radtke, Schrade F. (M) (C/S—A-M)

Washington
Spokane—Bardill, John D. (M) (R. C/S—S-M)

Canada
Ontario-Fonthill—Olson, George C. (A)

For the story of FERROCARBO in quality steelmaking, mail the coupon today—or phone or write the FERROCARBO distributor nearest you. You'll learn why steel deoxidized with FERROCARBO is "plus steel."

KERCHNER, MARSHALL & CO.
PITTSBURGH • Cleveland • Buffalo
Philadelphia • Birmingham • Los Angeles

MILLER & COMPANY
CHICAGO • St. Louis • Cincinnati

WILLIAMS & WILSON
TORONTO • Montreal • Windsor

THE CARBORUNDUM COMPANY, Dept. JM 84-31
Niagara Falls, New York

Gentlemen:

I would like to have the FERROCARBO story—no obligation on my part.

NAME AND TITLE

COMPANY

STREET AND NUMBER CITY ZONE STATE

FERROCARBO

TRADE MARK

by CARBORUNDUM

"Carborundum" and "Ferrocarbo" are trademarks which are registered in the U. S. by The Carborundum Company, Niagara Falls, New York, and in Canada by Canadian Carborundum Company, Ltd., Niagara Falls, Ontario.

64-310

Keep NATIONAL Carbon Brick on hand for MAINTENANCE

TRADE-MARK

KEEP THESE STANDARD SIZES ON HAND FOR EMERGENCY!

13½" x 6" x 3" series
9" x 6" x 3" series
9" x 4½" x 2½" series

☆

Write for Catalog Section S-6210

If you think of carbon only in terms of complete furnace linings, check these other important locations in and around the furnace where "National" carbon brick and shapes will also save time and money as a maintenance refractory:

- ✓ ***RUNOUT TROUGHS***
- ✓ ***CINDER NOTCH LINERS***
- ✓ ***CINDER NOTCH PLUGS***
- ✓ ***SPLASH PLATES***
- ✓ ***SKIMMER PLATES***

. . . and Many More!

The term "National" is a registered trade-mark of Union Carbide and Carbon Corporation

NATIONAL CARBON COMPANY

A Division of Union Carbide and Carbon Corporation, *30 East 42nd Street, New York 17, N. Y.*

District Sales Offices: Atlanta, Chicago, Dallas, Kansas City, New York, Pittsburgh, San Francisco

In Canada: National Carbon Limited, Montreal, Toronto, Winnipeg